



## **Terms and Conditions of Use of Digitised Theses from Trinity College Library Dublin**

### **Copyright statement**

All material supplied by Trinity College Library is protected by copyright (under the Copyright and Related Rights Act, 2000 as amended) and other relevant Intellectual Property Rights. By accessing and using a Digitised Thesis from Trinity College Library you acknowledge that all Intellectual Property Rights in any Works supplied are the sole and exclusive property of the copyright and/or other IPR holder. Specific copyright holders may not be explicitly identified. Use of materials from other sources within a thesis should not be construed as a claim over them.

A non-exclusive, non-transferable licence is hereby granted to those using or reproducing, in whole or in part, the material for valid purposes, providing the copyright owners are acknowledged using the normal conventions. Where specific permission to use material is required, this is identified and such permission must be sought from the copyright holder or agency cited.

### **Liability statement**

By using a Digitised Thesis, I accept that Trinity College Dublin bears no legal responsibility for the accuracy, legality or comprehensiveness of materials contained within the thesis, and that Trinity College Dublin accepts no liability for indirect, consequential, or incidental, damages or losses arising from use of the thesis for whatever reason. Information located in a thesis may be subject to specific use constraints, details of which may not be explicitly described. It is the responsibility of potential and actual users to be aware of such constraints and to abide by them. By making use of material from a digitised thesis, you accept these copyright and disclaimer provisions. Where it is brought to the attention of Trinity College Library that there may be a breach of copyright or other restraint, it is the policy to withdraw or take down access to a thesis while the issue is being resolved.

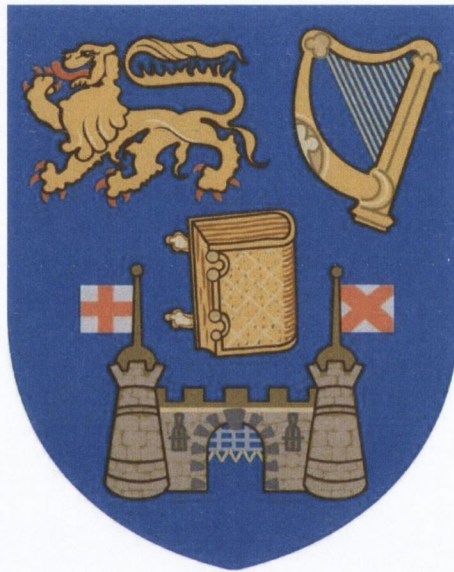
### **Access Agreement**

By using a Digitised Thesis from Trinity College Library you are bound by the following Terms & Conditions. Please read them carefully.

I have read and I understand the following statement: All material supplied via a Digitised Thesis from Trinity College Library is protected by copyright and other intellectual property rights, and duplication or sale of all or part of any of a thesis is not permitted, except that material may be duplicated by you for your research use or for educational purposes in electronic or print form providing the copyright owners are acknowledged using the normal conventions. You must obtain permission for any other use. Electronic or print copies may not be offered, whether for sale or otherwise to anyone. This copy has been supplied on the understanding that it is copyright material and that no quotation from the thesis may be published without proper acknowledgement.

# Biogrout

Pore scale bonding phenomena in saturated and unsaturated soils



Thesis submitted for the degree of  
Doctor of Philosophy in Civil, Structural and Environmental  
Engineering

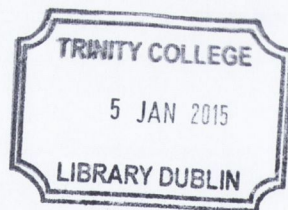
The University of Dublin, Trinity College

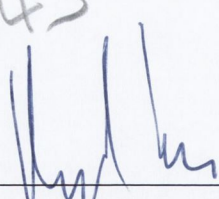
2014

**Matteo Viganotti**

I declare that this thesis has not been submitted as an exercise for a degree at this or any other university and it is entirely my own work.

I agree to deposit this thesis in the University's open access institutional repository or allow the library to do so on my behalf, subject to Irish Copyright Legislation and Trinity College Library conditions of use and acknowledgement.



Thesis 10743  


---

Matteo Viganotti

## SUMMARY

---

In the field of biogeocivil engineering one of the most promising *in-situ* ground improvement technologies is represented by Microbially Induced Carbonate Precipitation (MICP). Often referred to as biogrouting, MICP ground improvement is recognised as bioaugmentation technique employed to achieve the stabilisation of a granular soil by cementing its constituent particles together through calcium carbonate bonds. A substantial body of work has already gone into investigating the bulk properties of a biogROUTED granular material as well as the biogeochemical processes underpinning the technology. However, little research has systematically focussed on the mechanisms that control the formation and failure of the carbonate bond at the pore scale. A greater understanding of these mechanisms would lead to the development of a solid conceptual model which will become the basis for future improved computational modelling of MICP treatments. Therefore, the main aim of the research was to investigate the pore scale phenomena leading to the formation and mechanical failure of the calcium carbonate bonds between the particles of a granular medium.

Different treatment protocols were tested in saturated and unsaturated soils to investigate the effect that treatment protocols, saturation, soil particle size and soil mineralogy have on the formation and structure of the bonds. Traditional injection methods were employed to deliver the process reagents in saturated soils. Whereas the research was extended to include the atomised delivery of process reagents (an emerging technology in the bioremediation field) due to the potential it offers in the treatment of unsaturated soils. A multidisciplinary approach was taken throughout the project which was conducted by means of a literature review, followed by a set of experiments. The laboratory scale experiments were designed to: (1)

verify hypotheses derived from the review of the literature and (2) observe and interpret the bonding phenomena taking place at the pore scale. Data was collected using a diverse set of analytical testing, physical testing and visualization methods derived from the fields of applied microbiology, mineralogy and geotechnical engineering.

Overall the research has demonstrated that a number of parameters have a bearing on the formation, structure and failure of the inter-particle bond being formed during the MICP treatment of granular soils. Among these, the treatment protocol employed and the hydraulic regime of the soil being treated have shown to be the most critical. The addition of nutrients to the cementation solution was shown to control the abundance and distribution of bacteria at the pore scale and therefore affect the structure of bonds as well as the efficacy and homogeneity of a treatment. The establishment of partially saturated regimes during the treatment of unsaturated soils, instead, has shown to strongly control the structure of the bond: with relevant consequences extending to the macro scale. The mineralogical nature of the soil matrix has also shown to have an impact on the expected performance of treatments. Conversely, the impact of soil particle size is seen to be mostly limited to the bioaugmentation injection and its relevance is subject to the treatment protocol employed.

Ultimately, the results demonstrated the viability of aerosol delivery methods for *in-situ* MICP in unsaturated soils. A key advantage is represented by the ability to prevent the loss of liquid reagents by percolation. However, a number of limitations exist at the present stage of the technology development; these will need to be addressed in order to test the technology at a larger scale.

# TABLE OF CONTENTS

CHAPTER 1 .....	1
1) Microbiology in Geotechnical Engineering .....	1
2) MICP for Ground Improvement.....	3
3) Scope of the Research .....	4
3.1 Research framework.....	5
4) Structure of the Thesis.....	7
CHAPTER 2.....	8
1) Inspired by Natural Lithogenesis.....	8
1.1 The catalytic function of the urease enzyme.....	8
1.2 Sporosarcina pasteurii: a live source of urease.....	10
1.3 Alternative MICP processes .....	11
2) Bulk Properties of Soils Treated with MICP .....	12
2.1 Unconfined compressive strength.....	12
2.2 Stiffness and failure.....	13
2.3 Permeability and porosity .....	14
3) Bond Formation and Failure Model .....	14
4) Treatment Protocols: Transport and Growth of Bacteria.....	18
4.1 Transport and deposition of <i>S. pasteurii</i> .....	19
4.2 Growth of <i>S. pasteurii</i> and biofilm formation .....	24
5) Reagent Concentration in the Cementation Liquid.....	26
5.1 Effect of reagent concentrations on UCS .....	26
5.2 Effect of reagent concentrations on permeability.....	28
5.3 Pore scale conceptual model .....	28
6) Delivery methods and procedures .....	32

6.1 Macro scale effects of delivery methods.....	34
6.2 Pore scale effects of delivery methods .....	37
7) Soil mineralogy .....	40
8) Value of a Revised Conceptual Bond/Failure Model.....	42
9) Opportunities for Innovation .....	43
9.1 Atomised Delivery of MICP Process Liquids.....	43
9.2 Dolomite as an alternative cementation agent .....	45
CHAPTER 3.....	48
1) Solubility and Precipitation of Calcium Carbonate .....	48
1.1 Crystallisation and mineral morphology .....	51
2) Biological Catalysis of Urea Hydrolysis .....	54
2.1 Enzyme activity and kinetics .....	55
3) Atomised Delivery Technology .....	57
3.1 Deposition and Transport of Aerosols in Soils .....	59
CHAPTER 4.....	64
1) Introduction .....	64
2) Microbiological Methods .....	65
2.1 Chemicals and stock solutions .....	65
2.2 Culture preparation .....	66
2.3 Optical density and urease activity .....	68
3) Scanning Electron Microscopy .....	69
4) X-Ray Diffraction Peak Analysis .....	69
5) Soil and Geotechnical Testing Methods .....	71
5.1 Soil types .....	71
5.2 Barometric determination of calcium carbonate .....	72
5.3 Unconfined compressive strength test .....	73

6) Aerosol Delivery.....	73
6.1 Medical jet nebulisers .....	73
6.2 Test columns .....	75
CHAPTER 5.....	78
1) Experiment N. 1: Carbonate distribution .....	78
1.1 General.....	78
1.2 Experimental set-up .....	78
1.3 CaCO <sub>3</sub> determination and effect of particle size .....	81
1.4 Treatment protocols and CaCO <sub>3</sub> distribution.....	84
1.5 Soil mineralogy and CaCO <sub>3</sub> distribution.....	87
1.6 Interim conclusions.....	90
2) Experiment N. 2: Carbonate bond .....	92
2.1 General.....	92
2.2 Experimental set-up .....	92
2.3 Oligotrophic bond formation and failure .....	93
2.4 Eutrophic bond formation and failure .....	98
2.5 Interim conclusions.....	104
3) Experiment N. 3: Magnesium in MICP applications.....	106
3.1 General.....	106
3.2 Experimental set-up .....	106
3.3 Precipitated mineral forms.....	107
3.4 Precipitation rate.....	112
3.5 Interim conclusions.....	113
CHAPTER 6.....	115
1) Experiment N. 4: Feasibility of aerosol delivery .....	115
1.1 General.....	115



1.2 Experimental set-up .....	115
1.3 Carbonate content and UCS.....	117
1.4 Wetting front and deposition .....	118
1.5 Interim conclusions.....	120
2) Experiment N. 5: Aerosol delivery of MICP reagents.....	122
2.1 General.....	122
2.2 Experimental set-up .....	122
2.3 Calcium carbonate content.....	124
2.4 Conversion efficiency.....	126
2.5 Unconfined compressive strength.....	129
2.6 Structure of the inter-particle bond.....	131
2.7 Failure of the inter-particle bond.....	138
2.8 Interim conclusions.....	139
CHAPTER 7 .....	143
1) Bond formation, structure and failure .....	143
2) Atomised delivery of process reagents.....	146
3) Deposition of dolomite .....	147
4) Limitations of this study.....	148

# CHAPTER 1

## INTRODUCTION

---

### 1) MICROBIOLOGY IN GEOTECHNICAL ENGINEERING

Bacteria were the early inhabitant of Earth's primordial ecosystems. As such, microbes today form a significant part of the ecosystems in soils: typically accounting for  $10^9$  to  $10^{12}$  organisms per cubic meter of near surface soil (Mitchell and Santamarina 2005). Early examples of human exploitation of soil microbes can be traced as far back as Pre-Roman mining techniques (Rawlings 2002). Early miners were unaware of the role played by these microbial communities but throughout the XIX and XX century, theoretical and technological advancements have increasingly allowed researchers to study microbes and microbial communities in their natural environment. This has led to the development of innovative industrial and agricultural processes based on an improved understanding of the biogeochemical interactions that exists between microbes; and between microbial communities and their environment (Ehrlich and Newman 2009; Ivanov 2011).

Within the geotechnical discipline, it has only recently been recognised from an engineering perspective that soil is an active ecosystem (Mitchell and Santamarina 2005; DeJong, Soga et al. 2011). This new branch of geotechnics is building on the extensive knowledge already generated within the fields of agricultural soil science (van Veen, van Overbeek et al. 1997), wastewater treatment (Gray 2004), bioremediation (Wiedemeier 1999; Crawford and Crawford 2005) and geomicrobiology (Banfield and Nealson 1997; Ehrlich 1998). As a result it is possible to extend the interpretation of soil properties beyond physics, geology and chemistry into a single, holistic, biogeocivil engineering

framework (Mitchell and Santamarina 2005; Jonkers and van Loosdrecht 2010; Dejong, Soga et al. 2013).

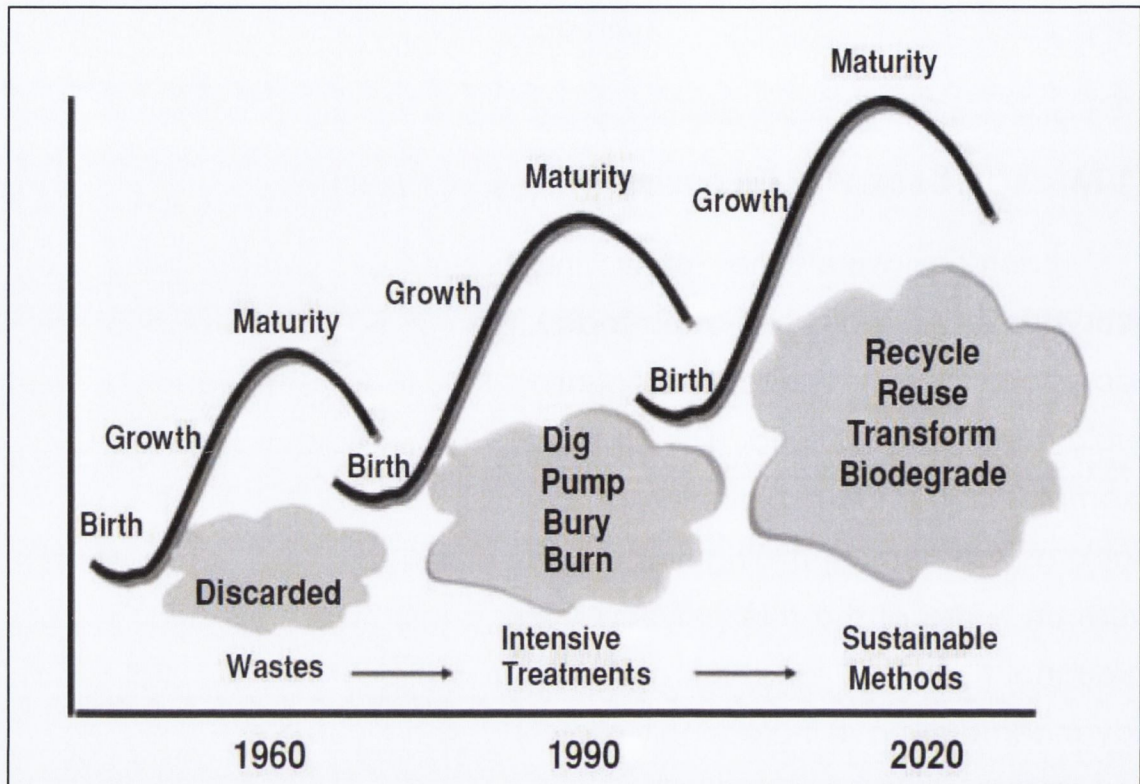


**Figure 1.1** Evolution of the thinking about wastes and cleanups: transforming our thought process (Ellis and Hadley 2009). A template for innovation trends in the geotechnical and civil engineering fields.

As illustrated in Figure 1.1, this paradigm shift repeats the trend followed by the closely related remediation industry: towards the much needed establishment of more sustainable practices. Therefore, biogeocivil engineering is deemed a young, vital field; and exciting research and development outcomes are expected for the future of the discipline. In fact, the significant potential for advancement offered by its principles has led the US National Research Council (2006) to identify biogeocivil engineering as one of the important research areas in the years to come. One such research effort is represented by the work presented here and focuses on the application of Microbially Induced Carbonate Precipitation (MICP) for soil improvement practices.

## 2) MICP FOR GROUND IMPROVEMENT

Settlement, erosion, slope stability and seismic activity can often represent a major threat to development projects around the world. Hence, modern engineers have learnt to resort to soil improvement techniques and design solutions to address many of the limitations imposed by the local ground conditions (Karol 2003; Chu, Varaksin et al. 2009). In the field of biogeocivil engineering, one of the most promising technologies for improving the mechanical properties of sands and gravels is represented by Microbially Induced Carbonate Precipitation, or MICP (Whiffin, van Paassen et al. 2007; van der Ruyt and van der Zon 2009; DeJong, Mortensen et al. 2010; Harkes, van Paassen et al. 2010).

MICP ground improvement, often referred to as biogrouting, falls within the category of non-displacement grouting techniques (Karol 2003) where microbial activities or products are used to reduce the permeability and/or increase the shear strength of a soil (Chu 2012). However, when compared to traditional grouting methods biogrouting would offer a more sustainable alternative (Suer, Hallberg et al. 2009) by taking inspiration from naturally occurring phenomena. In its typical concept, the treatment is delivered *in-situ* according to the following general procedure:

1. **Bioaugmentation:** the microbiological catalyst of the reaction is delivered into the soil by injecting a bacterial suspension;
2. **Cementation:** bioaugmentation is followed by the injection of one or more batches of a concentrated solution containing calcium chloride ( $\text{CaCl}_2$ ) and urea ( $\text{CO}(\text{NH}_2)_2$ ).

In the soil, urea is hydrolysed to ammonium and carbonate ions by the bacteria: in the presence of a high calcium concentration, the resulting pH increase and availability of carbonate ions causes the precipitation of calcium carbonate within the pore space (Stocks-Fischer, Galinat et al. 1999). Ultimately, biogrouting causes the transformation of loose

sediment, such as sand, into a more stable rock-like material (Montoya, DeJong et al. 2013): very much like the natural lithogenesis of carbonate rocks.

The increasing number of research efforts (Dejong, Soga et al. 2013) and the recent success of large scale experiments (van Paassen, Ghose et al. 2010) have made MICP by urea hydrolysis one of the biogeocivil technologies nearest to full scale and commercial implementation (Filet, Gadret et al. 2011): leading to the filing of several patents (Kucharski, Cord-Ruwisch et al. 2006; Balleur and Girinski 2008; Cheng and Shen 2008; Kucharski, Cord-Ruwisch et al. 2008)

### **3) SCOPE OF THE RESEARCH**

A substantial body of work has already gone into investigating the bulk properties of a biogROUTED granular material as well as the biogeochemical processes underpinning the technology. (Kucharski, Price et al. 1997; Whiffin, van Paassen et al. 2007; DeJong, Mortensen et al. 2010; van Paassen, Ghose et al. 2010; Tagliaferri, Waller et al. 2011). However, little research has systematically focussed on the mechanisms that control the formation and failure of the calcium carbonate bond at the pore scale.

Evidence suggests that the formation and failure of the bond is a crucial aspect of the technology and is expected to have a strong impact on the overall effectiveness of treatments. While some early conceptual models describing bonding and failure at the pore scale exist (DeJong, Mortensen et al. 2010; Al Qabany and Soga 2013), these would appear to be limited to very specific experimental conditions. Additionally, the literature appears to be mostly limited to the application of the technology in water saturated soils, with only one study investigating its application in unsaturated soils (Cheng and Cord-Ruwisch 2012).

Therefore, the main aim of the research was to investigate the pore scale phenomena leading to the formation and failure of the calcium carbonate bonds between the particles of a granular medium. It is hoped that a greater understanding of these mechanisms would lead to the development of a solid conceptual model which will become the basis for future improved computational modelling of MICP treatments. The objectives of the research were to critically assess the impact of the following factors on the bond formation and failure processes:

- The treatment protocols employed;
- The composition of the cementation solution;
- The delivery mechanisms and procedures employed;
- The mineralogy, size and saturation of the soil being treated.

The research has extended to include atomised delivery of process reagents due to the potential it offers in the treatment of unsaturated soils. Atomised delivery is an emerging method in the bioremediation field where small droplets ( $< 10 \mu\text{m}$ ) of reagents are delivered into the soil by a gas stream (Glew 2009; Riha, Murdoch et al. 2010; Dyer, Glew et al. 2012). Incidentally, the review of biomediated carbonate precipitation processes has also led to the identification of an opportunity for process innovation: the precipitation of the more durable dolomite mineral, in place of calcium carbonate polymorphs. This has also been investigated in the context of the research.

### 3.1 RESEARCH FRAMEWORK

The work presented here comprises of a literature review in which the possible impact of the identified factors was evaluated. The literature review also aimed at providing an understanding of how phenomena occurring at the pore scale might influence some of the bulk properties of the treated material. A multidisciplinary approach was

taken throughout the research which has led to the review of a diverse set of sources in the fields of microbiology, engineering, geology and mineralogy. Ultimately, the hypotheses derived from the literature review were explored through a series of small and medium scale experiments. A graphical representation of the research framework is presented in Figure 1.2.

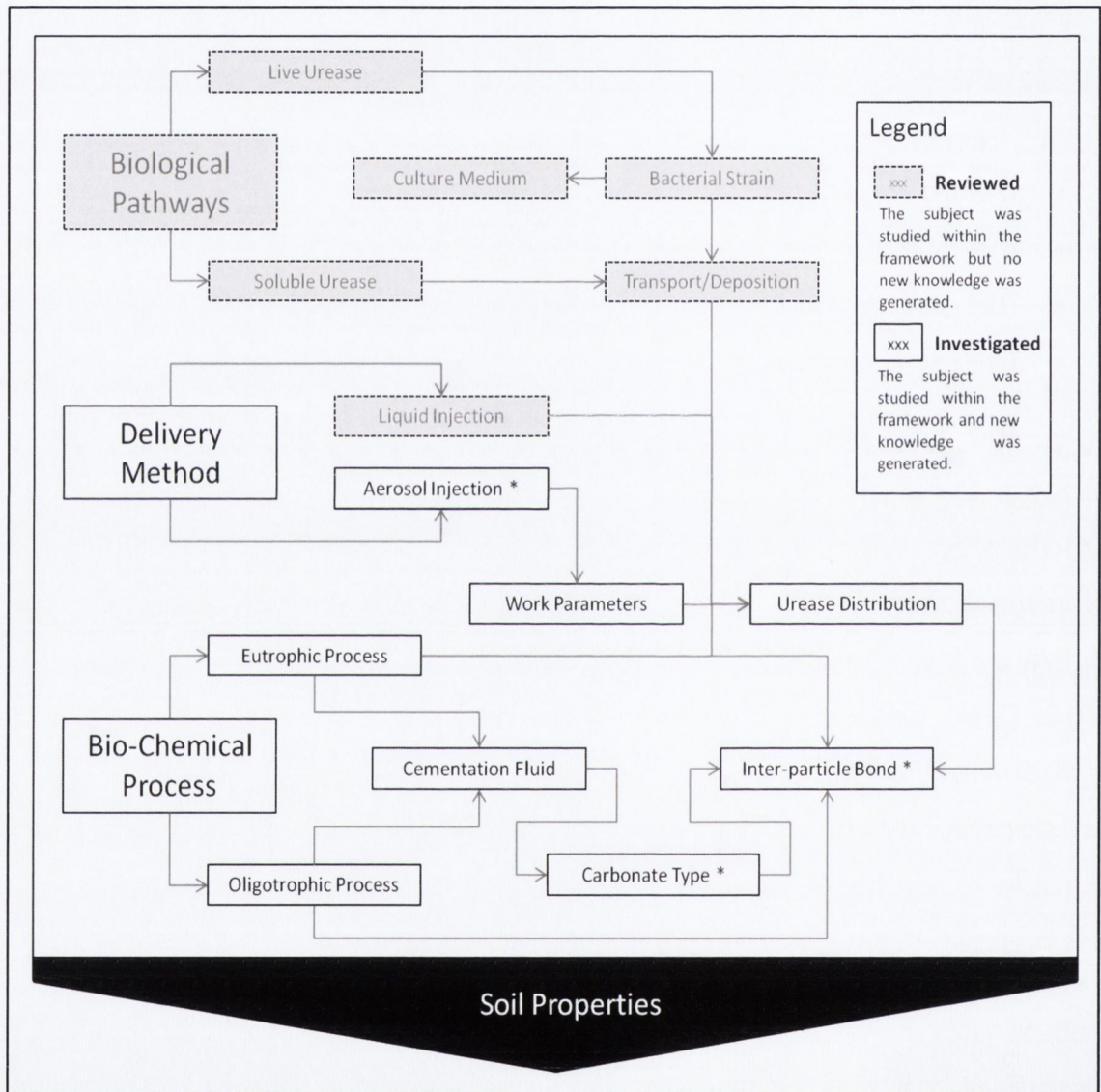


**Figure 1.2** Research framework showing the elements of the technology being investigated. Items marked with an asterisk were central to the research.

#### 4) STRUCTURE OF THE THESIS

This document is organised in six chapters:

- **Chapter 1** provides a general introduction to the field of biogeocivil engineering and to the work being presented.
- **Chapter 2 and 3** discuss the literature review together with the scientific principles that describe the key elements of MICP applications.
- **Chapter 4, 5 and 6** are dedicated to the experimental work carried out in the context of the research being presented. In particular, Chapter Four is dedicated to the description of the methods employed; Chapter Five and Chapter Six present and discuss the results of the experiments conducted in saturated and unsaturated soils respectively. Interim conclusions are also provided.
- **Chapter 7** is the concluding chapter in which the conclusions derived from the research will be presented.



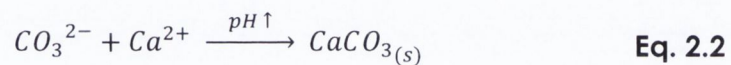
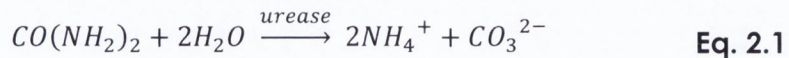
## **1) INSPIRED BY NATURAL LITHOGENESIS**

MICP takes inspiration from the formation process of one of the most significant groups of sedimentary rocks: calcium carbonate rocks. While the extent of the microbial contribution to the lithogenesis of carbonate rocks is still a matter of discussion (Castanier, Le Métayer-Levrel et al. 1999; Braissant, Verrecchia et al. 2002; Wright and Oren 2005), evidence exists, throughout the geological record, of the ability of microbes to intervene in their formation and diagenesis (Knoll and Swett 1990; Ehrlich 1999; Riding 2000; Mastandrea, Perri et al. 2006; Konhauser 2007). Well known examples are found in the formation of microbialites operated by complex microbial mats in marine environments (Dupraz and Visscher 2005; López-García, Kazmierczak et al. 2005). Additionally, the contribution of living organisms to the formation of large bioclastic carbonate deposits has been well documented and established (Ehrlich 1999).

### 1.1 THE CATALYTIC FUNCTION OF THE UREASE ENZYME

The research presented here will focus on aerobic metabolic processes leading to the nucleation and growth of calcium carbonate crystals from an interstitial supersaturated solution. In fact, most engineered applications of MICP take inspiration from one such naturally occurring processes, that is: the heterotrophic degradation of urea (Castanier, Le Métayer-Levrel et al. 1999). Applications involving the degradation of urea rely on a biological catalytic step to control the alkalinity and dissolved inorganic carbon (DIC) in a liquid medium; in turn inducing the precipitation of calcium carbonate:

As shown in Eq. 2.1, the catalytic function within the MICP process is performed by the enzyme urease (urea amidohydrolase) found in numerous bacteria, plant and animal species (Castanier, Le Métayer-Levrel et al. 1999; Krajewska 2009). Urea is hydrolysed by the enzyme to ammonium and carbonate ions. In the presence of a high calcium concentration, the precipitation of calcium carbonate, Eq. 2.2, is induced within the pore space (Stocks-Fischer, Galinat et al. 1999).



The reactions involved in the precipitation of calcium carbonate as described above, are abiotically possible. However, the presence of the urease enzyme (in the form of selected bacteria species) allows the reaction to proceed up to  $10^{14}$  times faster and achieve cementation in a useful timeframe (Ferris, Phoenix et al. 2004; Krajewska 2009).

In the context of MICP applications, optical density, urease activity and specific urease activity are often referred to when describing a bacterial culture employed in the process:

- **Optical Density** at 600nm ( $OD_{600}$ ): the measure of suspended biomass as determined by spectrophotometric absorbance at 600 nm;
- **Urease Activity** (UA): the amount of urea hydrolysed in the unit of time by a bacterial suspension (usually reported in  $\text{mM}\cdot\text{min}^{-1}$ );
- **Specific Urease Activity** (SUA): the amount of urea hydrolysed in the unit of time and biomass (usually reported in  $\text{mM}\cdot\text{min}^{-1}\cdot\text{OD}_{600}^{-1}$ ).

These parameters are, in fact, useful in evaluating the, rate, performance and effectiveness of a microbiological species employed in biogrouting applications.

## 1.2 SPOROSARCINA PASTEURII: A LIVE SOURCE OF UREASE

A readily available source of urease is represented by soluble forms of jack bean (*Canavalia ensiformis*) extract or grind. However, urea degrading bacteria are commonly found to participate in diagenetic processes by precipitating carbonates in natural soil and subsurface environments (Cacchio, Ercole et al. 2003; Banks, Taylor et al. 2010; Burbank, Weaver et al. 2012). Most importantly a live microbial sources of urease would present the advantage of being cost-effectively cultivable on-site as well as being able to become attached to the particles of a soil being treated (Whiffin 2004; Harkes, van Paassen et al. 2010). Whiffin (2004) has summarised the key characteristics of a suitable bacterial source of urease as follows:

- Non pathogenic and environmentally sound;
- High specific urease activity;
- The enzyme should not be strongly repressed by high concentrations of process reagents or by-products.

Consensus among researchers is that *Sporosarcina pasteurii* (formerly known as *Bacillus pasteurii*) mostly meets the requirements listed above. In fact, *S. pasteurii* is a common soil bacterium (Burbank, Weaver et al. 2012) with optimal growth pH of 9.25 (Whiffin 2004), as such its localised bioaugmentation would pose only a limited threat to the environment. Crucially, *S. pasteurii* does not represent a significant threat to human health (Whiffin 2004) and is classified by the Advisory Committee on Dangerous Pathogens as a Group 1 organism. While generally expressing a high specific urease activity (Mobley, Island et al. 1995; Krajewska 2009), this can be repressed by some of the reagents employed in MICP. In particular, concentrations of calcium ions above 1.5 M have shown to drastically reduce the performance of biogrouting applications (Whiffin 2004). However, such highly concentrated solution are not usually employed; therefore, *S. pasteurii* has become the species

of election in most engineering applications of MICP conducted using urea hydrolysis pathways (Gollapudi, Knutson et al. 1995; Stocks-Fischer, Galinat et al. 1999; Fujita, Ferris et al. 2000; DeJong, Fritzges et al. 2006; Whiffin, van Paassen et al. 2007; Bang, Lippert et al. 2010; van Paassen 2011; Al Qabany, Soga et al. 2012; Dejong, Soga et al. 2013).

### 1.3 ALTERNATIVE MICP PROCESSES

As shown in Figure 2.1, urea hydrolysis is less thermodynamically favoured when compared to alternative MICP processes. However, the relatively uncomplicated exploitation of the process has established urea hydrolysis as the main metabolic pathway employed. Alternative techniques that rely on the biological dissimilatory reduction of nitrate (or denitrification) are recently attracting the interest of researchers in the field.

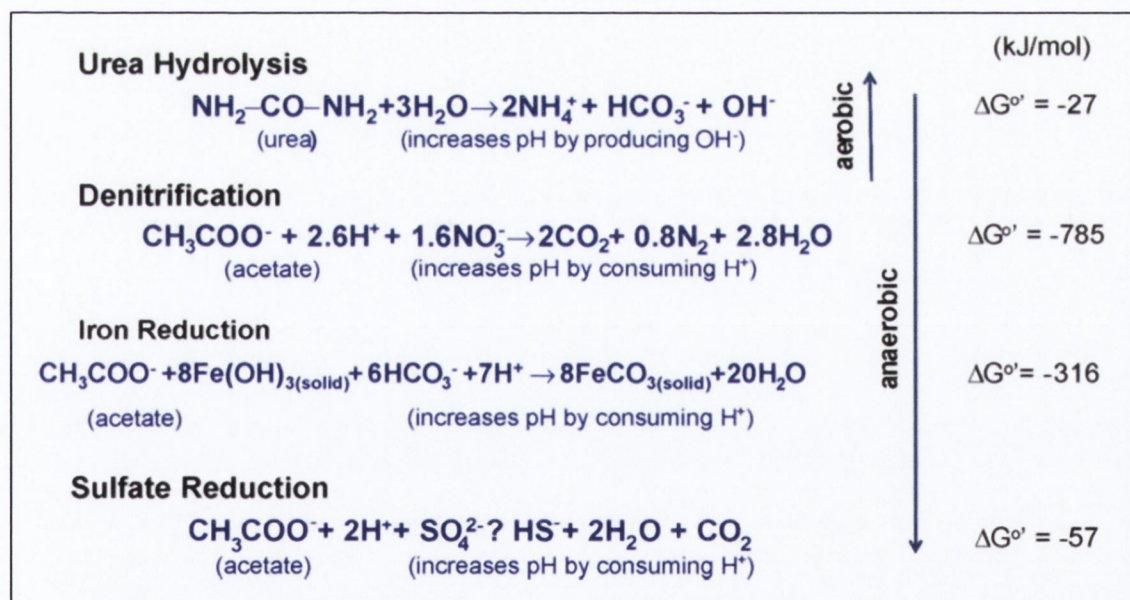


**Figure 2.1** Alternative bio-mediated processes potentially leading to calcium carbonate supersaturation. Gibbs free energy computed for standard conditions (DeJong, Mortensen et al. 2010).

The advantages with respect to urea hydrolysis would be: the reduced risk associated with the ammoniacal by-product of the process (van Paassen, Daza et al. 2010); the potentially higher calcium

carbonate yields (Hamdan, Kavazanjian et al. 2011); and the opportunity of using wastewater streams of different origin as a substrate source (van der Star, Taher et al. 2010). However, nitrate reduction as well as other alternative biological mechanisms, such as sulphate reduction, would be unsuitable for application in unsaturated soils due to their requirement for anaerobic conditions (Castanier, Le Métayer-Levrel et al. 1999; Dupraz, Reid et al. 2009).

## **2) BULK PROPERTIES OF SOILS TREATED WITH MICP**

In the geotechnical field, soil improvement technology is employed to modify, according to specific design requirements, the engineering parameters of a soil, namely: strength, stiffness, permeability and porosity. While pioneering examples of full scale field applications of biogrouting techniques exist (Filet, Gadret et al. 2011), at present MICP has been mostly investigated in controlled laboratory scale experiments employing poorly graded fine to medium silica sands (DeJong, Fritzges et al. 2006; Whiffin, van Paassen et al. 2007; van Paassen, Ghose et al. 2010; Al Qabany, Soga et al. 2012). Below are briefly introduced some of the key soil properties which can be improved or modified by means of MICP treatment.

### 2.1 UNCONFINED COMPRESSIVE STRENGTH

Due to the broad utility that the improvement of mechanical strength characteristics of sand and gravel soils would have in field applications, unconfined compressive strength (UCS) has been often used in the literature to assess the efficacy of MICP treatments. As shown in Figure 2.2, by controlling the amount of calcium carbonate precipitated, the process can be engineered to achieve a vast range of UCS. Reported UCS values for treated sand vary greatly with typical values ranging between 150 kPa and 20 MPa (Harkes, van Paassen et al.

2008; van der Ruyt and van der Zon 2009; van Paassen 2009; Al Qabany and Soga 2013). There is a general consensus that a strict relationship exists between calcium carbonate content and UCS (Whiffin, van Paassen et al. 2007; Harkes, van Paassen et al. 2008; van Paassen 2009). However, this is being recently challenged by the results presented by some authors (Cheng and Cord-Ruwisch 2012; Al Qabany and Soga 2013): suggesting that micro scale phenomena and methodological factors could have a bearing on the resulting effectiveness ( $[\text{CaCO}_3]/\text{UCS}$ ) of the treatment. These will be discussed in more detail in the following paragraphs

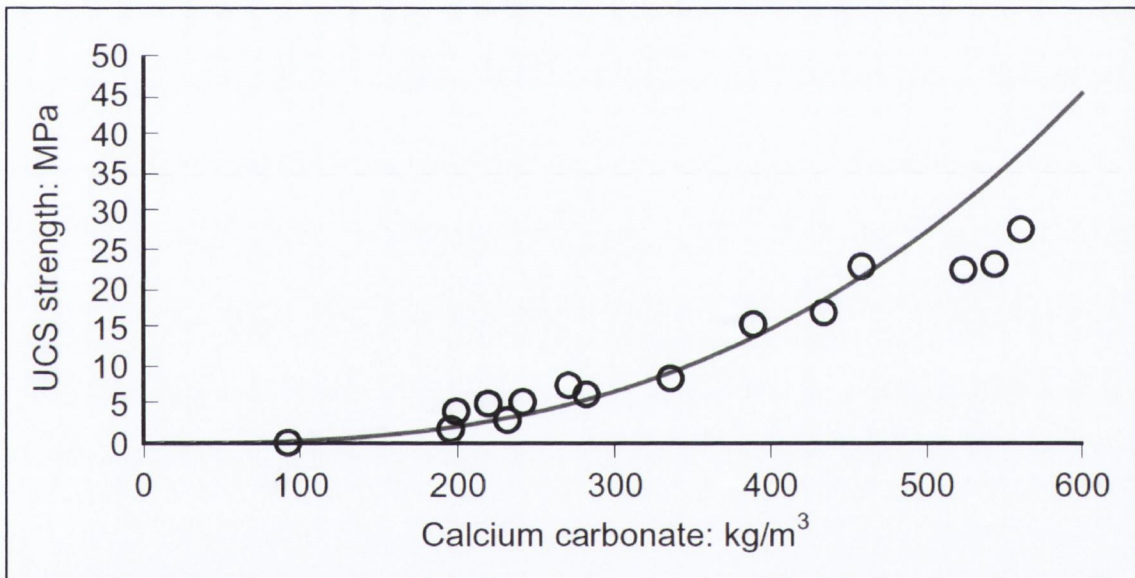


**Figure 2.2** Unconfined compressive strength versus calcium carbonate content (van der Ruyt and van der Zon 2009). By controlling the amount of calcium carbonate precipitated, it is possible to achieve a vast range of soil strength improvement.

## 2.2 STIFFNESS AND FAILURE

Biocemented sands display a stiff behaviour (van Paassen, Ghose et al. 2010), with recorded values of tangent Young modulus,  $E_{50}$ , ranging between 110 MPa and 2210 MPa and elastic Young modulus,  $E_{ur}$ , ranging between 1300 MPa and 13000 MPa. Due to its stiff behaviour, the cemented material displays little volumetric strain when loaded with

usually small differences in peak strength between drained and undrained compression tests (van Paassen 2009). Failure of biogROUTED samples is typically brittle. Shear failure is reported to occur along a thin active band in confined triaxial tests (Tagliaferri, Waller et al. 2011), whereas tensile failures (cracks) are reported as typical in unconfined compression strength tests (Al Qabany and Soga 2013). As a result of stiffness, small increases in pore-water pressure have been observed under loading: highlighting the potential of MICP as a soil liquefaction mitigation measure. To this effect, it is of particular significance that progressive weakening is reported to occur under dynamic loading (Montoya, DeJong et al. 2013) as sudden catastrophic failure of a treated mass would be a matter of concern in seismic areas.

### 2.3 PERMEABILITY AND POROSITY

Unlike traditional cement and chemical grouting, where a significant proportion of the soil's strength increase is a consequence of pores filling with grout (Karol 2003), biogROUTING can be successfully applied to increase a soil's strength with limited losses of porosity and permeability (Whiffin, van Paassen et al. 2007; van Paassen 2009). By controlling the amount of calcium carbonate and the precipitation conditions it is possible to control the resulting permeability reduction (Al Qabany and Soga 2013).

## **3) BOND FORMATION AND FAILURE MODEL**

There is general agreement among authors that the strength increase observed in biogROUTED sand samples is to be ascribed to the cementing effect of individual bonds between particles. As show in Figure 2.3, once failure occurs, the residual strength of the treated samples is comparable to that of an untreated sand: indicating that most of the improvement is caused by the formation of bonds between

particles and lost after failure thereof (van Paassen 2009; Tagliaferri, Waller et al. 2011). Once the bonds become broken, the contribution of the carbonate precipitated on the surface of the soil particles, or part-filling the pore space, is marginal (DeJong, Fritzges et al. 2006; Whiffin, van Paassen et al. 2007). This would highlight the relationship that exists between the strength increase observed at the macro scale and the formation and failure mechanisms controlling the bond at the pore scale.

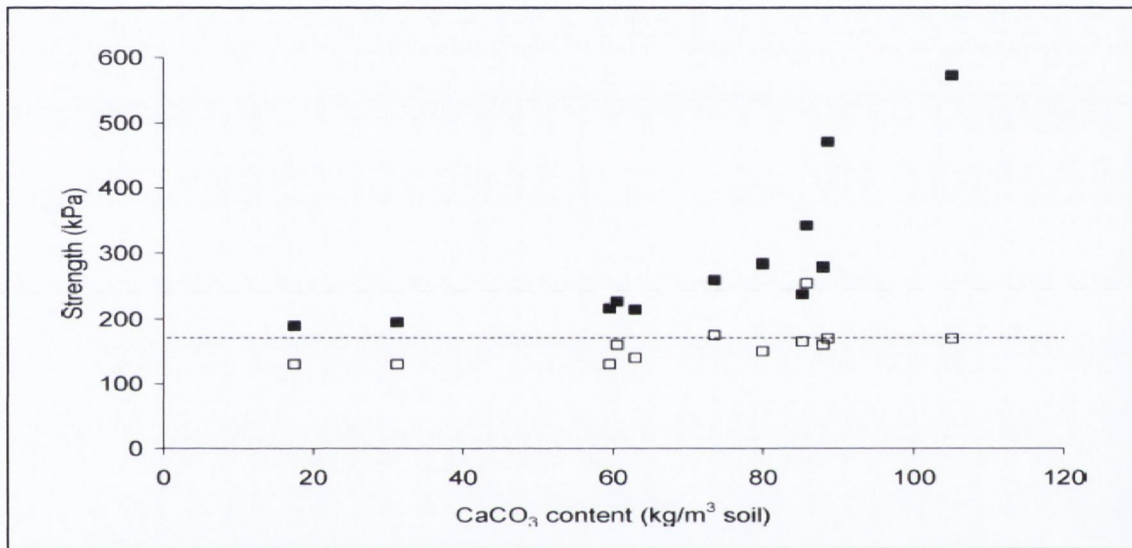


**Figure 2.3** Confined compressive strength (full squares) and residual strength of material after failure (empty squares) versus calcium carbonate content. Confining pressure was 50 kPa. Under the same consolidation conditions, untreated sand of the same density gave a strength value of 167 kPa and a residual strength of 130 kPa (Whiffin, van Paassen et al. 2007).

An early conceptual model of bond formation and failure mechanisms has been proposed by DeJong et al. (2010) and is reported in Figure 2.4. The model proposed shows the bond being formed as a hybrid between: the formation of a uniform carbonate crust around the sand particles, and the preferential deposition at (or close to) inter-particle contact points. The failure mechanism considered by the authors is presented as a failure surface involving both the bond-sand interface and fractures within the bond itself. While the model is an accurate and insightful interpretation of what observed by the authors in



scanning electron microscopy images, the experimental conditions employed were very specific. Therefore the conceptual model proposed is deemed limited by a lack of systematic investigation on the parameters that might have a bearing on the mechanisms leading to the establishment of a bonding structure. And in turn on the consequent failure mechanisms that might result.

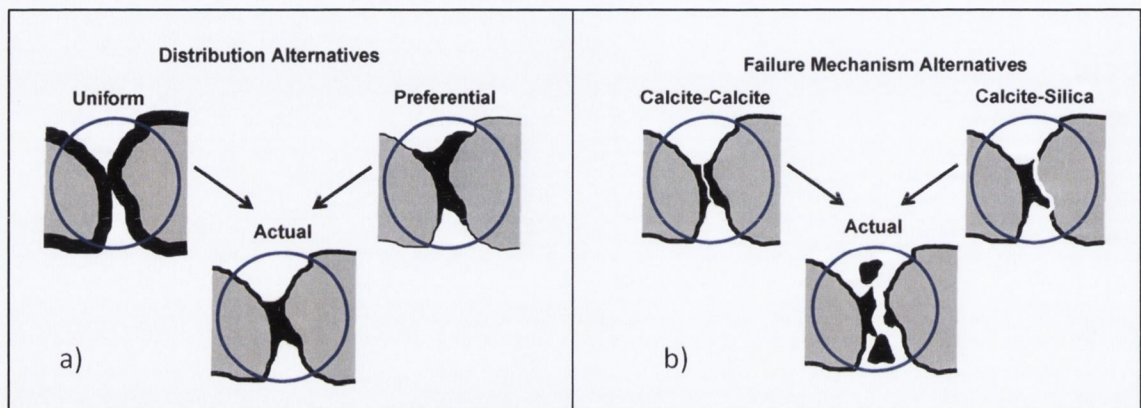


**Figure 2.4 (a)** Illustration of carbonate distribution patterns (bond formation) at the pore scale and **(b)** proposed failure mechanisms under shearing/loading (DeJong, Mortensen et al. 2010).

In addition to the factors affecting traditional grouting methodologies, biogrouting is complicated by the live nature of the biological catalyser: requiring to extend the interpretation beyond the biochemical reactions involved in the precipitation process alone. The key factors that have been identified in the work presented here as possibly impacting on the bond formation process are:

- The treatment protocols employed;
- The composition of the cementation solution;
- The delivery mechanisms and procedures employed;
- The mineralogy, size and saturation of the soil being treated.

These will be individually discussed in the following paragraphs within the context of the work being carried out. Table 2.1 provides a summary of the key publications that have been reviewed in the context of this research.

Table 2.1 Summary of key publications: investigation of MICP at the pore scale.

<b>Materials and Methods</b>	Enzyme source		<i>S. pasteurii</i>	<i>S. pasteurii</i>	<i>S. pasteurii</i>	<i>S. pasteurii</i>	<i>S. pasteurii</i>	<i>S. pasteurii</i>
	Delivery	Bioaugmentation	Injection	Inj. + fix	Injection	n.a.	Percolation	Injection
		Cementation	Injection	Inj. + ricirc.	Injection	n.a.	Percolation	Injection
	Trophic regime		Oligotrophic	Oligotrophic	Eutrophic	n.a.	Oligotrophic	Eutrophic
	Soil characteristics	Lithology	Silica sand Shale	Silica sand Carbonaceous	Silica sand	Perspex block Granite block	Silica sand	Silica sand
		Particle size	< 300 µm n.d.	n.d. n.d.	D <sub>50</sub> = 120 µm	n.a.	300-150 µm	300-150 µm 150-90 µm
		Saturation	Fully sat.	Fully sat.	Fully sat.	n.a.	Unsat.	Fully sat.
	Observation		Chemical Microscopy Physical	Microscopy	SEM Physical	Microscopy	SEM Chemical Physical	SEM Chemical Physical
Focus		Strength Efficiency	Crystal morphology	Strength Stiffness Review	Crack sealing Biofilm	Delivery Strength	Efficiency Permeability Strength	
<b>Parameters investigated at micro scale</b>	Bacteria	Distribution	Yes	Yes	No	No	Yes	Yes
		Growth	No	No	No	Yes	No	No
	Calcium carbonate	Distribution	No	Yes	Yes	Yes	Yes	Yes
		Form	No	Yes	No	No	No	Yes
	Delivery method		No	No	No	No	Yes	No
	Concentrations		Yes	No	No	Yes	No	Yes
	Trophic regime		No	No	No	No	No	No
	Soil characteristics		Yes	Yes	No	No	No	Yes
Bond		No	No	Yes	No	Yes	Yes	
<b>Reference</b>			Whiffin (2004)	van Paassen (2009)	DeJong et al. (2006)	Cuthbert et al. (2012)	Cheng et al. (2012)	Al Qabany et al. (2012, 2013)

#### 4) TREATMENT PROTOCOLS: TRANSPORT AND GROWTH OF BACTERIA

While the possibility of strictly biostimulation techniques is emerging in the literature (Cacchio, Ercole et al. 2003; Banks, Taylor et al. 2010; Burbank, Weaver et al. 2011; Burbank, Weaver et al. 2012; Dejong, Soga et al. 2013), most of the research so far has been concentrating on bioaugmentation treatment protocols for MICP *in-situ* applications. Typically, bioaugmentation is then followed by a number of injection rounds (determined by the design requirements) where a cementation solution is delivered into the soil.

**Table 2.2** Treatment protocols and relevant chemical composition of liquids employed in the literature for biogrout applications.

Bacteria Injection	Fixation	Cementation	Refs.
<i>S. pasteurii</i> (culture)* 20 g/L Yeast extract 190 mM NH <sub>4</sub> Cl (10 μM NiCl <sub>2</sub> )# pH 9.0	50mM CaCl <sub>2</sub>	0.5-1.0 M CaCl <sub>2</sub> 0.5-1.0 M CO(NH <sub>2</sub> ) <sub>2</sub>	(Whiffin, van Paassen et al. 2007) (van Paassen 2009) (Harkes, van Paassen et al. 2010) (Cheng and Cord-Ruwisch 2012)
<i>S. pasteurii</i> (cells)** 3 g/L Nutrient broth 330 mM CO(NH <sub>2</sub> ) <sub>2</sub> 20 mM CaCl <sub>2</sub> 190 mM NH <sub>4</sub> Cl 25 mM NaHCO <sub>3</sub> pH 6.0	Not employed	3 g/L Nutrient broth 330 mM CO(NH <sub>2</sub> ) <sub>2</sub> 20 mM CaCl <sub>2</sub> 190 mM NH <sub>4</sub> Cl 25 mM NaHCO <sub>3</sub> pH 6.0	(DeJong, Fritzsche et al. 2006) (Martinez and DeJong 2009) (Tagliaferri, Waller et al. 2011)
<i>S. pasteurii</i> (cells)** ??? g/L Nutrient broth ??? M NH <sub>4</sub> Cl ??? M NaHCO <sub>3</sub>	Not employed	3 g/L Nutrient broth 0.1-1.1 M CO(NH <sub>2</sub> ) <sub>2</sub> 0.1-1.1 M CaCl <sub>2</sub> 190 mM NH <sub>4</sub> Cl 25 mM NaHCO <sub>3</sub>	(Al Qabany, Soga et al. 2012) (Al Qabany and Soga 2013)

\* The culture is injected as is after it reaches late exponential

\*\* The culture is grown to late exponential, filtered and resuspended in the medium

# Not employed consistently throughout the literature

As shown in Table 2.2 two general protocols have been employed, albeit with some variations, in previous work; the key distinguishing parameters being: (1) the inclusion (or not) of a fixation treatment and (2) the presence (or absence) of nutrients in the cementation fluid employed. In order to distinguish between these two general protocols the terms “oligotrophic treatment” and “eutrophic treatment” will be introduced here and used throughout this document:

- **Oligotrophic treatment:** characterised by the absence of bacterial nutrients in the cementation liquid and usually includes a fixation phase;
- **Eutrophic treatment:** characterised by the addition of bacterial nutrients to the cementation liquid.

While both protocols have been applied successfully throughout the literature, this is the first time that the difference between the two is highlighted. Most crucially, the possible biostimulation of *S. pasteurii* resulting from the addition of nutrients to the cementation liquid has been mostly ignored by the literature. Additionally, the results obtained employing different protocols have often been compared or evaluated collectively without acknowledgment of the differences that might exist. However, the selection of one MICP treatment protocol over the other is deemed here to have a particular impact on the transport and growth mechanism regulating the abundance of bacteria within the pore space (Ghaly, A. et al. 2013).

#### 4.1 TRANSPORT AND DEPOSITION OF *S. PASTEURII*

Geometrical considerations have traditionally been assumed to determine the viability of bioaugmentation *in-situ* techniques (Crawford and Crawford 2005; Mitchell and Santamarina 2005; DeJong, Mortensen et al. 2010); one of the main limitations being the relative size of the biological component compared to that of the pores and pore throats

in the soil. As shown in the diagram in Figure 2.5, in fine soils (silts and clays) the small size of the pores can hinder the transport of bacterial cells and limit the flow of chemical or nutrient solutions for *in-situ* applications (Mitchell and Santamarina 2005).

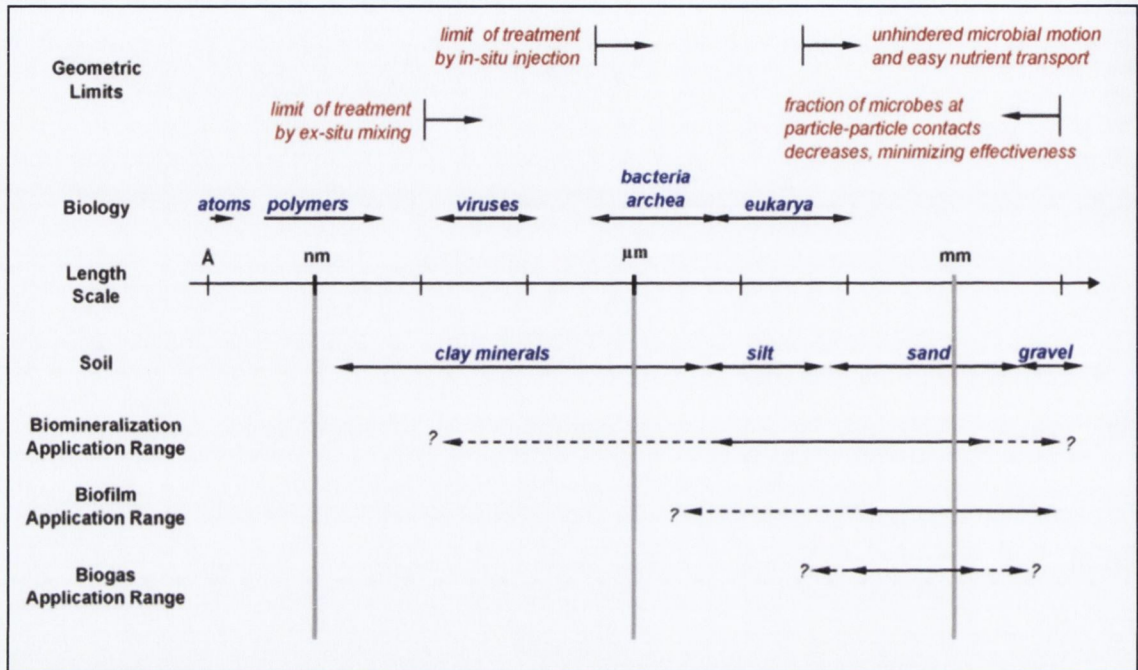


**Figure 2.5** Geometric limitations, and approximate limits of various biotreatment approaches (Mitchell and Santamarina 2005). Modified by DeJong et al. (2010).

This is a critical aspect in most *in-situ* bioremediation techniques (Crawford and Crawford 2005). However, in most ground improvement applications the size of the pore space is likely to be large enough to allow the transport of *S. pasteurii* cells. Conversely, in extremely coarse soils (very coarse sands and gravels), potentially fast flows and large pores could result in the bacteria being transported beyond the treatment area before these become deposited on a particle's surface (van Paassen 2009; Harkes, van Paassen et al. 2010). Additionally, the relatively small kissing number per unit volume of soil would imply that the contact surfaces between soil particles could be too few to ensure efficient cementation of very coarse matrixes (DeJong, Mortensen et al. 2010).

Noticeably, bacteria are known to act as nucleation sites during the heterogeneous nucleation of crystals (Ferris, Fyfe et al. 1987; Ehrlich 1999; Bosak and Newman 2003). Therefore the distribution of *S. pasteurii* within the pore space is expected to have consequences on the locations at which calcium carbonate will be precipitated.

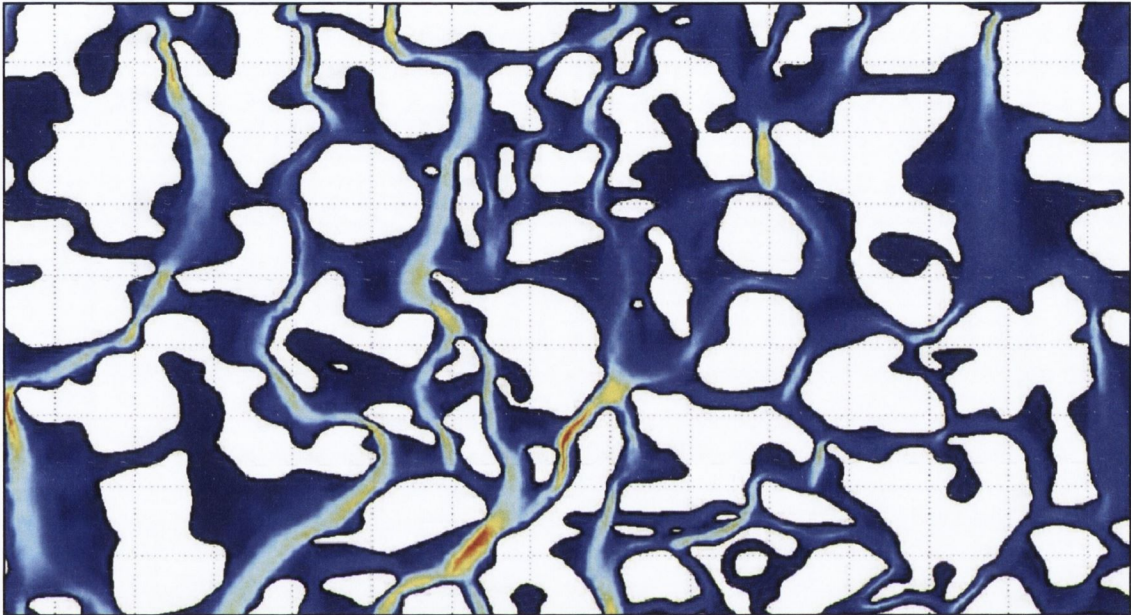


**Figure 2.6** Solution of Navier-Stokes equation for a complex pore space geometry using FEMLAB. Flow from top to bottom: dark blue, low velocity flow; red, high velocity flow (Keller and Auset 2007).

When biocolloids, such as bacteria, are transported through a soil, these can typically become attached (deposited) to: the soil-water interface, SWI; the air-water interface, AWI; or the triple contact of soil-water-air, SWA (Fang and Logan 1999; Keller and Auset 2007). The movement of bacteria within the pores of a porous medium is generally controlled by advection, diffusion, dispersion and active movement of the bacteria. These mechanisms can be described by referring to Figure 2.6. In such complex networks, larger particles tend to remain within the major stream lines (advection) while smaller particles and solutes are more likely to cross streamlines (diffusion and active movement) and become deposited (Gannon, Manilal et al. 1991; Abu-Ashour, Joyi et al. 1994; Keller and Auset 2007). Also, smaller particles have a larger number

of pathways available (dispersion) and can move through narrow pore throats to regions of almost stagnant flow precluded to larger particles (Sirivithayapakorn and Keller 2003). This phenomenon is often referred to as size exclusion. Size exclusion is, in strict terms, a transport process but can be associated with other deposition processes (Bradford, Simunek et al. 2006). Additionally, as a result of size exclusion, biocolloids (such as bacteria) can become retained in the column without direct contact with the soil particle surface (Johnson, Li et al. 2007).

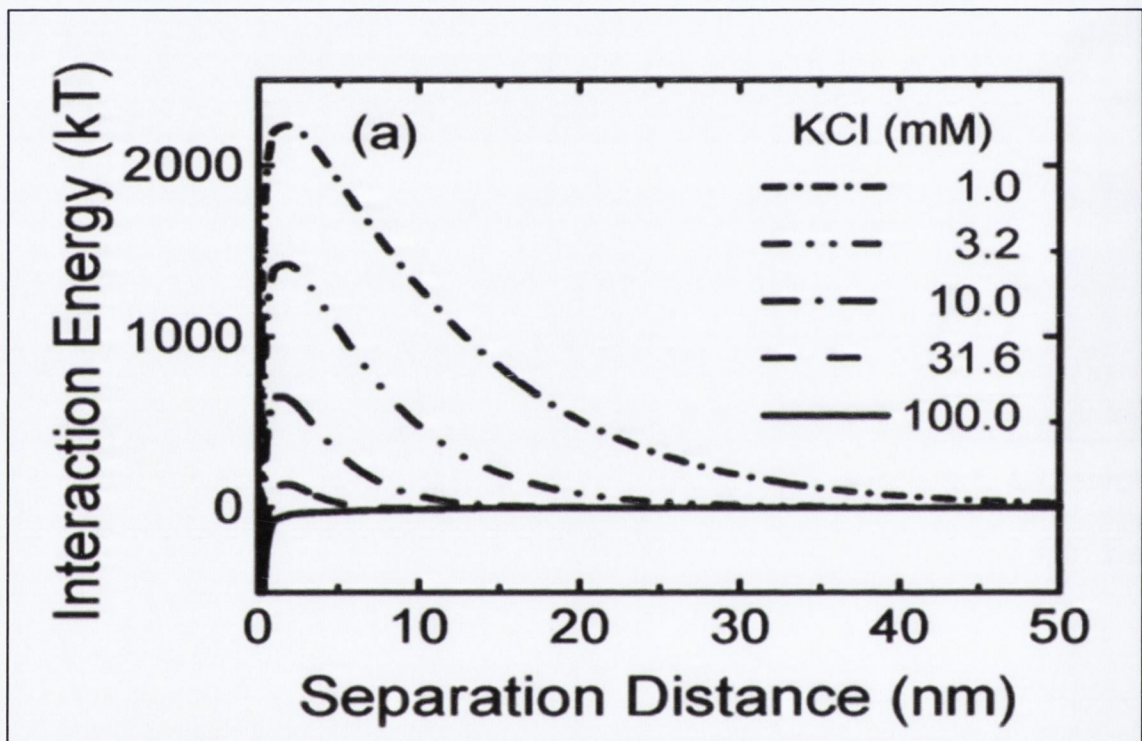


**Figure 2.7** Calculated Derjaguin-Landau-Verwey-Overbeek (DLVO) interaction energy between a collector and a bacteria cell as a function of separation distance and ionic strength of a KCl solution (Redman, Walker et al. 2004). Interaction energies were calculated from experimental data. Positive values indicate repulsion and negative values indicate attraction.

To limit the leaching of bacteria in sands, a fixation treatment, characterised by a relatively high ionic strength fluid (50 mM  $\text{CaCl}_2$ ), is proposed by some authors (Table 2.2). As shown in Figure 2.7, by changing the ionic strength of the pore-water, the energy barrier to deposition is reduced. As a result, the adsorption of bacteria cells on the

surface of soil particles (the collector) is increased (Redman, Walker et al. 2004; Torkzaban, Tazehkand et al. 2008); hence, limiting the leaching of urease. While the literature shows that the fixation treatment successfully increases the amount of bacteria retained in the soil column (van Paassen 2009; Harkes, van Paassen et al. 2010), it is of significance that colloid deposition occurs in porous media despite the expected presence of formidable energy barriers to deposition; and beyond what could be explained by traditional clean bed filtration theory (Bradford, Simunek et al. 2006; Johnson, Li et al. 2007). This was shown to be occurring when the ratio of the colloid diameter to the median collector diameter,  $D_{50}$ , is greater than  $5 \times 10^{-3}$  (Bradford, Simunek et al. 2003; Bradford, Torkzaban et al. 2007; Johnson, Li et al. 2007). In the context of Derjaguin-Landau-Verwey-Overbeek (DLVO) theory, several authors (Redman, Walker et al. 2004; Bradford, Simunek et al. 2006) suggest that the phenomenon could be the result of reversible attachment of bacteria cells in secondary energy minima (Figure 2.8).

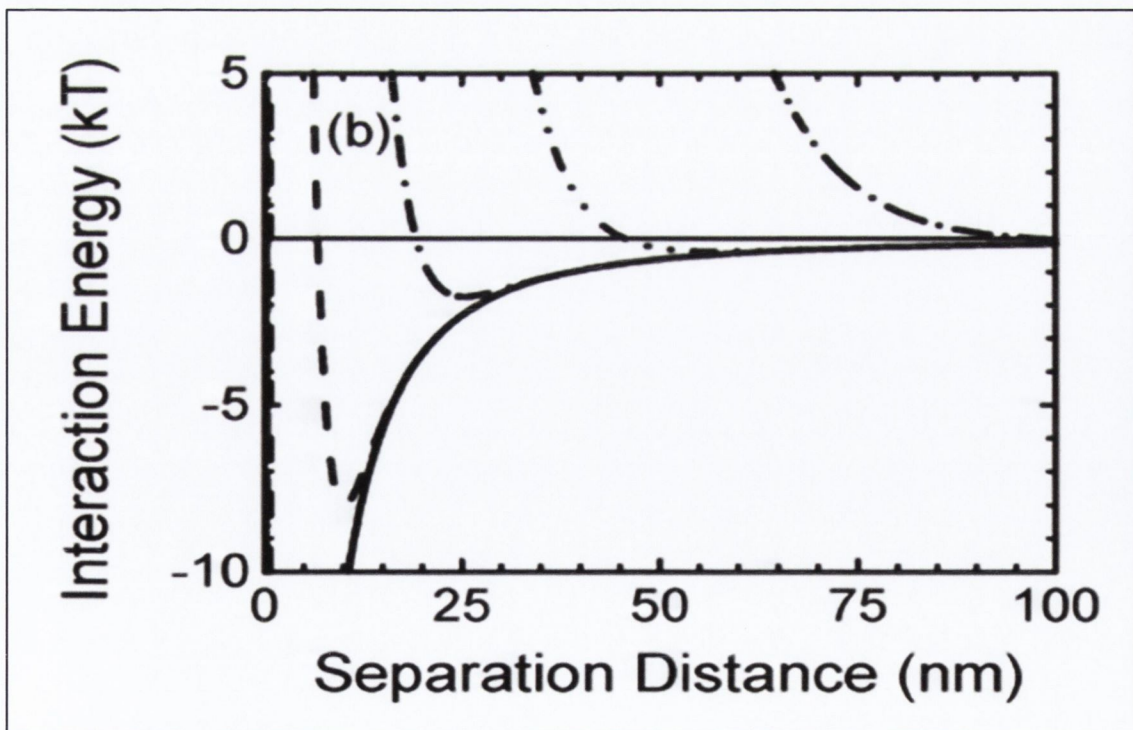


**Figure 2.8** Data from Figure 2.7 replotted to highlight the secondary energy minimum (Redman, Walker et al. 2004).



## 4.2 GROWTH OF *S. PASTEURII* AND BIOFILM FORMATION

In oligotrophic treatments, cell-bound urease has shown to remain active for over five days even though the bacteria cells are likely to become starved following the initial bioaugmentation (Whiffin, van Paassen et al. 2007; van Paassen, Ghose et al. 2010). Interestingly, the urea hydrolysis mechanism of *S. pasteurii* appears to be connected with the production of ATP (Jahns 1996), which would likely increase the endurance of the bacterium when low concentrations of nutrients are available. However, Cuthbert et al. (2012) have shown that the overall urease activity of *S. pasteurii* biofilms decreases in the absence of nutrients due to the encapsulation of bacteria cells within the newly formed carbonate crystals. The reduction of urease activity observed by Cuthbert et al. (2012) in oligotrophic conditions would therefore imply, from a biological perspective, the establishment of “no-growth” conditions (stationary phase). That is: in treatments where no nutrients are added during the cementation process, no new cells of *S. pasteurii* would be formed to replace those lost by encapsulation and cell lysis. Conversely, an eutrophic cementation solution would provide, albeit not in ideal conditions, the necessary nutrients for the growth of an urease active biofilm (Banfield and Nealson 1997; Cuthbert, Riley et al. 2012).

In practice, oligotrophic protocols would require the initial introduction of excess urease to complete the reaction whereas eutrophic methods can rely on the creation of new biomass to counter the depletion of urease. In fact, Al Qabany et al. (2012) employing eutrophic methods indicate that their experiments were not affected by the initial urease activity of the bacterial culture being injected; this despite introducing variably active cultures with measured urease activities in the range of 5 to 20 mM urea h<sup>-1</sup>. Furthermore, differences between the methods would be expected in the distribution of *S. pasteurii* (and the consequent calcium carbonate precipitation patterns) at the pore scale.

The conceptual model proposed by DeJong et al. (2010) was developed from the observation of samples treated eutrophically. Hence, the model could be specifically resulting from the formation of an active biofilm around the individual cells deposited during the augmentation exercise. Should this be the case, the mechanisms leading to the formation of a bond (and its failure) could be distinct from those occurring in oligotrophic treatments: with consequences on the resulting efficacy.

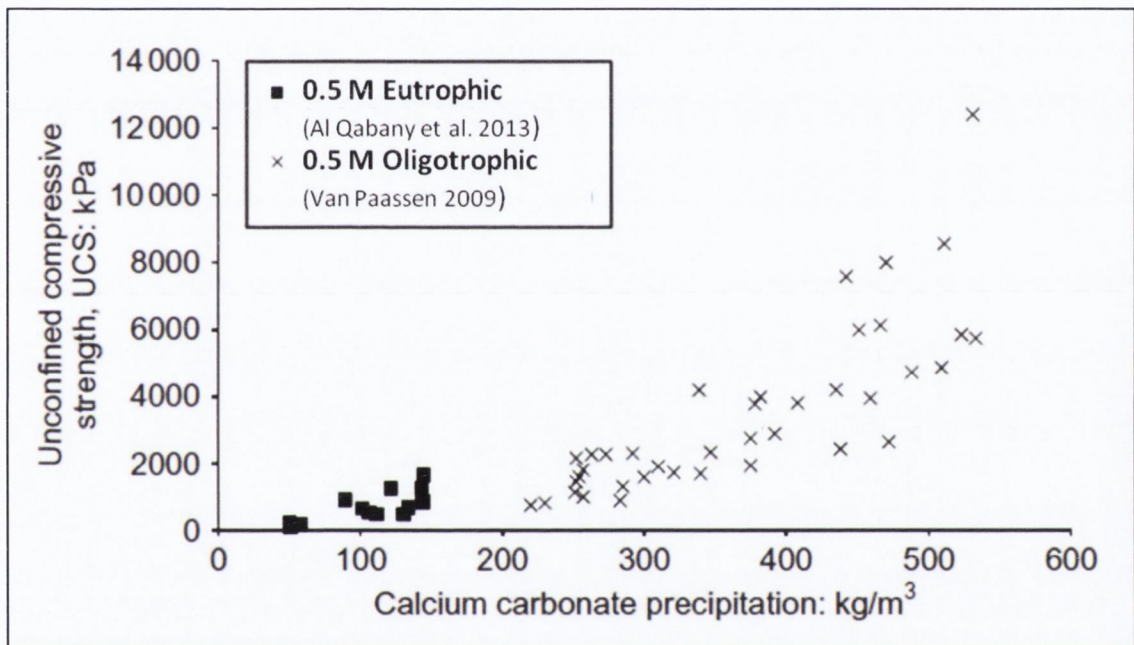


**Figure 2.9** Unconfined compressive strength plotted against calcium carbonate content in MICP soil treatment (Al Qabany and Soga 2013), modified to include the treatment protocol employed by different authors. Eutrophic protocols appear to require less calcium carbonate for a given increase in UCS when compared to oligotrophic protocols.

The hypothesis would be supported by the comparative analysis of unconfined compressive strength (UCS) values for samples treated with oligotrophic and eutrophic protocols. Figure 2.9 shows that approximately 140 Kg m<sup>-3</sup> were sufficient to obtain a UCS of c. 1500 kPa when employing eutrophic protocols. However, up to 260 Kg m<sup>-3</sup> were needed to achieve similar UCS values with oligotrophic methods employing the same concentration of process reagents in the

cementation solution (0.5 M). Additionally, while a large number of samples tested produced no measurable strength due to inhomogeneous cementation (Al Qabany and Soga 2013), a similar difference can also be inferred by referring to 1 M treatments in Figure 2.11 below.

## **5) REAGENT CONCENTRATION IN THE CEMENTATION LIQUID**

As shown in Eqs. 2.1 and 2.2, one mole of urea and calcium ions, respectively, are required to produce one mole of calcium carbonate. Consequently, the cementation solution is usually characterised by approximately equimolar concentrations of these reagents independent of the protocol employed. Interestingly, different equimolar concentrations of reagents have been employed in the literature and evidence exists that these have an impact on the resulting properties of the treated material. The literature on the subject is still scarce but the effects on permeability and UCS have been investigated specifically (Al Qabany, Soga et al. 2012; Al Qabany and Soga 2013).

### 5.1 EFFECT OF REAGENT CONCENTRATIONS ON UCS

Al Quabany et al. (2013) have shown that a relationship exists between the concentration of the chemical reagents and the resulting UCS. Figures 2.10 and 2.11 show the UCS of samples treated using different reagent concentrations for eutrophically treated samples. Despite some scatter, it is possible to observe that higher UCS values are obtained, for a given calcium carbonate content, when mildly concentrated (< 250 mM) solutions are employed. Conversely, treatments employing more concentrated solutions (> 0.5 M) present higher UCS/[CaCO<sub>3</sub>] ratios (referred to as effectiveness). 1 M solutions represent a limit case in that the treatment resulted in inhomogeneous localised reinforcement producing weak overall samples. Patchiness of

the cementation in these samples would be associated with the occurrence of localised rapid reduction of permeability as discussed in the next paragraphs (Al Qabany and Soga 2013).

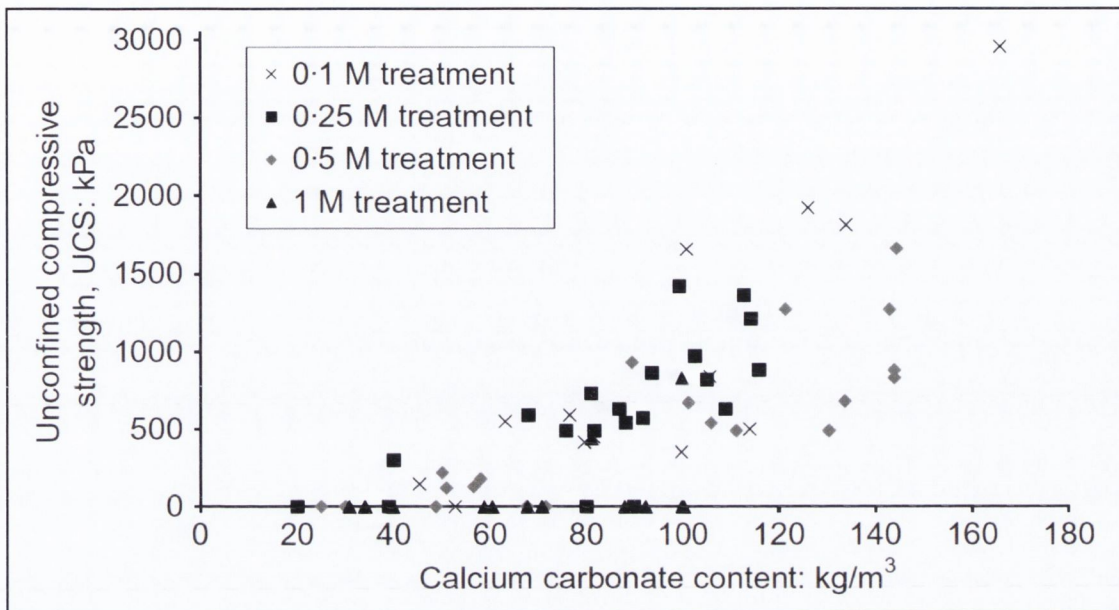


**Figure 2.10** UCS plotted against calcium carbonate precipitation for different eutrophic treatments (Al Qabany and Soga 2013). Mildly concentrated solutions are more effective than concentrated solutions.

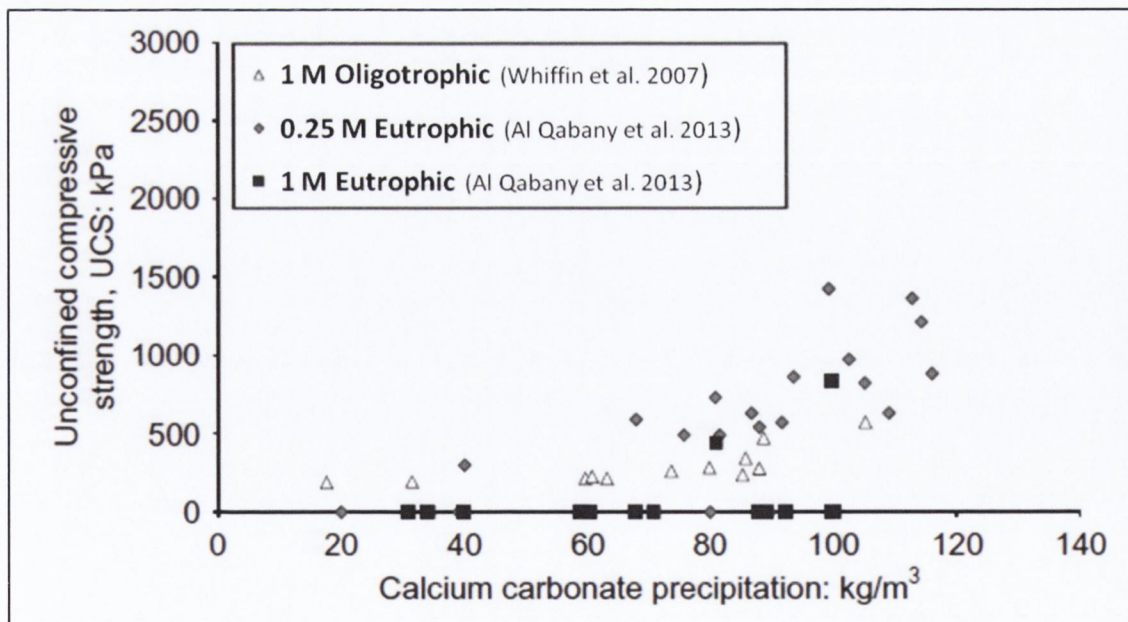


**Figure 2.11** Compressive strength plotted against calcium carbonate content in MICP soil treatment (Al Qabany and Soga 2013), modified to include the treatment protocol employed by different authors. (Values reported for Whiffin et al. (2007) were obtained at a confining pressure of 50 kPa).

## 5.2 EFFECT OF REAGENT CONCENTRATIONS ON PERMEABILITY

Figure 2.12 shows the decrease of normalised permeability (ratio between the actual permeability and the initial permeability) with increasing amounts of precipitated calcium carbonate in experiments conducted employing eutrophic protocols. The authors of the research conclude that the injection of highly concentrated ( $> 500$  mM) solutions results in a rapid decrease of permeability when compared with mildly concentrated ( $< 250$  mM) solutions (Al Qabany and Soga 2013).

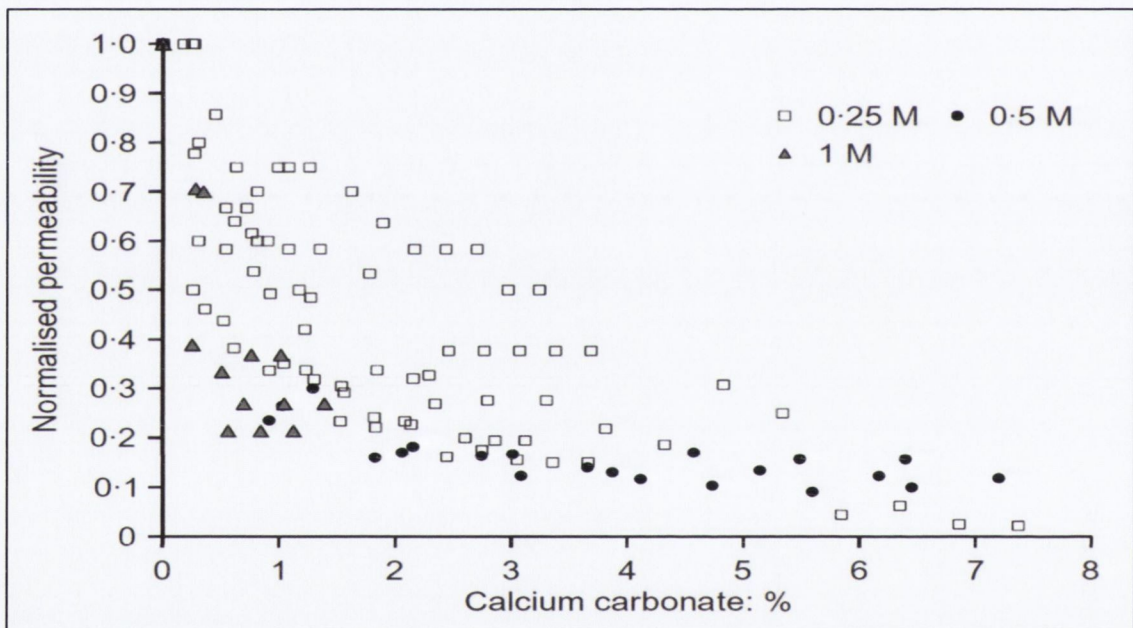


**Figure 2.12** Normalised permeability versus calcium carbonate precipitation for three reagent concentrations (Al Qabany and Soga 2013). Increasing the concentration of reagents in the cementation liquid results in the rapid reduction of permeability.

## 5.3 PORE SCALE CONCEPTUAL MODEL

According to Al Qabany et al. (2013), the effect of reagent concentration on both permeability and UCS could be explained by referring to previously published observations based on scanning

electron microscope images (Al Qabany, Soga et al. 2012). In fact, as shown in Figure 2.13, the images show that when mildly concentrated (250 mM) solutions are employed the resulting calcium carbonate is precipitated in small crystals over large portions of the sand particle (Figure 2.13(a)); whereas high concentrations (1 M) produced large individual structures, typically near inter-particle contact points (Figure 2.13(b)). Al Qabany et al. (2013) suggest that the rapid permeability reduction observed with 1M solutions is caused by the formation of these large crystals within the pore throats. Conversely, the numerous small crystals formed when mild solutions are employed result in a homogenous reduction of the permeability with increasing amounts of calcium carbonate.

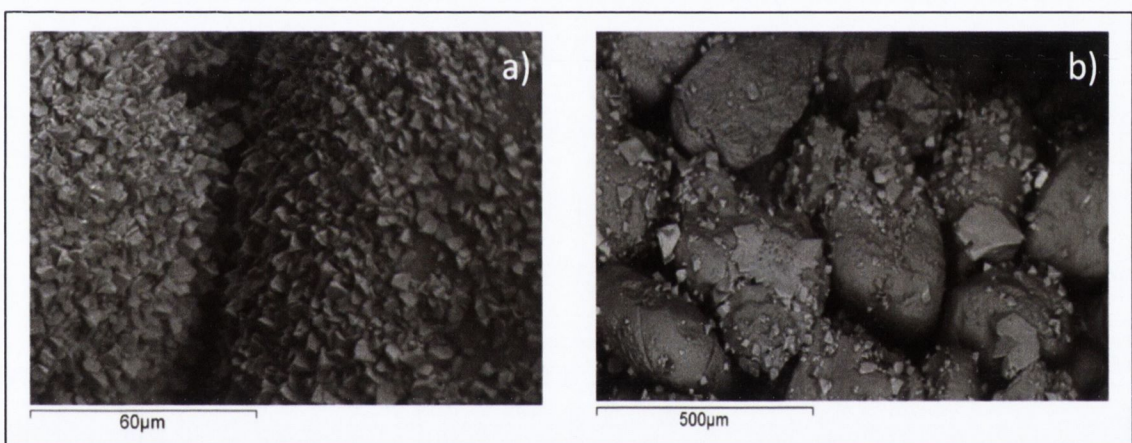


**Figure 2.13** SEM image of eutrophically treated biogrout samples employing: **(a)** 250 mM urea and  $\text{Ca}^{2+}$  solution which precipitated  $80 \text{ Kg m}^{-3}$  of  $\text{CaCO}_3$ ; **(b)** 1 M urea and  $\text{Ca}^{2+}$  solution which precipitated  $65 \text{ Kg m}^{-3}$  of  $\text{CaCO}_3$  (Al Qabany, Soga et al. 2012). Small crystals are formed when mild solutions are employed **(a)** whereas larger crystals are produced by concentrated treatments **(b)**.

While debatable, the reasoning proposed by the authors to explain the different precipitation patterns shown in the SEM images provides a very good starting point for understanding the precipitation phenomena that affect the distribution of calcium carbonate at the pore scale. These are central to the research being carried out and therefore will be discussed in further detail here. Two concurrent mechanisms are proposed (Al Qabany, Soga et al. 2012):

**1) Higher urea concentrations would cause a higher and localised pH increase. This would promote the formation of thicker/larger precipitates.**

This seems an unlikely occurrence. In fact, despite the bioaugmentation, the available urease enzyme is likely to become saturated even at very low urea concentrations (refer to Chapter 3 paragraph 2.1): implying that the circumcellular pH variations remain comparable despite the higher urea concentrations. It should be noted that the cultures employed during bioaugmentation displayed a urease activity of 5 to 20 mM h<sup>-1</sup>. Speculatively, an alternative explanation could be provided by the larger number of treatment rounds delivered when employing 250 mM solutions. To achieve comparable amounts of precipitated calcium carbonate, four times as many treatment rounds would be required when compared with 1 M treatments; albeit with shorter retention times. The authors assume that the distribution of bacteria is comparable between different treatments; however, in this case, four times as many nutrients (in the form of added nutrient broth) would have been delivered with a relatively rapid turnover: better supporting the formation of a biofilm. Hence, increasing the number and spreading of cells (nucleation sites) as well as the amount of urease activity contained in the soil. The precipitation process is further complicated by the polymorphic nature of calcium carbonate minerals (refer to Chapter 3 paragraph 1.1). In fact, increased urease activity has been shown to reduce the size of the crystals and, in extreme cases, promote the formation of metastable intermediates (van Paassen 2009).

**2) The high supersaturation resulting from concentrated solutions would privilege crystal growth over nucleation.**

Supersaturation alone would not appear to explain the phenomenon (refer to Chapter 3 paragraph 1.1). In fact, in the absence of poisons or additives and in sterile conditions, elevated supersaturation

is expected to favour nucleation over growth (Meldrum and Cölfen 2008; van Paassen 2009). Additionally, the results reported by Al Qabany et al. (2012) would appear to contradict those reported by Cuthbert et al. (2012), which showed that higher reagent concentrations produce smaller crystals during MICP (Table 2.3).

**Table 2.3** Average crystal size formed over *S. pasteurii* biofilms by MICP using variably concentrated reagents (Cuthbert, Riley et al. 2012). Increasing the concentration of reagents had the effect of reducing the average crystal size.

<b>Samp. ID</b>	<b>Nutrients*</b> (Biofilm formation)	<b>Reagents**</b> (Urea and CaCl <sub>2</sub> )	<b>Average</b> (Crystal size)	<b>St. Dev.</b> (Crystal size)
L6	0.13 g/l (NB) 33 mM (Urea)	6 mM	100.5 μm	55.3 μm
H6	13 g/l (NB) 330 mM (Urea)	6 mM	55.7 μm	13.6 μm
L200	0.13 g/l (NB) 33 mM (Urea)	200 mM	214.4 μm	116.0 μm
H200	13 g/l (NB) 330 mM (Urea)	200 mM	18.0 μm	5.0 μm
L500	0.13 g/l (NB) 33 mM (Urea)	500 mM	42.7 μm	13.4 μm
H500	13 g/l (NB) 330 mM (Urea)	500 mM	8.4 μm	2.4 μm

\* NB = Nutrient Broth

\*\* Reagents were applied in fresh solutions without the addition of nutrients.

This highlights how the introduction of a biological component in engineering processes requires to extend the interpretation beyond chemical-physical considerations. Biofilm development appears to be a key element in the process. In fact, Cuthbert et al. (2012) report that, in identically treated samples, larger crystals are deposited when *S. pasteurii* produced a biofilm under low nutrient conditions (Table 2.3). In this case, stressed cultures would be expected to display lower urease activities which would in turn lead to higher [Ca<sup>2+</sup>]/[CO<sub>3</sub><sup>2-</sup>] ratios during



the steady state of the reaction. Interestingly, the results presented by Han et al. (2006) in abiotic precipitation conditions show that, provided supersaturation is achieved, calcite is preferentially precipitated (over less stable vaterite) at high  $[Ca^{2+}]/[CO_3^{2-}]$  ratios. Speculatively, in Al Qabany et al. (2012) experiments the low concentration of reagents could have led, assisted by the abundance of nutrients, to the widespread precipitation of vaterite, which would then have transitioned (Oswald's ripening) into small calcite crystals. Conversely, 1M treatments would have produced the relatively rapid nucleation of calcite crystals which, combined with the slower bacterial growth, resulted in large isolated crystals.

## **6) DELIVERY METHODS AND PROCEDURES**

One of the key features of biogrouting is that treatment can be employed for *in-situ* applications. As such, the delivery techniques employed have been developed by borrowing from the remediation industry (Suthersan 1997). In fact, the experimental literature has mostly focussed on flow-through column tests; while field scale piloting and pioneering full-scale tests have employed arrays of injection and extraction wells as would be typical of bioaugmentation set-ups (Whiffin, van Paassen et al. 2007; Filet, Gadret et al. 2011). Mixing techniques have occasionally been employed for the bioaugmentation step at laboratory scale, albeit not systematically (Al Qabany and Soga 2013). However, *in-situ* mixing techniques would be a least preferable option in the field due to: cost, site disruption and biological stress implications (van Paassen 2009; Dejong, Soga et al. 2013).

While most of the literature has focussed on the application of biogrout in fully saturated soils, treatment of unsaturated soils has been largely disregarded. Cheng et al. (2012) propose a methodology for the treatment of unsaturated soils by percolating alternate volumes of bacterial suspension and concentrated (1 M), oligotrophic cementation

solution. The surface percolation method proposed (Figure 2.14) resulted in a successful treatment for some of the regimes tested. However, a major limitation in the treatment of unsaturated soils would be represented by the relatively high permeability of the soils typically being treated. In fact, significant percolation losses have been observed by Cheng et al. (2012), where urease activity losses of up to 60 % occurred in the treatment by percolation of unsaturated columns. This is a well known issue in irrigation practices where coarse sands are generally not recommended for surface flood irrigation (Heibloem, Prins et al. 1990).

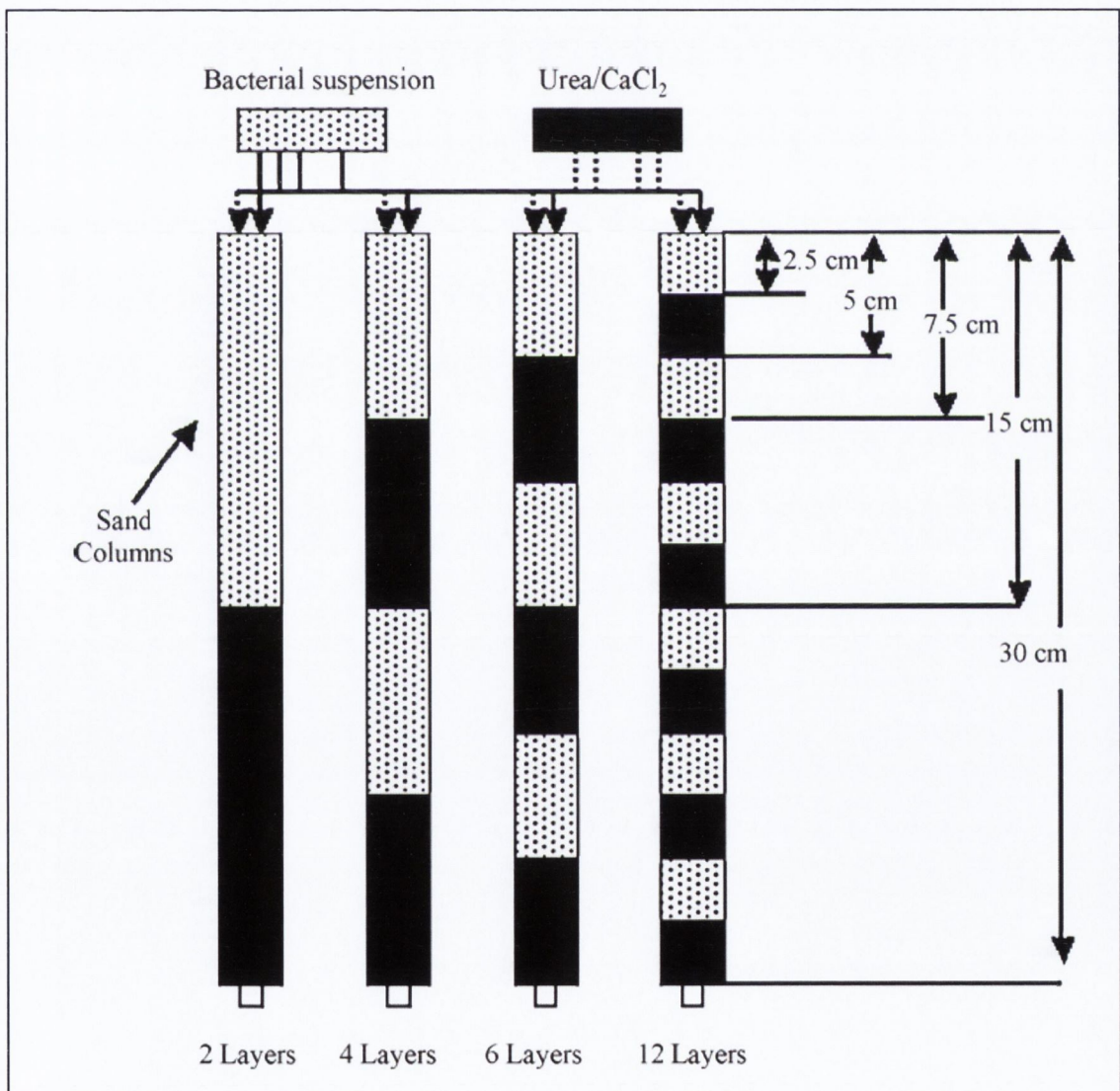


**Figure 2.14** Diagram of the treatment regimes employed in surface percolation biogROUT tests. Each "layer" alternatively represents a volume of *S. pasteurii* suspension and of the 1M, oligotrophic cementation solution (Cheng and Cord-Ruwisch 2012).

## 6.1 MACRO SCALE EFFECTS OF DELIVERY METHODS

Figure 2.15 shows the set-up and results, in terms of calcium carbonate precipitated, of a 100 m<sup>3</sup> oligotrophic pilot test (Whiffin, van Paassen et al. 2007; van Paassen 2009; van Paassen, Ghose et al. 2010). In the pilot test the flow direction and intensity was kept constant by means of continued pumping as a way of simulating the groundwater flow in an aquifer (saturated).

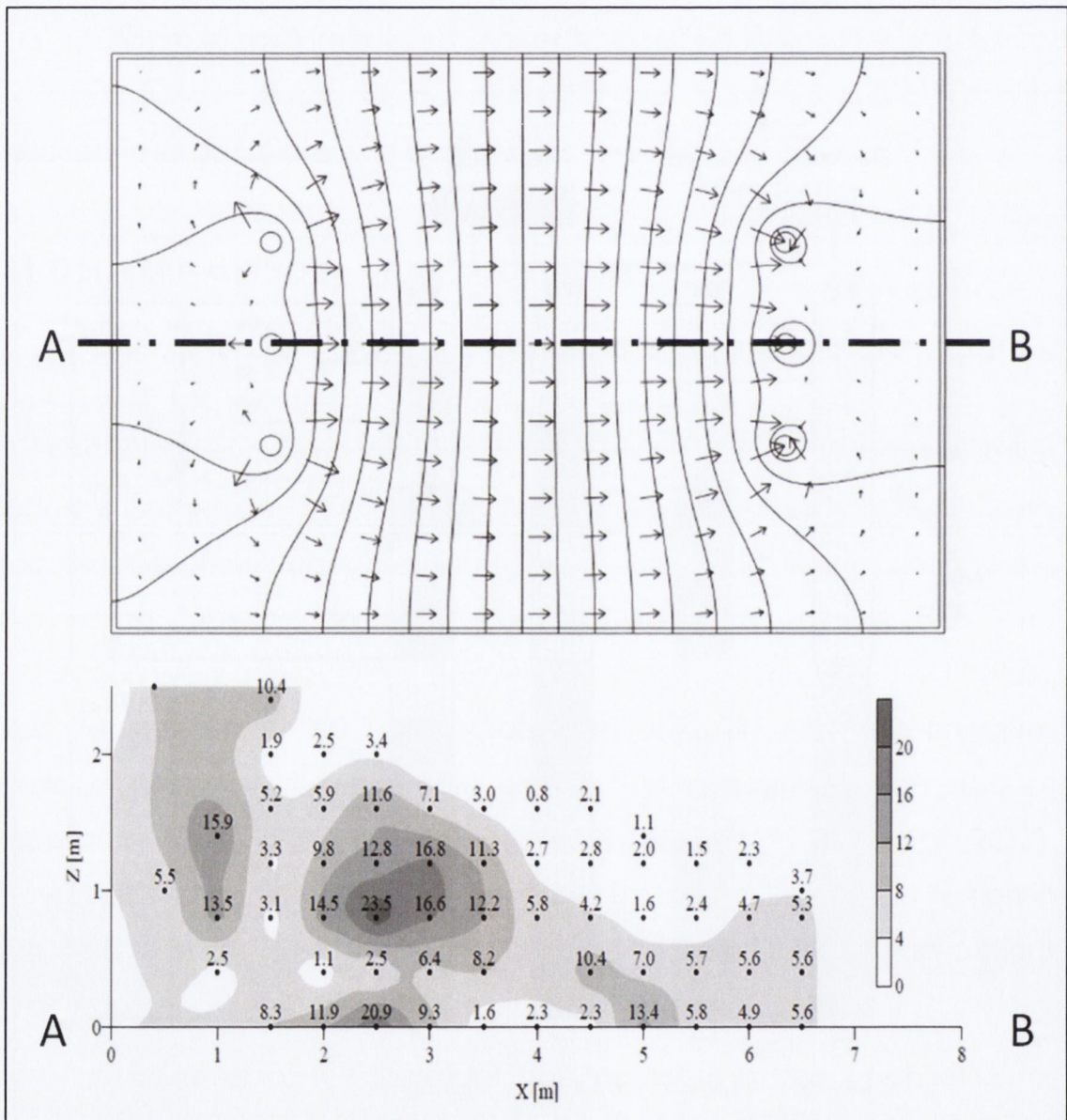


**Figure 2.15** Percentage of CaCO<sub>3</sub> (w/w) along the cross section of a 100m<sup>3</sup> biogROUT experiment. The circles indicate the locations of the injection well (left) and the extraction well (right). A continuous gradient was maintained with water during curing of the cement (van Paassen, Ghose et al. 2010).

The resulting uneven distribution of calcium carbonate within the soil mass is a consequence of several macro scale factors, namely:

- **Transport and retainment of bacteria** affecting the homogeneity of the urease distribution (previously discussed in this Chapter), and in turn of carbonate distribution (Harkes, van Paassen et al. 2010);
- **Dilution with *in-situ* groundwater** has shown to create treatment gradients along the three axis of the mass (van Paassen 2009);
- **Depletion of urea and calcium ions in solution** has shown to result in a limited availability of reagents further along the flow direction (van Paassen 2009; Barkouki, Martinez et al. 2011).

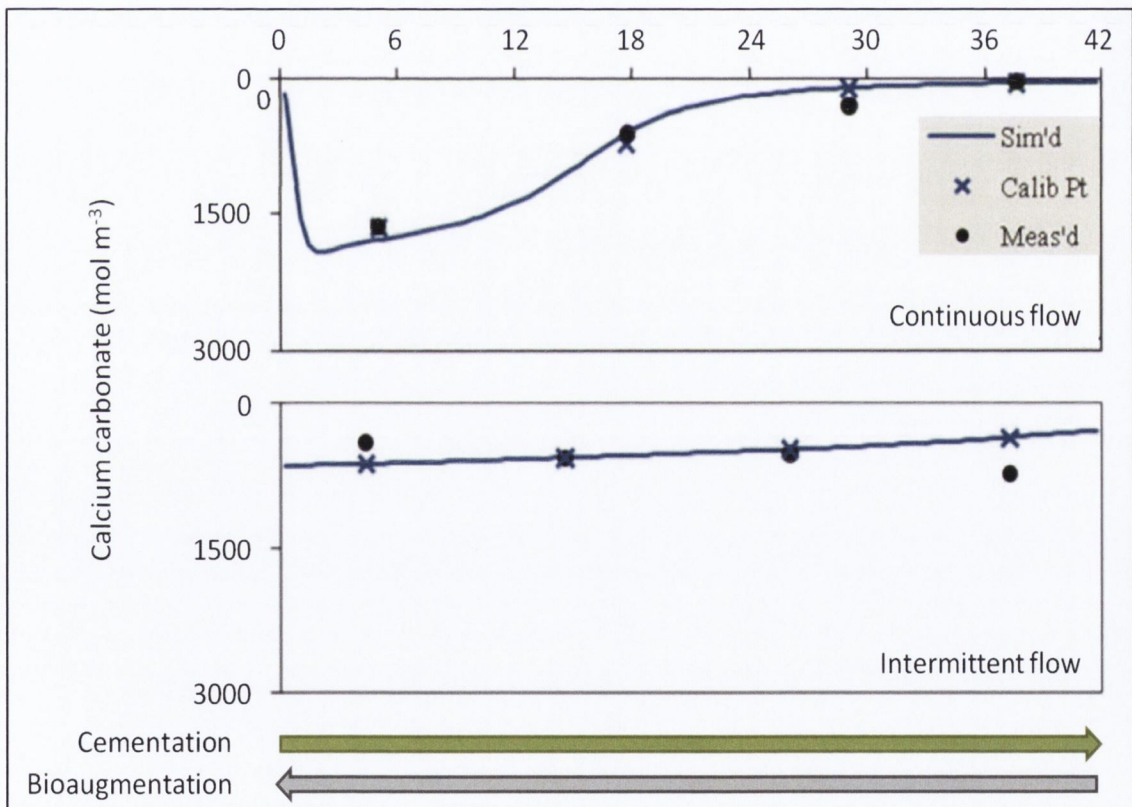


**Figure 2.16** Calcium carbonate profiles in a 1D experiment employing continuous flow and intermittent flow injection protocols. The cementation solution and bacterial suspension were injected in opposite directions. Results of a proposed computational model simulation are also shown, blue line (Barkouki, Martinez et al. 2011).

While dilution with groundwater cannot be avoided, it would be possible to mitigate the effect of bacteria distribution and reagent depletion. In fact, to improve the homogeneity of large scale treatments, Barkouki et al. (2011) have tested two alternative injection protocols in 0.5 m columns. Both injection protocols proposed by Barkouki et al. (2011) involved injecting the cementation solution with a flow direction opposite that of the bioaugmentation injection. The distribution would be more even as higher concentrations of reagents would be first exposed to areas with lesser deposited biomass. Additionally, one of the columns was treated using an intermittent pattern of short, high flow injections. The results are reported in Figure 2.16 and provide a very strong argument for the use of intermittent inverse flows as a way to improve homogeneity.

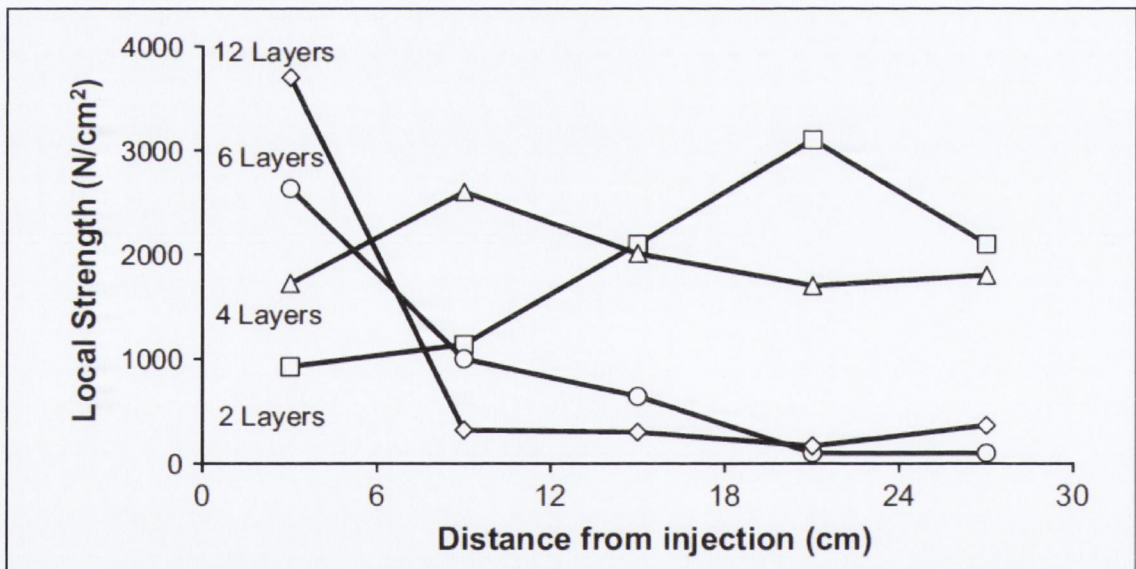


**Figure 2.17** Strength profiles (pocket penetrometer) of 30 cm sand samples treated using different regimes of surface percolation (Cheng and Cord-Ruwisch 2012). Layers are defined in Figure 2.14.

As previously mentioned, Cheng et al. (2012) have investigated the treatment of unsaturated soil employing surface percolation delivery methods. The results reported in Figure 2.17 show that in two layer treatments, the strength increase is mostly concentrated towards the lower part of the column where larger amounts of *S. pasteurii* and

reagents accumulate due to gravity. Instead, when six and twelve layers are employed, the rapid alternation of small volumes causes the bacteria and cementation fluid to react close to the surface very soon in the treatment: resulting in the formation of an almost impervious crust at the top of the column. The crust limits the penetration of the reagents and the reaction remains confined to within the top centimetres of the column. An ideal situation would be the result obtained employing a four layer treatment regime, where the treatment produced a relatively homogeneous distribution in terms of soil strength. Most interestingly, this does not imply a homogeneous distribution of calcium carbonate as will be discussed in more detail in Paragraph 6.2 below.

## 6.2 PORE SCALE EFFECTS OF DELIVERY METHODS

The pore scale conceptual models discussed so far have all been developed on the basis of tests conducted employing eutrophic reagents injected in fully saturated soils. Despite the differences highlighted above in this document, eutrophic and oligotrophic methods have shown a similar direct relationship between the amount of calcium carbonate and UCS of treated samples. However, Cheng et al. (2012) have observed a deviation from this behaviour in unsaturated soils treated by surface percolation with oligotrophic protocols. Figure 2.18 shows, comparatively, the results obtained by Cheng et al. (2012) in a 1 m unsaturated column treated using oligotrophic surface percolation, and in a 1 m saturated column using an oligotrophic injection protocol. In the figure, "local strength" is measured with a calibrated pocket penetrometer on 3 cm samples and correlated to the calcium carbonate content.

Despite the different (in absolute terms) strength values measured due to the method employed, the results of the saturated column are generally comparable to those presented by others in the literature. However, there does not appear to be a correlation between

precipitated calcium carbonate and strength in the unsaturated sample. In fact, the local strength remains constant, at about 20 MPa, whereas calcium carbonate increases with depth from c. 20 Kg m<sup>-3</sup> to c. 100 Kg m<sup>-3</sup>.

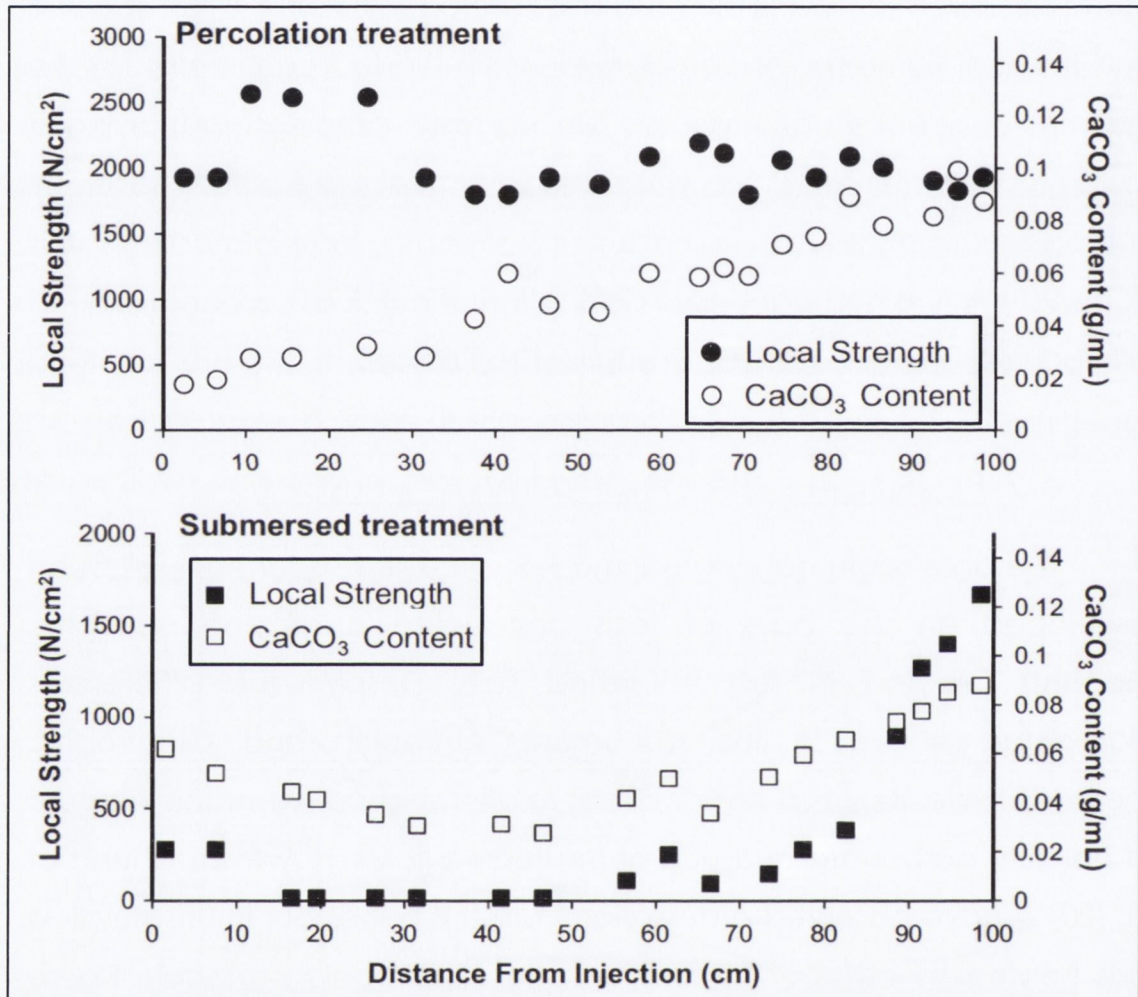


**Figure 2.18** Strength (pocket penetrometer) and precipitated calcium carbonate content obtained treating: (above) unsaturated soils by percolation and (below) saturated soils by injection. Oligotrophic protocols were employed in both columns (Cheng and Cord-Ruwisch 2012).

The observed lack of correlation is explained by the authors by considering the hydraulic regime that might ensue in the unsaturated sample during treatment (Cheng and Cord-Ruwisch 2012). By referring to Figure 2.19, it is possible to appreciate how, during the reaction period, the top of the column would become characterised by a pendular regime in which small volumes of reagents are retained near

inter-particle contact points or in the pore throats. According to the authors, smaller amounts of calcium carbonate would therefore be precipitated here but in areas of the pore network ideally located to produce a strength increase: forming bonds between particles. The transition from pendular regime to capillary fringe determines the volume of reagents retained in the column's section; and in turn, the amount of carbonate being precipitated. At the bottom of the column, relatively large volumes of reagents would be available, resulting in a larger amount of calcium carbonate potentially precipitated. However, this would be precipitated over a larger surface (wet surface) of the sand particle: without necessarily contributing to the soil's cementation.

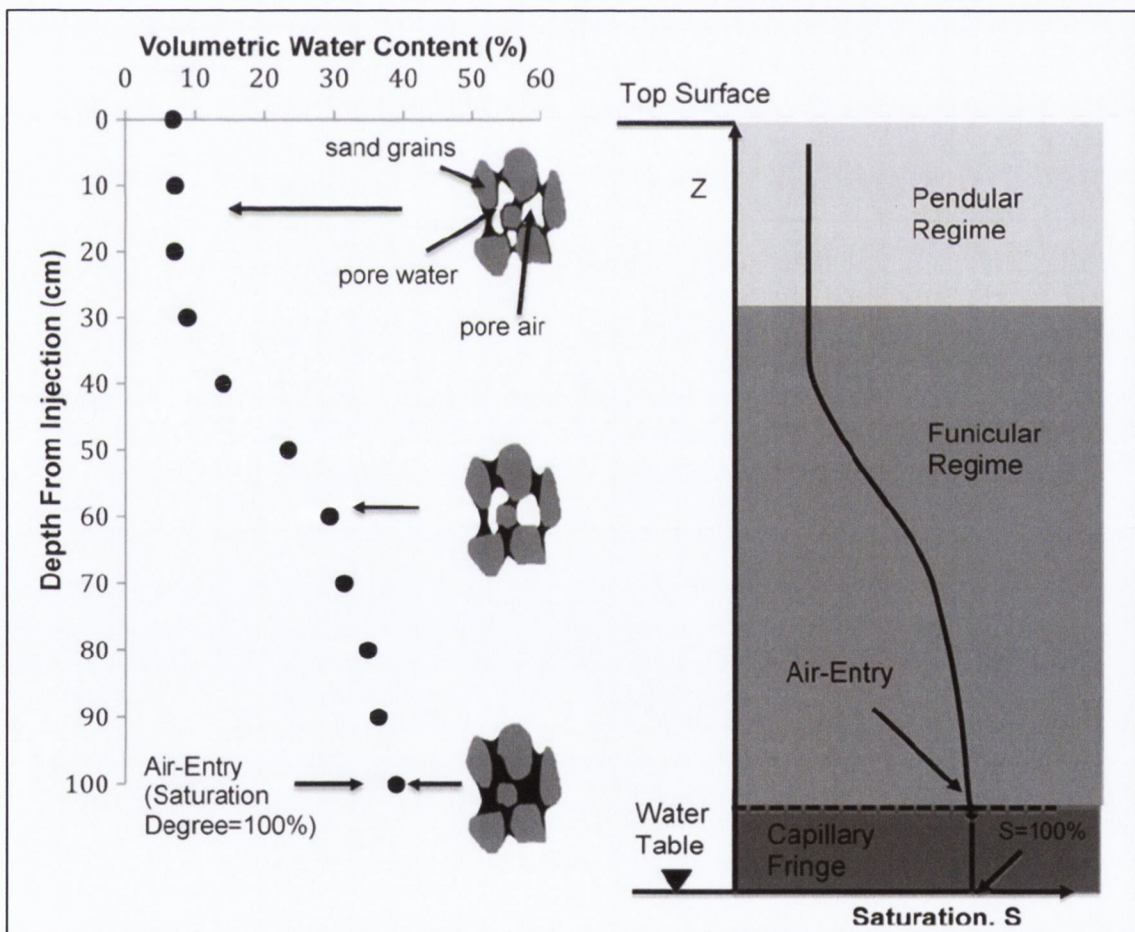


**Figure 2.19 (left)** Profile of volumetric water content in a 1 m sand column under surface percolation (unsaturated) conditions (porosity 37.7%) and **(right)** conceptual illustration of saturation in the unsaturated soil zone and water regime of the unsaturated soil zone (Cheng and Cord-Ruwisch 2012).



The results and interpretation presented by Cheng et al. (2012) are very interesting in that: despite a potentially low efficiency (up to 60% percolation losses) when compared to injection delivery methods (Harkes, van Paassen et al. 2010; Al Qabany, Soga et al. 2012), the ensuing of a pendular or funicular regime could actually result in higher efficacy of the treatment (in terms of UCS/[CaCO<sub>3</sub>] ratios).

## **7) SOIL MINERALOGY**

In the interest of repeatability, most of the published research work to date has been conducted employing standardised silica sand as a test soil matrix. Therefore, the literature regarding the effect of soil mineralogy on the MICP process is scarce (Whiffin 2004; van Paassen 2009). However, soil mineralogy is known to impact on the transport of bacteria (Scholl, Mills et al. 1990; Foppen and Schijven 2005) as well as potentially affecting the heterogeneous nucleation of calcium carbonate (Lioliou, Paraskeva et al. 2007). As shown in Figure 2.20, carbonaceous sand particles present a higher surface heterogeneity when compared to silica particles.

The rough micromorphology of carbonaceous particles is a key element in promoting the attachment of bacteria cells to the surface of the particle. Scholl et al. (1990) suggest that limestone particles would provide a larger area for the attachment of the bacteria and shielding from shear forces (drag). Additionally, morphological and chemical heterogeneities are known to impact on the energy interactions between colloidal particles and surfaces (Bhattacharjee, Ko et al. 1998; Shellenberger and Logan 2002). In fact, Bhattacharjee et al. (1998) have demonstrated that the interaction energies are substantially reduced even in the presence of asperities which are very small compared to the particle radius. Furthermore, Foppen et al. (2005) have shown that the addition of as small an amount as 5% w/w of calcite grains can significantly increase the retention of *E. coli* in a quartz sand column due

to the increased Zero Point of Charge pH,  $pH_{zpc}$ , of the soil matrix (Banfield and Nealson 1997).

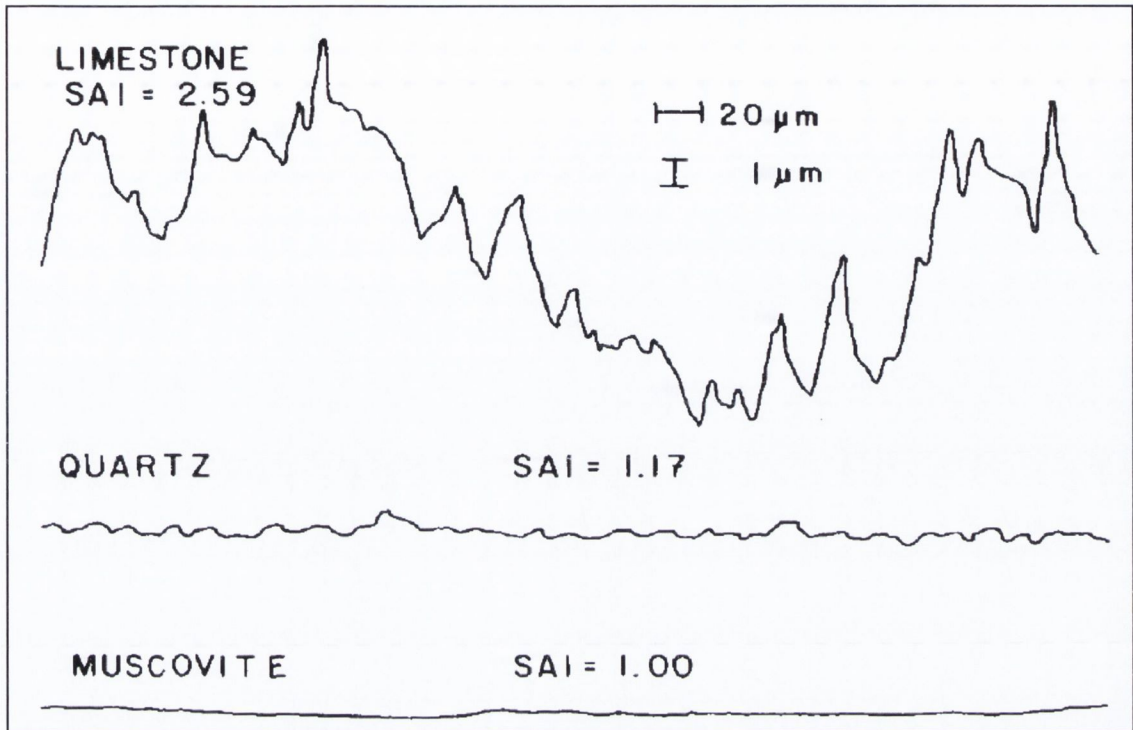


**Figure 2.20** Examples of sections of surface profiles of limestone, quartz and muscovite chips used in the experiments of Scholl et al. (1990). Surface area index (SAI) values are reported for each mineral species.

Noticeably, the increased affinity of bacteria to the matrix's carbonate surfaces would promote a homogeneous distribution of cells over the particle's surface, reducing the relative number of cells strained at inter-particle contact points. In addition to an increased retention of bacteria, Lioliou et al. (2007) have shown that the seeding of supersaturated solutions with calcite promotes the precipitation of calcium carbonate; whereas the addition of quartz seeds is unable to initiate the nucleation and precipitation process.

When treating carbonaceous sands, the combination of these effects would possibly result in calcium carbonate precipitates forming homogeneously over the whole soil particle. In fact, this phenomenon was already identified by Van Paassen (2009) in oligotrophic treatments employing 500 mM cementation solutions. In his work, Van Paassen

shows that, similarly treated silica and carbonaceous sand, respectively, produce isolated groups of mineral precipitates, and a homogeneous coating of carbonate crystals. The interpretation he provided was mostly focussed on the carbonate polymorph being precipitated. However, the occurrence of such a homogeneous precipitation would have consequences on the resulting bulk properties. When generally compared to silica sand treatment, the large deposition area typical of carbonaceous sands would result in higher efficiencies (actual/potential  $\text{CaCO}_3$  precipitation ratio) but lower efficacies (in terms of strength increase). In fact, only a small portion of the carbonate precipitated would be actually forming bonds between particles, while most of the crystals are formed on free surfaces exposed to the pore liquid. Additionally, the permeability in carbonaceous sands would be progressively reduced as described by Al Qabany et al. (2013) for mildly concentrated cementation solutions.

## **8) VALUE OF A REVISED CONCEPTUAL BOND/FAILURE MODEL**

At the time of writing it is found that a limited number of computational models have been developed for MICP soil improvement applications (Barkouki, Martinez et al. 2011; van Wijngaarden, Vermolen et al. 2013). While these models provide a sound starting point, the review of the literature shows that, in the field, the variability of ground conditions could introduce significant errors. A main limitation is represented by the assumption that the distribution of biomass is independent of the soils mineralogy. Additionally, it is also assumed that the active biomass remains quantitatively stable once the bioaugmentation is completed. However, the literature suggests that this is unlikely as competing phenomena, such as growth and encapsulation, occur during the cementation phase. Most crucially, the computational models developed so far have focussed on predicting the amount of calcium carbonate precipitated, then assuming a

correlation with the engineering parameters of the treated soil. However, the experience of Cheng et al. (2012) with unsaturated soils treated by surface percolation, as well as the comparison between eutrophic and oligotrophic effectiveness (Paragraph 4.2), suggests that this assumption could be fallacious. Phenomena taking place at the pore scale have, in fact, shown to be relevant when considering the resulting bulk properties of the treated material. Despite having provided an insight on the parameters that might be involved in the bond formation process, the conceptual models proposed by DeJong et al. (2009; 2010) and Al Qabany et al. (2012; 2013) would be characterised by a narrow field of validity. A revised conceptual model would therefore have to account for an increased number of variables in order to provide a solid base to the development of improved computational models.

## **9) OPPORTUNITIES FOR INNOVATION**

### **9.1 ATOMISED DELIVERY OF MICP PROCESS LIQUIDS**

In the field of soil remediation technology, a pioneering example of large scale application of aerosol delivery methods is provided by the Liner® system (Dyer, Marnette et al. 2006). The system was employed to deliver atomised nutrient solutions for the anaerobic degradation of chlorinated solvents in a contaminated aquifer. The use of atomised liquids was employed as a way of improving the distribution homogeneity of the treatment reagents. Similarly, US Patent N. 2010/0307754 describes a process for the treatment of chlorinated solvents in the vadose zone employing nebulised liquids (Riha, Murdoch et al. 2010). Nebulisers have also been employed in experimental bioremediation work (Glew 2009). By taking cue from the similarities that exist between the structure of a human lung and that of granular soils,

Glew (2009) proposes the use of medical jet nebulisers for the atomisation of process reagents at a laboratory scale.

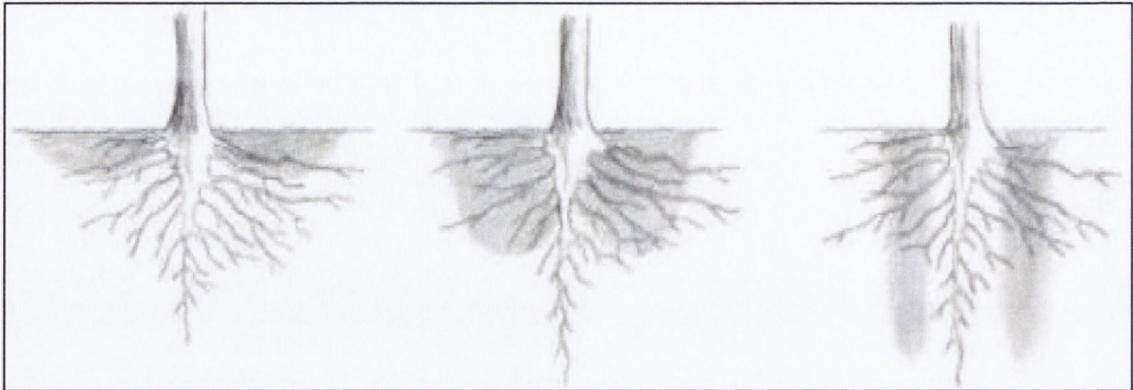


**Figure 2.21** Schematic representation of drip irrigation wetting patterns in: **(left)** clay soils, **(centre)** sandy loam and **(right)** sand. In sandy soils, percolation can lead to significant amounts of reagents being transported beyond the treatment area by gravity.

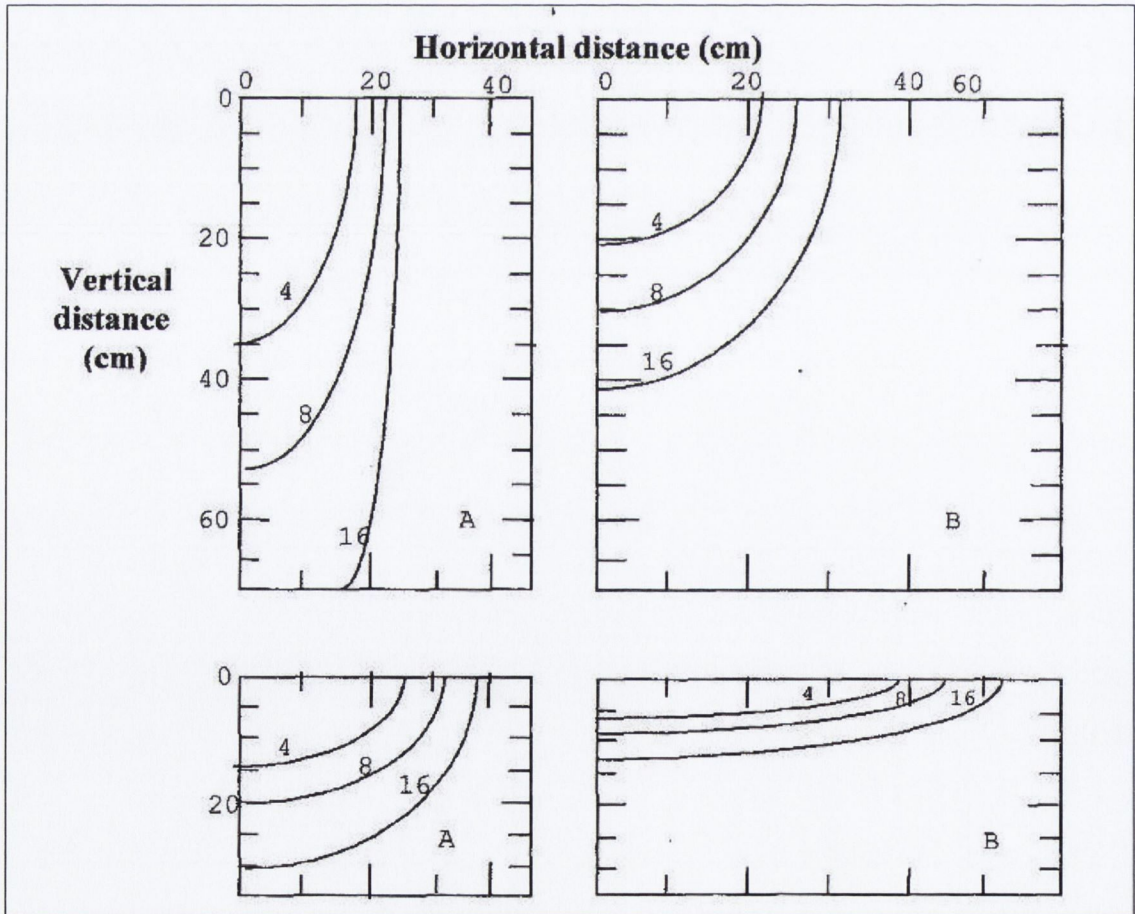


**Figure 2.22** Water distribution from point source emitters in sandy soils (above) and loam soils (below) at 4 l/h (A) and 20 l/h (B) flow rates. Profiles are drawn after 4l, 8l and 16l (Bressler 1977).

Atomised delivery of process reagents has been shown to be a viable, albeit emerging, technique and it is deemed to offer several possible advantages to the application of MICP soil improvement in unsaturated soils. Figures 2.21 and 2.22 illustrate how the horizontal distribution of the injected biogROUT liquids, characterised by a viscosity similar to that of water, would be negatively affected by the relatively high permeability of granular soils: resulting in heavy percolation losses as observed by Cheng et al. (Cheng and Cord-Ruwisch 2012). Above all, atomised delivery could increase the treatment efficiency and efficacy of unsaturated soils by reducing the percolation losses observed in surface percolation delivery (Cheng and Cord-Ruwisch 2012). Additionally, when the atomised droplets are deposited in granular soils these tend to form water menisci between soil particles (Dyer, Glew et al. 2012; Lourenço, Gallipoli et al. 2012). This could result in pore scale cementation patterns similar to those observed by Cheng et al. (2012) in pendular hydraulic regimes; and hence, lead to highly effective treatment in unsaturated soils.

## 9.2 DOLOMITE AS AN ALTERNATIVE CEMENTATION AGENT

The reactivity of calcium carbonate with acid solutions is a well known phenomenon. In natural subsurface environments, acidic conditions can ensue as a result of numerous factors, such as: dissolved carbonic acid, decomposing organic matter or an acidic soil matrix. Whereas acid rain as well as other aggressive substances can be formed in urban environments. This generates concerns for the long term performance of MICP treatments in both semi-natural and anthropogenic environments. An opportunity for improvement would be provided by the substitution of the calcium carbonate minerals employed as cementing agents with dolomite which is less susceptible to acid attack.

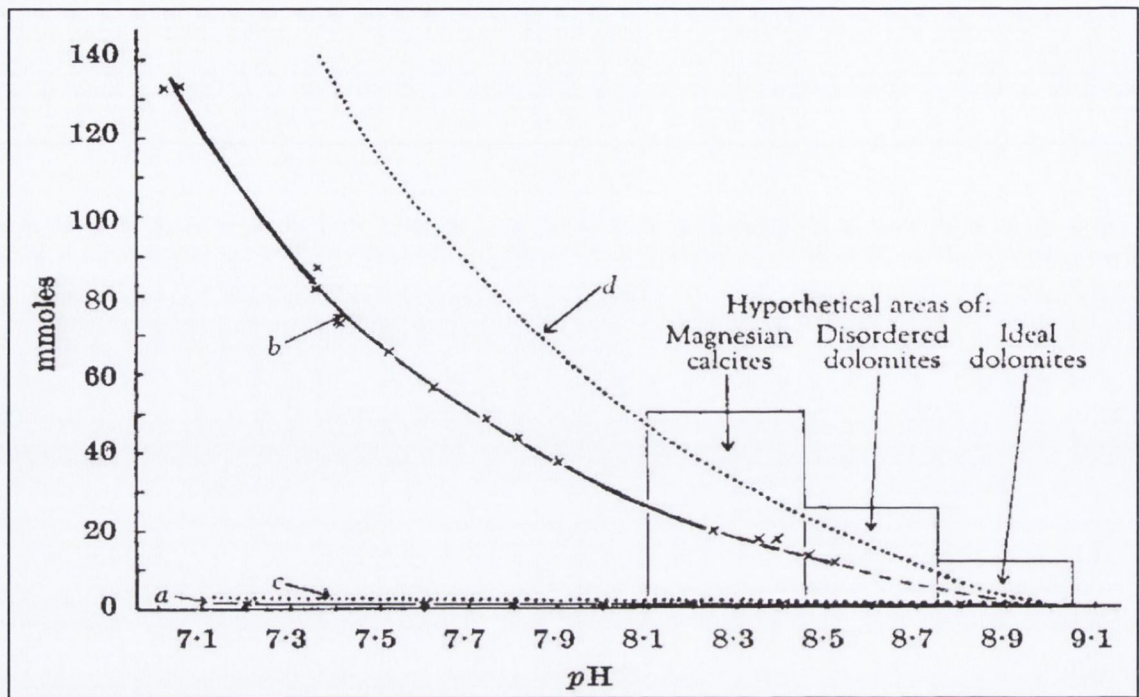


**Figure 2.23** Solubilities of calcium carbonate (**a**) and magnesium carbonate (**b**) in normal sea water at 25 °C and hypothetical solubilities of calcium carbonate (**c**) and magnesium carbonate (**d**) in hypersaline water as function of pH (Liebermann 1967).

Dolomite is a double salt mineral ( $\text{CaCO}_3 \cdot \text{MgCO}_3$ ) mostly encountered as the result of late diagenetic processes within a carbonate rock (secondary dolomite). Dolomitisation can involve the substitution of  $\text{Ca}^{2+}$  ions in the crystal matrix with  $\text{Mg}^{2+}$  ions or more complicated multiphase processes controlled by temperature and other factors (Di Cuia, Riva et al. 2011). While calcium carbonates are directly precipitated in various low-temperature diagenetic environments (McConnaughey and Whelan 1997; Castanier, Le Métayer-Level et al. 1999; Dupraz and Visscher 2005), literature shows that unassisted low-temperature precipitation of primary dolomite is generally a very limited phenomenon (Land 1998; Long, Ma et al. 2011). This is mostly due to kinetic limitations favouring the precipitation of calcium carbonate over that of dolomite (Liebermann 1967; Deelman 1999). As shown in Figure 2.23, the relative solubility of the constituents of a double (or multiple) salt should be equal or nearly equal at the moment of co-precipitation.

At those conditions encountered in most depositional environments this would require, for dolomite to precipitate, relatively high  $Mg^{2+}/Ca^{2+}$  ratios (Liebermann 1967; Vasconcelos and McKenzie 1997). However, literature suggests that, at low salinity (Folk and Land 1975) and high pH conditions (Liebermann 1967), dolomite would be able to nucleate at  $Mg^{2+}/Ca^{2+}$  ratios approaching unity.

In an attempt to precipitate primary dolomite *sensu stricto*, Deelman (1999) reports his repetition of one of Liebermann's experiments. Interestingly, his experiment included the addition of urea to Liebermann's experiment and found that it favoured the nucleation of dolomite. Since Deelman's experiments, several other authors report successful low-temperature precipitation of primary dolomite in natural bio-mediated settings (van Lith, Warthmann et al. 2003; Mastandrea, Perri et al. 2006) as well as in controlled, urease positive (Table 2.4) experiments on solid substrates (Sánchez-Román, Vasconcelos et al. 2008; Sánchez-Román, McKenzie et al. 2009).

**Table 2.4** Microbial species successfully employed in primary dolomite precipitation experiments by Sánchez-Roman et al. (2008; 2009).

<b>Microorganism</b>	<b>Aerobic</b>	<b>Urease</b>	<b>Source</b>
<i>Virgibacillus marismortui</i> (AJ009793)	YES	YES	(De Vos, Garrity et al. 2009)
<i>Halomonas meridiana</i> (ACAM 246 / UQM 3342)	YES	YES	(James, Dobson et al. 1990)



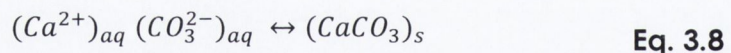
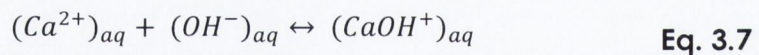
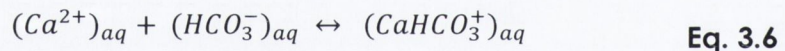
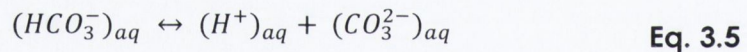
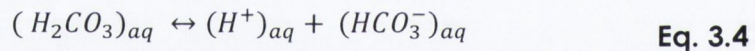
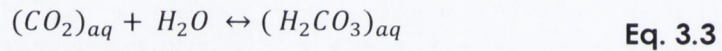
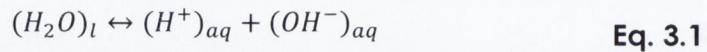
## CHAPTER 3

# THEORETICAL BACKGROUND

---

### 1) SOLUBILITY AND PRECIPITATION OF CALCIUM CARBONATE

The main geochemical reactions controlling the precipitation and dissolution of calcium carbonate in water are well known due to the importance that these have in the geochemical cycling of carbon (Zeebe and Wolf-Gladrow 2001):



The thermodynamic state of the precipitation-dissolution reaction of calcium carbonate, Eq. 3.8, is determined by the relative supersaturation:

$$S = \frac{\{Ca^{2+}\}\{CO_3^{2-}\}}{K_{sp}} \quad \text{Eq. 3.9}$$

where  $S$  is the relative supersaturation, the numerator represents the ionic activity product ( $IAP$ ) in the solution and  $K_{sp}$  is the solubility product:

$$\text{at equilibrium} \quad K_{sp} = IAP = \{Ca^{2+}\}\{CO_3^{2-}\} \quad \text{Eq. 3.10}$$

The  $K_{sp}$  of a soluble salt is a measure of its solubility and is a function of the mineral form being considered. A low  $K_{sp}$  corresponds to low solubility minerals. Therefore, when  $S > 1$  the solution is said to be supersaturated and precipitation is favoured. Conversely, when  $S < 1$  the solution is said to be undersaturated and dissolution is favoured.

The activity of a generic ion, A, can be correlated to its concentration [A] as follows:

$$\{A\} = \gamma_A[A] \quad \text{Eq. 3.11}$$

where,  $\gamma_A$  is the activity coefficient and in dilute solutions of simple electrolytes can be considered equal to unity (Zeebe and Wolf-Gladrow 2001). By combining Eq. 3.9 and Eq. 3.11 and assuming a dilute solution the following is obtained:

$$S = \frac{[Ca^{2+}][CO_3^{2-}]}{K_{sp}} \quad \text{Eq. 3.12}$$

As seen in Figure 3.1, calcium carbonate can precipitate in numerous different mineral forms each with a different  $K_{sp}$ ; the different forms of calcium carbonate will be discussed in more detail further in this Chapter.

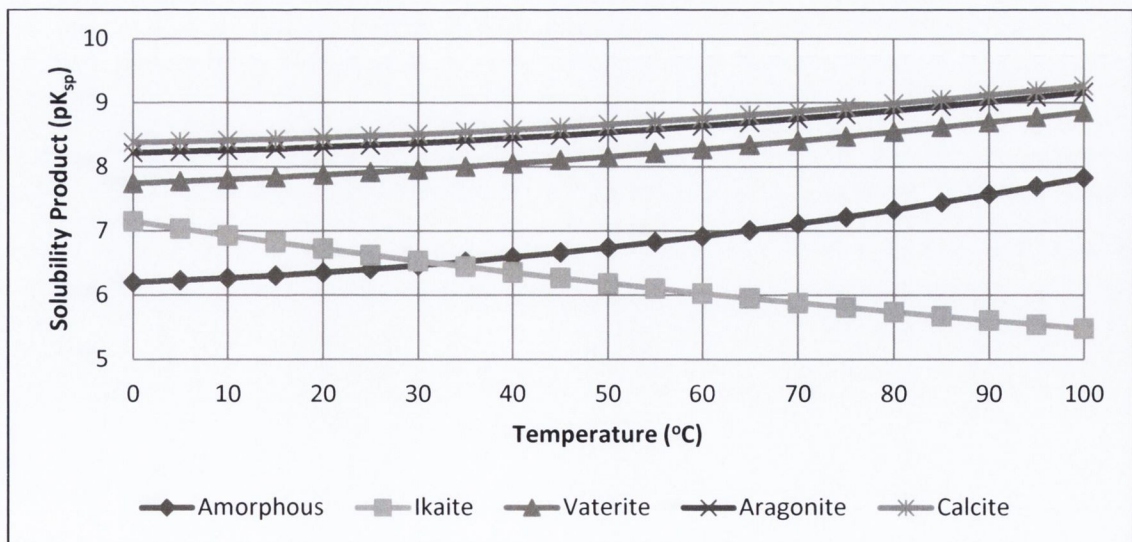


**Figure 3.1** Variation with temperature of the solubility product of calcium carbonate polymorphs (Gal, Bollinger et al. 1996).

As for all salts of weak acids, the solubility product of calcium carbonate is heavily dependent on pH (Figure 3.2) and can be shown to be:

$$K_{sp}^* = \sqrt{K_{sp}' * \frac{[H^+]}{K_a'}} = \sqrt{K_{sp}' * \frac{10^{-pH}}{4.8 * 10^{-11}}} \quad \text{Eq. 3.13}$$

where  $K_{sp}^*$  is the solubility product at the given pH,  $K_{sp}'$  is the solubility product of the species (standard conditions) and  $K_a'$  is the dissociation constant for the bicarbonate ion.

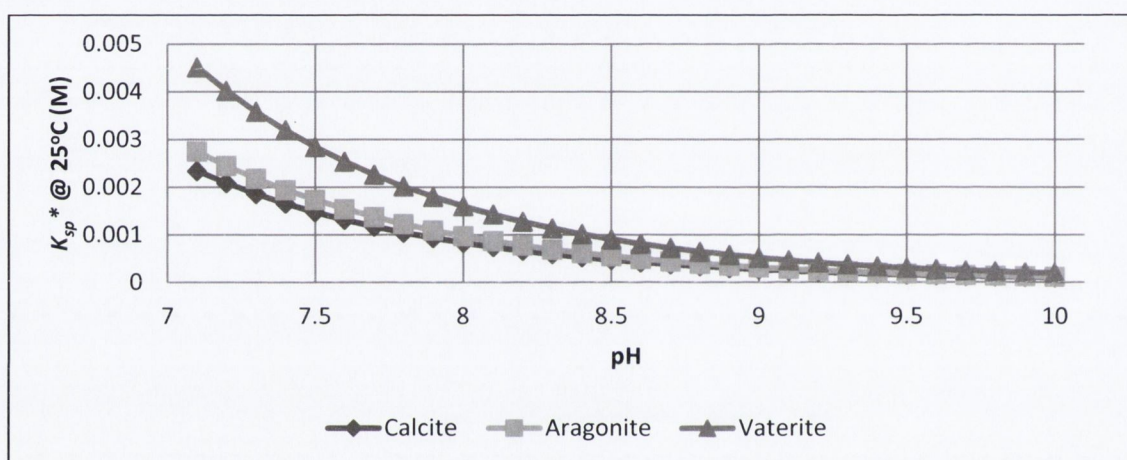
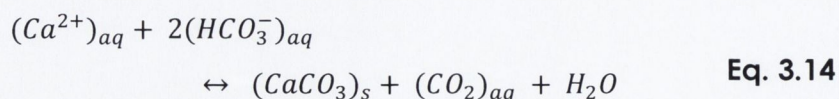


**Figure 3.2** Variation with pH of the solubility of different calcium carbonate polymorphs.

The pH dependency is complicated by the close relationship with the dissolve inorganic carbon (DIC): resulting in a counterintuitive precipitation of calcium carbonate following the sequestration (or degassing) of carbon dioxide from water (Zeebe and Wolf-Gladrow 2001). The phenomena can be understood by rewriting the reaction as follows:



The removal of carbon dioxide will shift the equilibrium to the right, resulting in the precipitation of calcium carbonate. Conversely an increase in carbon dioxide could lead to the dissolution of calcium

carbonate. Abiotic enrichment and degassing of carbon dioxide can play a significant role in shaping cave environments (Short, Baygents et al. 2005).

### 1.1 CRYSTALLISATION AND MINERAL MORPHOLOGY

The driving force behind the formation of a mineral species is the change of chemical potential,  $\Delta\mu$  (Meldrum and Cölfen 2008):

$$\Delta\mu = -kT \ln S \qquad \text{Eq. 3.15}$$

where  $k$  is Boltzmann's constant,  $T$  is the thermodynamic temperature and  $S$  is the super saturation. Once the supersaturation threshold is surpassed ( $S > 1$ ) precipitation can take place. However, for a particle to grow, a nucleus that resists re-dissolution needs to be formed. During homogeneous nucleation, energy is consumed for the formation of new surfaces, posing a thermodynamic barrier to the precipitation process. The barrier is reduced in heterogeneous nucleation by the presence of dispersed components (e.g. crystal seeds or dust particles) that furnish an already formed surface from which to grow (Meldrum and Cölfen 2008). The nature of the dispersed component is also a known factor: Lioliou et al. (2007) have shown that the addition of calcite seeds to a supersaturated solution promotes the precipitation of calcium carbonate, whereas quartz particles had no effect.

While the precipitation of calcite is favoured over other calcium carbonate forms from a thermodynamic point of view, the precipitation of calcium carbonate is complicated by the possibility of less stable but kinetically favoured polymorphs. Figure 3.3 illustrates the mechanisms of thermodynamic and kinetic control that might be established. The theoretical homogeneous nucleation rate of calcium carbonate can be described using an Arrhenius equation for spherical molecular clusters (Mullin 2001):

$$\frac{dN}{dt} = Ae^{-\frac{\Delta G_{crit}}{kT}} \quad \text{Eq. 3.16}$$

where  $A$  is the pre-exponential constant (empirically determined),  $\Delta G_{crit}$  is the energy required to form a stable (critical size) nucleus and  $k$  is Boltzmann's constant. The nucleation rate can therefore be correlated to the supersaturation,  $S$  (Mullin 2001):

$$\frac{dN}{dt} = Ae^{-\frac{16\pi\gamma^3v^2}{3k^3T^3(\ln S)^2}} \quad \text{Eq. 3.17}$$

where  $\gamma$  is the interfacial tension and  $v$  is the number of ions involved in the reaction and is equal to two for calcium carbonate.

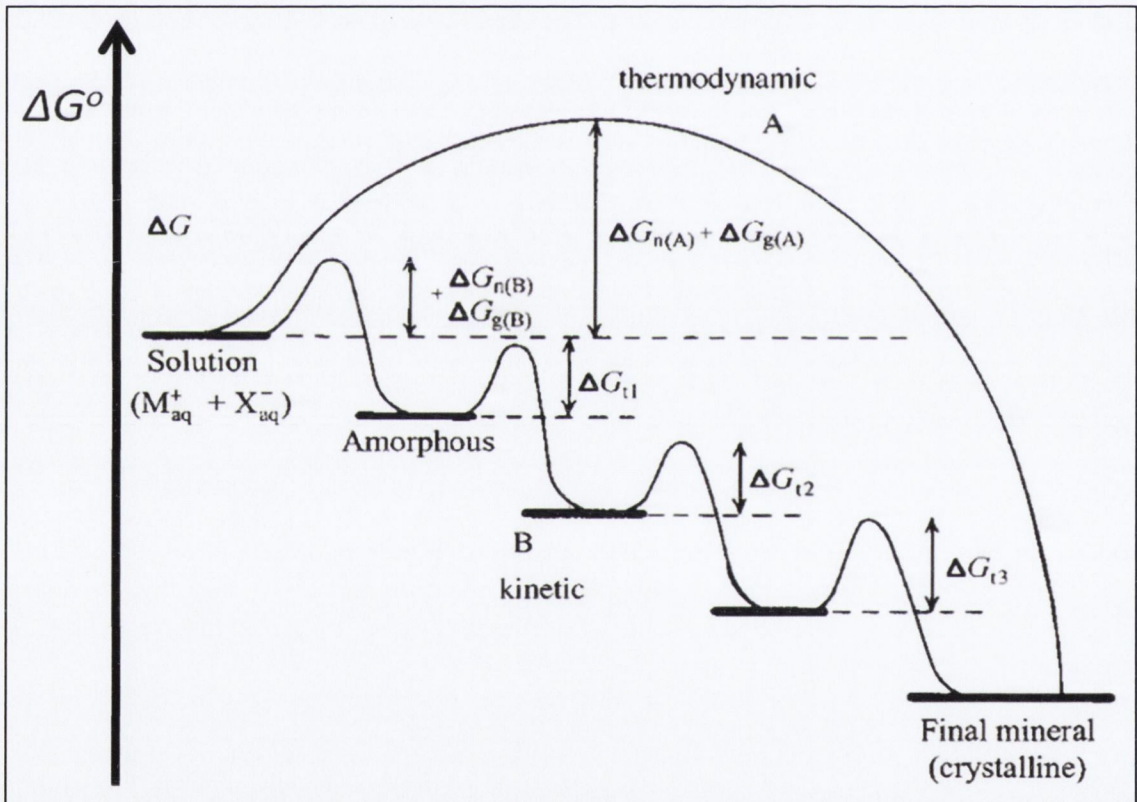


**Figure 3.3** Crystallisation pathways under thermodynamic and kinetic control. Whether a system follows a one-step route to the final mineral phase (pathway A) or proceeds by sequential precipitation (pathway B), depends on the free energy of activation ( $\Delta G_{crit}$ ) associated with nucleation (n), growth (g), and phase transformation (t). Amorphous phases are common under kinetic conditions (Cölfen and Mann 2003).

Once a crystal nucleus is formed, crystal growth is initiated. Assuming carbonate crystals grow spherically with a mononuclear mechanism the growth rate can be described as (Mullin 2001):

$$\frac{dR}{dt} = k_g(S - 1)^2 \quad \text{Eq. 3.18}$$

where  $R$  is the crystal radius,  $S$  the supersaturation of the mineral phase considered and  $k_g$  is the empirical rate constant. As seen in Figure 3.4 at supersaturation of calcite above 7.0 vaterite growth is kinetically favoured over calcite.

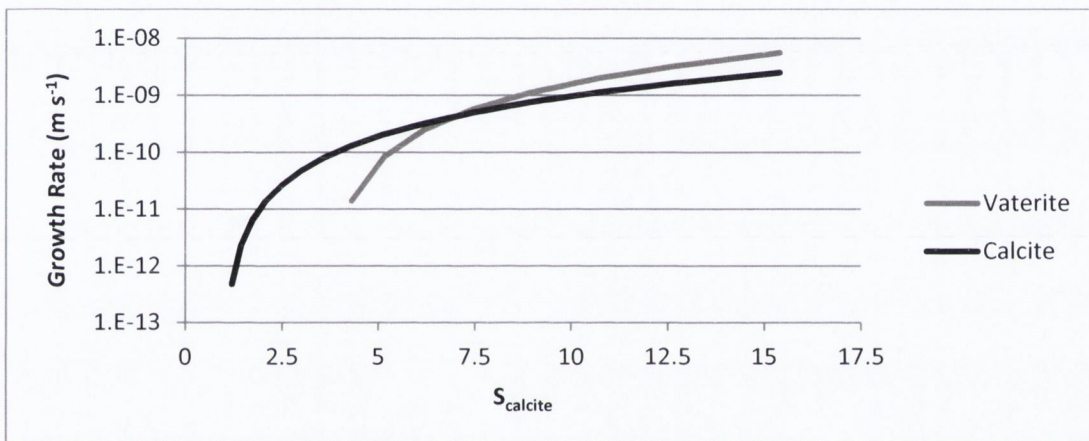


**Figure 3.4** Crystal growth of calcite and vaterite for varying calcite supersaturation (Eq. 3.18).  $pK_{sp}$  for calcite and vaterite are 8.48 and 7.91 respectively. Rate constant,  $k_g$ , for calcite and vaterite are  $1.2 \times 10^{-11} \text{ m s}^{-1}$  and  $5.6 \times 10^{-10} \text{ m s}^{-1}$  respectively. Rate constant values after Kralj et al. (1990; 1994; 1997).

The kinetic cascade of transformations shown in Figure 3.3 (pathway B) exemplifies Oswald's step rule (Threlfall 2003). The rule implies that, following the early formation of the least thermodynamically stable polymorph (but kinetically favoured), the solid phase transitions in steps to form the most stable (i.e. "ripens"). Calcium carbonate, generally adheres to the rule. Typically, a short-lived amorphous or hydrated phase is followed by the formation of vaterite which then transforms into secondary calcite (Kralj, Brečević et al. 1997). It should be noted that aragonite is often missing in the sequence as it is generally

hard to nucleate in the absence of additives (Berner 1975; Loste, Wilson et al. 2003; Meldrum and Cölfen 2008). The transition time from vaterite to calcite has been shown to be inversely proportional to the pH of the starting solution: complete transformation was observed in less than 24 hours at pH 6.9 (Zhou, Yao et al. 2010). While numerous studies on industrial additives and biological molecules have demonstrated the opportunity of controlling the morphology of calcium carbonate precipitates with additives or crystal poisons (Meldrum and Cölfen 2008), several authors have investigated the effect of modifying the carbonate morphology by acting solely on the reaction parameters. In fact, decreasing the starting pH at which the reaction takes place has been shown to result in more ordered crystals (calcite) being precipitated (Han, Hadiko et al. 2006; Zhou, Yao et al. 2010). Whereas, Han et al. (2005) have shown that it is possible to preferentially precipitate vaterite by increasing the flow rate of carbon dioxide in a bubbling precipitation set-up. This observation is expected and consistent with the fact that higher carbonate concentrations result in higher supersaturation and lower pH. When the carbonate content is kept constant however, the same authors have shown that high  $[Ca^{2+}]/[CO_3^{2-}]$  ratios in the reagent solution favour the precipitation of calcite over that of vaterite (Han, Hadiko et al. 2006).

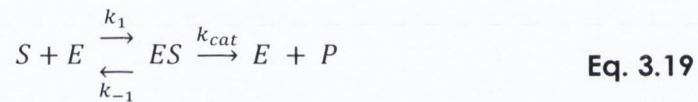
## **2) BIOLOGICAL CATALYSIS OF UREA HYDROLYSIS**

At the conditions normally encountered in the shallow subsoil, urea is a fairly stable compound. The uncatalysed degradation is usually obtained with a slow elimination reaction (Krajewska 2009), which would be unsuitable for ground improvement applications. Probably in response to the abundance of urea and the universal requirement for nitrogen, numerous plant and microbial species have developed a strategy to enzymatically catalyse a hydrolysis reaction and accelerate the degradation of urea (Castanier, Le Métayer-Levrel et al. 1999; Wang,

Köhler et al. 2008; Krajewska 2009). Noticeably, some urease positive microbial species are found associated with human infections of the excretory and digestive tract due to the presence of urea in such systems (Mobley, Island et al. 1995).

## 2.1 ENZYME ACTIVITY AND KINETICS

Enzymes are specialised biological molecules able to reduce the activation energy of selected reactions, hence substantially increasing the rate at which these reactions take place (Chieffi 1994). However, enzyme-catalysed reactions depend on the availability of free active sites on the enzyme to occur and as such are saturable. The catalytic reaction can be described as a two step reaction:



where  $S$  is the substrate (i.e. urea),  $E$  is the enzyme (i.e. urease),  $P$  is the product (or products) and  $k_1$ ,  $k_{-1}$  and  $k_{cat}$  are the rate constants of the reaction. While the enzymatic mechanism can be quite complex, it is useful to model the reaction as a single catalytic step by introducing the apparent unimolecular rate constant,  $k_{cat}$ . The kinetics of an enzyme-catalysed reaction can be described using Michaelis-Menten equation (Li, Qian et al. 2013):

$$v_i = \frac{V_{max}[S]}{K_M + [S]} \quad \text{Eq. 3.20}$$

where  $v_i$  is the reaction rate (assuming irreversible reactions),  $V_{max}$  is the maximum rate reached at saturation of the enzyme,  $[S]$  is the concentration of the substrate and  $K_M$  is Michaelis–Menten constant, describing the affinity of the enzyme for the substrate:

$$K_M = \frac{k_{cat} + k_{-1}}{k_1} \quad \text{Eq. 3.21}$$



$V_{max}$  can be defined as a function of the enzyme's concentration,  $[E]$ :

$$V_{max} = k_{cat}[E] \quad \text{Eq. 3.22}$$

In the context of MICP applications the reported values for  $K_M$  range from 26 mM for cell free extract at pH 7.7 to 200 mM for a cell suspension (van Paassen 2009). For more general reference values, Krajewska (2009) compiled a list of typical activities,  $K_M$  and  $k_{cat}$  of ureases produced by different organisms.

The specific activity of an enzyme is a common way of measuring the catalytic performance of an enzyme and is defined as the amount of substrate the enzyme converts per minute per mg protein in the enzyme preparation. Interestingly, while all ureases display characteristic active sites containing nickel ions (Benini, Rypniewski et al. 1999), not all ureases are identical and those extracted by different species can perform drastically different. It should be noted that when employing live cultures in the context of MICP applications it is useful to define the specific activity on the basis of the suspended biomass ( $OD_{600}$ ) as discussed in Chapter Two.

Enzymes can be inhibited through different mechanisms that can reduce the values of  $V_{max}$  and  $K_M$  (Walsh 2012). A list of known urease inhibitors is presented by Krajewska (2009) and includes: ammonium, urea and its analogues, other organic molecules, boron compounds and various heavy metals. However, inhibition mechanisms can depend on the source and type of urease considered (Bachmeier, Williams et al. 2002). Whiffin (2004) has investigated the impact of pH on the UA and SUA of *S. pasteurii* identifying pH 7 as the optimal pH. Whereas the optimum observed for the free enzyme by Stocks-Fisher et al. (1999) was pH 8.5. In the same study, Whiffin proposes a correlation for the standardisation at pH 7 of measured UAs. While only limited inhibitory effects appear to be caused by high concentration of the ammonium

by-product, concentrations of calcium ions above 1.5 M have shown to significantly reduce the urease activity of *S. pasteurii* (Whiffin 2004). However it is not clear if the inhibitory effect acts upon the enzyme or the more general cellular activities.

### 3) ATOMISED DELIVERY TECHNOLOGY

An aerosol or spray can be defined as “a stable suspension of solid or liquid particles in a gas phase such as air” (Taylor and Gumbleton 2004). Atomisation (or nebulisation) is the transformation of bulk liquid into sprays (and other physical dispersions of small particles) in a gaseous atmosphere (Lefebvre 1989). The dispersed or discrete phase is defined as drops or droplets and the gas is known as the continuous, or carrier, phase. Figure 3.5 illustrates the range of droplet sizes found in nature and in atomised liquids.

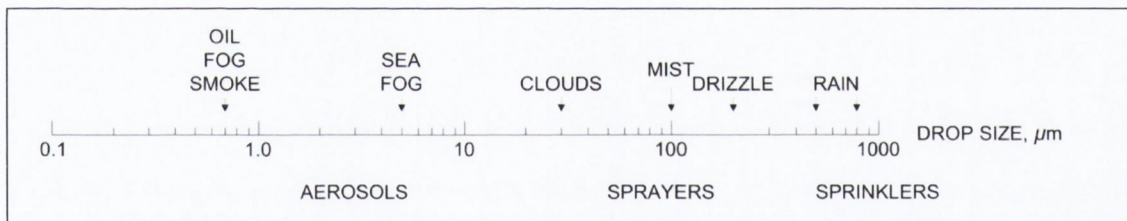


**Figure 3.5** Range of droplet sizes in atomised liquids and natural processes (Lefebvre 1989).

As shown in Figure 3.6, atomisers are generally classified as belonging to one of four groups depending on the type of energy used to initiate the disintegration of the bulk liquid: liquid, gaseous, mechanical and vibration energies. Among these, medical nebulisers are jet nebulisers (gas energy): designed to atomise a wide range of liquid drug solutions for delivery to the lower respiratory tract of the human lung. Commonly used in the treatment of pulmonary conditions, medical jet nebulisers also offer the advantage of being propellant free in that they solely use air (McCallion, Taylor et al. 1996).

The typical design and functioning of a medical jet nebuliser is shown in Figure 3.7. As described by O'Callaghan et al. (1997) air from the compressor passes through a small hole (Venturi). Rapid expansion of air causes a negative pressure which sucks fluid up the feeding tube system where it is atomised. Larger particles impact on the baffle and walls of the chamber and are returned for re-nebulisation. Small aerosol particles are released continuously from the nebuliser chamber.

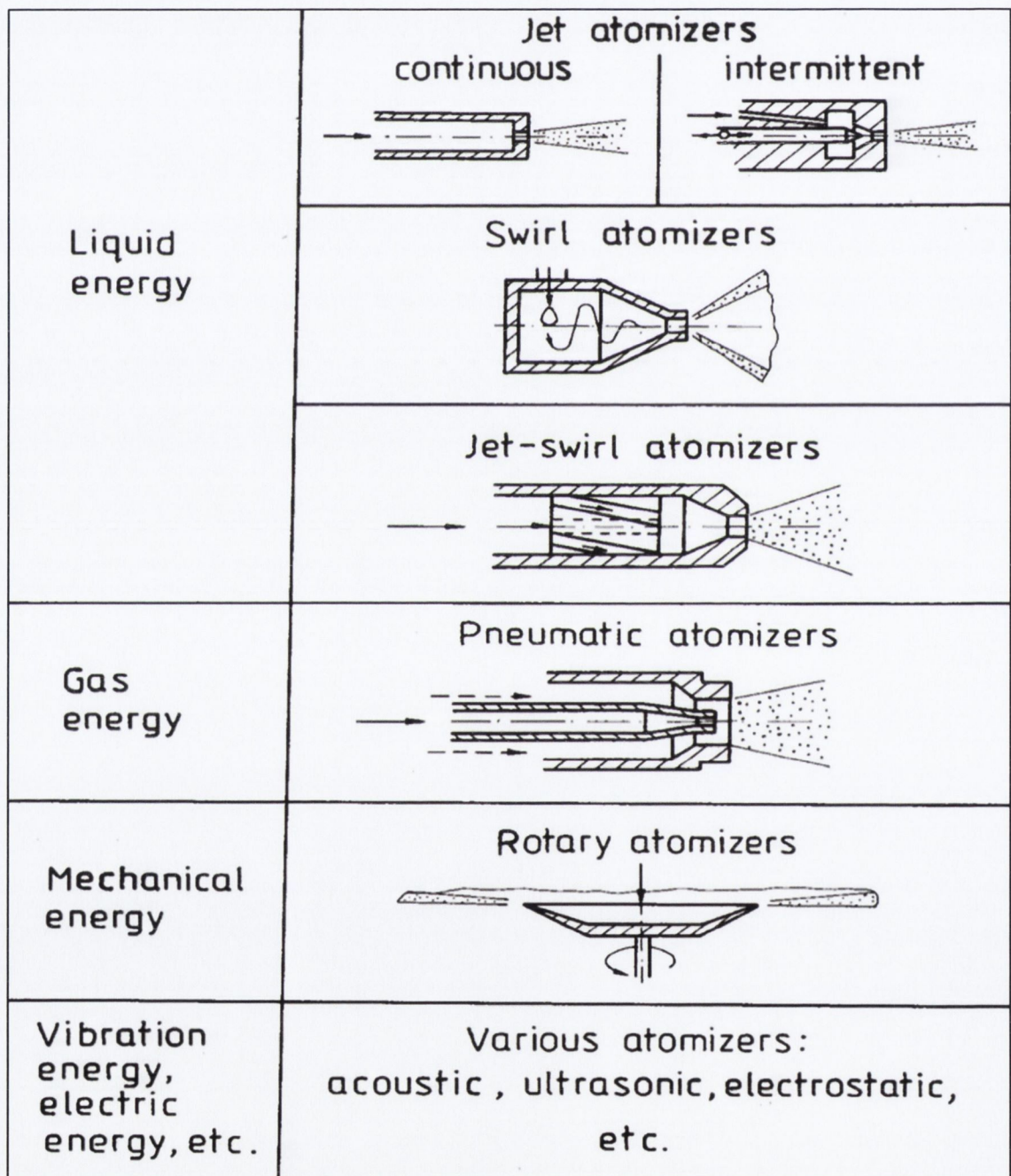


**Figure 3.6** Classification of atomisers based on the source of energy employed for atomisation (Bayvel and Orzechowski 1993).

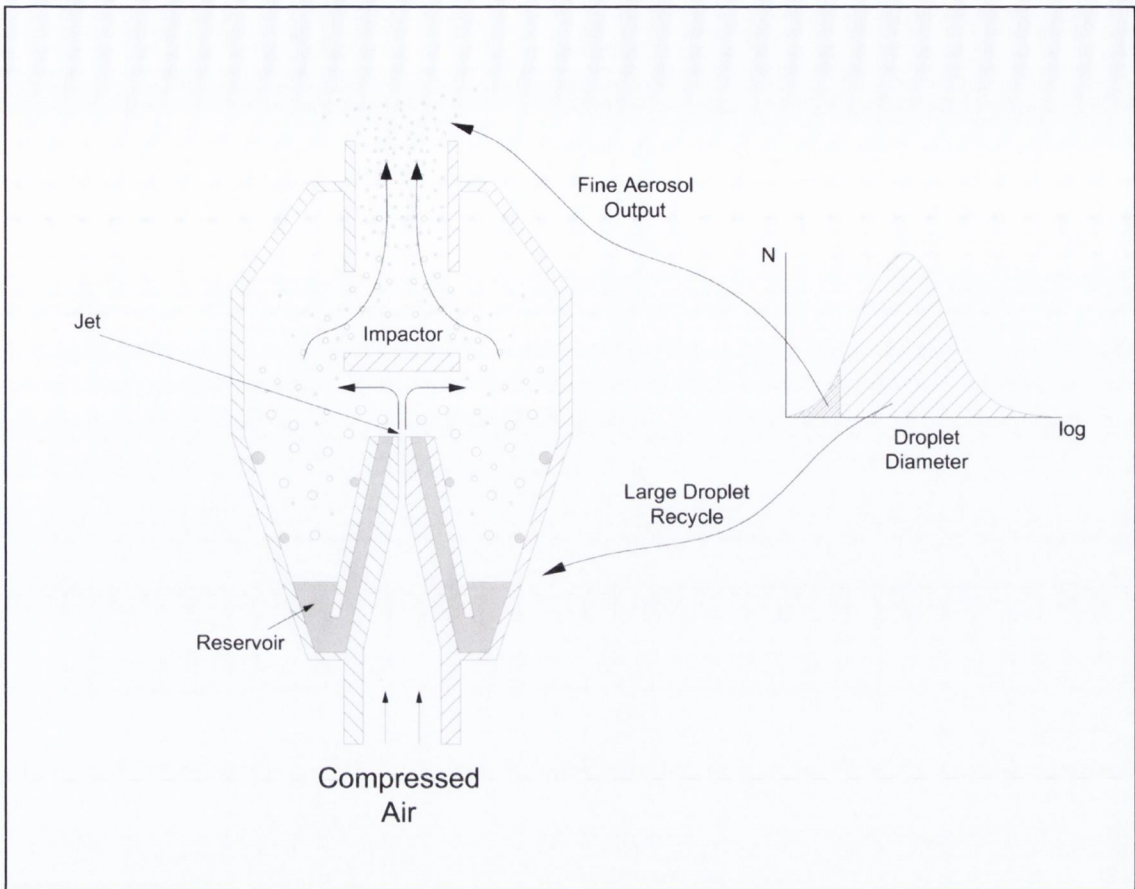


**Figure 3.7** Conventional medical jet nebuliser design (Dyer, Glew et al. 2012).

### 3.1 DEPOSITION AND TRANSPORT OF AEROSOLS IN SOILS

Research on the transportation of aerosol droplets in soils is limited. However, the deposition of droplet sizes for medical aerosols is generally understood to depend on three mechanisms (Schulz 1998): inertial impaction, gravitational sedimentation and Brownian diffusion. Figure 3.8 shows the typical deposition distribution of unit density droplets in a human lung. It can be seen that droplets larger than  $1 \mu\text{m}$  are increasingly more likely deposited by impaction. Whereas only a small proportion of droplets in the  $0.1 - 1 \mu\text{m}$  are deposited and are usually exhaled from the lung. Droplets smaller than  $0.1 \mu\text{m}$  are quickly diffused onto surfaces and deposited.

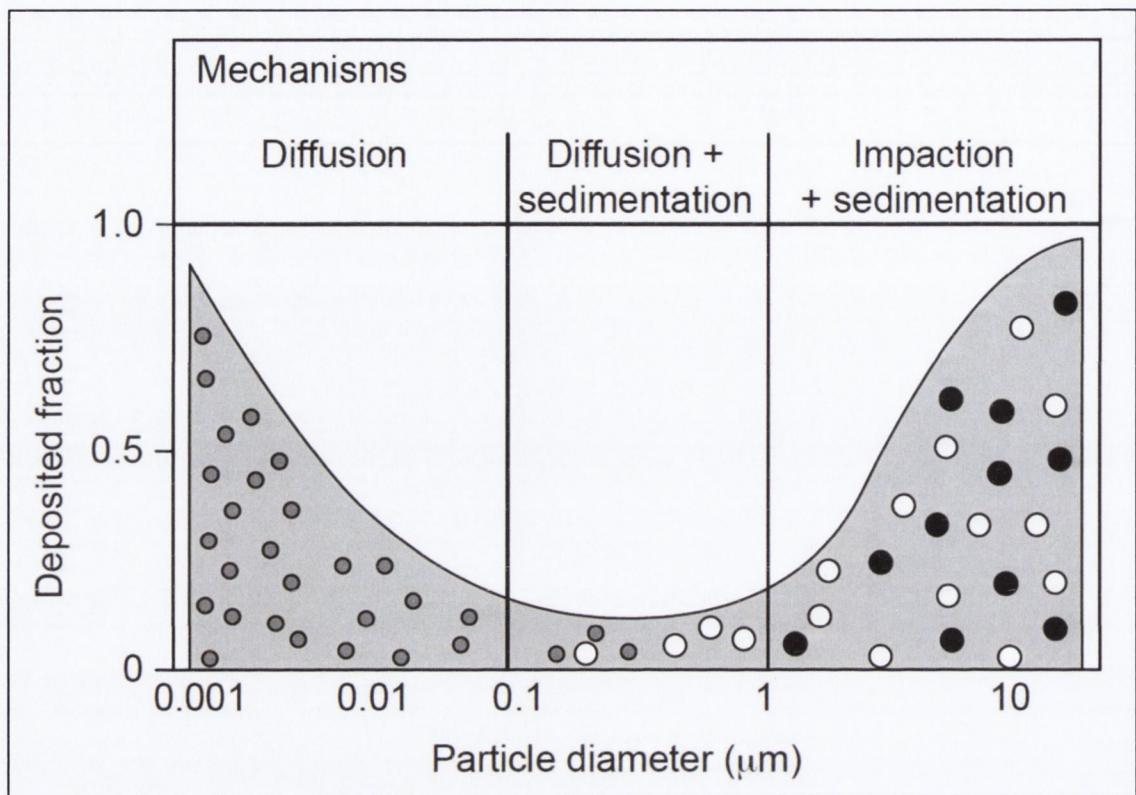


**Figure 3.8** Schematic overview of total particle deposition in the respiratory system for unit density spheres. Typical deposition values of an adult during quiet mouth breathing are given as a function of the inhaled particle diameter. Dominant deposition mechanisms are indicated (Schulz 1998).

In soils, saturation has shown to impact on the transport and deposition of nebulised liquids. Dyer et al. (2012) indicate that higher saturation levels reduce the maximum size of the particles transported outside a test column. This would be the result of water menisci acting as filters or traps for the coarser aerosol droplets. In the same paper Dyer et al. (2012) describe the mass balance of transported and deposited volumes of liquid using the dimensionless parameter  $A_t$ :

$$A_t = \frac{\Delta m_1 - (\Delta m_2 + \Delta m_3)}{\Delta m_1} \quad \text{Eq. 3.23}$$

where,  $\Delta m_1$  is the change in mass of nebuliser,  $\Delta m_2$  is the change in mass of column and  $\Delta m_3$  is the change in mass of pore fluid due to sparging. For  $A_t = 1$ , all the atomised liquid is transported outside the column. Whereas  $A_t < 1$  indicates that liquid is being deposited.

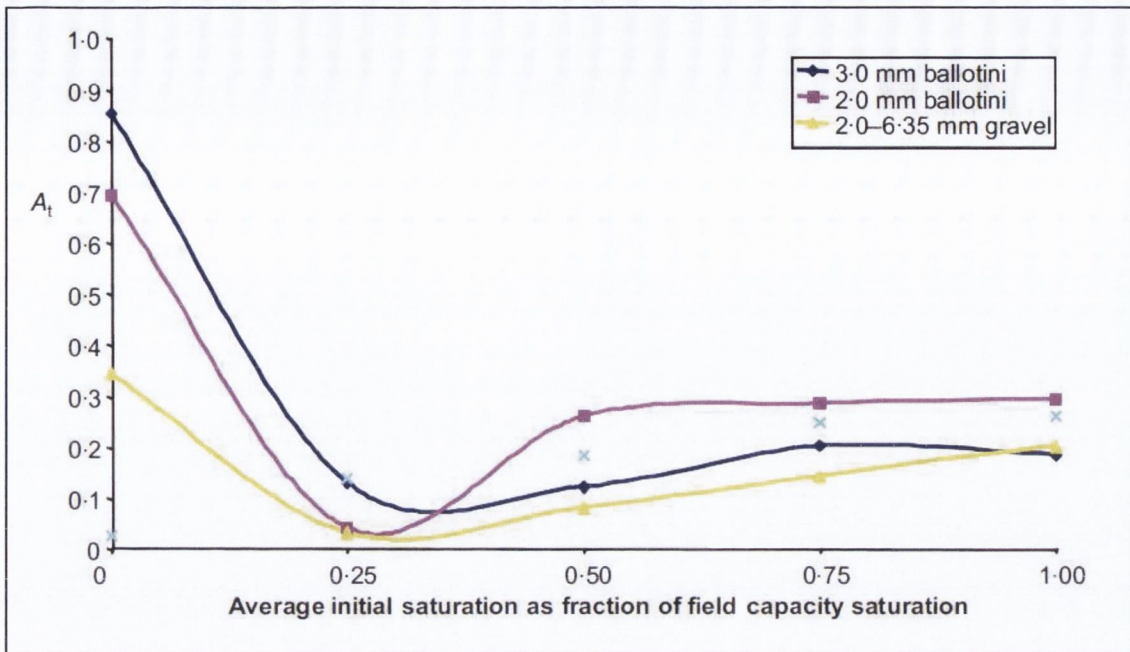


**Figure 3.9** Calculated transportation parameter ( $A_t$ ) for aerosol transported through soil columns with varying moisture content using medical jet nebulisers (Dyer, Glew et al. 2012).

As shown in Figure 3.9 the mass balance of the deposition is significantly impacted by the moisture content. Dry soils are shown to behave hydrophobically (Lourenço, Gallipoli et al. 2012) and most droplets are transported outside the column (low wettability). However, this phenomenon reduces rapidly with only small increases in moisture content. When field capacity is approached retention reaches a steady state. A similar dependency on wettability has been reported by Riha et al. (2010) in the supporting documentation of US Patent N. 2010/0307754. The results reported by Riha et al. (2010) indicate that oil coated sand particles would inhibit the deposition of relatively large water droplets. Hence, limiting the volume of water being deposited in short columns.

A set of large scale aerosol experiments was carried out by Glew (2009) to determine the expected distribution of bioremediation reagents in a field application (Figure 3.10). Approximately 2 m<sup>3</sup> of saturated sand was injected with a nebulised tracer solution. The concentration of the tracer was measured through a number of

sampling ports fitted on the test cylinder. Consistent with airsparging theory (Boelsma, Marnette et al. 2000), the results show that a pulsed injection would be able to distribute the tracer more evenly across the volume when compared to a continuous flow. As inferred from the larger volume of displaced liquid (6.3 L and 7.2 L for continued and pulsed respectively), the pulsating regime has resulted in a greater number of air channels being developed. Hence, in an increased lateral penetration of the air flow carrying the tracer droplets. Conversely, a more vertical transport pattern was observed in the continued flow injection exercise.

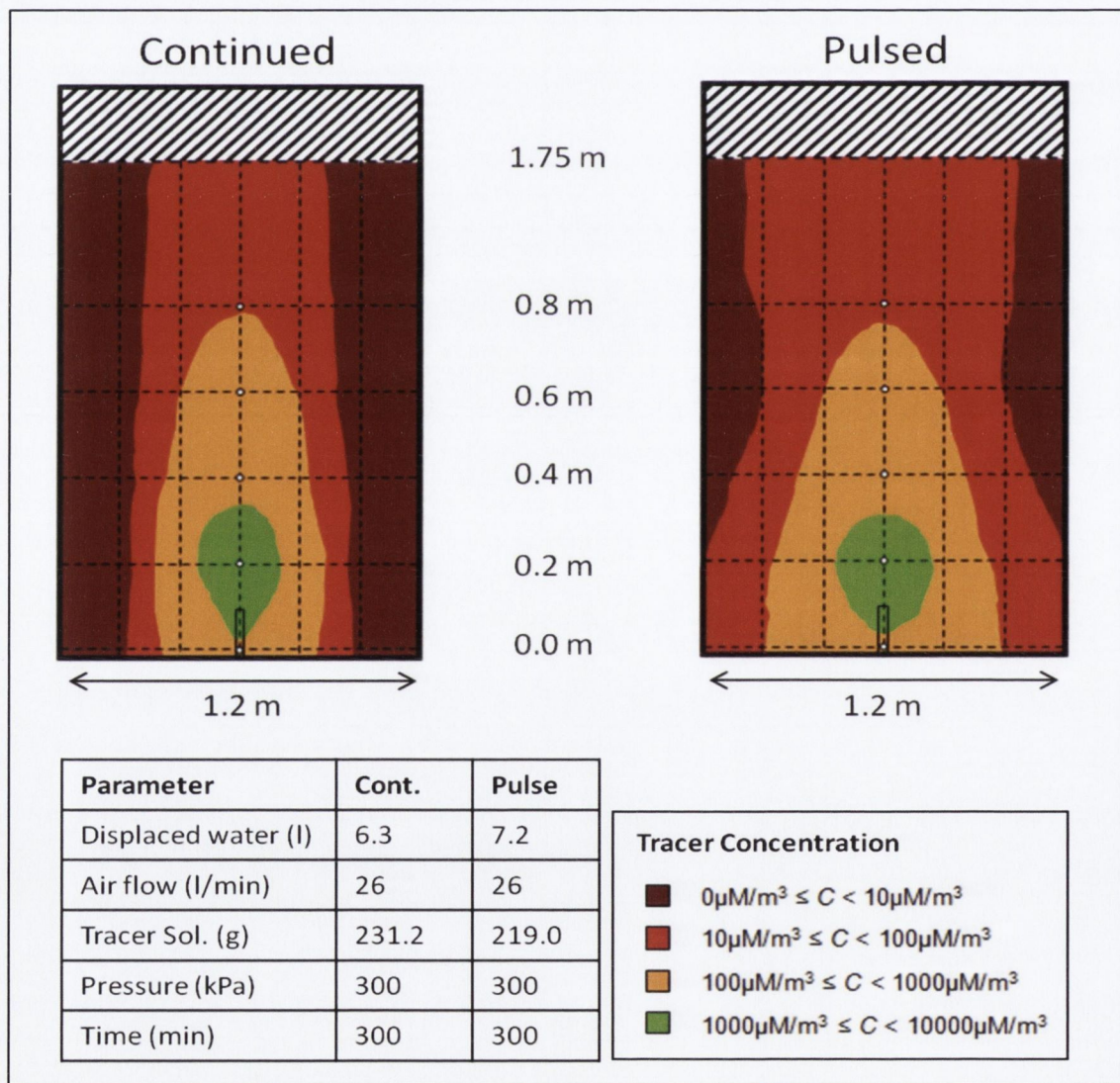


**Figure 3.10** Concentration of rhodamine tracer solution in a saturated sand treated using aerosol injections (Glew 2009).

To describe the uniformity of a treatment in medium scale 1D columns, Glew introduced the concept of molar concentration difference,  $C_{diff}$ :

$$C_{diff} = 1 - \left( \frac{C_{top}}{C_{bot}} \right) \quad \text{Eq. 3.24}$$

where  $C_{top}$  is the concentration of the tracer (or reagent) at the top of the column and  $C_{bot}$  is the concentration of the tracer (or reagent) at the bottom of the column. According to Glew (2009),  $C_{diff}$ , is a useful parameter for assessing the uniformity of droplet deposition.



# CHAPTER 4

## MATERIALS AND METHODS

---

### 1) INTRODUCTION

This Chapter is dedicated to the description of the general materials and methods employed in the research. While most of the methods employed have been derived from the established literature, some adaptations have been introduced in order to suit the experimental requirements. Among these, the medical nebulisers employed required the most significant design adaptations due to the high back pressures being formed during injection. Further details of such modifications and additional information regarding the materials and methods employed can also be found in Appendix One.

**Table 4.1** Summary of MICP treatment protocols and delivery methods employed in this study.

Step	Injection/Oligotrophic	Injection/Eutrophic	Atomised/Eutrophic
1	Injection of bacterial suspension	Injection of bacterial suspension	Delivery of atomised droplets of bacterial suspension
2	Injection of fixation fluid	—	—
3	Injection of cementation liquid	Injection of cementation liquid with nutrients	Delivery of atomised droplets of cementation liquid with nutrients
4	Reaction pause	Reaction pause	Reaction pause
5	Repeat 3 and 4 until the required cementation is achieved	Repeat 3 and 4 until the required cementation is achieved	Repeat 3 and 4 until the required cementation is achieved

Due to the diverse nature of the experiments carried out, the set-up of each individual experiment will be described in Chapters 5 and 6 by referring to this Chapter for the general methodologies and materials.

Unless otherwise specified, experiments were conducted at room temperatures between 18 °C and 23 °C. A summary of the treatment techniques used is presented in Table 4.1.

## 2) MICROBIOLOGICAL METHODS

### 2.1 CHEMICALS AND STOCK SOLUTIONS

All chemicals employed in the work carried out were analytical grade reagents supplied by Fisher Scientific Ireland Ltd. For practical purposes a set of stock solutions was prepared as detailed in Table 4.2 and used to prepare the solutions employed in the experimental work. In order to ensure the highest quality of the stock solutions, these were prepared fresh every two months and stored at 4 °C. Sterilisation of the stock solutions, and of the double deionised water employed in the preparation of the work solutions, was obtained by appropriate treatment (Table 4.2).

**Table 4.2** Preparation of stock solutions.

<b>Stock solution</b>	<b>M</b>	<b>g/L</b>	<b>Sterilisation</b>
Yeast extract	n.a.	100	Autoclave (20 mins @ 121 °C)
Urea, CO(NH <sub>2</sub> ) <sub>2</sub>	4.0	240	Filter (0.22 µm)
Calcium chloride dihydrate, CaCl <sub>2</sub> ·2H <sub>2</sub> O	4.0	588	Autoclave (20 mins @ 121 °C)
Magnesium chloride, MgCl <sub>2</sub>	4.0	380	Autoclave (20 mins @ 121 °C)
Sodium chloride (saline), NaCl	0.15	9.0	Autoclave (20 mins @ 121 °C)
Doble deionised water, H <sub>2</sub> O	n.a.	n.a.	Autoclave (20 mins @ 121 °C)

## 2.2 CULTURE PREPARATION

*Sporosarcina pasteurii* (NCIMB Accession Number 8841) was employed throughout the work presented here. Optimal and cost efficient culturing of *S. pasteurii* for biogrouting applications has been extensively investigated by Whiffin (2004). The growth medium employed in this study was derived from her work. In particular, yeast extract has been employed as sole source of proteins and nutrients. Urea, instead, was the source of ammoniacal nitrogen: selected *in-lieu* of cheaper ammonium sources proposed by Whiffin and often employed in the literature. The choice was made in order to ensure consistency with the source present in the cementation solution: of particular relevance when evaluating the effects of eutrophic treatment. Table 4.3 provides details of the key parameters of *S. pasteurii* liquid cultures employed in this study.

**Table 4.3** Range of parameters characterising *S. pasteurii* liquid cultures employed in this study.

Parameter	Range
Optical density (OD <sub>600</sub> )	5.02 – 5.38
Urease activity (mM·min <sup>-1</sup> )	5.11 – 6.80
Specific urease activity (mM·min <sup>-1</sup> ·OD <sub>600</sub> <sup>-1</sup> )	1.02 – 1.51

*Sporosarcina pasteurii*, was received dry frozen and revived aseptically (triplicate) in a liquid reviving medium and plated on solid reviving medium (Table 4.4) in accordance with the suppliers recommendations (NCIMB 2008; NCIMB 2010). Incubation was carried out aerobically at 30 °C for 48 hours; the liquid culture was agitated at 200 rpm. Following incubation, the plated culture was employed as a backup and stored at 4 °C. A collection sample on ceramic beads was also prepared from the plated culture and stored at -80 °C for future use.

**Table 4.4** Reviving medium composition.

<b>Ingredients (in 1 L distilled water)*</b>	
Lab-Lemco nutrient broth powder	13.0 g
<i>Lab-Lemco beef extract (1.0 g)</i>	
<i>Yeast extract (2.0 g)</i>	
<i>Peptone (5.0 g)</i>	
<i>NaCl (5.0 g)</i>	
Agar (solid medium only)	15.0 g
Urea stock 20% (w/w) solution - filter sterilised#	10 ml

\* Solution is sterilised by autoclaving at 121 °C for 15 min

# Urea is added to cooling media after autoclaving to avoid decomposition

The revived liquid culture was consequently sub-cultured a total of three times in the selected growth medium (Table 4.5) with 5% (v/v) inoculums. This was carried out to ensure full recovery and adaptation of the culture to the new medium. Sub-cultures were incubated to late exponential phase aerobically at 30 °C, under agitation (200 rpm) for 28 hours. The third sub-culture was stored at 4 °C as a stock liquid culture and refreshed (sub-cultured) approximately every three to four weeks.

**Table 4.5** Growth medium composition. Stock solutions as in Table 4.2.

<b>Ingredients</b>		<b>Stock*</b>
Yeast extract	20 g/L	200 ml
Urea	6 g/L (100 mM)	25 ml
pH (not adjusted)	~ 7.5	n.a.

\* Calculated for 1 L of growth medium

Working cultures (liquid) were prepared fresh employing the growth medium inoculated with 5% (v/v) of stock liquid culture. Work cultures were incubated aerobically at 30 °C, under agitation (200 rpm) for 28 hours (late exponential phase). Aseptic conditions were maintained at all times when working with cultures. Purity of each liquid

culture was verified by plating on urea agar (Table 4.4) and spot checks were carried out on the stock liquid culture by observation under the microscope after Gram staining.

### 2.3 OPTICAL DENSITY AND UREASE ACTIVITY

Optical density (OD) is a well established method for the determination of the concentration of bacteria cells in a solution. OD is photometrically determined by measuring the absorbance of the suspension at the conventional wavelength of 600 nm (OD<sub>600</sub>). In this study, OD<sub>600</sub> of each sample was measured in triplicate against a blank prepared by syringe filtering an aliquot of sample (0.22 µm filters). Average values were then employed. Measurements were taken using a ND1000 NanoDrop (Thermo Scientific Inc.) spectrophotometer. It should be noted that the NanoDrop instrument measures absorbance across 1 mm of sample. In order to ensure consistency with literature values, where 10 mm spectrophotometer cells are typically used, all measured values were multiplied by a factor of ten and reported accordingly.

**Table 4.6** Sample preparation for EC determination of urease activity.

Double deionised water	20 ml
Urea stock solution (4M)	10 ml
<i>S. pasteurii</i> culture*	10 ml
Temperature	25 °C

\* *S. pasteurii* should be added last to avoid osmotic shock.

Urease activity (UA) has been commonly employed in the literature on biogrowth as a measure of the rate of urea hydrolysed by a bacterial suspension. In this study, UA was derived from Electric Conductivity (EC) readings over fixed time intervals (Grunwald 1984). EC and pH were measured with a Multi340i (WTW GmbH) on samples prepared as indicated in Table 4.6. EC change rate values were

correlated to UA values of urea consumed per minute ( $\text{mM min}^{-1}$ ) and corrected to pH 7 according to Whiffin (2004). Final values were calculated by accounting for dilution of the culture in the analytical sample (factor of 4). Further details can be found in Appendix One.

Specific urease activity (SUA) is a measure of the amount of urease produced per unit of bacteria biomass. In the literature on biogrowth, it has commonly been determined indirectly as  $\text{UA}/\text{OD}_{600}$ . This approach will be maintained in this study and SUA is reported as  $\text{mM min}^{-1} \text{OD}_{600}^{-1}$ .

### **3) SCANNING ELECTRON MICROSCOPY**

Scanning electron microscopy (SEM) was employed to observe structures developed at the micro scale. Images were acquired using Tescan Mira Variable Pressure Field Emission Scanning Electron Microscope with Energy Dispersive X-ray (EDX) microanalysis capability for elemental composition analysis. Samples were prepared after overnight drying at  $105\text{ }^{\circ}\text{C}$  and carbon coated. With few exceptions carbonaceous sand samples were imaged using secondary electron detection (SED). This allowed the distinction between the particle material and the deposited calcium carbonate to be more easily made based on topography and structure of the crystals. Silica sand samples, instead, were imaged employing backscatter electron detection (BSD) to enhance the contrast between the particle material and the carbonate precipitates. Further details on the method can be found in Appendix One, Annexes 3 to 6.

### **4) X-RAY DIFFRACTION PEAK ANALYSIS**

Powder X-Ray Diffraction (XRD) is a well established technique for the analysis of crystalline compounds and minerals (Moore and Reynolds 1997). When an X-ray is shined on a crystal or powder, it diffracts in a

pattern characteristic of the structure allowing the identification of the mineral(s) using a set of reference diffraction patterns. Powdered XRD can be employed to determine the purity of a sample, as well as the composition of any impurities present. Most importantly, it can be used to determine the lattice parameters of a crystal and therefore, the Mg : Ca ratio of a carbonate mineral. This is determined from the shift of the peak generated by the [104] calcite plane (Lumsden 1979; Sánchez-Román, Romanek et al. 2011):

$$N_{Ca} = \frac{(333.33 * d_{104}) - 911.99}{100} \quad \text{Eq. 4.1}$$

where  $N_{Ca}$  is the percentage mole of calcium ions in the lattice and  $d_{104}$  is the distance between the ion layers of the [104] plane. Further details of the method can be found in Appendix One.

In this study, analysis was carried out using a Phillips PW1720 with a Philips PW1050/80 goniometer and a Philips PW3313/20 Cu k-alpha anode tube that was run with standard conditions of 40kV and 20mA. A soller slit and a 1° divergence slit were used on the incident x-ray beam and a 0.2° receiving slit followed by a 1° anti-scatter slit were used on the diffracted beam. A Philips PW 1752/00 curved graphite monochromator was used in front of the PW1711 proportional counter detector. The detector controller was a Philips 1710. Each sample was washed with acetone, rinsed using deionised water and ethanol, and physically dried at 105 °C for 24 hours. A quartz internal standard was added to the samples prior to grinding to produce a benchmark peak for comparative data analysis. Prior to analysis each sample was hand ground for 15 minutes using mortar and pestle to ensure good reproducibility for replicate scans (Lumsden 1979). All measurements were taken from 25 to 55 degrees ( $2\theta$ ) at a step size of 0.01 degrees/second.

## 5) SOIL AND GEOTECHNICAL TESTING METHODS

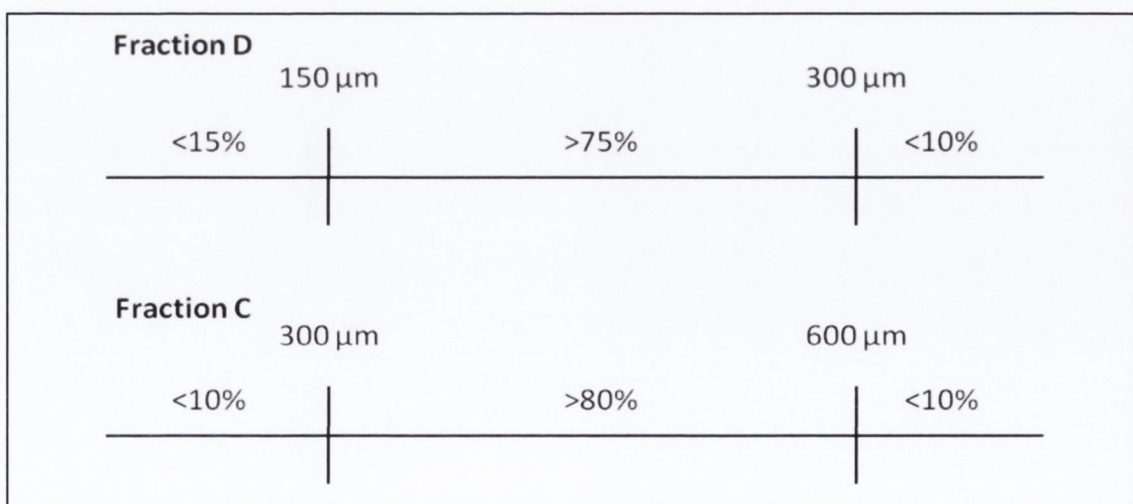
### 5.1 SOIL TYPES

Table 4.7 and Table 4.8 describe the salient characteristics of the soil types employed in the work presented here. Silica sand materials were supplied by David Ball Ltd, UK. Carbonaceous sand materials were obtained by wet sieving to the required size range multi-purpose limestone sand. For practical reasons the terms fine sand and medium sand will be used throughout the text as indicated in Tables 4.7 and 4.8.

**Table 4.7** Description of the silica sand materials employed in this study (DavidBall Ltd. 2011).

	<b>Fine Silica Sand</b>	<b>Medium Silica Sand</b>
Fraction*	D	C
Nominal size range	300 - 150 $\mu\text{m}$	600 - 300 $\mu\text{m}$
Bulk density ( $\text{kg m}^{-3}$ )	1310 (loose) 1510 (compact)	1560 (loose)
Classification	Lower Greensand, Leighton Buzzard sand	

\*As defined in BS 1881-131:1998



**Figure 4.1** Size distribution (% dry mass) of the silica materials employed in this study (DavidBall Ltd. 2011).



**Table 4.8** Description of the carbonaceous materials employed in this study.

	<b>Fine Carbonaceous Sand</b>	<b>Medium Carbonaceous Sand</b>
Size range	300 - 150 $\mu\text{m}$	600 -300 $\mu\text{m}$
Classification	Multi-purpose limestone sand	

## 5.2 BAROMETRIC DETERMINATION OF CALCIUM CARBONATE

Barometric determination of calcium carbonate equivalent was carried out in compliance with ASTM D4373 standard. The test consists of digesting a known amount of sample soil with hydrochloric acid in a sealed container equipped with a pressure gauge. Carbon dioxide is evolved during the reaction of carbonates with the acid: increasing the pressure in the vessel. The pressure increase inside the vessel can then be correlated to the equivalent calcite content by means of a calibration curve.

In this study, 10 g or 20 g (depending on the expected amount of precipitate) of soil sample were hand ground (mortar and pestle) for two minutes after drying at 105 °C for 24 hours. Ground samples were digested with 20 ml of 1 N reagent grade hydrochloric acid (Fisher Scientific Ltd.) in a specifically designed pressure vessel, HM-4501 apparatus (Interplant Ireland Ltd.). Calcium carbonate equivalent content was then determined from a calibration curve obtained with 0.2 g, 0.4 g, 0.6 g 0.8 g and 1.0 g of analytical grade calcium carbonate (Fisher Scientific Ltd.). Limestone sand samples could not be tested due to the carbonate nature of the particles. Further details of the method are provided in Appendix One.

### 5.3 UNCONFINED COMPRESSIVE STRENGTH TEST

Unconfined compressive strength is a well established soil testing methodology (Craig 2004). In particular, wet unconfined compressive strength (UCS) has been often employed in the literature for the rapid assessment of the effectiveness of biogrouting applications. The test is relatively simple but is conducted in drained conditions. This would, therefore, be considered to limit the interpretation of the findings when considering phenomena, such as soil liquefaction, where the increase of pore water pressure could become relevant. However, it has been shown that the cemented material displays little volumetric strain when loaded: resulting in small differences in peak strength between drained and undrained triaxial tests (van Paassen 2009; Montoya, DeJong et al. 2013).

In this study, the test has been conducted in accordance with standard BS 1377-7:1990 using a mechanical load frame testing device. Testing was conducted at 0.5 % min<sup>-1</sup> strain rate. Samples had a diameter of approximately 38 mm and a length to diameter ratio of approximately 2:1. Treated samples were flushed with 3 pore-water volumes of double deionised water to remove the process reagents and left to drain for 24 hours prior to testing. Further details of the method are provided in Appendix One.

## **6) AEROSOL DELIVERY**

### 6.1 MEDICAL JET NEBULISERS

Cirrus® (Intersurgical Ltd.) medical jet nebulisers were previously employed by Glew (2009) and Dyer et al. (2012) to deliver atomised carbon substrates for the bioremediation of chlorinated solvents in saturated soils. Continuing the line of research, Cirrus® nebulisers were

employed in this study to deliver the bioaugmentation and cementation liquids in unsaturated soils.

**Table 4.9** Range of working pressures and flows for Cirrus® medical jet nebulisers.

	Gas flow	Pressure	Liquid flow*
Max	8 L min <sup>-1</sup>	180 kPa	0.25 mL min <sup>-1</sup>
Min	6 L min <sup>-1</sup>	110 kPa	0.20 mL min <sup>-1</sup>

The Cirrus® nebuliser is designed to atomise liquid solutions suitable for deposition of drugs in the tracheobronchial airways of the human lung. To avoid calcium carbonate precipitation occurring inside the nebuliser, dedicated units and tubing were employed for the bioaugmentation and the treatment process respectively. During operation, the pressure drop across the nebuliser was maintained within the range indicated by the manufacturer and reported in Table 4.9.

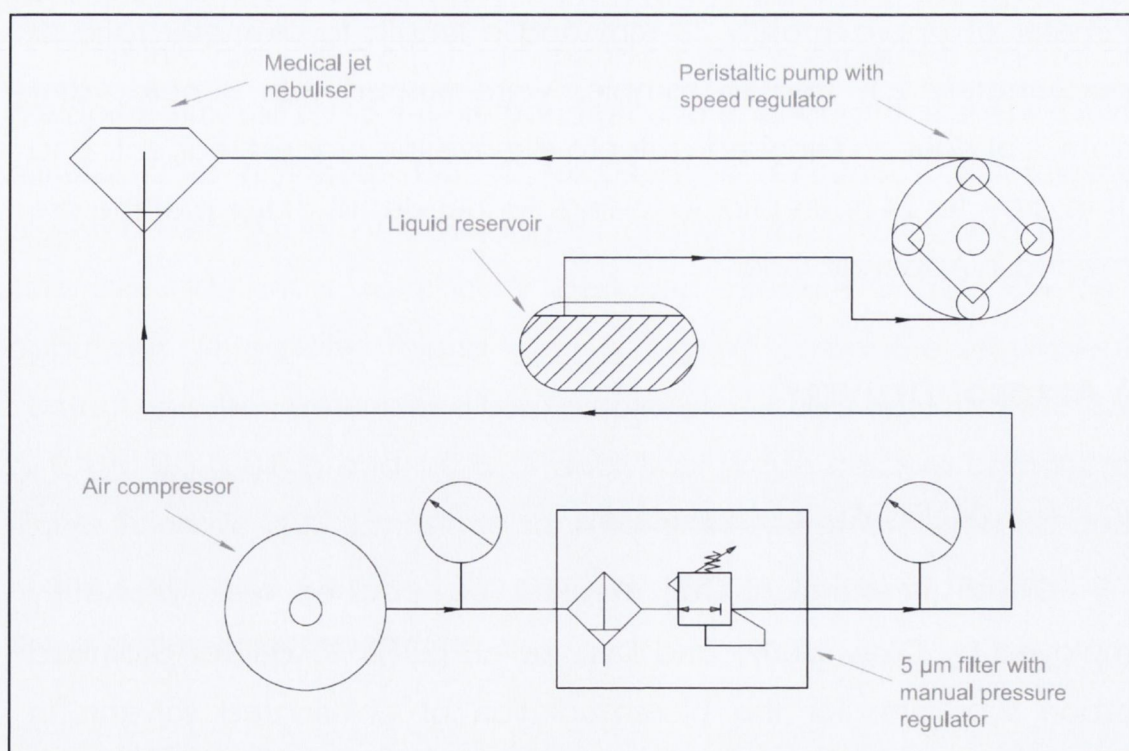


**Figure 4.2** Schematic representation of the nebuliser set-up employed in the experiments.

Some modifications to the nebuliser's design were required by the working conditions encountered during the experiments. In particular, the nebuliser's chamber had to be sealed to prevent leakage caused by the pressure build up at the head of the nebuliser. Sealing the chamber meant that it was no longer possible to fill the nebuliser manually. Therefore, this was modified to receive flow from a peristaltic pump connected to a reservoir containing the process liquids. The amount of liquid delivered as aerosol was measured by employing a graduated container as reservoir. A schematic representation of the set-up is presented in Figure 4.2. The air compressor employed was a Jun-Air 3-4 fitted with a 5  $\mu\text{m}$  filter with manual drain and a manual pressure regulator. The peristaltic pump employed was a 4 channel 323/MC8 low-pulse pump with manual control capable of delivering between 2  $\mu\text{L min}^{-1}$  and 36  $\text{mL min}^{-1}$  per channel.

## 6.2 TEST COLUMNS

The test columns were designed to accommodate a vertical aerosol flow directed from bottom to top. This had two distinct advantages: (1) simplify the design of the connections by allowing to connect the nebuliser in series with the column without U bends; (2) allow the discrimination between liquid displaced by the airflow (accumulating at the top) and liquid percolating by gravity and accumulating at the bottom of the column. Figure 4.3 illustrates the set-up of the columns employed in the experiments involving the delivery of atomised liquids. A 140 mm long perspex tube with an internal diameter of 40 mm (50 mm OD) was mounted between two perspex plates and sealed. A thin plastic sheet (0.15 mm) was employed to line the internal wall of the perspex tube (Appendix One). This was introduced to enable the extraction of the sample which would otherwise become cemented to the walls. Once extracted the core could then be easily "unwrapped" from the lining material without damaging the sample.

The top plate was necessary to provide a confinement in order to avoid rupturing of the samples during injection (Appendix One). A smaller perspex tube (28 mm ID, 32 mm OD) was employed to connect the nebuliser to the column and a pressure gauge was fitted to the side. The small tube was also employed to construct the out-let.

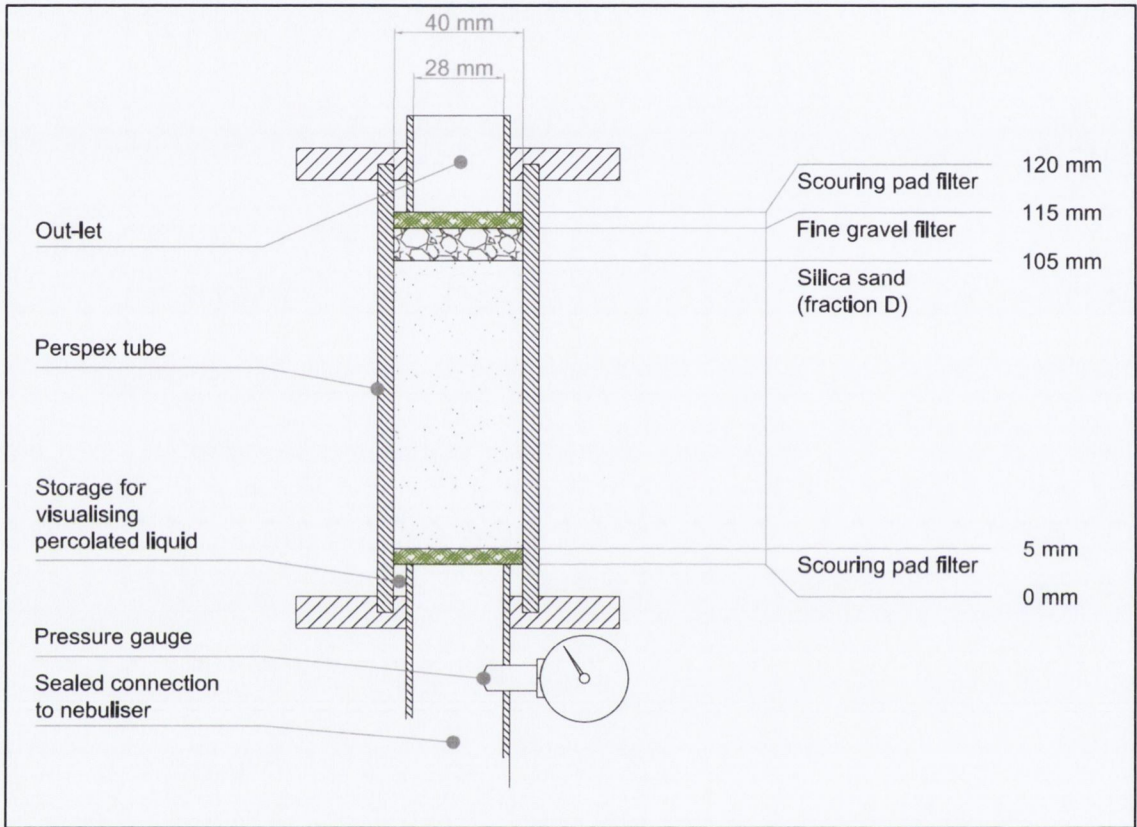


**Figure 4.3** Schematic representation of the test columns employed in this study.

The inlet was raised (10 mm) above the bottom of the column in order to allow for the visual assessment of any occurring percolation. The column was packed with 100 mm of fine silica sand. A 10 mm thick layer of fine silica gravel ( $d_{50} = 2$  mm) was employed as ballast and filter at the top of the column. The gravel also had the purpose of spreading the confining load at the top. Two filters ( $h = 5$  mm) were constructed using commercially available scouring pad (TESCO Ireland) and added to prevent the sand from falling in to the nebuliser unit or exiting the column at the top. The weave of the pads was deemed sufficiently fine

to stop the sand, but not the aerosol, from passing the filter. An image of a complete column is found in Appendix One.

## 1) EXPERIMENT N. 1: CARBONATE DISTRIBUTION

### 1.1 GENERAL

Experiment N. 1 was carried out to investigate the carbonate precipitation patterns and distribution at the pore scale when employing liquid injection methods in saturated soils. The effect of different treated materials and different treatment protocols was evaluated. The test method used both oligotrophic and eutrophic injection protocols in small columns prepared using four different sand materials. The treated materials were subsequently transferred under the scanning electron microscope to observe the distribution of calcium carbonate. Calcium carbonate content was determined in order to allow comparison between samples containing similar amounts of carbonate. Preliminary work (Appendix Two) showed that in order to observe the formation of individual crystals and structures the experiment should be conducted by limiting the amount of bioaugmentation. This allowed for the clear observation of isolated deposits which might have been obscured by the coalescence or overgrowth of carbonate in the presence of large amounts of urease.

### 1.2 EXPERIMENTAL SET-UP

A total of 24 miniature test columns were prepared as shown in Figure 5.1 using plastic vials with 25 mm diameter and 110 mm height. Six test samples were prepared using medium silica sand and 6 test samples were prepared using fine silica sand. The sand was pluviated under water to avoid the inclusion of air pockets and vibrated to an

approximate porosity of 40% and 44% for fine and medium sand respectively. In order to evaluate the impact of different geological substrates, 12 identical size-range (fine and medium sand) samples were obtained by wet sieving multi-purpose limestone sand (carbonaceous).

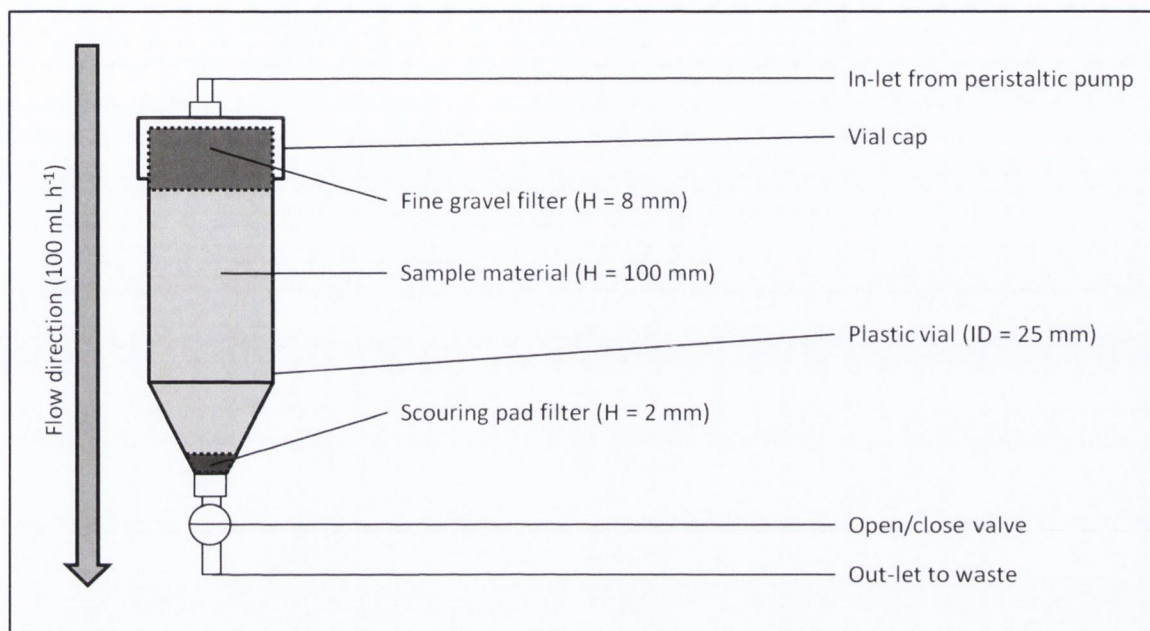


**Figure 5.1** Schematic representation of the experimental set-up.

All 24 columns were initially flushed from top to bottom at a flow rate of  $100 \text{ mL h}^{-1}$  with double deionised water. Bioaugmentation was subsequently achieved by injecting, at the same rate,  $5 \text{ mL}$  of *S. pasteurii* suspension having  $5.38 \text{ OD}_{600}$  and UA of  $6.71 \text{ mM min}^{-1}$ . Following bioaugmentation, 16 samples were treated employing an oligotrophic protocol and immediately received  $30 \text{ mL}$  (approximately 1.5 pore volumes) of saline fixation fluid aseptically prepared with  $7.35 \text{ g/L}$  ( $50 \text{ mM}$ ) of calcium chloride dehydrate. After the fixation phase, a schedule of  $30 \text{ mL}$  injection rounds ( $100 \text{ mL h}^{-1}$ ) and sample harvesting was selected in order to produce samples with varying amounts of precipitated calcium carbonate (Table 5.1). The oligotrophic cementation medium was composed as follows:  $60 \text{ g/l}$  ( $1 \text{ M}$ ) of urea and  $147 \text{ g/l}$  ( $1 \text{ M}$ ) of calcium chloride dihydrate.



**Table 5.1** Oligotrophic treatment and sampling regime.  $t_0$  was set at the end of bioaugmentation injection and treatments were applied at 24 hour intervals.

ID	Min.	Frac.#	R1*	R2*	R3*	R4*	Harvest
OA1	Silica	C	$t_0$				$t_0+24h$
OA2	Silica	C	$t_0$	$t_0+24h$			$t_0+48h$
OA3	Silica	C	$t_0$	$t_0+24h$	$t_0+48h$		$t_0+72h$
OA4	Silica	C	$t_0$	$t_0+24h$	$t_0+48h$	$t_0+72h$	$t_0+96h$
OB1	Silica	D	$t_0$				$t_0+24h$
OB2	Silica	D	$t_0$	$t_0+24h$			$t_0+48h$
OB3	Silica	D	$t_0$	$t_0+24h$	$t_0+48h$		$t_0+72h$
OB4	Silica	D	$t_0$	$t_0+24h$	$t_0+48h$	$t_0+72h$	$t_0+96h$
OC1	Carb.	C	$t_0$				$t_0+24h$
OC2	Carb.	C	$t_0$	$t_0+24h$			$t_0+48h$
OC3	Carb.	C	$t_0$	$t_0+24h$	$t_0+48h$		$t_0+72h$
OC4	Carb.	C	$t_0$	$t_0+24h$	$t_0+48h$	$t_0+72h$	$t_0+96h$
OD1	Carb.	D	$t_0$				$t_0+24h$
OD2	Carb.	D	$t_0$	$t_0+24h$			$t_0+48h$
OD3	Carb.	D	$t_0$	$t_0+24h$	$t_0+48h$		$t_0+72h$
OD4	Carb.	D	$t_0$	$t_0+24h$	$t_0+48h$	$t_0+72h$	$t_0+96h$

\* Round of oligotrophic treatment (30 mL injections)

# C = 600  $\mu\text{m}$  – 300  $\mu\text{m}$  (medium sand); D = 300  $\mu\text{m}$  – 150  $\mu\text{m}$  (fine sand)

**Table 5.2** Eutrophic treatment and sampling regime.  $t_0$  was set at the end of the bioaugmentation injection and treatments were applied at 3 hour intervals.

ID	Min.	Frac.#	R1*	R2*	R3*	R4*	Harvest
EA1	Silica	C	$t_0$	$t_0+3h$			$t_0+6h$
EA2	Silica	C	$t_0$	$t_0+3h$	$t_0+6h$	$t_0+9h$	$t_0+12h$
EB1	Silica	D	$t_0$	$t_0+3h$			$t_0+6h$
EB2	Silica	D	$t_0$	$t_0+3h$	$t_0+6h$	$t_0+9h$	$t_0+12h$
EC1	Carb.	C	$t_0$	$t_0+3h$			$t_0+6h$
EC2	Carb.	C	$t_0$	$t_0+3h$	$t_0+6h$	$t_0+9h$	$t_0+12h$
ED1	Carb.	D	$t_0$	$t_0+3h$			$t_0+6h$
ED2	Carb.	D	$t_0$	$t_0+3h$	$t_0+6h$	$t_0+9h$	$t_0+12h$

\* Round of eutrophic treatment (30 mL injections)

# D = 600  $\mu\text{m}$  – 300  $\mu\text{m}$  (medium sand); C = 300  $\mu\text{m}$  – 150  $\mu\text{m}$  (fine sand)

The remaining 8 columns were treated employing eutrophic protocols. In these, bioaugmentation was followed by 30 mL of eutrophic cementation liquid prepared aseptically as follows: 5 g/L yeast extract, 10 g/L (170 mM) urea and 22 g/L (150 mM) of calcium chloride dihydrate. A schedule of 30 mL injection rounds (100 mL h<sup>-1</sup>) and sample harvesting was selected in order to produce samples with varying amounts of precipitated calcium carbonate (Table 5.2). Two sets of samples were harvested from each of the silica sand columns. One set was prepared for the determination of calcium carbonate content and a second set was employed for SEM imaging and analysis. Only SEM samples were taken from the carbonaceous sand columns.

### 1.3 CACO<sub>3</sub> DETERMINATION AND EFFECT OF PARTICLE SIZE

Table 5.3 shows the content of calcium carbonate contained in the silica sand samples treated with an oligotrophic protocol. As expected, the treatment generally resulted in a limited precipitation of carbonate (< 0.94% w/w) due to the small amount of bioaugmentation applied. For the same reason the overall conversion efficiency,  $OC_{eff}$ , (< 7.14%) was also low.  $OC_{eff}$ , is here defined as:

$$OC_{eff} = \frac{[CaCO_3]}{Max[CaCO_3]} \quad \text{Eq. 5.1}$$

where  $[CaCO_3]$  is the calcium carbonate content actually achieved (% w/w) and  $Max[CaCO_3]$  is the calcium carbonate content potentially achieved assuming the total conversion of urea into calcium carbonate (% w/w). Three of the values recorded for calcium carbonate content were below the detection limit of 0.9% (w/w). These extremely low values were recorded for mildly treated samples which were subjected to less than two and one cementation rounds for medium and fine sand respectively.

**Table 5.3** Calcium carbonate content of oligotrophically treated silica sand. Precipitation was more abundant in fine sand (OB series) when compared with medium sand (OA series).

ID	Total CaCO <sub>3</sub> (g)#	Actual CaCO <sub>3</sub> (w/w)	Max CaCO <sub>3</sub> (w/w)*	OC <sub>eff</sub>
OA1	n.a.	b.d.l.	3.85%	n.a.
OA2	n.a.	b.d.l.	7.69%	n.a.
OA3	0.133	0.17%	11.54%	1.47%
OA4	0.534	0.68%	15.38%	4.45%
OB1	n.a.	b.d.l.	4.0%	n.a.
OB2	0.192	0.26%	8.0%	3.19%
OB3	0.643	0.86%	12.0%	7.14%
OB4	0.707	0.94%	16.0%	5.89%

# Calculated for the entire sample

\* The difference between the OA and the OB series is due to the different bulk density.

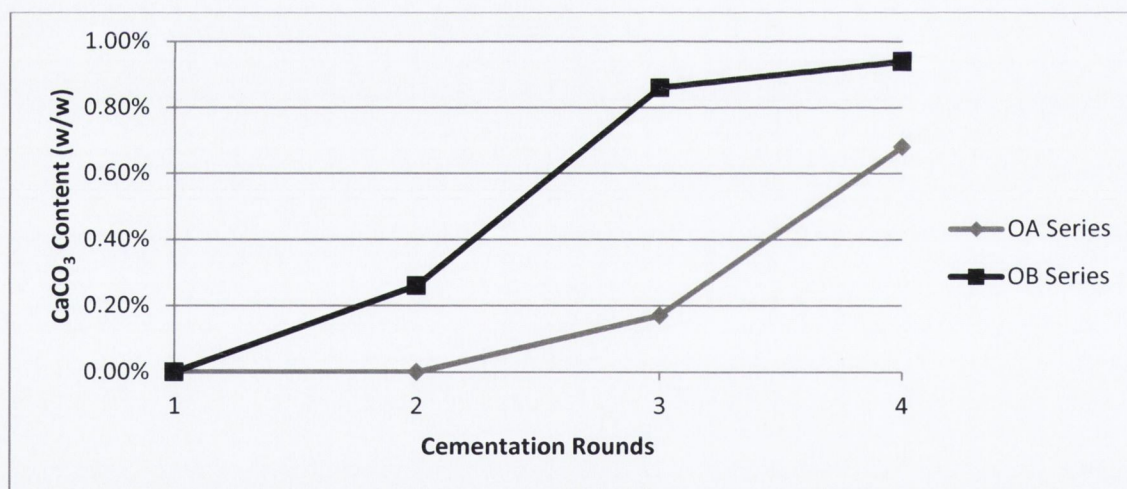


**Figure 5.2** Calcium carbonate content of oligotrophically treated silica sand plotted against the number of cementation rounds applied. Precipitation was more abundant in fine sand (OB series) when compared with medium sand (OA series). The precipitation rate is seen to reduce overtime (OB series).

As evident in Figure 5.2, medium sand samples (OA series) resulted in smaller amounts of carbonate being precipitated when compared with identically treated fine sand samples (OB series). This would indicate that less biomass (urease activity) was retained by the coarser fraction C soil: confirming the relevance of bacterial straining and wedging

phenomena occurring near or at inter-particle contact points (Bradford, Simunek et al. 2006). Figure 5.2 also shows that the precipitation rate in fine sand samples is reducing over time due to bacteria encapsulation (Cuthbert, Riley et al. 2012) and cell lysis (van Paassen 2009). The phenomenon is not observed in medium sand samples, possibly because smaller amounts of carbonate are precipitated over the time span of this experiment and encapsulation is therefore less prominent. However, it would be expected that a similar reduction would be observed if the experiment was progressed further.

Table 5.4 shows the content of calcium carbonate contained in the silica sand samples treated with an eutrophic protocol. As for the samples treated oligotrophically, the amounts of calcium carbonate precipitated are generally low. The maximum concentration achieved was 0.77% (w/w). The low concentrations of urea and calcium (150 mM) employed in the cementation liquid resulted in efficiencies as high as 35.5% being recorded despite the limited bioaugmentation.

**Table 5.4** Calcium carbonate content of eutrophically treated silica sand. Early precipitation was more abundant in fine sand (EB1) when compared with medium sand (EA1). The difference is less evident at the later stages of the treatment (EB2 and EB1).

ID	Total CaCO <sub>3</sub> (g) <sup>#</sup>	Actual CaCO <sub>3</sub> (w/w)	Max CaCO <sub>3</sub> (w/w) <sup>*</sup>	OC <sub>eff</sub>
EA1	0.066	0.09%	1.15%	7.37%
EA2	0.533	0.68%	2.31%	29.7%
EB1	0.320	0.43%	1.20%	35.5%
EB2	0.578	0.77%	2.40%	32.1%

<sup>#</sup> Calculated for the entire sample

<sup>\*</sup> The difference between the OA and the OB series is due to the different bulk density.

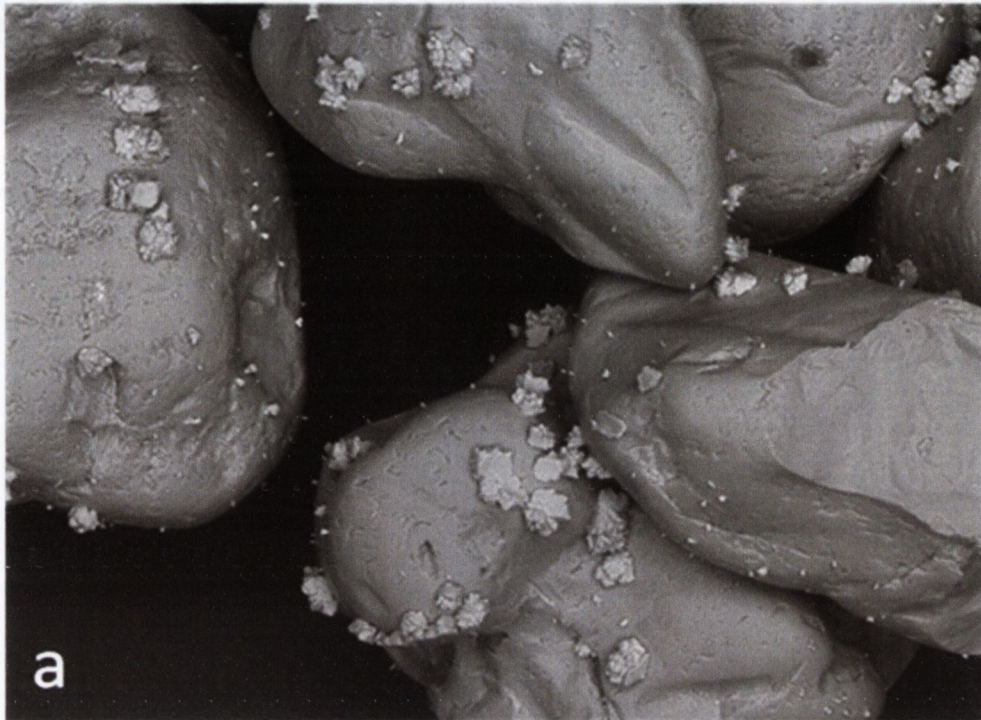
As for oligotrophic samples, the retained biomass (as inferred from the amount of precipitated carbonate) is less abundant in medium sand (sample EA1) than in fine sand (EB1). However, this appears to become

less evident when the treatment is progressed (samples EA2 and EB2). In fact, while the number of data points is limited, it is interesting to note that the efficiency recorded in the eutrophic samples appears to converge over time towards a value of approximately 30%. It could be speculated that this is the value determined by the biomass sustained by 5 g L<sup>-1</sup> of yeast extract in the experimental conditions encountered: suggesting a control on the biomass of *S. pasteurii* present in the soil.

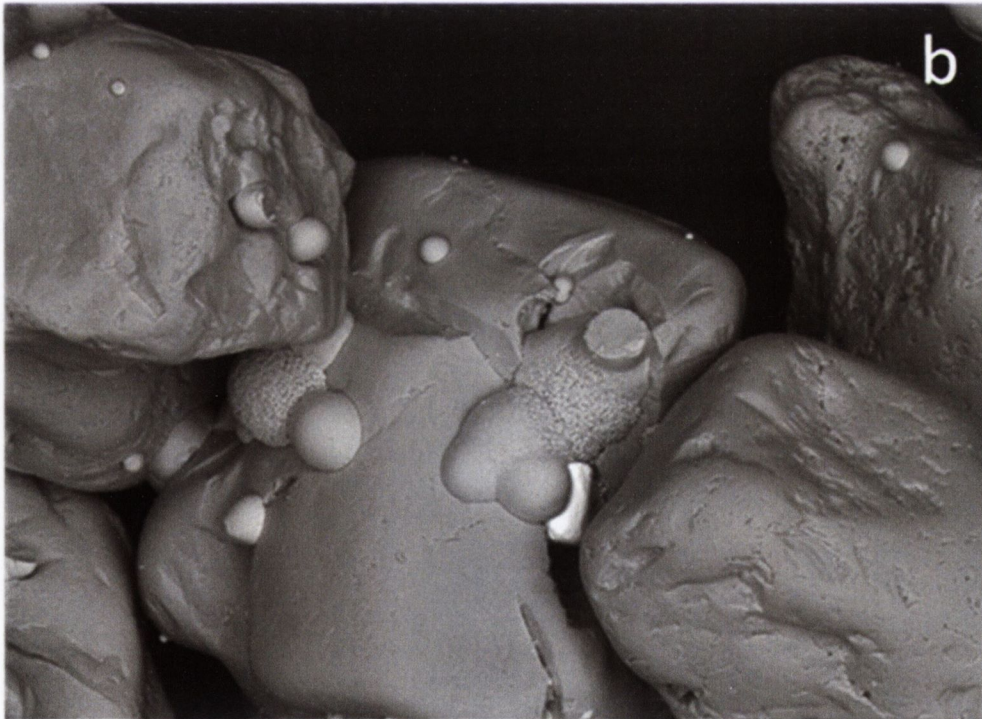
#### 1.4 TREATMENT PROTOCOLS AND CaCO<sub>3</sub> DISTRIBUTION

The SEM images illustrate distinctly different patterns for the precipitation of calcium carbonate on the surface of sand particles depending on whether oligotrophic or eutrophic protocols were employed. The effect of the different protocols can be observed in Figure 5.3.

The SEM images compare two identical medium silica sand samples (samples OA4 and EA2) where one was treated using an oligotrophic protocol, Figure 5.3(a), and the second employed an eutrophic protocol, Figure 5.3(b). Both treatments resulted in 0.68% w/w calcium carbonate being precipitated. However, the precipitation of the crystals over the surface of soil particles (indicative of bacterial attachment locations) is noticeably different. In Figure 5.3(a), the oligotrophic treatment resulted in a greater dispersion of calcium carbonate with numerous small crystals deposited on more exposed surfaces away from inter-particle contact points. In contrast the image reproduced in Figure 5.3(b) for the eutrophic treatment shows calcium carbonate being precipitated at a relatively smaller number of locations and predominantly at or near inter-particle contact points; where, in the absence of a fixation phase, restricted passage ways would allow accumulation of bacteria as a result of mechanical filtration, straining and wedging (Li, Lin et al. 2006; Bradford, Torkzaban et al. 2007).



200  $\mu\text{m}$



200  $\mu\text{m}$

**Figure 5.3** Medium silica samples (OA4, EA2) treated with: **(a)** oligotrophic methods, and **(b)** eutrophic methods. Calcium carbonate is visible over the smooth particle surface as: **(a)** wide spread and variably sized crystal formations; and **(b)** hemispherical or dome-like masses. Both samples contained 0.68% w/w of precipitated calcium carbonate.

This observation confirms that a fixation phase promotes a relatively homogeneous bacterial attachment throughout the soil sample as a result of the indiscriminate reduction of energy barriers to deposition (Redman, Walker et al. 2004). Conversely, eutrophic protocols distinctly promote preferential attachment at pore throat or near inter-particle contact points (Chapter 2, Paragraph 4.1). The resulting different deposition patterns would be expected to have markedly different effects on the mechanical strength of the soil. In the case of oligotrophic protocol the portion of crystals grown on the exposed surface of a sand particle would increase surface roughness but would not contribute to inter-particle bond formation and so have a lesser influence on the soil's mechanical properties as previously presumed by DeJong et al. (2010). Conversely, in this series of test the eutrophic protocol is shown to produce greater calcium carbonate precipitation at the inter-particle interface leading to a greater likelihood for an increased cementation and mechanical strength.

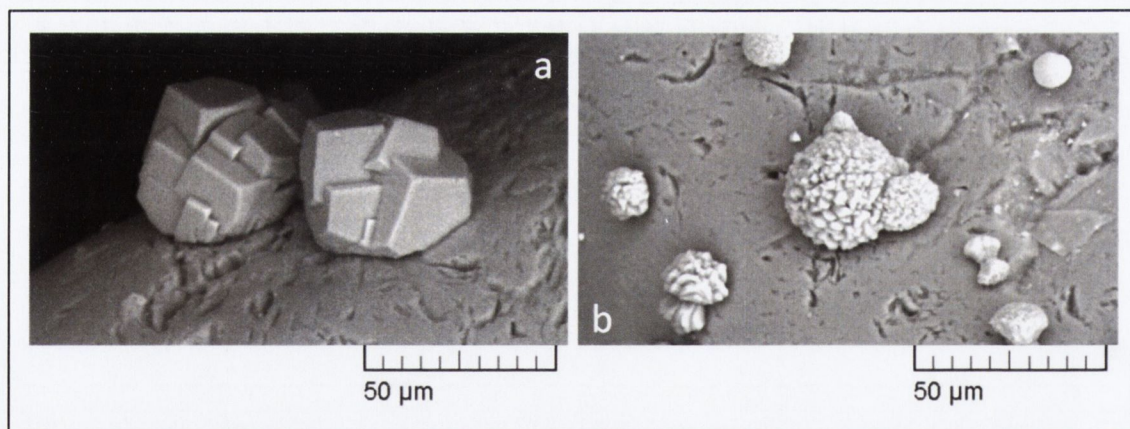


**Figure 5.4** Typical calcium carbonate crystals formed in medium silica samples (OA1, EA1) treated with: **(a)** oligotrophic protocol and **(b)** eutrophic protocol. The minerals can be respectively interpreted as calcite **(a)** and vaterite **(b)** on the basis of crystal morphology.

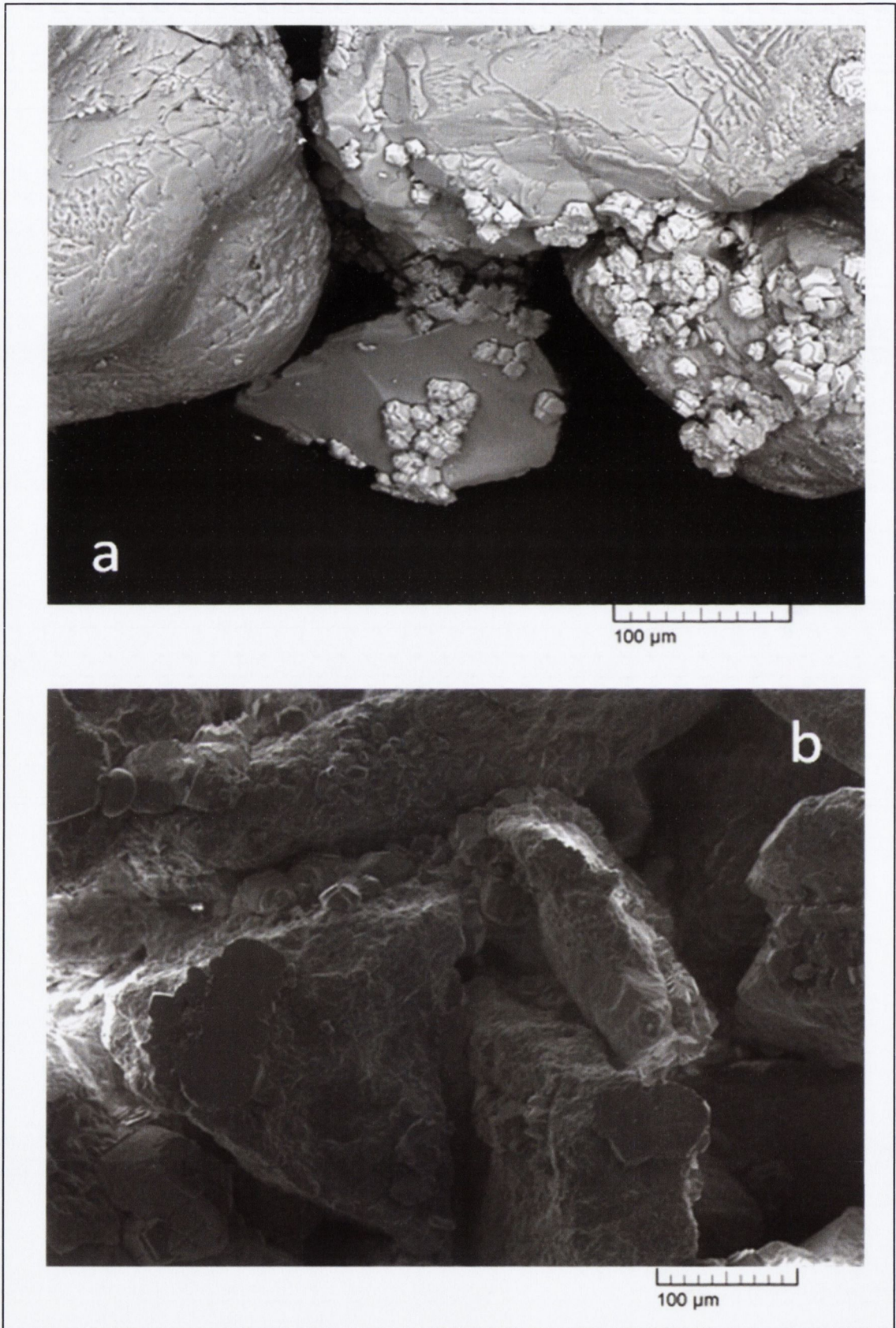
In addition to a different precipitation pattern observed for oligotrophic and eutrophic protocols, the treatment methods resulted in a different crystal mineralogy. This phenomenon is well illustrated in

Figure 5.4 which compares two medium samples of silica sand treated separately with an oligotrophic protocol and an eutrophic protocol (samples OA1 and EA1). The oligotrophic process is shown to predominantly produce large rhombohedra shaped crystals as illustrated in Figure 5.4(a). In contrast, the eutrophic process is shown to mostly produce the micritic dome-like structures seen in Figure 5.4(b). While positive identification of mineral species cannot be positively determined by SEM techniques, the minerals can be respectively interpreted as calcite and vaterite on the basis of crystal morphology (Zhou, Yao et al. 2010). Assuming that in both treatments the enzyme available was saturated, the high concentration of calcium ions (1 M) present in the oligotrophic cementation liquid meant that a relatively high  $[Ca^{2+}]/[CO_3^{2-}]$  ratio was determined in the circum-cellular space. Hence promoting the formation of calcite (Han, Hadiko et al. 2006). Conversely, the lower  $[Ca^{2+}]/[CO_3^{2-}]$  ratio determined in the eutrophic samples would promote the precipitation of vaterite (Chapter 3, Paragraph 1.1). Additionally, the nutrients supplied with the eutrophic process could have enabled further bacteria growth: locally increasing the amount of urease activity in the soil and in turn the level of local supersaturation. Hence, further contributing to the preferential precipitation of vaterite (van Paassen 2009).

### 1.5 SOIL MINERALOGY AND $CaCO_3$ DISTRIBUTION

A comparison was made between the distribution pattern of crystals precipitated on the surface of silica and carbonaceous sand particles for both oligotrophic and eutrophic protocols. The SEM observations reveal a widespread and abundant precipitation in carbonaceous soils whether oligotrophic or eutrophic methods were employed. This is particularly evident when referring to Figure 5.5 in which two fine sand samples of different mineralogy were identically treated with oligotrophic protocols (samples OB4 and OD4).





**Figure 5.5** Fine sand samples (OB4, OD4) identically treated with oligotrophic protocols: **(a)** silica sand, **(b)** carbonaceous sand. Precipitation is distinctly more abundant and widespread in carbonaceous sand.

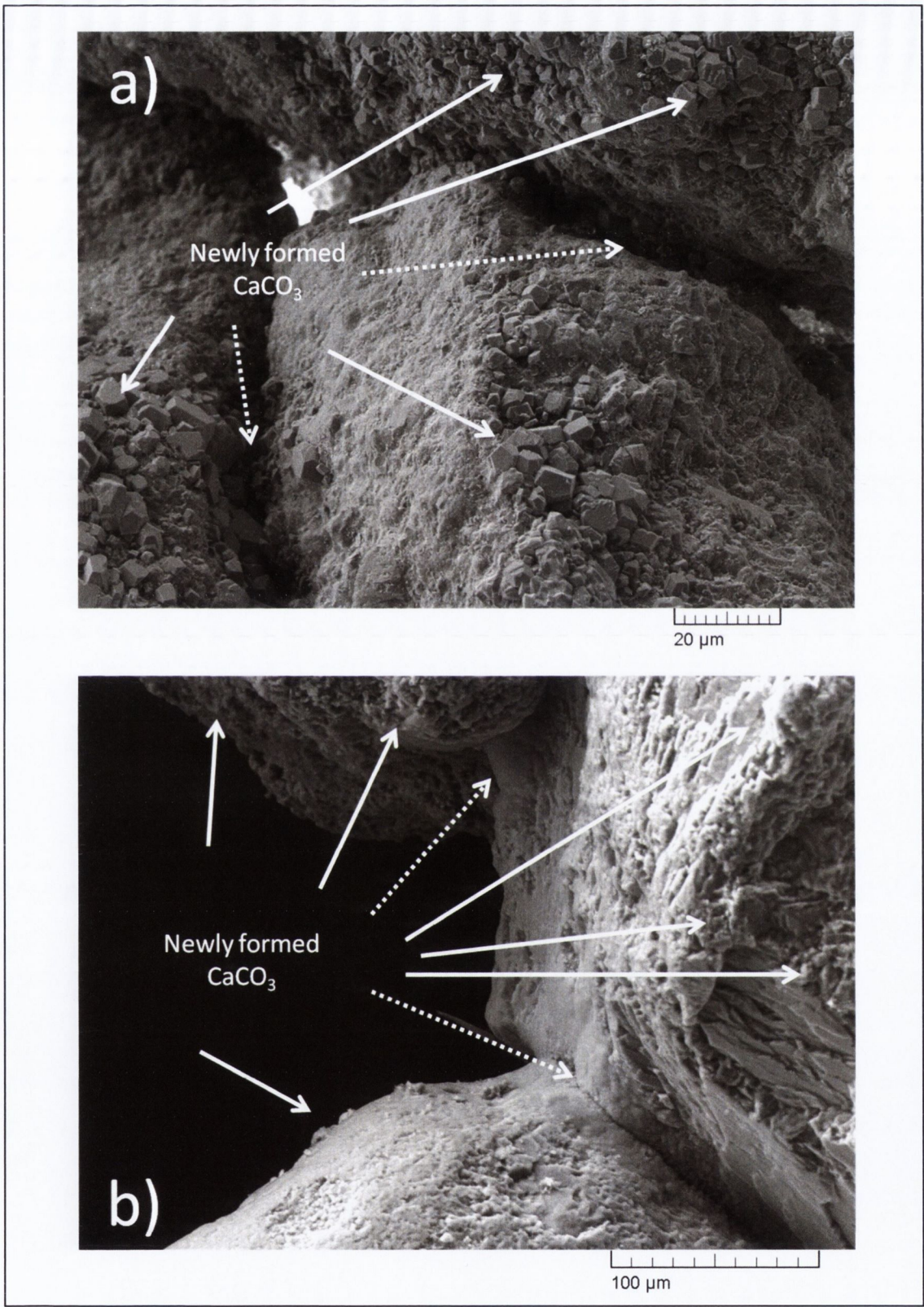


**Figure 5.6** Medium carbonaceous sand treated with **(a)** oligotrophic (sample OC4) and **(b)** eutrophic protocols (sample EC2). Arrows indicate large areas covered by newly formed carbonate as indicated by close observation of the topography (Appendix Two). Dashed arrows indicate bond-forming precipitates.

As expected, for oligotrophic treatments both samples show a relatively broad distribution of the precipitated carbonate but, as also observed by Van Paassen (2009), precipitation is distinctly more abundant and widespread in carbonaceous sand, Figures 5.5(b) and 5.6(a). A similar trend is observed in eutrophic samples. However, in carbonaceous samples, it is often difficult to detect the boundary between the precipitate and the host sand particle (Appendix Two, Annexes 4 and 10). This is due to the similarity of the mineral compositions and the micritic nature of the cement being precipitated (Figure 5.6(b)). The widespread distribution observed is attributed to the combination of abiotic precipitation processes promoted by the carbonate component of the sand particle (Lioliou, Paraskeva et al. 2007) and increased bacterial attachment on rough, carbonaceous surfaces (Scholl, Mills et al. 1990; Bhattacharjee, Ko et al. 1998; Shellenberger and Logan 2002). It is reasonable to assume that the consequence of this depositional pattern for carbonaceous sands would be an increase in efficiency. However, a corresponding decrease in the effectiveness would also be observed as a significant proportion of the precipitated calcium carbonate would not contribute to particle bonding.

## 1.6 INTERIM CONCLUSIONS

The results show that soil particle size has an impact on the amount of biomass retained during bioaugmentation. In fact, the calcium carbonate determination exercise shows that fine sand samples resulted in larger amounts of calcium carbonate being precipitated when compared with medium sand samples. The same results would also suggest that eutrophic protocols are less affected as a result of what is interpreted as ongoing bacterial growth during the treatment (Chapter 2, Paragraph 4). Particle size would therefore mostly impact on the viability of field applications of oligotrophic protocols. In fact, in this

case, the initial amount of bioaugmentation will have to account for encapsulation and cell lysis in order to achieve the specified calcium carbonate content. However, biofilm formation and bacterial growth in eutrophic treatments remain to be confirmed due to the experimental limitations of the work carried out.

Different deposition patterns are to be expected depending on the treatment protocol employed. While fixation promotes the attachment of bacteria and improved precipitation rates (Harkes, van Paassen et al. 2010), a significant proportion of the precipitated carbonate would not produce an increase in strength as it is not contributing to the formation of bonds between particles (Chapter 2, Paragraph 3). This appears to be less significant in eutrophically treated samples. In fact, in the mildly cemented samples obtained in this experiment, a substantial portion of bacteria became deposited at or near inter-particle contact points resulting in preferential deposition of carbonate at these locations. It is therefore expected that eutrophic treatment would result in higher efficacy of the treatment.

The mineralogical nature of the sand particles has a substantial impact on the distribution pattern of calcium carbonate. Carbonaceous matrixes produced visibly larger amounts of carbonate precipitation when compared to silica sand. This was attributed to abiotic processes which have enhanced the biomediated precipitation of calcium carbonate (Chapter 2, Paragraph 7 and Chapter 3, Paragraph 1). However, calcium carbonate was broadly distributed over the particle surface indicating that higher precipitation efficiency could come at the cost of reduced efficacy of the treatment.

## 2) EXPERIMENT N. 2: CARBONATE BOND

### 2.1 GENERAL

Experiment N. 2 was carried out to investigate in more detail the carbonate bond being formed at the pore scale when employing liquid injection methods in saturated soils. The effect of different treated materials and different treatment protocols was evaluated. The test method used both oligotrophic and eutrophic injection protocols in small columns prepared using two different sand materials. The treated materials were subsequently observed under the scanning electron microscope to describe the bonding structures being formed and failure thereof. In order to observe the formation of individual bonds and structures the experiment was conducted by limiting the amount of bioaugmentation. This allowed for the clear observation of isolated deposits which might have been obscured by the coalescence or overgrowth of carbonate in the presence of large amounts of urease.

### 2.2 EXPERIMENTAL SET-UP

A total of 4 miniature test columns were prepared as for Experiment N. 1 (Figure 5.1) using plastic vials with 25 mm diameter and 110 mm height. The test samples were prepared using fine (300  $\mu\text{m}$  -150  $\mu\text{m}$ ) silica and carbonaceous sand. The sand was pluviated under water to avoid the inclusion of air pockets and vibrated to an approximate porosity of 40%. Details of each column are provided in Table 5.5. All 4 columns were initially flushed from top to bottom at a flow rate of 100 mL  $\text{h}^{-1}$  with double deionised water. Bioaugmentation was achieved by injecting, at the same rate, 5 mL of *S. pasteurii* suspension having 5.38  $\text{OD}_{600}$  and UA of 6.71  $\text{mM min}^{-1}$ .

Following bioaugmentation, 2 samples were treated employing an oligotrophic protocol and immediately received 30 mL

(approximately 1.5 pore volumes) of saline fixation fluid aseptically prepared with 7.35 g/L (50 mM) of calcium chloride dehydrate. After the fixation phase, a schedule of five 30 mL injection rounds (100 mL h<sup>-1</sup>) was applied at 24 hour intervals and samples were harvested 24 hours after the last treatment. The oligotrophic cementation medium was composed as follows: 60 g/l (1 M) of urea and 147 g/l (1 M) of calcium chloride dihydrate.

**Table 5.5** Salient characteristics of the columns and treatments employed. Treatments were delivered by means of injection methods.

<b>ID</b>	<b>Mineralogy</b>	<b>Fraction</b>	<b>Treatment</b>
OE1	Silica	D (fine sand)	Oligotrophic
OE2	Carbonaceous	D (fine sand)	Oligotrophic
EE1	Silica	D (fine sand)	Eutrophic
EE2	Carbonaceous	D (fine sand)	Eutrophic

The remaining 2 columns were treated employing eutrophic protocols. In these, bioaugmentation was followed by five 30 mL rounds of eutrophic cementation liquid applied at 3 hour intervals (100 mL h<sup>-1</sup>) and samples were harvested 3 hours after the last treatment. The eutrophic cementation liquid was prepared aseptically as follows: 5 g/L yeast extract, 10 g/L (170 mM) urea and 22 g/L (150 mM) of calcium chloride dihydrate.

### 2.3 OLIGOTROPHIC BOND FORMATION AND FAILURE

Figure 5.7 shows a typical bond structure formed between silica sand particles treated with an oligotrophic protocol (sample OE1). The image illustrates that for the oligotrophic process the bond was formed by one large structure that grew continuously over time and with increasing treatment rounds until the soil particles were cemented together. The image also shows the presence of globular deposits which

were previously interpreted by Van Paassen (2009) as spherulites (sphere-shaped amorphous calcium carbonate): consequence of localised high supersaturation. However, amorphous calcium carbonate was only very occasionally observed in this experiment due to the limited bioaugmentation employed.

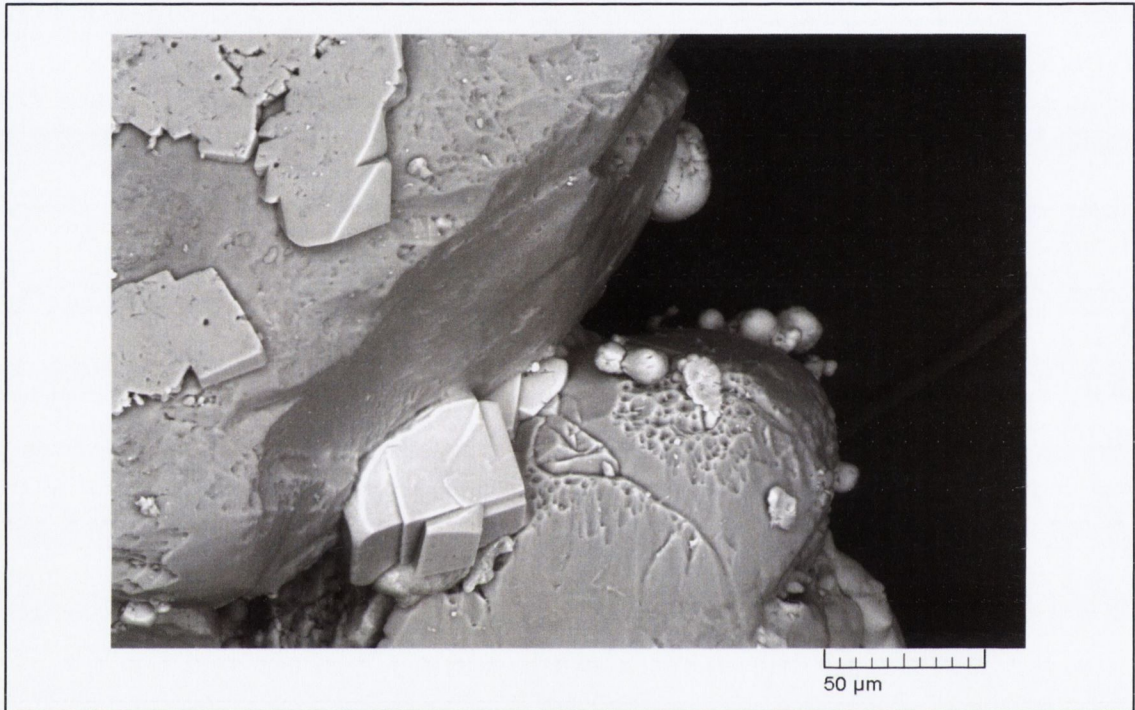


**Figure 5.7** Detail of a large calcite structure bonding two silica sand particles after oligotrophic treatment (sample OE1).

Failure of the bond was seen to usually occur along the bond-particle interface and can be clearly observed in Figure 5.8. The image shows a clean break between two silica particles that were previously connected by a carbonate bond. The concave imprint of the detached particle is discernible in the exposed surface of the carbonate bond. At the level of cementation obtained during the experiment, individual bonds such as those shown in Figures 5.7 and 5.8 are a limit case and a rare occurrence. Complex bonds, such as the one seen in Figure 5.9, are more often observed. In the image, it is possible to discern the partial imprint of the detached particle in each individual crystal. It would appear that these small polycrystalline structures increase in size while

treatment progresses: ultimately producing the monolithic bonds observed in the previous figures.

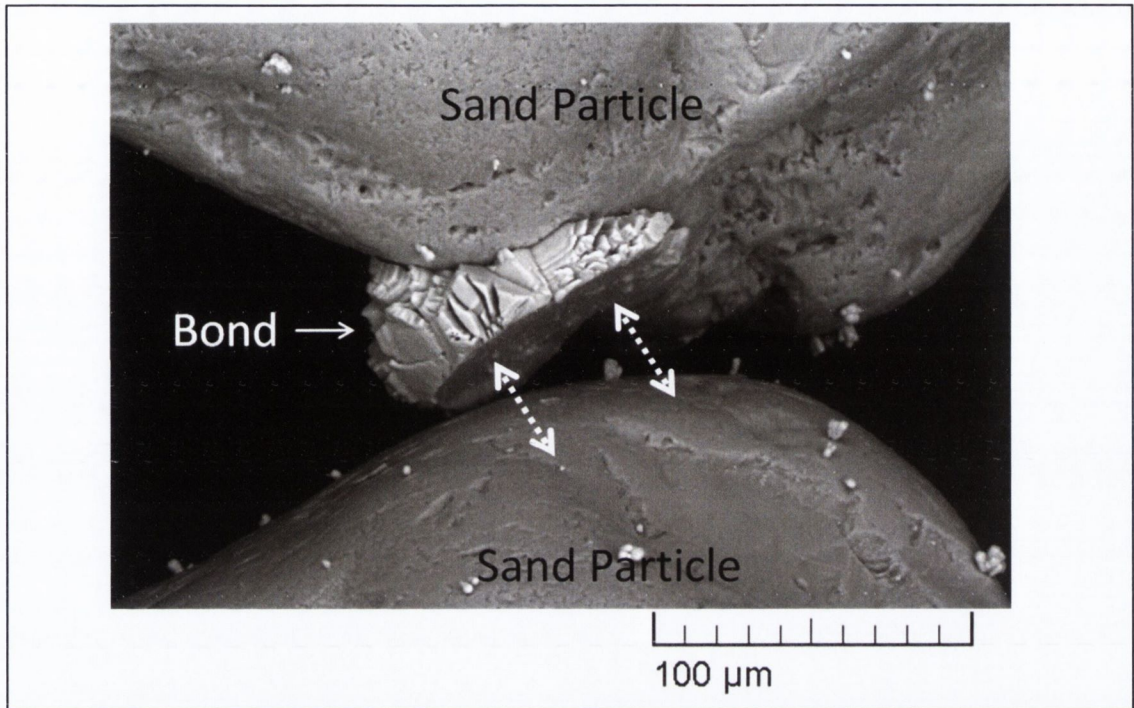


**Figure 5.8** Detail of a bond-particle failure system observed in silica sand treated with oligotrophic protocols (sample OE1).

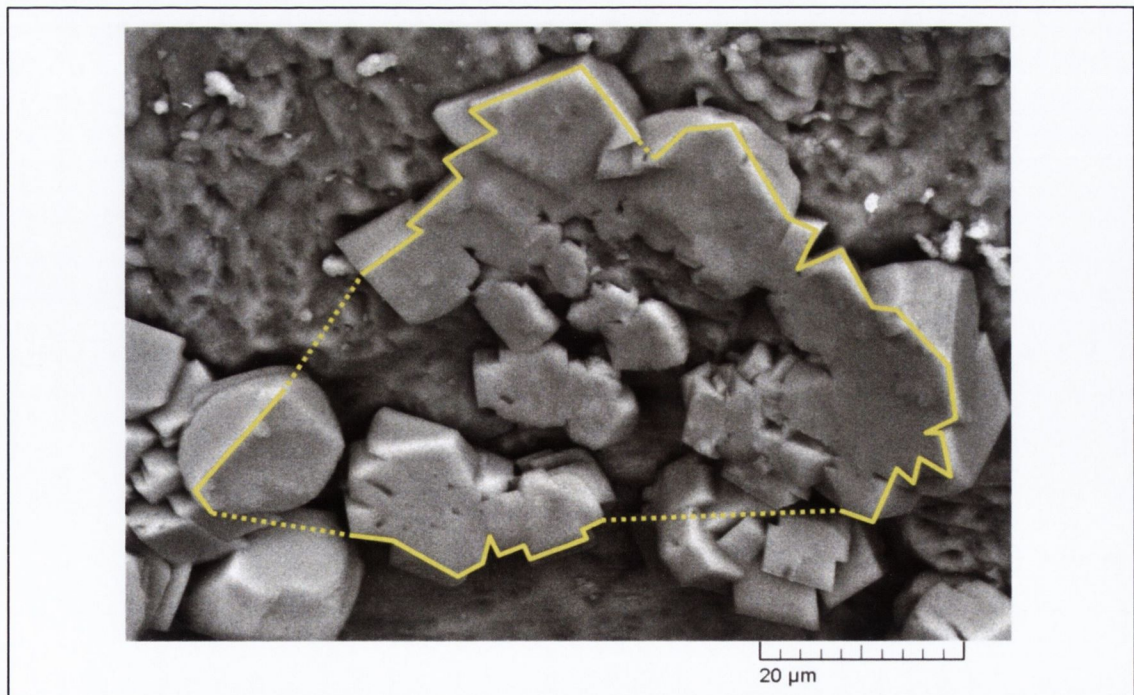


**Figure 5.9** Detail of a bonding structure (polycrystalline) observed in silica sand treated with oligotrophic protocols (sample OE1). The outline of the imprint left from a detached sand particle is traced over the image.



A detail of an exposed bond-particle failure surface is shown in Figure 5.10. In the image, it is possible to observe the mark left by individual bacteria, visible as rod-shaped gaps in the carbonate. Strained and wedged bacteria were deposited during bioaugmentation and were then encapsulated by the cementing material (Cuthbert, Riley et al. 2012). This would indicate that late precipitation, leading to the increased size of the bond, would mostly occur as a result of thermodynamically favoured processes where the carbonate surface of the bond would act as a preferential surface for deposition.

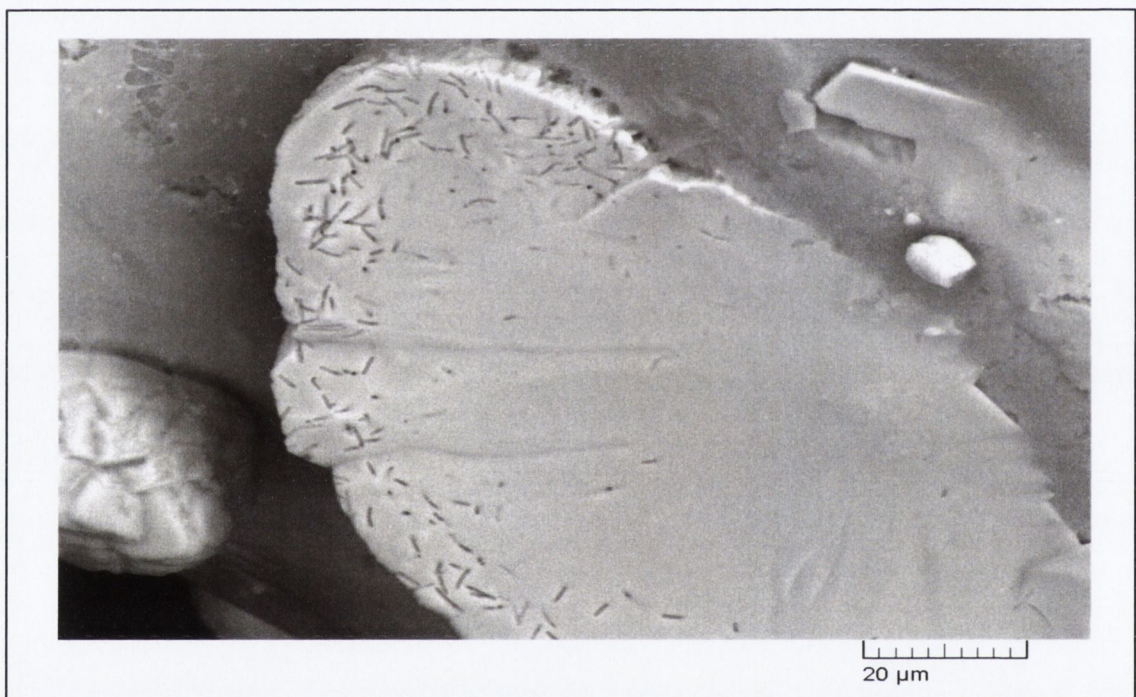


**Figure 5.10** Close-up of an exposed bond-particle (silica) failure surface. Bacteria imprints are visible as small cylindrical gaps (dark grey) in the bond surface (Appendix 2, Annex 12). The convex shape of the surface is a cast of the detached particle surface (sample OE1).

The large majority of failure surface observed in silica sand samples was located along the bond-particle surface. However, in carbonaceous sand samples, it was not possible to identify such clear failure surfaces. As expected, carbonaceous samples resulted in larger amounts of calcite being precipitated after oligotrophic treatment (Experiment N. 1). Although it was difficult to make a distinction between

newly formed carbonate and the sand particles, the structure of the bonds was similar to that observed in silica sand samples, as shown in Figure 5.11.

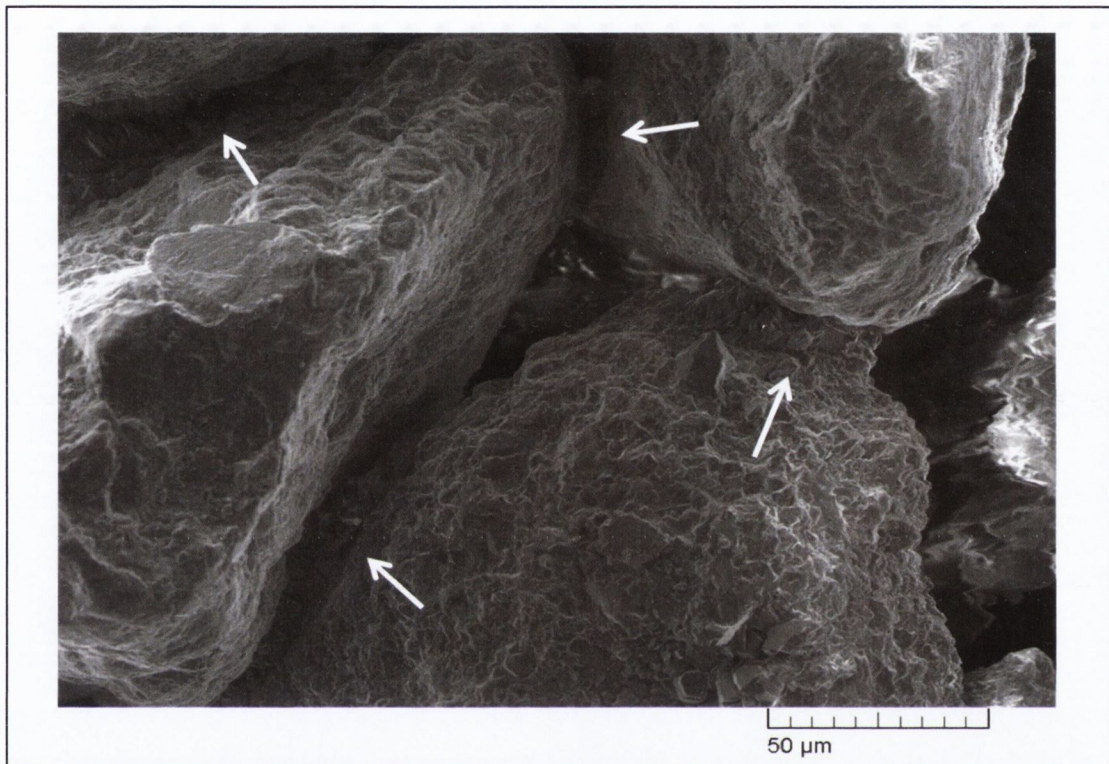


**Figure 5.11** Carbonaceous sand treated with oligotrophic protocols. Arrows indicate where bonds between particles are formed (sample OE2). The bonds are formed by monolithic/polycrystalline structures similar to those observed for silica sand. However, these are more extended and less isolated due to the abundant and widespread precipitation of calcite.

The absence of clear bond-particle failure surfaces can be explained by taking into account the mineral nature of the particle. Carbonaceous particles would provide a relatively rough surface (Scholl, Mills et al. 1990) to which the bond structure is attached providing a larger contact surface and a strong physical link between the two. Additionally, the chemical affinity between the particle surface and the bonding mineral would result in strong chemical links being formed. The two phenomena combined would therefore explain the irregular failure patterns observed.

## 2.4 EUTROPHIC BOND FORMATION AND FAILURE

As evident in Figure 5.12, the structure of the carbonate bond developed under eutrophic conditions is significantly different from that obtained with oligotrophic treatments. The inter-particle bonds formed during an eutrophic process display a more complex structure, characterised by the presence of a suture line.

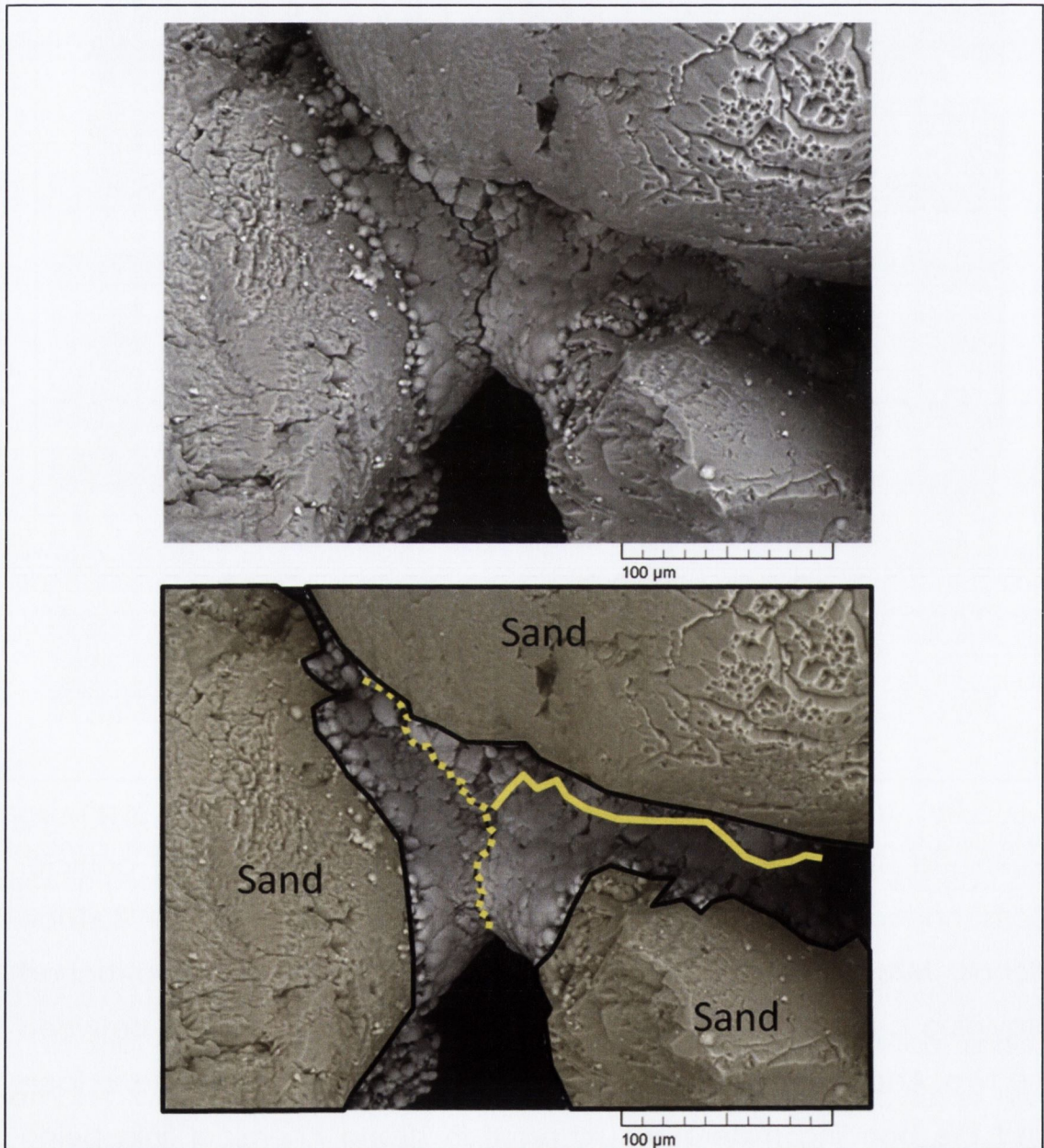


**Figure 5.12** Detail of a carbonate structure bonding three silica sand particles after eutrophic treatment. Incipient failure (crack) can be observed along one side of the suture line (sample EE1). The suture line is highlighted in the image at the bottom. The dotted line indicates the incipient failure.

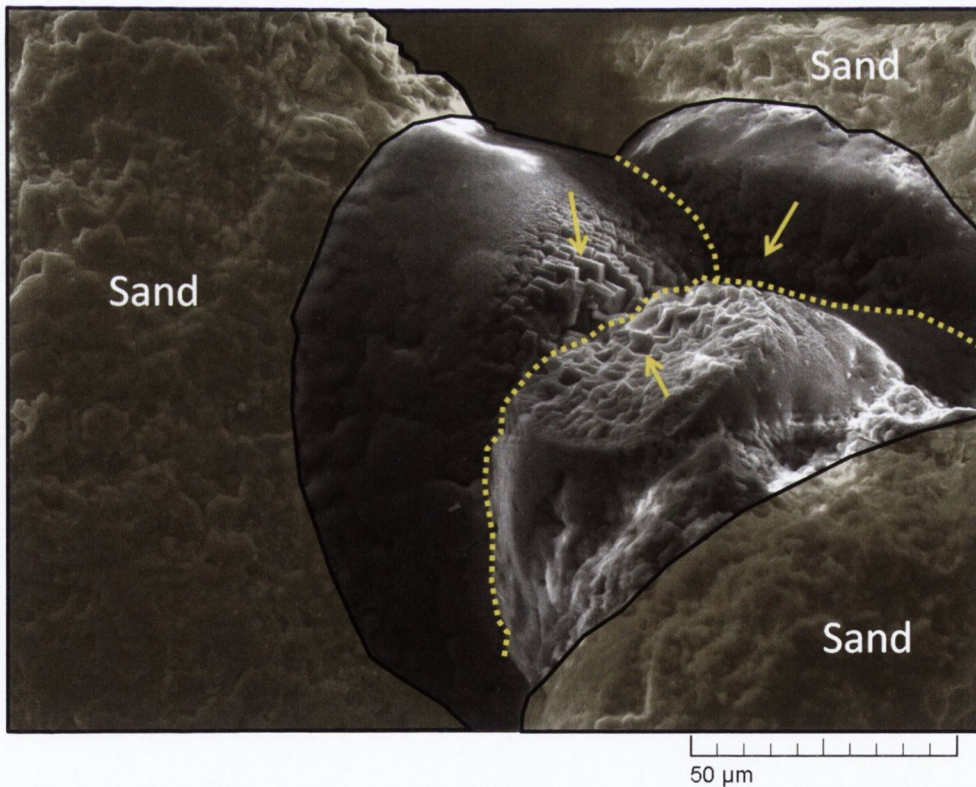
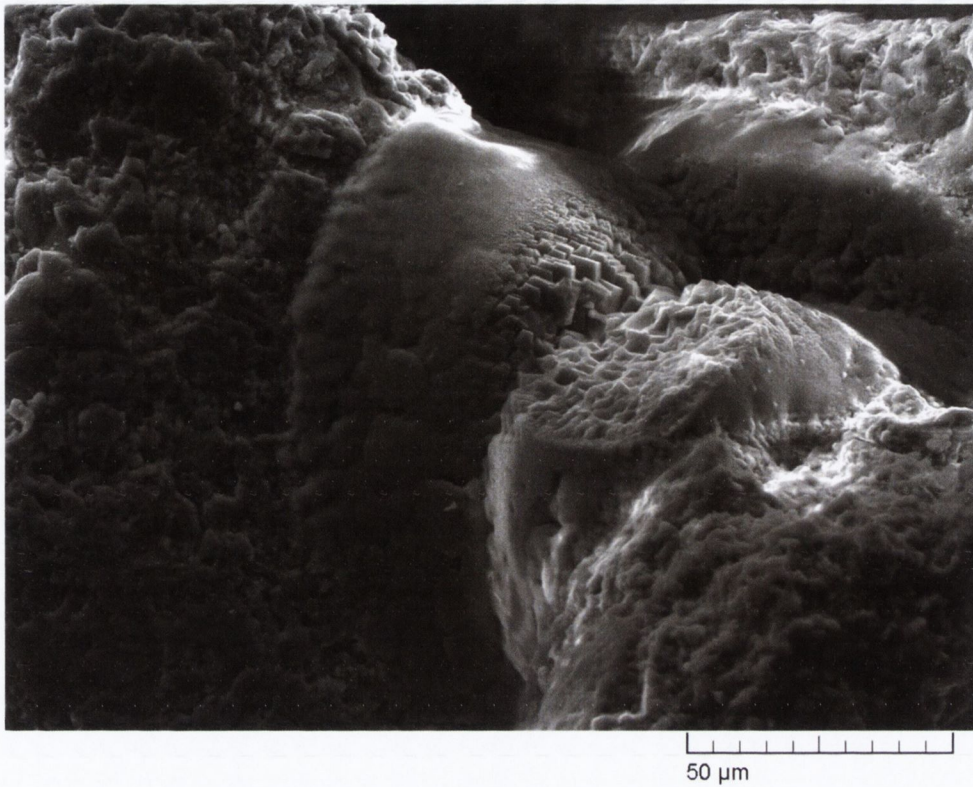


**Figure 5.13** Detail of a carbonate structure bonding three carbonaceous sand particles after eutrophic treatment (sample EE2). At bottom, crystalline calcite (arrows) can be observed along the suture lines (dash-dot line). The bond structure is consistent with that observed in silica sand samples.

The bond is formed by the coalescing of numerous individual domes into an interlocking structure between the particles. The suture is formed when the deposition occurring on the surface of one particle meets that occurring on the other particle. In Figure 5.12 the suture line is visible in the shape of an approximate upside down Y where one side shows an incipient failure (fracture). As shown in Experiment N. 1, vaterite domes are preferentially precipitated in the early stages of carbonate precipitation during eutrophic treatments. However, as more clearly seen in Figure 5.13, the suture is typically characterised by a jagged edge where the mineral form precipitated is more evidently crystalline calcite. Diffusion is a main limiting factor in these tight spaces and would shift the controls of the reaction towards the thermodynamically favoured precipitation of calcite.

When compared with oligotrophically treated samples, the failure patterns observed in eutrophically treated silica sand displayed a more diverse set of patterns. Hybrid failure surfaces intersecting the suture line (bond-bond failure), as well as bond-particle surfaces, were the most common where bonds larger than 100  $\mu\text{m}$  were involved. Instead, bond-particle failures as that observed in Figure 5.14, were more common in bonds smaller than 100  $\mu\text{m}$ : probably a result of the relatively small contact area between the bond and the particle. It should be noted that a failure pattern as the incipient one seen in Figure 5.12 would produce a hybrid failure mechanism as described by the conceptual model proposed by DeJong et al. (2010).

Eutrophic carbonaceous samples displayed the same absence of clear failure surfaces noticed in oligotrophic samples: confirming the relevance of surface roughness and chemical affinity in determining the formation and consequent failure mechanism observed at the pore scale.



**Figure 5.14** Detail of a carbonate structure bonding three silica sand particles after eutrophic treatment. The arrow indicates where a detached particle left behind a smooth concave imprint (sample EE1).

The bond formation mechanism occurring during an eutrophic treatment can be understood by referring to Figure 5.15. In this image, the bond side of a bond-particle failure surface is exposed to reveal sets of concentric circles, marked A to C, that can be interpreted as the cross-section of the carbonate domes formed by subsequent generations of bacteria. It is reasonable to conclude that the rings formed in the calcium carbonate formations (marked as I to V) are the result of environmental variations induced in the pore space by the consecutive injection rounds of cementation liquid. It can therefore be assumed that the dome characterised by 5 concentric rings, A, has started its formation at the very beginning of the treatment while domes

with 4 rings, *B*, were initiated between the first and the second injection of cementation fluid by a new generation of bacteria.

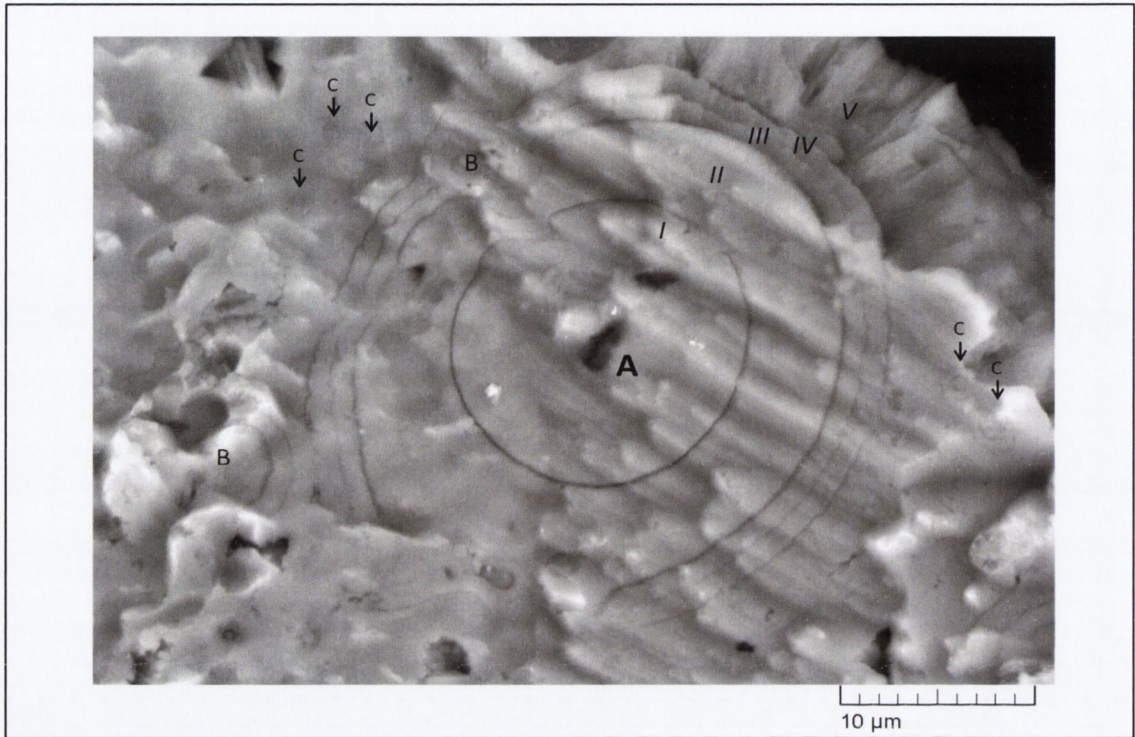


**Figure 5.15** Close-up of the surface along a particle-bond failure surface showing a time record of the precipitation process during the five round eutrophic treatment. Letters A, B and C indicate subsequent generations of crystal domes. Numbers I to V identify the calcium carbonate rings formed between treatments (sample EE1).

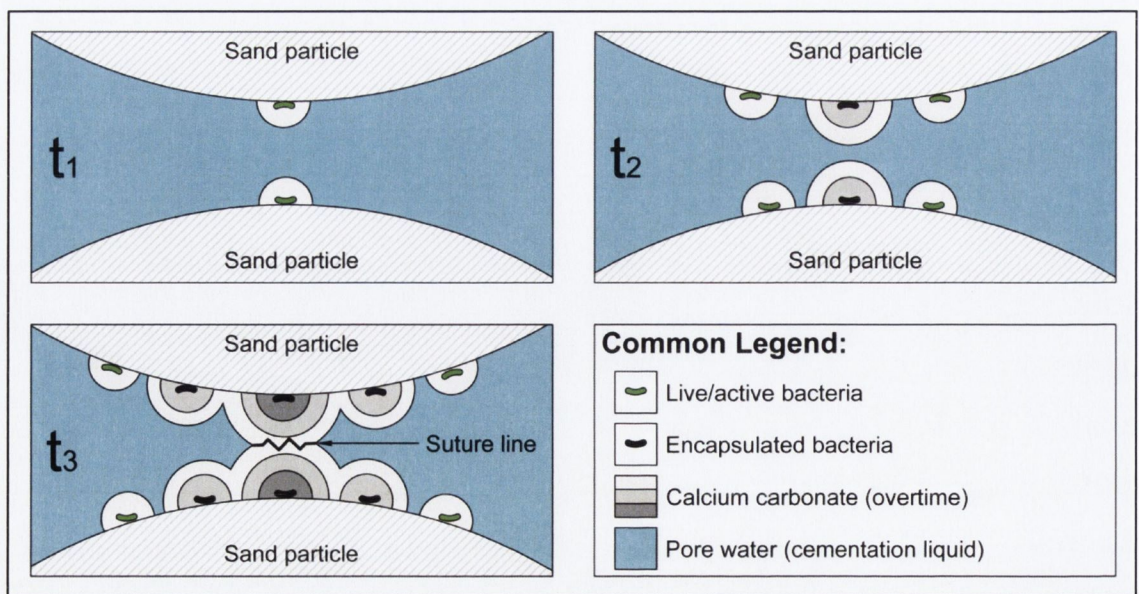


**Figure 5.16** Schematic representation of bond formation under eutrophic treatment conditions.

A schematic representation of the process is provided in Figure 5.16. This formation model is corroborated by the fact that the youngest generations visible, marked as C and characterised by 3 rings, are located the farthest away from the centre of what is considered to be the ancestral set of five rings, A. Bacterial growth and the formation of a urease active biofilm can also be inferred from Figure 5.17. The image shows the surface of a fine gravel (approximately 2 mm) taken from the filter packing of an eutrophically treated test column (EE2). The development of the carbonate concretion visible over the gravel's surface follows the typical growth pattern of *S. pasteurii* colonies formed on agar plates. Transition from micritic dome-like structures, visible on the margins of the concretion, to larger crystals, visible in the centre, would be evidence that Oswald ripening is also occurring where the biological activity is reduced by encapsulation. Rapid, biomediated precipitation is, however, occurring on the fringes of the biofilm where live, multiplying bacteria are present.

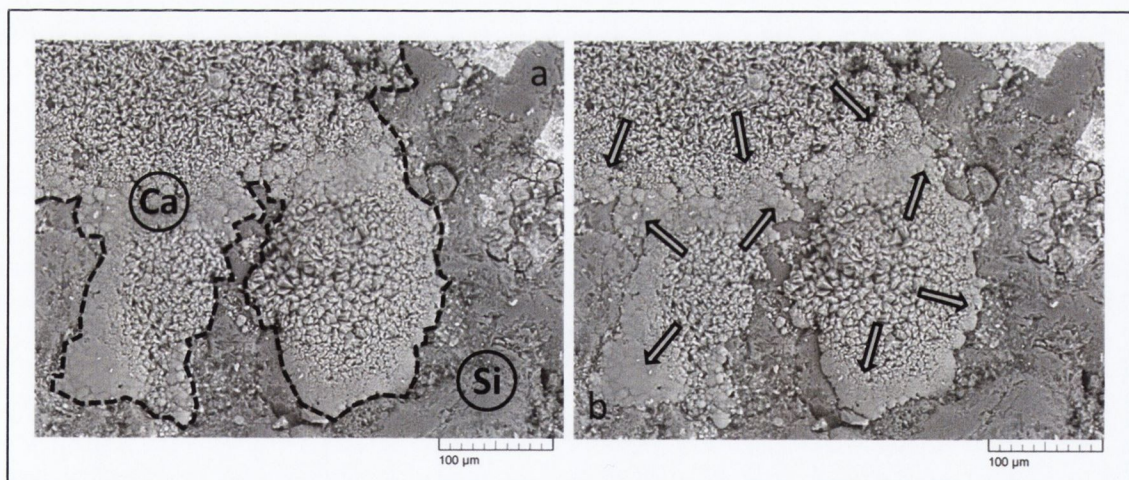


**Figure 5.17** Surface of a fine gravel grain (approximately 2 mm) taken from the filter packing of an eutrophic sample: **(a)** limit between areas covered by calcium carbonate and exposed surface of the silica grain; **(b)** arrows indicate the direction in which three colonies of ureolytic bacteria are expanding over the particle's surface.



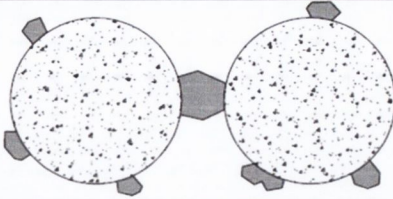
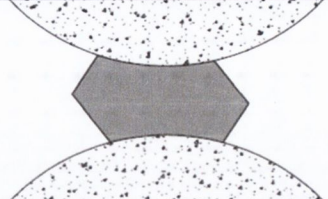
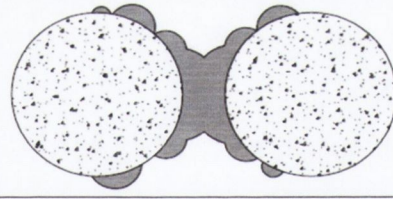
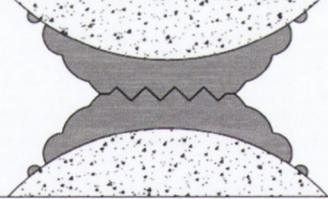
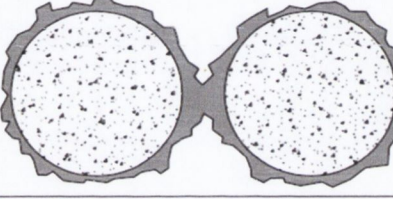
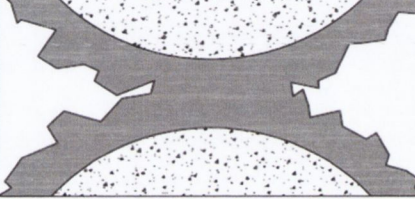
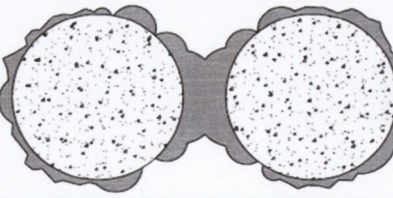
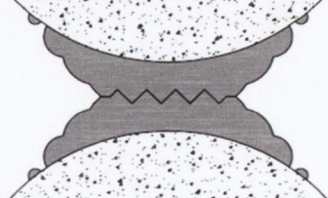
It is noted that progressing the cementation beyond what achieved in this experiment, would likely produce a coating of small carbonate crystals over the whole surface as observed in the SEM images produced employing mildly concentrated eutrophic cementation liquids (Al Qabany, Soga et al. 2012). Additionally, if it is assumed that bacterial deposition is predominant at inter-particle contact points (Experiment N. 1), the resulting bond formation model would closely relate to the hybrid model proposed by DeJong et al. (2010).

## 2.5 INTERIM CONCLUSIONS

The cementation observed in the SEM images assisted in describing the mechanisms leading to the formation of a bond between sand particles. The results obtained with eutrophic protocols support the validity of the conceptual formation/failure model proposed by DeJong et al. (2010) for eutrophic treatment of silica sand (Chapter 2, Paragraph 3). However the broader scope of this experiment highlighted the limitations of its validity when considering different mineral matrixes, or different treatment protocols (Figure 5.18). Additionally, the significance of bacterial growth during eutrophic treatment was highlighted by the effects that this has on the bond formation process as well as the covering of particle surfaces with calcium carbonate.

The difference between the failure mechanisms observed in oligotrophic silica samples and carbonaceous samples would indicate that the resulting strength increase is affected by the nature of the soil matrix. This would be mostly due to the material (or interface) involved in the failure. Instead, SEM images of eutrophic samples have shown that the limited size of the bond during the early stages of treatment could determine weak bond-particle failure surfaces and therefore result in limited strength increase. However, it should be noted that the relevance of this observation in field applications could be limited as the

level of cementation required in such cases would be higher than what obtained in the experiment.

<b>Oligotrophic Protocol</b>	<b>Silica</b>		
		<p>Bacterial attachment occurs over the whole surface of the particles with a slight preference for inter-particle contact areas. Isolated precipitation of calcium carbonate results from biological processes at the locations of attachment. Crystals are loosely fixed on the surface. The bond usually forms from the growth of one or more crystals that bridge between particles.</p>	<p>Once the bond is formed particle-bond interfaces are likely failure surfaces. Stress, surface roughness and chemical affinity will determine the forces acting on the interface.</p>
<b>Eutrophic Protocol</b>	<b>Silica</b>		
		<p>Bacterial attachment is markedly preferential around inter-particle contact areas. Precipitation results from biological processes at the locations of attachment. The area interested by precipitation extends as a result of biofilm formation. Crystals are loosely fixed on the surface. The bond forms by interpenetration of complex structures being formed on each side of the gap.</p>	<p>The bond being formed can be geometrically complex along the suture line. The most likely failure surface is along the suture and the pattern will depend on the geometry of the suture. At early stages of the cementation process the particle-bond interface has shown to be a potential failure surface in light of (1) the limited chemical affinity between the particle and the bond material and (2) the relatively low roughness of the particle surface.</p>
<b>Oligotrophic Protocol</b>	<b>Carbonaceous</b>		
		<p>Bacterial attachment homogeneously occurs over the whole surface of the particles. Widespread precipitation of calcium carbonate results from the combination of biological processes (localised) and abiotic processes. New crystals are intimately connected to the particle. The bond forms as a result of the increasing thickness of precipitate.</p>	<p>The bond being formed can be geometrically complex. The failure pattern and surface depend on (1) the geometry of the bond and (2) localised weaknesses in the particle. A clear particle-bond interface cannot be identified due to the chemical/mineralogical affinity between particle and bond.</p>
<b>Eutrophic Protocol</b>	<b>Carbonaceous</b>		
		<p>Bacterial attachment is markedly preferential around inter-particle contact areas. Widespread precipitation of calcium carbonate results from the combination of biological processes (localised) and abiotic processes. The area interested by biological precipitation extends as a result of biofilm formation. New crystals are intimately connected to the particle. The bond forms by interpenetration of complex structures being formed on each side.</p>	<p>The bond being formed can be geometrically complex. The failure pattern and surface depend on (1) the geometry of the bond and (2) localised weaknesses in the particle. A clear particle-bond interface cannot be identified due to the chemical/mineralogical affinity between particle and bond.</p>

**Figure 5.18** Conceptual model: bond formation and failure at the pore scale for different treatment protocols and soil mineral matrixes.

### 3) EXPERIMENT N. 3: MAGNESIUM IN MICP APPLICATIONS

#### 3.1 GENERAL

Experiment N. 3 was designed to evaluate the potential offered to the MICP method by the addition of magnesium ions to the cementation solution. Magnesium additions were investigated because magnesium carbonate is known to co-precipitate with calcium carbonate to potentially produce dolomite *in-lieu* of calcite. In particular, primary dolomite,  $MgCa(CO_3)_2$ , is known to precipitate in biomediated ureolytic reactions in the presence of magnesium ions. Precipitating dolomite would potentially improve the long term performance of MICP soil improvement applications due to its higher resistance to chemical weathering when compared to calcite.

#### 3.2 EXPERIMENTAL SET-UP

Two sets of plastic test chambers were prepared in sealable 200 mL sterile tubs. A first set of four chambers was prepared, as shown in Table 5.6, to investigate the addition of magnesium ions to the cementation solution in the context of oligotrophic protocol.

**Table 5.6** Preparation of Mg-rich oligotrophic reaction liquids used in the test chambers.

ID	UA	[Ca <sup>2+</sup> ]	[Mg <sup>2+</sup> ]	Urea	pH
OA1	5 mM h <sup>-1</sup>	0.4 M	0.6 M	1.0 M	8.9
OA2	10 mM h <sup>-1</sup>	0.4 M	0.6 M	1.0 M	8.9
OB1	5 mM h <sup>-1</sup>	0.5 M	0.5 M	1.0 M	8.9
OB2	10 mM h <sup>-1</sup>	0.5 M	0.5 M	1.0 M	8.9

An additional eight chambers were prepared, as shown in Table 5.7, to investigate the addition of magnesium ions in the context of

oligotrophic protocols. All the work solutions were prepared aseptically using previously prepared stock solution and volume was adjusted with double dionised sterile water. pH was adjusted using 4 M NaOH. The required urease activity for each set-up was achieved by adding appropriate volumes of a fresh *S. pasteurii* culture having an OD<sub>600</sub> of 5.02 and a UA of 5.11 mM min<sup>-1</sup>.

**Table 5.7** Preparation of Mg-rich eutrophic reaction liquids used in the test chambers.

ID	UA	[Ca <sup>2+</sup> ]	[Mg <sup>2+</sup> ]	Urea	Y.E.*	pH
EA1	5 mM h <sup>-1</sup>	0.1 M	0.1 M	0.2 M	10 g/L	8.9
EA2	5 mM h <sup>-1</sup>	0.1 M	0.15 M	0.25 M	10 g/L	8.9
EA3	5 mM h <sup>-1</sup>	0.1 M	0.2 M	0.3 M	10 g/L	8.9
EA4	5 mM h <sup>-1</sup>	0.1 M	0.25 M	0.35 M	10 g/L	8.9
EB1	5 mM h <sup>-1</sup>	0.2 M	0.2 M	0.4 M	10 g/L	8.9
EB2	5 mM h <sup>-1</sup>	0.2 M	0.25 M	0.45 M	10 g/L	8.9
EB3	5 mM h <sup>-1</sup>	0.2 M	0.3 M	0.5 M	10 g/L	8.9
EB4	5 mM h <sup>-1</sup>	0.2 M	0.35 M	0.55 M	10 g/L	8.9

After inoculation with *S. pasteurii*, each chamber was left to react at room temperature (approximately 20° C) for 72 hours. Samples were collected by filtering the liquid from the chamber after having scraped the internal surfaces with a metal blunt-edge instrument to dislodge the precipitate formed on the surfaces. The precipitate was collected on 0.22 µm filter pads and prepared for XRD analysis.

### 3.3 PRECIPITATED MINERAL FORMS

Overall, the experimental conditions employed failed to induce the formation of dolomite. Figure 5.19 shows the full XRD peak analysis plot produced for sample OA2. While sample OA2 is presented for

illustrative purposes, the present discussion applies to all of the samples analysed. Plots of the full set of samples are provided in Appendix Two.

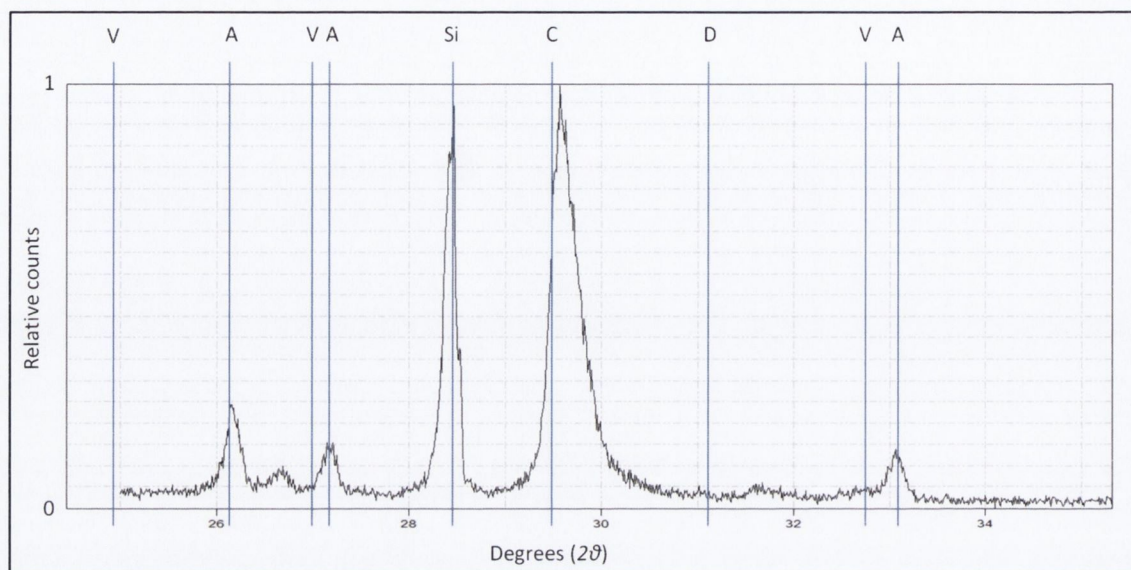


**Figure 5.19** XRD peak analysis of sample OA2. Vertical lines indicate the position of diagnostic peaks for: **(V)** vaterite, **(A)** aragonite, **(C)** calcite, **(D)** dolomite and **(Si)** quartz standard.

The vertical lines in Figure 5.19 illustrate the position of the diagnostic peaks for different minerals. OA2 was the only sample in which the formation of aragonite was observed. This could not be definitively explained and was interpreted as an experimental anomaly. Vaterite, present in similar experiments without magnesium (van Paassen 2009), was absent in all of the samples. This would indicate that, consistently with the literature (Meldrum and Cölfen 2008), the presence of magnesium promoted the formation of more stable forms of calcium carbonate. Interestingly, Mg-calcite was formed *in-lieu* of pure calcite.

This can be observed in Figure 5.20. The graph shows a close-up, around the  $d_{104}$  peak for calcite, of the plot recorded for sample OA2 (blue curve) against a pure calcite sample (black curve). The C to C' peak shift observed in Figure 5.20 is a consequence of the substitution of magnesium ions in the crystal lattice (Lumsden 1979).

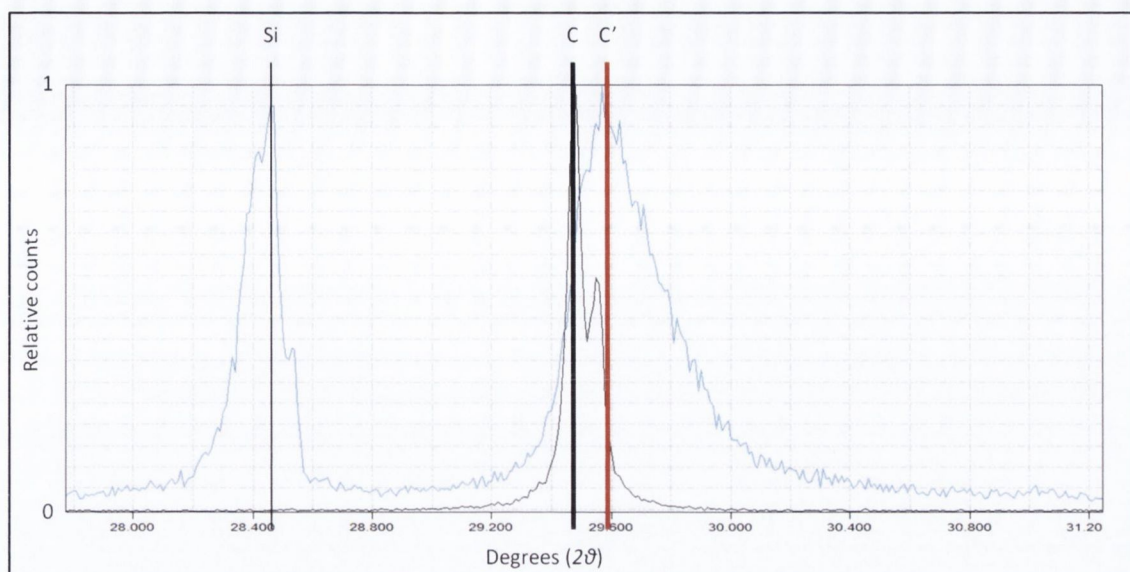


**Figure 5.20** XRD peak analysis of sample OA2 (blue) and of a pure calcite standard (black). Detail of the  $d_{104}$  calcite peak highlighting the shift in the sample's peak (C→C').

**Table 5.8** XRD determination of calcium content in Mg-calcite (oligotrophic). The calcium content was determined by the shift in the peak for the [104] plane. Computed values of d-spacing are also reported (Chapter Four, Paragraph 4).

ID	[104] Peak ( $2\theta$ )	d-Spacing (Å)	[CaCO <sub>3</sub> ] (% mole)
OA1	29.60°	3.0143	92.8%
OA2	29.57°	3.0173	93.8%
OB1	29.54°	3.0203	94.8%
OB2	29.53°	3.0213	95.1%

Tables 5.8 and 5.9 show the content (% mole) of calcium carbonate within the lattice of the Mg-calcite precipitated in each set-up. As shown by the values reported in the tables, the addition of magnesium resulted in the formation of low Mg-calcite with magnesium substituting up to 10.53% mole of calcium. By plotting the data obtained for oligotrophic samples (Figure 5.21), it is possible to observe that higher initial urease activity resulted in a lower level of substitution. This would indicate that the higher supersaturation achieved by employing an

initial UA of 10 mM h<sup>-1</sup> increased the precipitation rate of calcium carbonate but had only limited effect on the inclusion rate of magnesium. Figure 5.21 also shows that an increase in the Ca<sup>2+</sup> : Mg<sup>2+</sup> molar ratio of the initial solution produces a higher grade of magnesium inclusion.

**Table 5.9** XRD determination of calcium content in Mg-calcite (eutrophic). The calcium content was determined by the shift in the peak for the [104] plane. Computed values of d-spacing are also reported (Chapter Four, Paragraph 4).

ID	[104] Peak (2θ)	d-Spacing (Å)	[CaCO <sub>3</sub> ] (% mole)
EA1	29.53°	3.0213	95.11%
EA2	29.60°	3.0143	92.78%
EA3	29.63°	3.0114	91.78%
EA4	29.70°	3.0044	89.47%
EB1	29.53°	3.0213	95.11%
EB2	29.58°	3.0163	93.44%
EB3	29.61°	3.0133	92.45%
EB4	29.62°	3.0123	92.12%

This can better be observed in Figure 5.22 where the results of all the samples (oligotrophic and eutrophic) treated with 5 mM h<sup>-1</sup> initial UA are plotted against the initial Ca<sup>2+</sup> : Mg<sup>2+</sup> ratio. As expected, the percentage of substitution increases when lowering the ratio (Liebermann 1967; Loste, Wilson et al. 2003). However, the results show that the initial molar ratio is a controlling factor over the initial calcium concentration: starting concentrations of 0.1 M (EA series), 0.2 M (EB series), 0.4 M (sample OA1) and 0.5 M (sample OB1) had no noticeable effect (Figure 5.23).

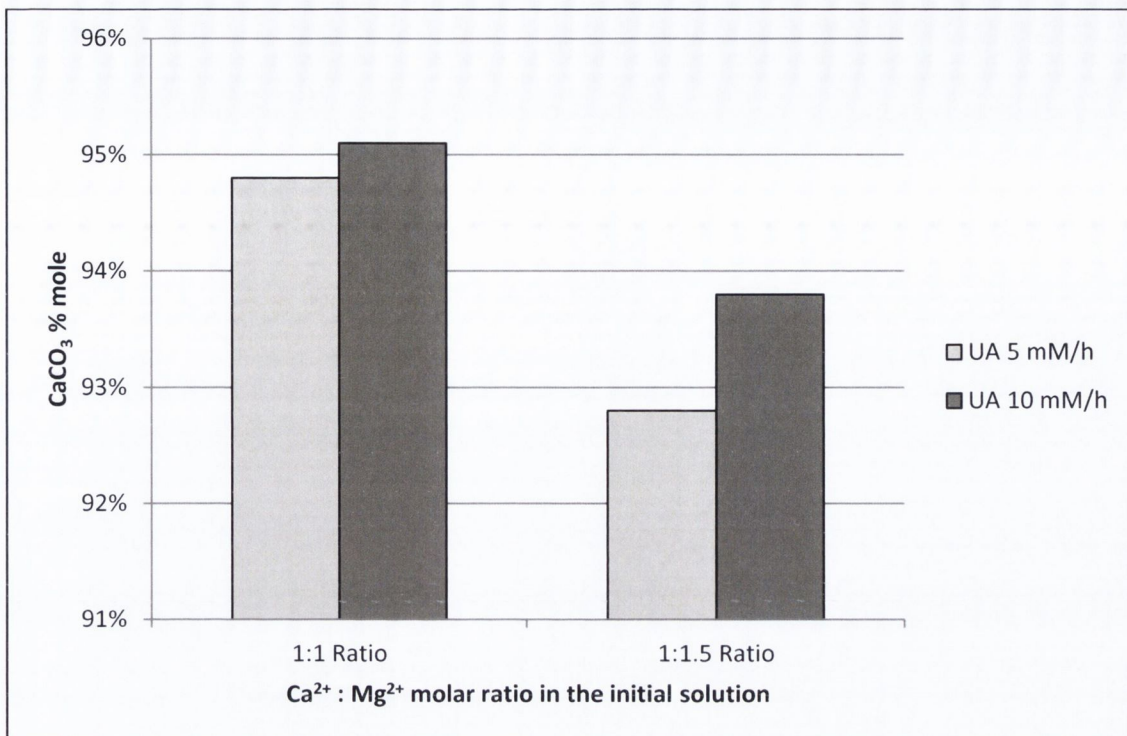


**Figure 5.21** Calcium content of Mg-calcite precipitated in oligotrophic MICP test chambers prepared with different initial Ca<sup>2+</sup> : Mg<sup>2+</sup> molar ratios. Low urease activity and low Ca<sup>2+</sup> : Mg<sup>2+</sup> molar ratios promote the inclusion of magnesium ions in the crystal lattice.

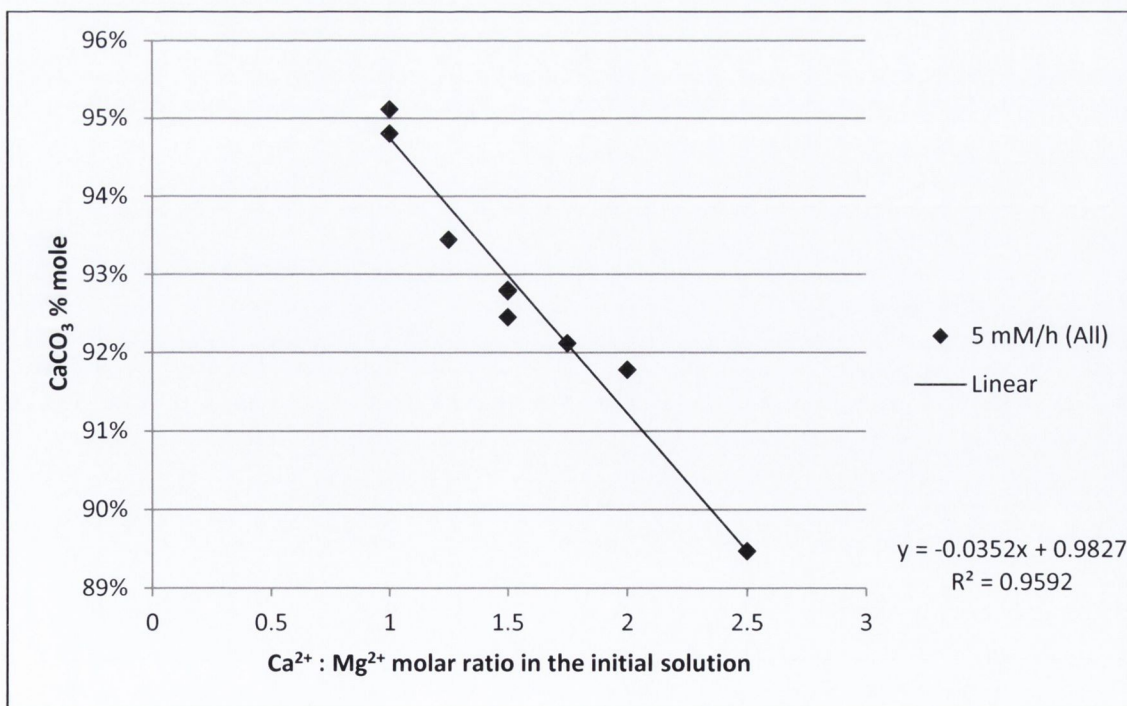


**Figure 5.22** Calcium content of Mg-calcite samples formed in chambers having an initial UA of 5 mM h<sup>-1</sup>. Initial Ca<sup>2+</sup> : Mg<sup>2+</sup> molar ratios are shown on the horizontal axis.



Additionally, eutrophic chambers did not appear to perform differently than oligotrophic chambers as would have been expected. In fact, biological growth should have increased the urease activity of the solution over time. In turn, this would have resulted in a lower magnesium content of the Mg-calcite being formed as observed for oligotrophic treatments (Figure 5.21). It is speculated, however, that limiting oxygen conditions in the sealed container could have impeded the growth of *S. pasteurii* as already observed by Whiffin (2004).

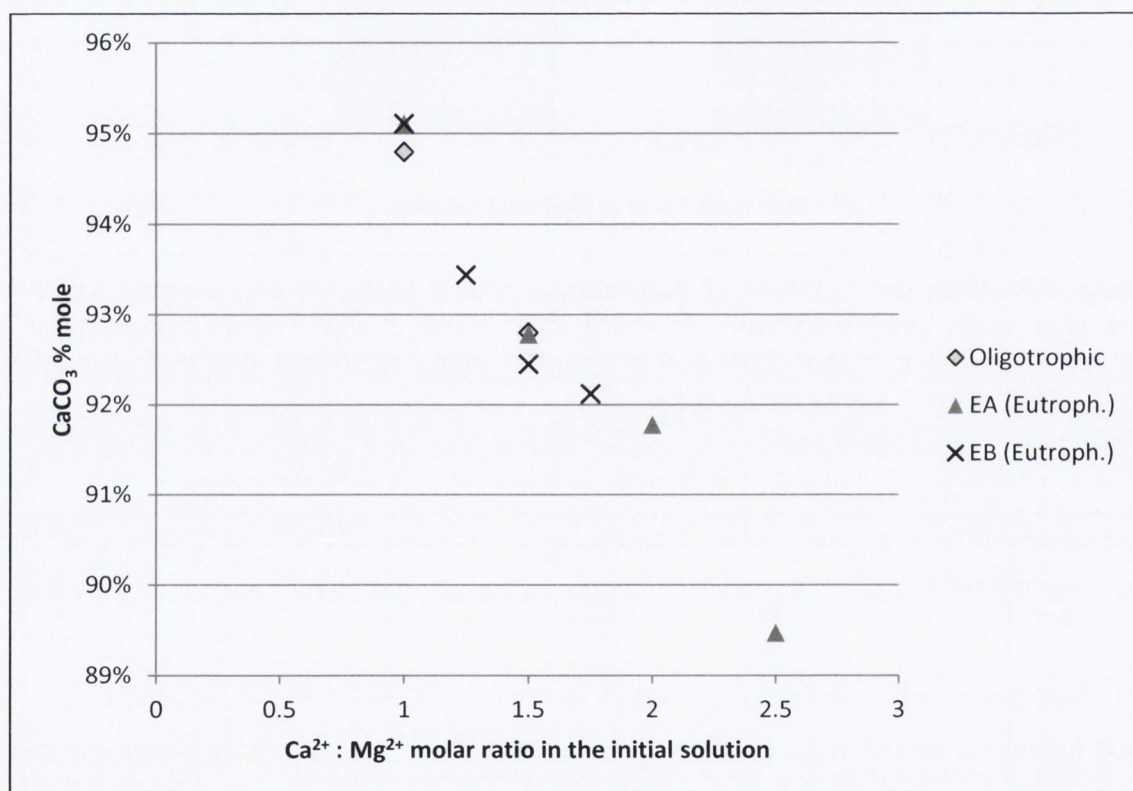


**Figure 5.23** Re-plot of Figure 5.22 showing the individual groups of samples and highlighting that the initial molar ratio is a controlling factor over the initial calcium concentration. [Ca<sup>2+</sup>] = 0.1 M (EA series), 0.2 M (EB series), 0.4 M (sample OA1) and 0.5 M (sample OB1).

### 3.4 PRECIPITATION RATE

In Figure 5.24, the dry weight of the precipitate recovered from each of the eutrophic chambers is plotted against the initial molar concentration of magnesium ions. The graph clearly shows that

increasing concentrations of magnesium have a detrimental effect on the precipitation rate observed; in particular when the initial  $\text{Ca}^{2+} : \text{Mg}^{2+}$  ratio is higher than 1:1.5. The phenomenon could be explained by the stabilising role played by magnesium ions in the precipitation process of calcite (Loste, Wilson et al. 2003; Meldrum and Cölfen 2008). In fact, during the precipitation reaction, magnesium ions are adsorbed onto the surface of growing calcite. While this promotes the incorporation of magnesium in the calcite lattice, magnesium ions are more hydrated than calcium ions, creating a barrier to the growth of the crystal nuclei.

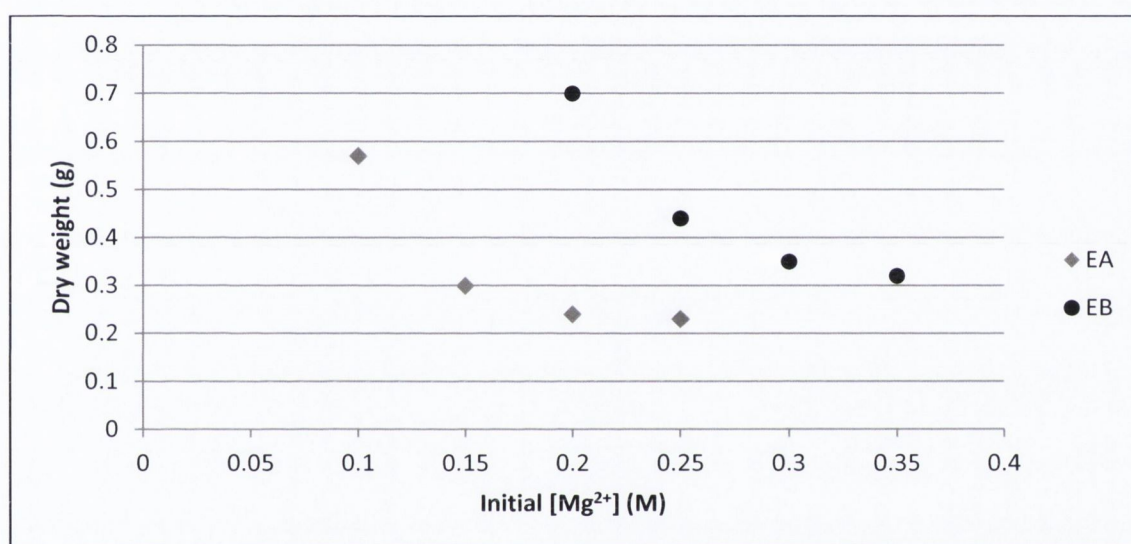


**Figure 5.24** Dry weight of recovered precipitates in relation to the initial concentration of magnesium ions. Initial calcium ion concentrations were 0.1 M (EA series) and 0.2 M (EB series). The graph shows that increasing concentrations of magnesium have a detrimental effect on the precipitation rate observed.

### 3.5 INTERIM CONCLUSIONS

While the availability of magnesium ions can lead to the formation of primary dolomite in abiotic diluted solutions (Folk and Land 1975) and in biomediated ureolytic processes on solid mediums (Sánchez-Román, Vasconcelos et al. 2008), the results show that this cannot be achieved in the context of MICP soil improvement applications. The addition of

magnesium to the reaction environment, instead, produced low Mg-calcite precipitates (Chapter 2, Paragraph 9.1).

The results show that reducing the initial  $\text{Ca}^{2+} : \text{Mg}^{2+}$  ratio could possibly result in the production of high Mg-calcites or even dolomite. However, this could require ratios below 1:10 (Loste, Wilson et al. 2003; Sánchez-Román, Vasconcelos et al. 2008) and the results show that the overall precipitation rate is significantly reduced by the presence of large amounts of magnesium ions, posing a practical limit to field applications. The results also indicate that this could not be countered by increasing the urease activity retained in the soil as this would consequently limit the inclusion of magnesium in the crystal lattice.

It is noted that only a portion of the magnesium ions provided would be contributing to the mass of cementing material, leading to a low economical and environmental performance of the treatment. Treatment with diluted solutions with an initial  $\text{Ca}^{2+} : \text{Mg}^{2+}$  ratio close to one could be considered as an alternative approach. However, this would require large volumes of cementation liquid when employed in field applications, with significant economical and environmental implications. For these reasons MICP of dolomite has not been investigated further in the context of this research.

## RESULTS AND DISCUSSION: UNSATURATED SOILS

## 1) EXPERIMENT N. 4: FEASIBILITY OF AEROSOL DELIVERY

1.1 GENERAL

Experiment N. 4 was designed to preliminarily establish the viability of aerosol delivery methods for MICP soil improvement in unsaturated soils. A provisional treatment regime was adopted for oligotrophic and eutrophic protocols and tested on fine silica sand samples.

1.2 EXPERIMENTAL SET-UP

Four test columns were prepared with fine silica sand (300  $\mu\text{m}$  – 150  $\mu\text{m}$ ) as illustrated in Chapter 4, Paragraph 6.2. Two columns were treated using oligotrophic protocols and 2 columns using eutrophic protocols.

**Table 6.1** Summary of the treatment protocols employed. Blank samples were prepared by introducing dead *S. pasteurii* cells.

ID	Protocol	Bioaugmentation
O1	Oligotrophic	100 mL - Live cells
O1B	Oligotrophic	100 mL - Dead cells (blank)
E1	Eutrophic	100 mL - Live cells
E1B	Eutrophic	100 mL - Dead cells (blank)

As summarised in Tables 6.1 and 6.2, of the two columns composing each set, one was initially treated with 0.1 L (approximately 2 pore volumes) of *S. pasteurii* suspension (5.04 OD<sub>600</sub>; UA = 6.49 mM min<sup>-1</sup>)

delivered continuously at a rate of 0.25 mL min<sup>-1</sup> with a Cirrus® nebuliser. The second column was prepared as a blank and initially treated with dead *S. pasteurii* cells prepared by autoclave sterilisation of a live culture (20 mins @ 120° C).

**Table 6.2** Composition of the cementation fluids employed.

<b>Protocol</b>	<b>[Urea]</b>	<b>[Ca<sup>2+</sup>]</b>	<b>[Yeast extract]</b>
Oligotrophic	1 M	1 M	0 g L <sup>-1</sup>
Eutrophic	1 M	1 M	5 g L <sup>-1</sup>

After injecting the bacteria, the columns were left to rest for 12 hours following which the cementation liquid was applied in four batches as detailed in Table 6.3. The cementation liquid was delivered continuously at a rate of 0.25 mL min<sup>-1</sup> with a Cirrus® nebuliser. Following the last treatment, each sample was left to react for 24 hours and then tested for unconfined compression strength (UCS) and carbonate content as detailed in Chapter Four.

**Table 6.3** Cementation treatment regime followed in Experiment N. 4.  $t_0$  was set as the end of the bioaugmentation treatment. The samples were left to react for 24 hours after each injection round.

<b>Round 1</b>	<b>Round 2</b>	<b>Round 3</b>	<b>Round 4</b>	<b>Injection time</b>
<b>(<math>t_0+12h</math>)</b>	<b>(<math>t_0+36h</math>)</b>	<b>(<math>t_0+60h</math>)</b>	<b>(<math>t_0+84h</math>)</b>	<b>(continuous)</b>
100 mL	100 mL	100 mL	100 mL	400 min @ 25 mL min <sup>-1</sup>

The development of the wetting front of samples O1 and E1 was observed during the injection of the process reagents. The advancement of the front was monitored by measuring the height of the front as observed through the transparent column along an arbitrarily fixed vertical axis. Once the front reached the top of the column, the liquid accumulating on the surface was regularly removed

using a syringe to avoid any backflow once air pressure was removed in-between treatments.

### 1.3 CARBONATE CONTENT AND UCS

All four samples were very poorly cemented. As shown in Table 6.4, only the samples treated with live cells resulted in the deposition of measurable amounts of calcium carbonate. The low calcium carbonate content recorded, 0.72% and 0.13% w/w for eutrophic and oligotrophic treatments respectively, provides a justification for the low unconfined compressive strength (UCS) measured in both samples.

**Table 6.4** Calcium carbonate determination results and overall conversion efficiency ( $OC_{eff}$ ). While values are generally low, eutrophic treatment (E1) performed better than oligotrophic treatment (O1).

ID	CaCO <sub>3</sub> (g) <sup>#</sup>	CaCO <sub>3</sub> (w/w)	Max CaCO <sub>3</sub> (g) <sup>*</sup>	Max CaCO <sub>3</sub> (w/w)	OC <sub>eff</sub>
O1	0.219	0.13%	40	23.4%	0.54%
O1B	b.d.l.	b.d.l.	40	22.5%	n.a.
E1	1.328	0.72%	40	21.7%	3.32%
E1B	b.d.l.	b.d.l.	40	20.7%	n.a.

<sup>#</sup> Total for the entire column

<sup>\*</sup> Assuming total conversion of CaCl<sub>2</sub> into CaCO<sub>3</sub>

**Table 6.5** Unconfined compression strength test results. The very low values recorded are evidence of poor treatment performance.

ID	Protocol	UCS (wet)
O1	Oligotrophic	8.5 kPa
E1	Eutrophic	7.0 kPa

Due to the lack of cohesion, only the two samples treated with live cells could be tested for UCS. The results of the tests are listed in Table 6.5. Despite displaying comparable UCS values, the eutrophic treatment

performed better than the oligotrophic treatment and overall conversion efficiencies,  $OC_{eff}$ , of 3.32% and 0.54% were respectively recorded. The different  $OC_{eff}$  is interpreted as the effect of biological stress during nebulisation. In fact, the addition of nutrients in eutrophic treatments would have assisted the recovery of the bacteria during cementation.

However, both  $OC_{eff}$  values are very low when compared with efficiencies between 80% and 100% reported by Al Qabany et al. (2012). Low efficiency could be associated with the stripping of ammonia and carbon dioxide from the deposited liquid. In fact, during the 400 minutes required to deliver the reagents, up to 3.2 m<sup>3</sup> of air flow through the column which could lead to significant losses (volumetric air flow to volumetric water flow ratio:  $3.2 \cdot 10^4$ ). The consequent low ammonium concentrations and unavailability of carbonate ions in the pore liquid would severely limit the calcium carbonate precipitation process (Ferris, Phoenix et al. 2004).

#### 1.4 WETTING FRONT AND DEPOSITION

The two samples (O1 and E1) displayed a distinct behaviour in the advancement of the wetting front. O1 displayed a regular advancement of the front until liquid started accumulating at the top of the column. The results of the monitoring are shown in Figure 6.1. Up to 3 pore volumes of liquid were necessary before the wetting front reached the surface of the column. This confirms that a large portion of the liquid droplets being injected in dry soils is transported through and outside the column (Dyer, Glew et al. 2012).

The wetting front of E1 was consistent with what observed for O1 over the first 60 mL of injected liquid. Following that, fingers started to develop where the rapid displacement of liquid was observed (Figure 6.2). Liquid started to accumulate at the top of the column after 80 mL

were delivered. As a result the advancement of the wetting front could not be monitored.

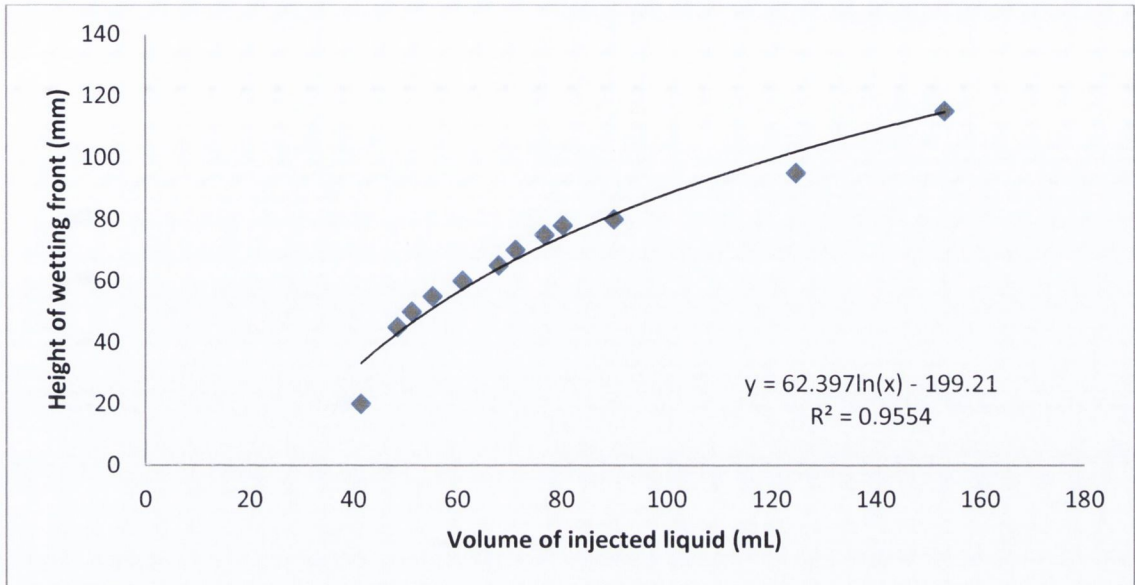


**Figure 6.1** Advancement of the wetting front observed in column O1. The high injected volumes required to advance the front would be evidence of liquid being transported outside the column as a result of inefficient droplet deposition and stripping.

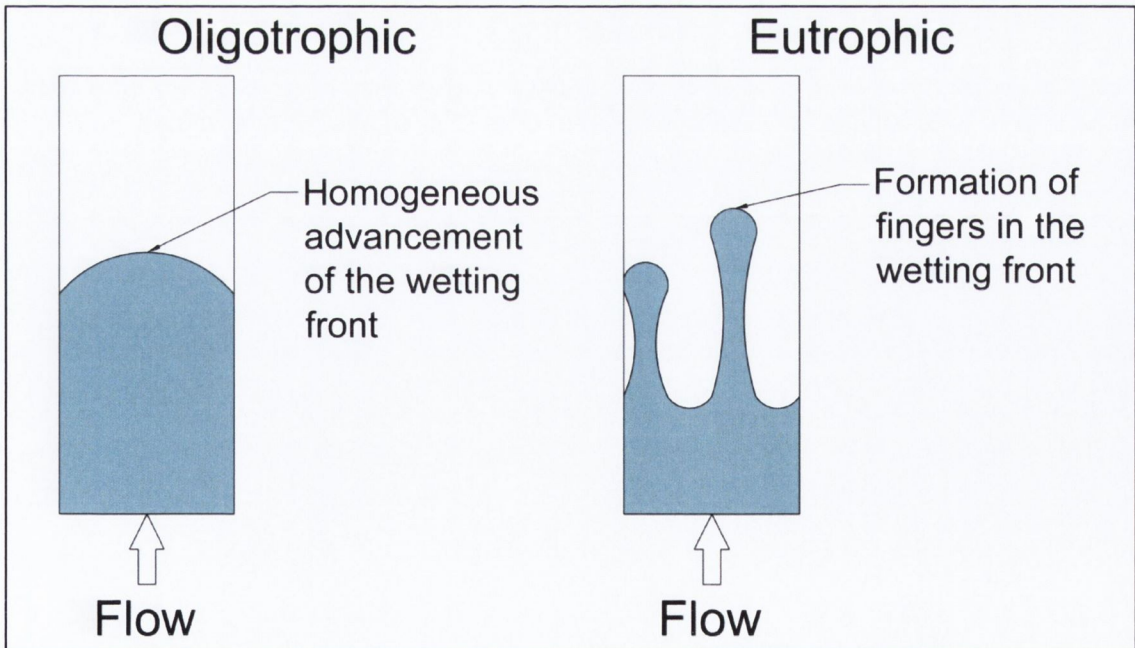


**Figure 6.2** Schematic representation of the different wetting front observed employing oligotrophic and eutrophic protocols with nebulised delivery systems.



The phenomenon could be associated with the higher viscosity and wetting of the eutrophic liquid caused by the addition of yeast extract. As a result of the increased viscosity and wetting, larger volumes of nebulised liquid would become deposited at the base of the column. When approaching localised soil saturation at the bottom of the column, the air pressure applied through the nebuliser would be sufficient to displace and drag the liquid along preferential pathways in the soil mass.

It should be noted that no percolation was observed throughout the experiment. Indicating that gravitational forces were insufficient to displace the liquid retained in the column during the reaction pauses. It can therefore be inferred that the moisture content of the samples was maintained at all times below the field capacity limit (pendular or funicular regime).

### 1.5 INTERIM CONCLUSIONS

The results show that atomised delivery methods could be a viable approach for biogrouting applications of unsaturated soils. It is of significance, however, that the  $OC_{eff}$  of the treatment appears to be seriously undermined by the necessity of prolonged injection periods which are required to deliver sufficient volumes of cementation liquid. Eutrophic treatment protocols appear to perform better than oligotrophic methods as a result of stresses on the biological component caused by the atomisation process. However, due to the likely stripping of reagents from the reaction environment both protocols resulted in very low treatment efficiencies (Chapter 2, Paragraph 1). A revised treatment regime, where treatments are delivered by alternating short injection rounds with short reaction pauses, could potentially improve the performance. By employing such a regime, most of the reagents delivered with the first batch would have been depleted before the second injection round could initiate the stripping process.

Crucially, the absence of percolation losses, as seen in the context of bioremediation applications, provides a strong argument for the use of nebulised delivery methods in unsaturated soils (Chapter 2, Paragraph 9.1). The value of atomised delivery is further increased when considering MICP treatments as higher treatment efficacy is expected when precipitation occurs in soils characterised by pendular and funicular regimes (Cheng and Cord-Ruwisch 2012).

## 2) EXPERIMENT N. 5: AEROSOL DELIVERY OF MICP REAGENTS

### 2.1 GENERAL

Experiment N. 5 was designed to assess the performance of a revised injection regime for the delivery of nebulised MICP reagents in unsaturated soils. Taking cue from the results of Experiment N. 2 (Chapter 5, Paragraph 2) and Experiment N. 4 (Chapter 6, Paragraph 1), an eutrophic treatment protocol was selected based on the following observations:

- Development of a urease active biofilm around inter-particle contact points would increase the efficacy of the treatment;
- Biological stress during atomisation results in low performance of oligotrophic treatments delivered by atomisation.

A pulsed injection regime is proposed as a possible way of improving efficiency by limiting the stripping of ammonia and carbon dioxide from the reaction environment. Additionally, a pulsed regime would also increase the number and density of air channels formed in the partially saturated soil at the later stages of the treatment (Chapter 3, Paragraph 3.1). An increased number of air channels per unit of soil volume (were process reagents travel in the form of aerosols) would benefit the treatment by increasing homogeneity, and increase the retention of liquid reagents in the column by distributing the treatment to a larger portion of the soil mass (Glew 2009).

### 2.2 EXPERIMENTAL SET-UP

A total of three columns were prepared as detailed in Chapter 4 with fine (300  $\mu\text{m}$  -150  $\mu\text{m}$ ) silica sand. The bioaugmentation of each column was achieved by injecting 90 mL (approximately 2 pore volumes) of nebulised *S. pasteurii* suspension (Table 6.6) at a rate of 0.25 mL min<sup>-1</sup>. Following bioaugmentation, the columns were left to rest for 12

hours in order to allow for bacterial attachment. Each column was then treated with a cementation solution prepared as detailed in Table 6.7.

**Table 6.6** Atomised delivery of *S. pasteurii* (bioaugmentation step). The ureolysis rate of the column is reported assuming 100% retention of bacteria. The relevance of this parameter will be discussed in Paragraph 2.4 below.

Column ID	Volume	Urease Activity	OD <sub>600</sub>	Ureolysis Rate*
E150	90 mL	5.20 mM min <sup>-1</sup>	4.49	0.028 mol h <sup>-1</sup>
E500	90 mL	6.18 mM min <sup>-1</sup>	5.24	0.033 mol h <sup>-1</sup>
E1000	90 mL	6.80 mM min <sup>-1</sup>	5.31	0.036 mol h <sup>-1</sup>

\* Ureaolysis rate of the column, assuming 100% retention of bacteria

**Table 6.7** Reagent concentration in the eutrophic cementation fluid.

Column ID	[Urea]	[Ca <sup>2+</sup> ]	[Yeast Extract]
E150	0.15 M	0.15 M	5.0 g L <sup>-1</sup>
E500	0.50 M	0.50 M	5.0 g L <sup>-1</sup>
E1000	1.00 M	1.00 M	5.0 g L <sup>-1</sup>

**Table 6.8** Actual volumes and injection rate of atomised cementation fluid. The cementation treatment was delivered by alternating one hour injection periods with one hour reaction pauses, five times daily.

	E150		E500		E1000	
	mL	mL min <sup>-1</sup>	mL	mL min <sup>-1</sup>	mL	mL min <sup>-1</sup>
<b>Day 1</b>	75	0.25	75	0.25	75	0.25
<b>Day 2</b>	70	0.23	70	0.23	66	0.22
<b>Day 3</b>	60	0.20	60	0.20	60	0.20
<b>Day 4</b>	60	0.20	60	0.20	60	0.20

The cementation treatment was delivered by alternating one hour injection periods with one hour reaction pauses, five times daily for a period of 4 days. As reported in Table 6.8, the volume of cementation liquid delivered daily could not be kept constant. This was due to the establishment of increasingly higher backpressures (> 150kPa) at the

head of the nebuliser which limited the achievable airflow (range: 8 L min<sup>-1</sup> to 6 L min<sup>-1</sup>). The increase of backpressure was interpreted as caused by a decrease of porosity in the sample brought about by the formation of calcium carbonate within the pore space. The reaction was stopped 12 hours after the last treatment by flushing 4 pore volumes of deionised water through each column.

As for Experiment N.4, any liquid seen to accumulate on the top surface of the column was manually removed with a syringe and the volume recorded. Despite removing the accumulating liquid, however, small volumes of cementation liquid were seen to percolate from the gravel pack into the sand column during the reaction period: resulting in increased availability of reagents in the top 20 mm (circa) of the column. During extraction, this section of the column was therefore carefully sawn off from the samples by pushing out the core and cutting it (together with the lining material) flush with the column edge. The samples were then prepared for UCS testing. Following UCS testing, two sub-samples were taken from the bottom and top of the sample and prepared for calcium carbonate determination and SEM imaging.

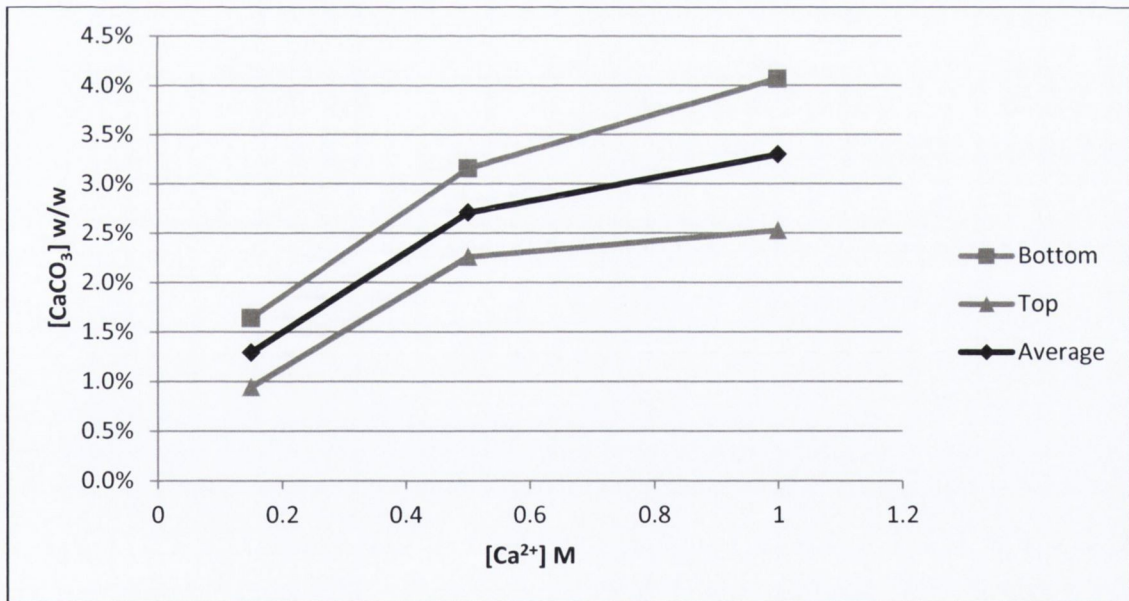
### 2.3 CALCIUM CARBONATE CONTENT

Figure 6.3 illustrates the results of the calcium carbonate determination. Overall, the results indicate that there is a non-linear correlation between the concentration of calcium ions in the cementation liquid and the amount of calcium carbonate being precipitated. However, the graph highlights that precipitation did not occur homogeneously along the column. As a result of preferential deposition of droplets, larger amounts of calcium carbonate were precipitated close to the inlet. A coefficient of uniformity,  $C_{uni}$ , can be used to evaluate the homogeneity of treatment along the column (Glew 2009):

$$C_{uni} = 1 - \left( \frac{C_{top}}{C_{bot}} \right) \quad \text{Eq. 6.1}$$

where  $C_{top}$  is the calcium carbonate content measured at the top of the column and  $C_{bot}$  is the calcium carbonate content measured at the bottom of the column. Values of  $C_{uni}$  close to zero indicate a uniform distribution whereas values close to one indicate a low uniformity of the treatment. Negative values would indicate a higher deposition further away from the injection point but, while possible, this is an unlikely occurrence with the set-up employed.

Care should however be taken in relating the  $C_{uni}$  to the homogeneity of droplet deposition. In fact, the formation of fingers (Experiment N. 4) would indicate that additional transport mechanisms (such as displacement and convection of previously deposited liquid) contribute to the distribution of reagents in the soil mass.



**Figure 6.3** Calcium carbonate content of E150, E500 and E1000 presented as a function of  $[Ca^{2+}]$  in the cementation liquid. Values are reported for sub-samples taken from the bottom and top of each UCS sample.

**Table 6.9** Calculated coefficient of uniformity.

	E150	E500	E1000
Coefficient of Uniformity ( $C_{uni}$ )	0.427	0.282	0.380

The values of  $C_{uni}$  calculated for the columns in this experiment are reported in Table 6.9. E500 was the most homogeneously treated sample ( $C_{uni} = 0.282$ ) whereas E150 showed the lowest homogeneity with a  $C_{uni}$  value of 0.427. While variability in the parameter is noted the limited data set does not allow for further interpretation.

## 2.4 CONVERSION EFFICIENCY

As seen in Table 6.10, the overall conversion efficiency,  $OC_{eff}$ , recorded for Experiment N. 5, where a pulsed injection regime was employed, is significantly higher than what obtained with a continuous flow in Experiment N. 4. In fact, for similarly treated columns,  $OC_{eff}$  went from 3.3% (sample E1, Experiment N. 4) to 23% (sample E1000, Experiment N. 5).

**Table 6.10** Calcium carbonate content and overall conversion efficiency,  $OC_{eff}$ , of E150, E500 and E1000. A drastic drop in  $OC_{eff}$  occurs when highly concentrated solutions are employed.

ID	CaCO <sub>3</sub> (g) <sup>#</sup>	[CaCO <sub>3</sub> ] (w/w)	Max CaCO <sub>3</sub> (g) <sup>*</sup>	Max [CaCO <sub>3</sub> ] (w/w)	OC <sub>eff</sub>
E150	2.20	1.3%	3.97	2.3%	55%
E500	4.79	2.7%	13.2	7.5%	36%
E1000	6.03	3.3%	26.1	14.3%	23%

<sup>#</sup> Total for the entire column (calculated from average values)

<sup>\*</sup> Assuming total conversion of CaCl<sub>2</sub> into CaCO<sub>3</sub>

However, efficiency remains generally low (< 55%) due to the inefficient deposition of droplets into the column. The volumetric deposition ratio,  $A_d$ , is defined here as:

$$A_d = \frac{\Delta V_1 - (\Delta V_2 + \Delta V_3)}{\Delta V_1} \quad \text{Eq. 6.2}$$

where,  $\Delta V_1$  is the volume of atomised liquid delivered by the nebuliser,  $\Delta V_2$  is the volume of atomised liquid directly transported outside of the

column and  $\Delta V_3$  is the volume of liquid removed by sparging. The values of  $A_d$  recorded over the 4 days of treatment are reported in Figure 6.4.

It is therefore possible to define the effective conversion efficiency,  $EC_{eff}$ , by considering that only a portion,  $A_d$ , of the injected cementation solution was actually available for the precipitation reaction:

$$EC_{eff} = \frac{OC_{eff}}{A_d} \quad \text{Eq. 6.3}$$

The computed values of  $EC_{eff}$  are reported in Table 6.11.  $EC_{eff}$  values exceeding 100% (E150 and E500) are evidence of stripping (water).

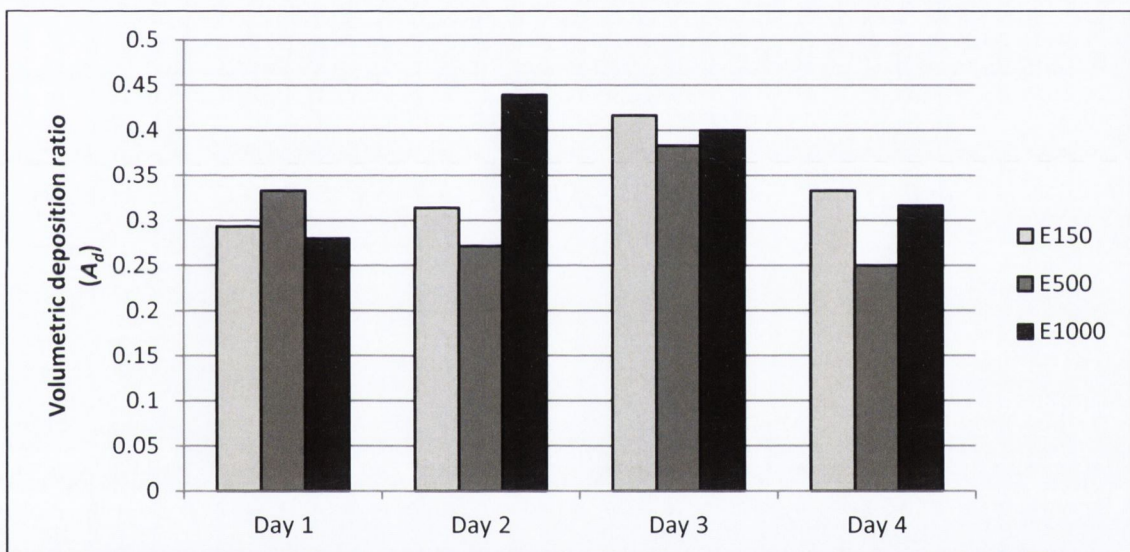


**Figure 6.4** Volumetric deposition ratio,  $A_d$ , over the 4 days of treatment.

**Table 6.11** Effective conversion efficiency,  $EC_{eff}$ , calculated from average volumetric deposition ratios,  $A_d$  (Eqs. 6.2 and 6.3). Values of  $EC_{eff}$  higher than 100% are evidence of stripping of water caused by the air flow.

ID	$OC_{eff}$	$A_d^*$	$EC_{eff}$
E150	55%	0.34	162%
E500	36%	0.31	116%
E1000	23%	0.36	64%

\* Average values were computed from values reported in Figure 6.4



While stripping of water can be considered negligible during short injection periods (Dyer, Glew et al. 2012), the prolonged exposure of wetted pore surfaces to air flow from the nebuliser (8 L min<sup>-1</sup> to 6 Lmin<sup>-1</sup>) can result in significant losses of water (solvent). These losses would therefore result in higher reagent concentrations being present in the deposited liquid and in turn in  $EC_{eff} > 100\%$  being recorded. The data indicates that, for the set-up employed during the experiment, over 60% of the water (solvent) can be removed by air sparging.

The drop in  $EC_{eff}$  observed for increasing concentrations is explained by considering the residence time of the reagents in the column. In fact, one hour reaction periods were equally allowed for all the columns. This would be sufficient time for the near complete reaction of the reagents deposited in E150 but not in E500 and E1000. Table 6.12 reports the ureolysis rates of each column calculated by assuming that all of the precipitation took place during the one hour reaction pause. Despite introducing some approximation, the average ureolysis rates so calculated suggest, as indicated by the drop in  $EC_{eff}$ , that a limit of approximately  $3 \cdot 10^{-3}$  mol h<sup>-1</sup> exists for the particular set-up employed. It is noted, that this value is one order of magnitude smaller than the potentially achievable rate if all of the injected bacteria were retained in the column during bioaugmentation (Table 6.6). The low value ( $1.053 \cdot 10^{-3}$  mol h<sup>-1</sup>) recorded in sample E150 is evidence of the reaction being completed in less than one hour due to the smaller amounts of reagents in the cementation liquid.

**Table 6.12** Average ureolysis rates calculated for E150, E500 and E1000 (whole columns). The values are one order of magnitude smaller than those achievable considering 100% retention of bacteria during bioaugmentation.

	<b>E150</b>	<b>E500</b>	<b>E1000</b>
Ureolysis Rate (mol h <sup>-1</sup> )	$1.053 \cdot 10^{-3}$	$2.782 \cdot 10^{-3}$	$3.001 \cdot 10^{-3}$

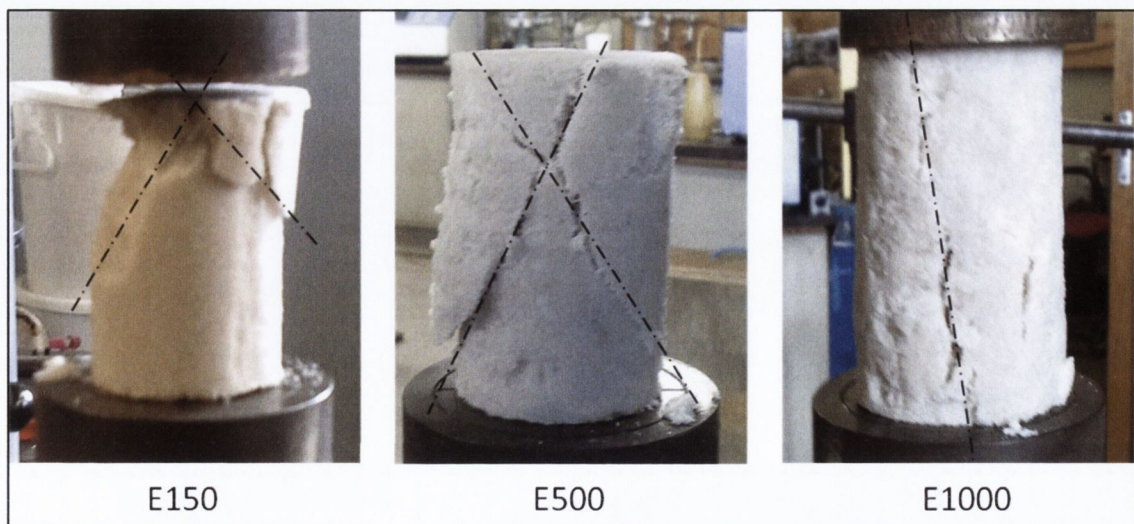
## 2.5 UNCONFINED COMPRESSIVE STRENGTH

Table 6.13 reports the UCS (wet) values recorded for each of the samples. As expected the highest value, 374 kPa, was recorded for sample E1000 where the average calcium carbonate content was 3.3% w/w (approximately 50 Kg m<sup>-3</sup>); whereas, no measurable improvement was observed in sample E150 where on average 1.3% w/w (approximately 18 Kg m<sup>-3</sup>) of calcium carbonate was precipitated.

**Table 6.13** Unconfined compressive strength and average calcium carbonate content.

Column ID	UCS (wet)	[CaCO <sub>3</sub> ]
E150	6.6 kPa	1.3% w/w (18 Kg m <sup>-3</sup> )
E500	121 kPa	2.7% w/w (40 Kg m <sup>-3</sup> )
E1000	374 kPa	3.3% w/w (50 Kg m <sup>-3</sup> )

As shown in Figure 6.5, the increasingly rock-like nature and brittleness of the material leads to the formation of typical multiple shear planes and tensile failure surfaces (Zhao 2008). This is most evident in sample E1000 and is consistent with failure mechanisms observed in columns treated with conventional injection methods (Appendix Two).



**Figure 6.5** Failure surfaces during unconfined compression strength test.

Figures 6.6 and 6.7 show a comparative analysis of the UCS and calcium carbonate data collected in this study, with the values recorded by Al Qabany et al. (2013) employing eutrophic protocols and delivered with conventional injection methods. While the data set of this study is relatively small, the results appear to confirm that higher efficacies (i.e. UCS/CaCO<sub>3</sub> ratios) are to be expected when treating unsaturated soils. As indicated by Cheng et al. (2012), this could be attributed to the presence of a partially saturated hydraulic regime which is, in turn, a result of the nebulised injection technique employed. This will be discussed in detail in Paragraph 5.5 of this chapter.

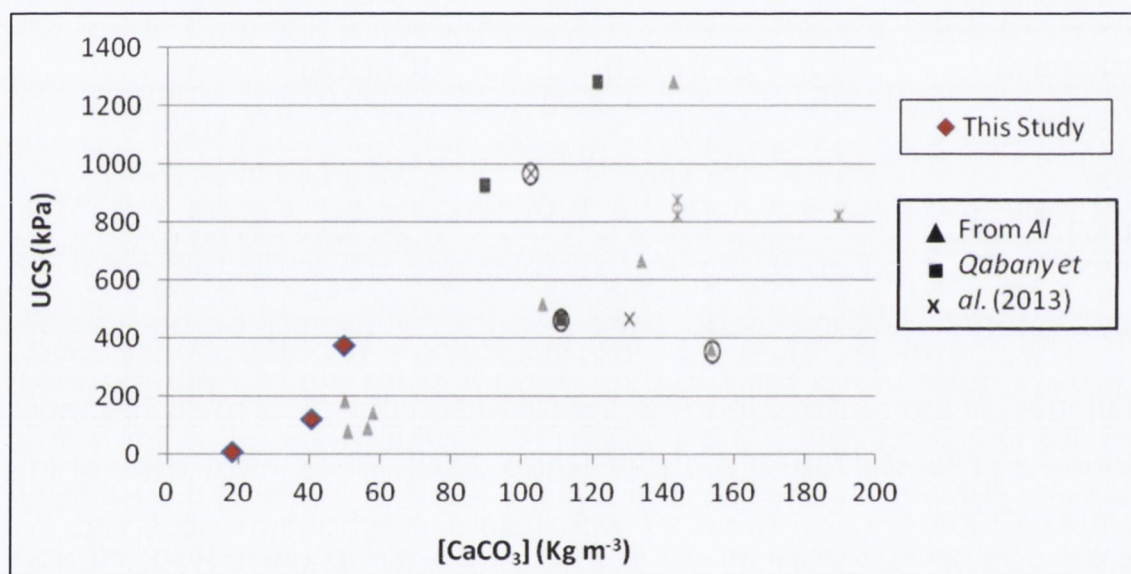


**Figure 6.6** Unconfined compressive strength and calcium carbonate content obtained. Data from this study (♦) is compared to 0.5 M eutrophic treatments (▲, ■, and x) using conventional injection methods in saturated soils (Al Qabany and Soga 2013).

A more definitive comparison can be made with oligotrophic treatments. In this study, a measurable increase in strength was recorded where 40 Kg m<sup>-3</sup> were deposited (sample E500). This value is significantly lower than what reported by several authors in oligotrophic treatments of saturated soils where at least 60 Kg m<sup>-3</sup> were required for MICP to measurably improve strength (Whiffin, van Paassen et al. 2007; van Paassen 2009).

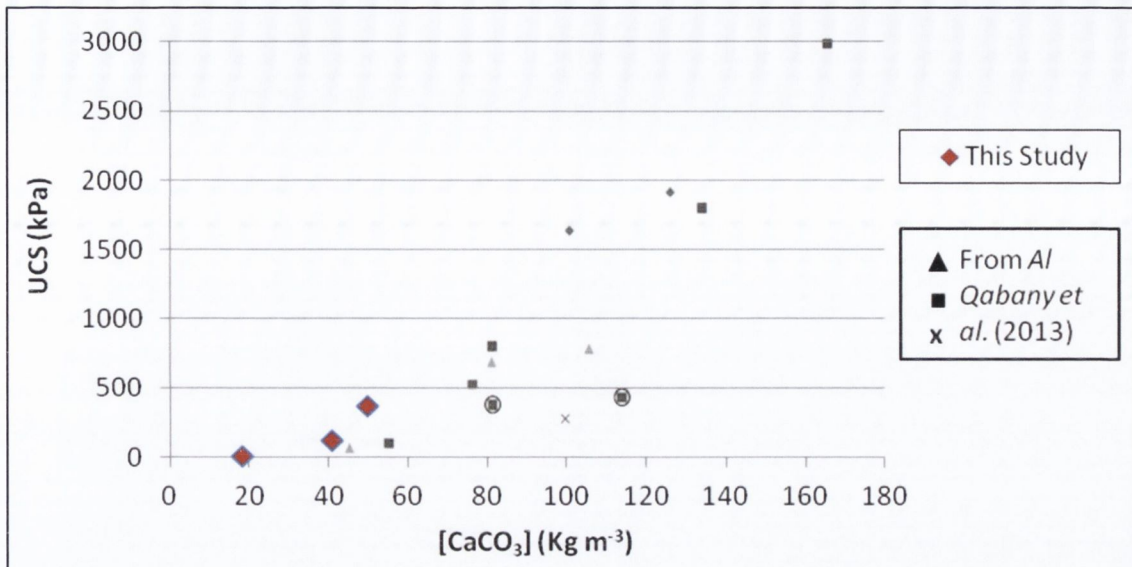


**Figure 6.7** Unconfined compressive strength and calcium carbonate content obtained. Data from this study (♦) is compared to 1.0 M eutrophic treatments (▲, ■, and x) using conventional injection methods in saturated soils (Al Qabanyet and Soga 2013).

## 2.6 STRUCTURE OF THE INTER-PARTICLE BOND

As hypothesised earlier the bonding structures being formed in unsaturated soils are substantially different from those observed in saturated soils (Experiment N. 2). Figure 6.8 illustrates how calcium carbonate was precipitated within the confines of pore liquid retained by capillary forces. In the SEM image it is possible to clearly identify smooth carbonate surfaces, reminiscence of the menisci formed by the pore liquid. Interestingly, the air-water interface (AWI) becomes available as an additional surface for both bacterial attachment (Fang and Logan 1999; Keller and Auset 2007) and carbonate precipitation (Loste, Wilson et al. 2003). As illustrated in Figure 6.9, this led to the formation of a characteristic dual bond meniscus structure between soil particles.



**Figure 6.8** Cluster of sand particles held together by calcium carbonate bonds formed during the atomised delivery of cementing agents (sample E150). The calcium carbonate precipitated traces the shape of water menisci formed during the reaction time.

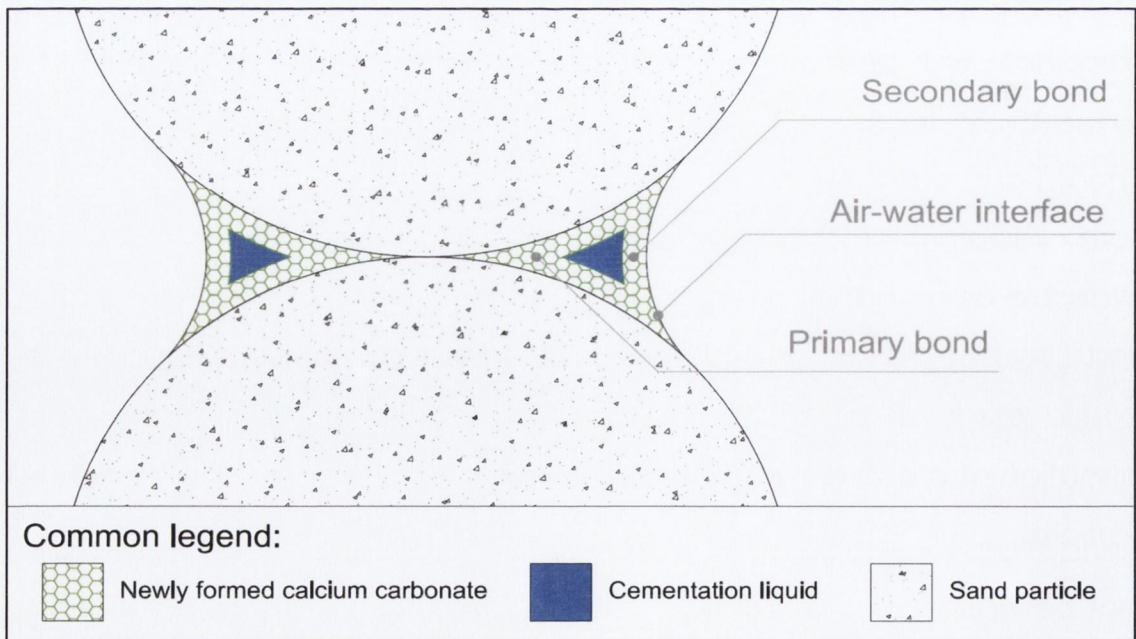
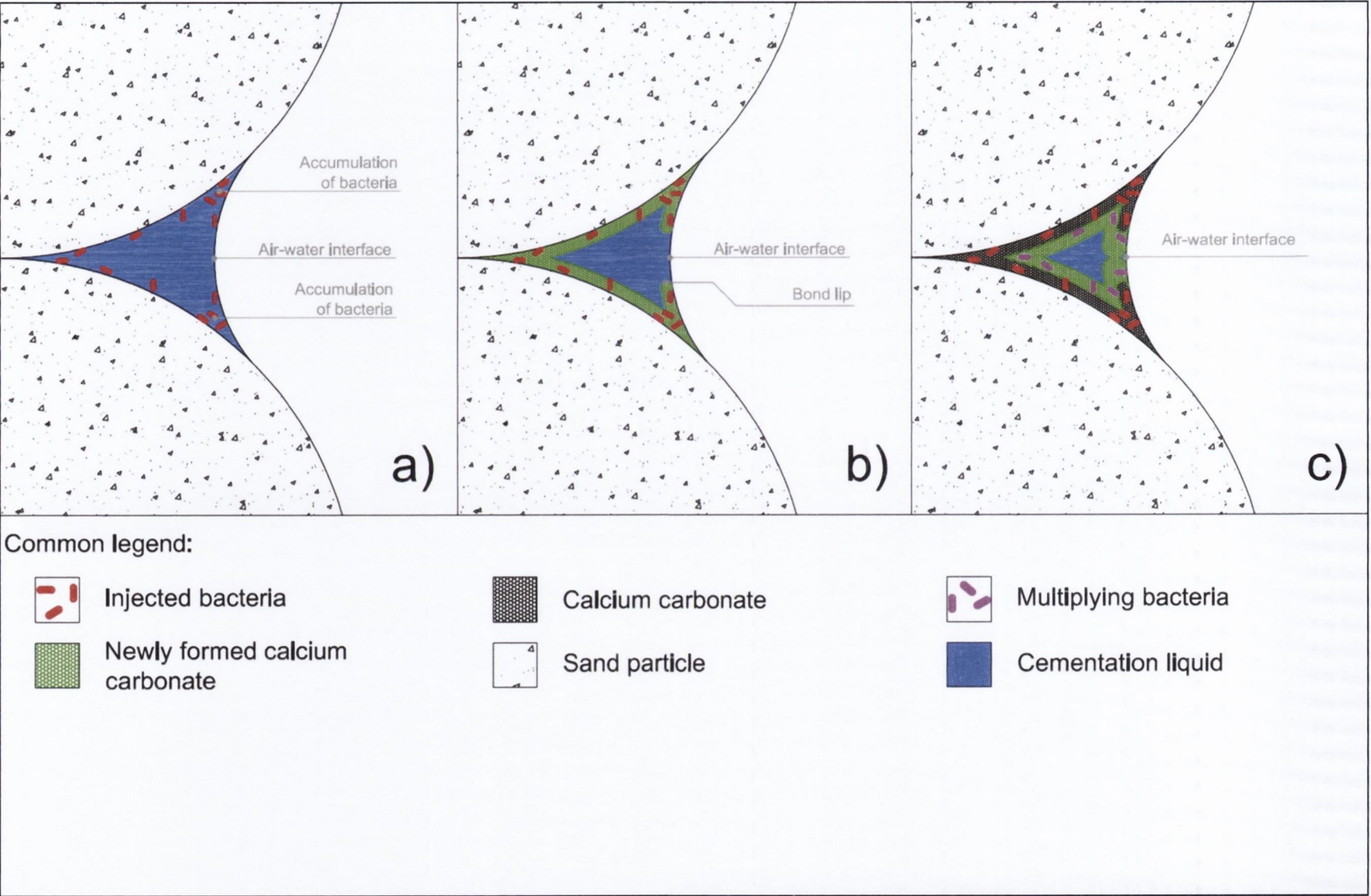


**Figure 6.9** Schematic representation of a fully formed dual bond meniscus.



While the formation mechanism of the primary bond is consistent with observations in Experiment N. 2 for eutrophic samples, the formation process of the secondary bond is unique and can be described as follows:

1. Droplets of liquid are deposited on the surface of soil particles: forming characteristic menisci. Bacteria attach to the particle surfaces. Also, bacteria attached to the AWI accumulate at the edges of the menisci as a result of reduced surface tension forces (Zevi, Dathe et al. 2005), Figure 6.10(a).
2. Precipitation of calcium carbonate is initiated. The primary bond is formed within the confines of the menisci as described for saturated soils. At the same time calcium carbonate is precipitated on the surface of the AWI and close to the triple contact point air-water-soil. A lip of carbonate is therefore formed: raised above the particle's surface (Figure 6.10(b)).
3. The precipitation process can continue until the secondary bond is formed. Noting that, the extent of the AWI is reduced and triple contact point is now air-water-carbonate (Figure 6.10(c)).

Figure 6.11 shows the detail of the carbonate lip in which it is possible to distinguish the rod-shaped cavities left behind by the bacteria attached to the AWI. While the carbonate lip is consistently formed throughout the samples, in samples E500 and E1000 the secondary bond often remains unformed (Figure 6.12). Complete formation of a secondary bond appears to be specifically subject to the amount of precipitation occurring at the AWI. It is, in fact, observed that E150 displayed a widespread occurrence of fully formed secondary bonds, this despite the fact that lower amounts of calcium carbonate were precipitated in E150 when compared to the other samples.

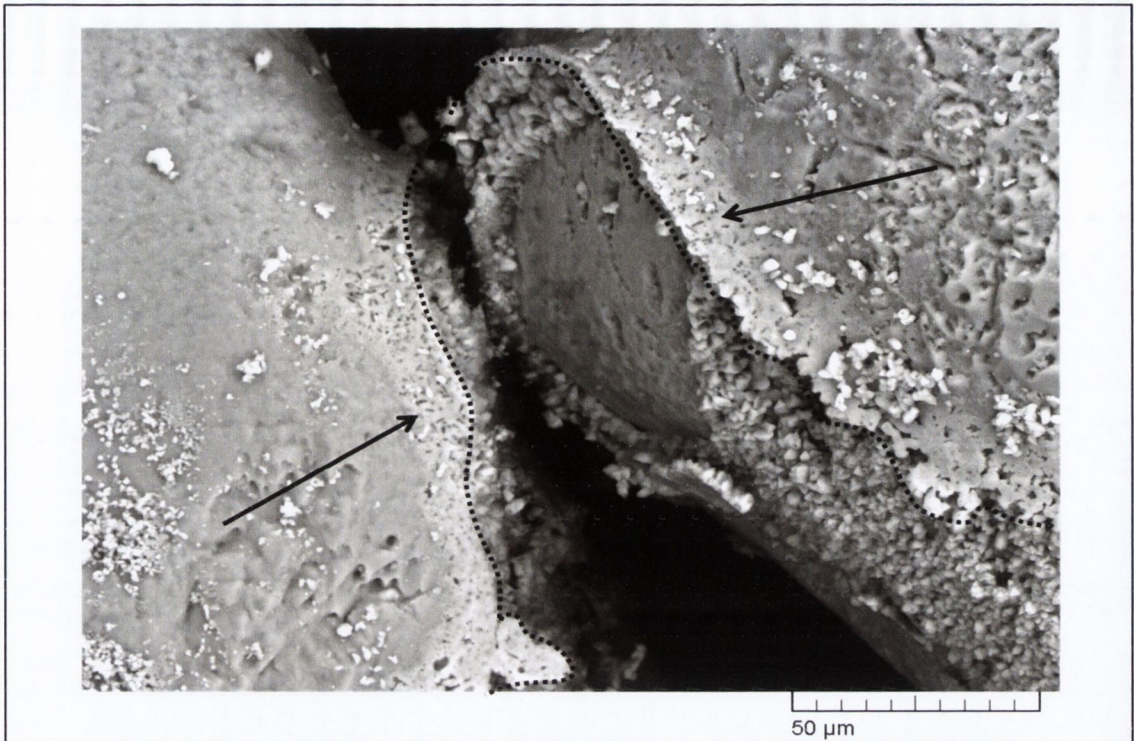


**Figure 6.11** Detail of a carbonate lip (dashed line), sample E150. Arrows indicate where rod-shaped imprints of bacteria attached to the AWI are mostly visible.

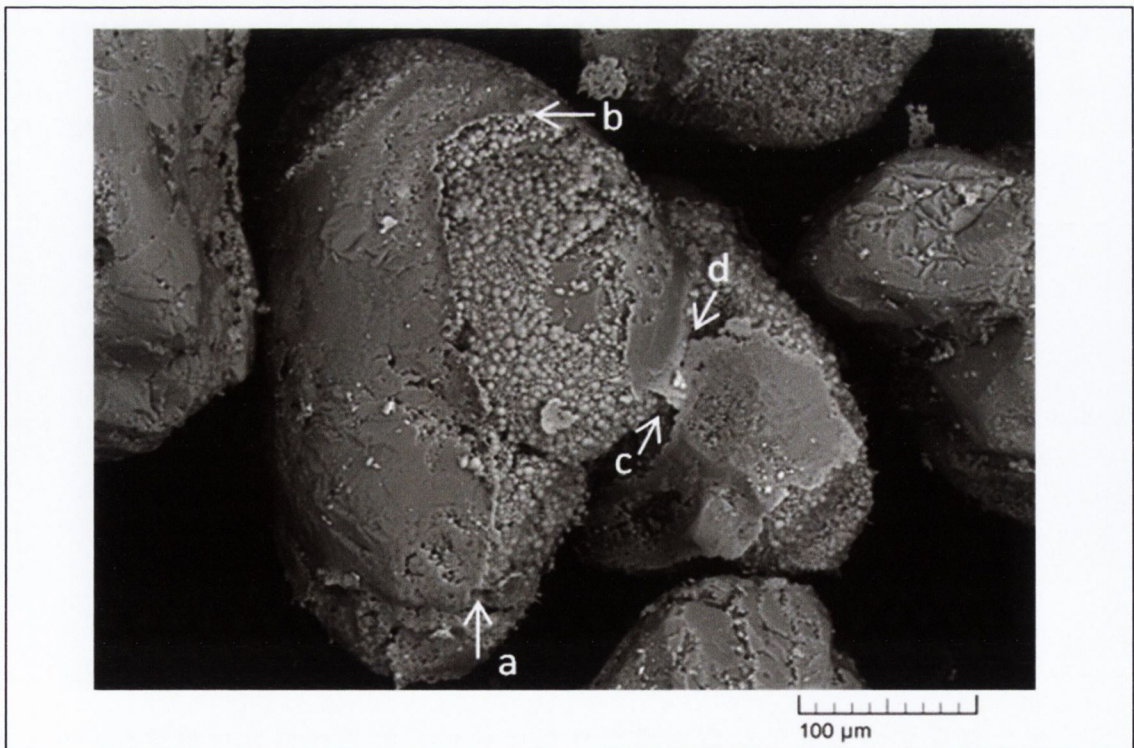


**Figure 6.12** Sample E500 showing the exposed edge of a carbonate lip (a-b) where a secondary bond failed to form, and a fully formed secondary bond (c-d).



The scarcity of secondary bonds in heavily treated samples is interpreted as mostly being a consequence of: (1) relatively high supersaturation occurring in the reaction environment; (2) the surface tension of the cementation liquid. As shown in Figures 6.13 and 6.14, copious amounts of amorphous spherulites are precipitated on the surface of sand particles in both E500 and E1000 samples. E150, however, showed predominant formation of calcite, which would lead to conclude that the localised rapid depletion of the reagents in highly supersaturated environments made them unavailable for the precipitation at the AWI. It should be noted that presence of empty spherulites in Figure 6.14 would be indication of Oswald ripening taking place (Zhou, Yao et al. 2010).

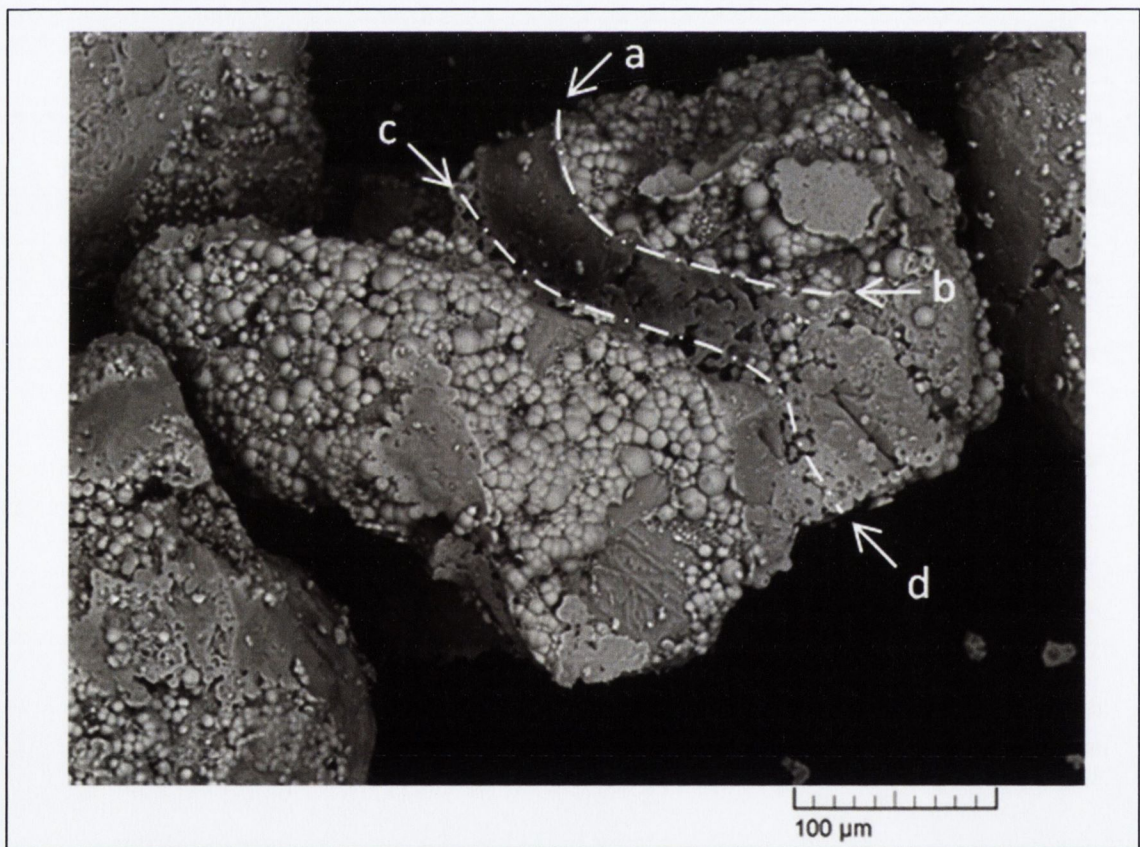


**Figure 6.13** Sample E1000 showing the exposed edge of a carbonate lip (a-b), and a partially formed secondary bond (c-d). Vaterite spherulites formed within the confines of the menisci are clearly visible.

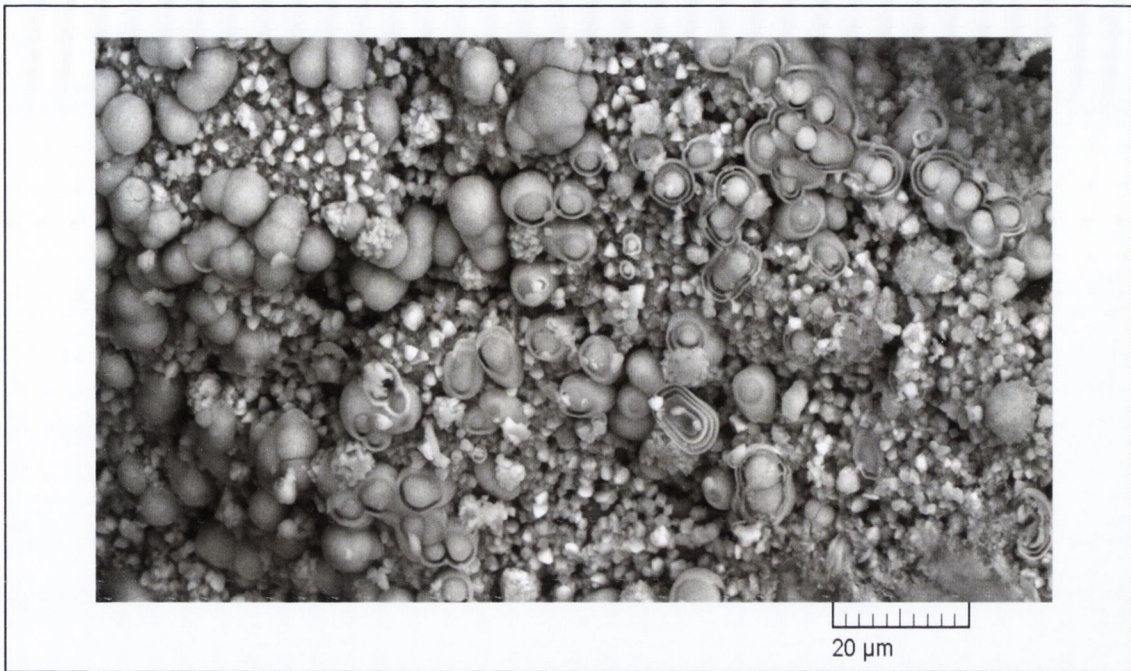


**Figure 6.14** Detail of vaterite spherulites and calcite crystals (E500).

The curvature of an air-liquid interface where a pressure difference,  $\Delta P$ , causes the surface to curve is related to the surface tension of the interface (Amyx, Bass et al. 1960; Gennes, Brochard-Wyart et al. 2004):

$$\Delta P = \gamma \left( \frac{1}{r_x} + \frac{1}{r_y} \right) \quad \text{Eq. 6.4}$$

where  $\Delta P$  is the pressure difference curving the surface,  $\gamma$  is the surface tension, and  $r_x$  and  $r_y$  are the radii of curvature along perpendicular planes normal to the surface.  $\Delta P$ , here is generated by capillary forces. Because the surface tension of a solution is directly proportional to its ionic strength (Adamson and Gast 1997), it is possible to conclude that the three liquids employed in the experiment would produce different AWI surfaces (Figure 6.15). At equilibrium, the ionic strength of E500 and E1000 would result in larger AWI surfaces (Figure 6.13) when compared with E150 (Figure 6.11). Therefore, significantly larger amounts of calcium carbonate would be required to complete the secondary bond.

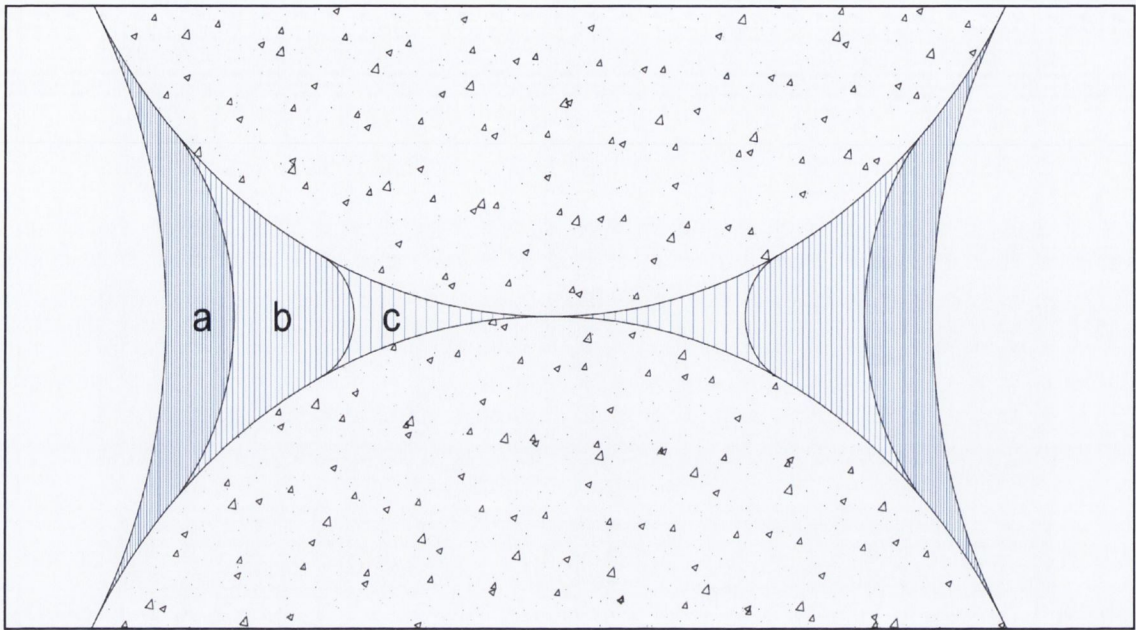


**Figure 6.15** Schematic representation of the water meniscus between two soil particles for different ionic strengths of the solution and fixed capillary pressure: **(a)** high ionic strength, **(b)** medium ionic strength and **(c)** low ionic strength.

## 2.7 FAILURE OF THE INTER-PARTICLE BOND

The failure mechanism observed was consistent among all samples and is best illustrated in Figure 6.16. Failure of the primary bond occurs with the same mode observed for eutrophic samples in Experiment N. 2. A hybrid failure surface, involving the bond-bond as well as the bond-particle interface, represents the typical mechanism for primary bond failure. When present, the secondary bond typically fails at the bond-bond interface. The failure surface usually runs along the suture where the lips touched before forming the secondary bond. While it could be speculated that the secondary bond is likely to be the first to fail, the order in which the bonds fail could not be confidently determined from the data available.

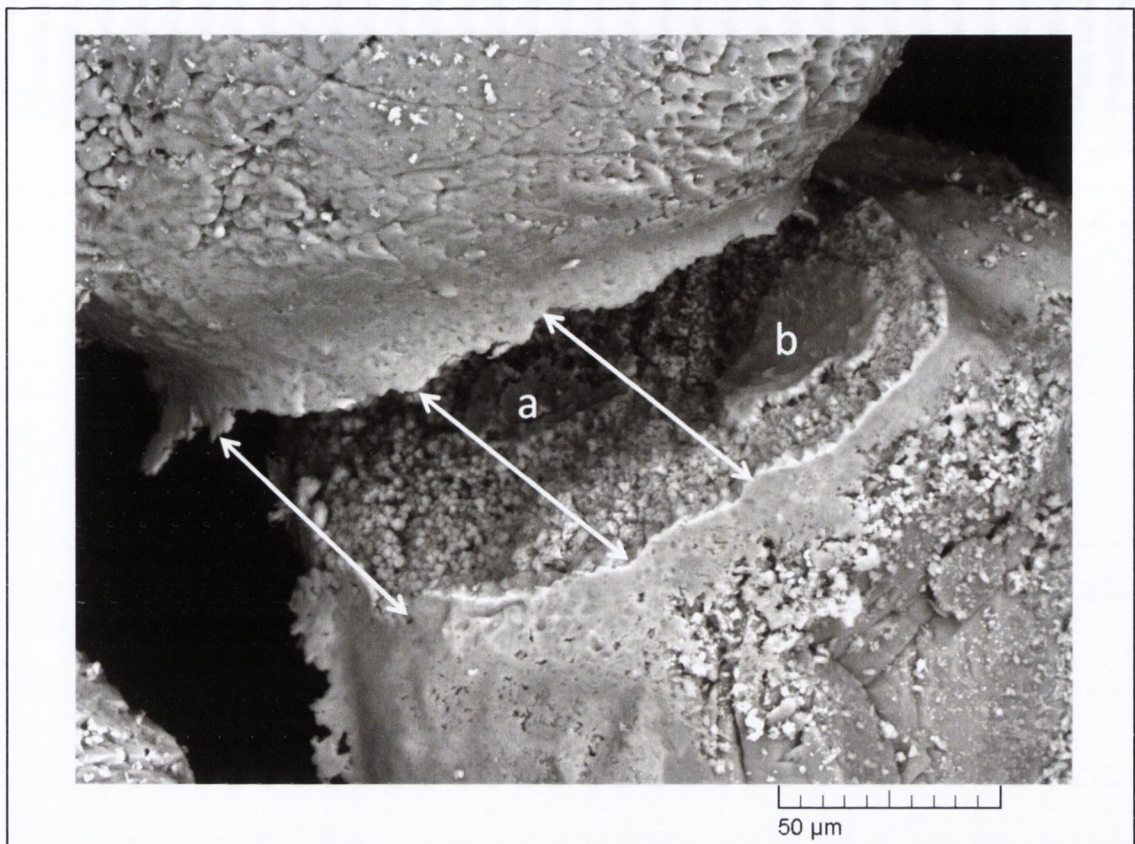


**Figure 6.16** Failure of the primary and secondary bond. Imprint in the calcium carbonate surface of the top sand particle (a, b) along a bond-particle failure of the primary bond. Matching points along the failure surface of the secondary bond (arrows).

## 2.8 INTERIM CONCLUSIONS

The experiment successfully demonstrated the viability of aerosol delivery methods for *in-situ* MICP using eutrophic protocols. In particular, adopting a pulsed injection regime significantly increased the overall performance of the method by delaying the stripping of volatile molecules to a time when the reagents were fully exploited by the process. While stripping of water was also observed, this had no impact on the efficiency due to the mitigating effect of increasing reagent concentrations.

Some limitations have been identified in the present technology which make medical jet nebuliser unsuitable for large scale applications.

Among these, during the late stages of the treatment it was necessary to increase the pressure of the air entering the column to up to 150 kPa in order to maintain an airflow between 6 L min<sup>-1</sup> and 8 L min<sup>-1</sup> (an operational requirement of the nebuliser unit). This raises concern as it might lead to soil fracturing and weakening of the bonds so far formed; more so in a full scale application that usually would require larger amounts of cement to be precipitated. However, the use of alternative nebulisation units, where the nebulisation process is disjoint from the air feed, could address this limitation.

Additionally, the low overall conversion efficiency,  $OC_{eff}$ , is a matter of concern with regards to the economical viability of aerosol delivery. However, low  $OC_{eff}$  values are associated with the deposition rate of droplets which is bound to increase should larger volumes of soil be considered: increased retention time as a result of longer pathways through the soil and decreasing airflow speed (Chapter 3, Paragraph 3). As previously observed by Glew (2009), a relatively low homogeneity of the treatment is also among the limitations.

The concentration of the process reagents in the cementation liquid has shown to be a key factor for the design of the treatment regime and holding times. However, the length of the reaction pauses should be reviewed in the context of the biological potential of the eutrophic liquids employed as these appear to determine the ureolytic potential of the soil column. In fact, in Experiment N. 5 the average ureolysis rate of the columns was found to be significantly lower (one order of magnitude) than what would have been granted by the initial urease injected in the column (up to  $3.6 \cdot 10^{-2}$  mol h<sup>-1</sup>). Interestingly, the limit value recorded in Experiment N. 5 (circa  $3 \cdot 10^{-3}$  mol h<sup>-1</sup>) was comparable with that recorded for similarly sized columns by other authors (circa  $1.5 \cdot 10^{-3}$  mol h<sup>-1</sup>) which instead saw an increase from initial values of approximately  $2 \cdot 10^{-5}$  mol h<sup>-1</sup> (Al Qabany, Soga et al. 2012). Differences in the parameters between the two experiments do not

allow for a definitive determination of the effect of nutrients but the results indicate that bacterial growth (or limits to it) should be considered as a relevant control factor (Chapter 2, Table 4.1 and Paragraph 5).

As hypothesised during the review of the work presented by Cheng et al. (2012), the UCS results and the SEM images indicate that a more effective treatment (higher UCS/[CaCO<sub>3</sub>] ratio) of unsaturated soil should be expected when compared with treatment of saturated soils. Calcium carbonate is deposited within the confines of the menisci formed between particles. Therefore, calcium carbonate is formed at locations conveniently positioned to increase strength.

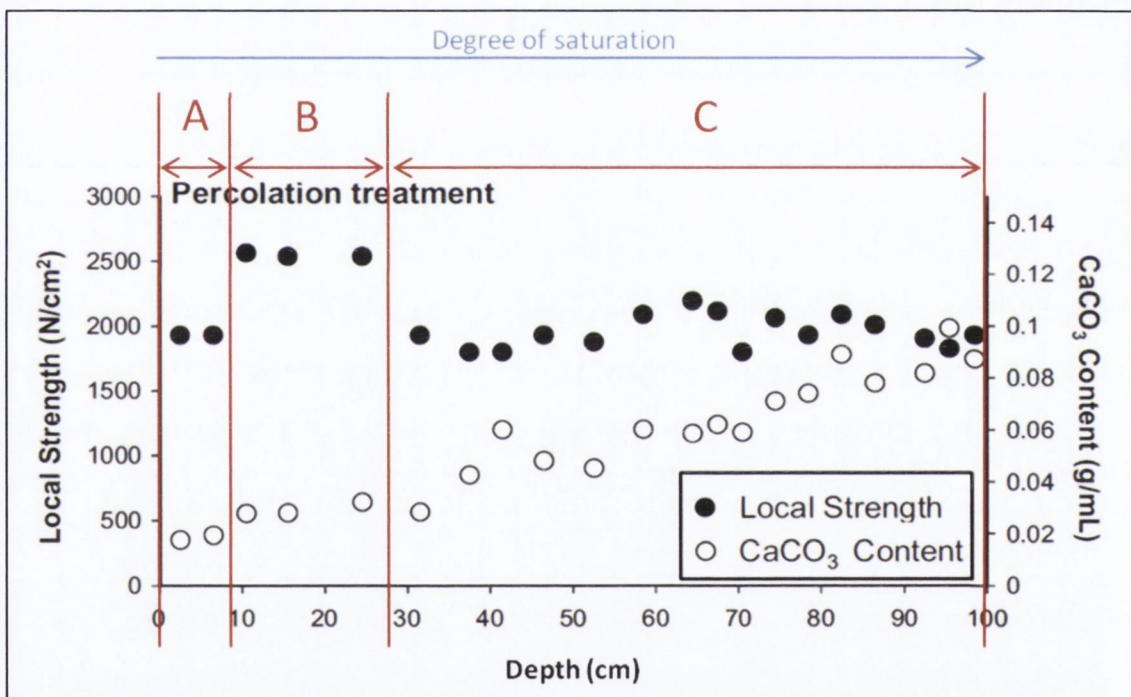


**Figure 6.17** Dual bond interpretation of the results presented by Cheng et al. (2012). **(A)** Pendular regime, the meniscus is too small and no distinction exists between primary and secondary bond. **(B)** Pendular regime, a secondary bond is formed producing a strength increase. **(C)** Funicular regime, the secondary bond is not complete and only the primary bond is contributing to strength; calcium carbonate content increases but is deposited on the surface of particles and at the AWI without increasing strength.

A key feature of the inter-particle bond formation process in unsaturated soils is the presence of a dual bond meniscus structure, where the AWI acted as an additional deposition surface for both

bacteria and calcium carbonate. The SEM images highlighted the role of local super saturation and ionic strength of the solution as factors controlling the formation of the secondary bond. Interestingly, the concept can be extended to the results presented by Cheng et al. (2012). When the ionic strength of the solution is kept constant, the shape of the meniscus in transitioning from pendular regime to capillary fringe would be consisted with Figure 6.15, where (c) represents the pendular regime and, (b) and (a) represent increasingly wet funicular regimes (Chapter 2, Paragraph 6.2). As seen in Figure 6.17 the presence of a dual bond could explain the results obtained using percolation treatment methods.

## **1) BOND FORMATION, STRUCTURE AND FAILURE**

Overall the research has demonstrated that a significant number of parameters have a bearing on the formation, structure and failure of the carbonate bond being formed during the MICP treatment of soils. Among these, the treatment protocol employed is considered to be the most relevant. In fact, the addition of nutrients, in the form of yeast extract or nutrient broth, was shown to control the abundance and distribution of *S. pasteurii* in the context of pore scale phenomena. This is the first time that a distinction between the two protocols is highlighted and the results indicate that the consequences of their effect on pore scale phenomena extend to the macro scale. While oligotrophic treatment has been shown to be a viable protocol in this and other studies, eutrophic protocols would present the following advantages:

- Preferential retention of bacteria at or near inter-particle contact points;
- Constant biomass as determined by the amount of nutrients provided;
- Requires less biomass to be injected during bioaugmentation.

However, these advantages are partially off-set by the increased cost of the treatment associated with the addition of nutrients. Additionally, application in natural environments could be adversely affected by the growth of indigenous bacteria species (biofouling).

Most crucially, the research presented here suggests that eutrophic protocols, when compared with oligotrophic treatments, would produce a larger increase in a soil's strength for a given increase



in carbonate content. Therefore a correlation between calcium carbonate content and unconfined compressive strength should be assumed limited to within the context of a specific treatment protocol. However, while the presence or absence of nutrients in the cementation solution has shown to control the structure of the bond, it is unclear if the higher efficacy of eutrophic protocols is to be ascribed to stronger bonds or to strategically located precipitation of calcium carbonate. The latter aspect would appear to be more relevant but the different failure surfaces observed for oligotrophic and eutrophic samples imply that further investigation would be required.

The mineral composition of the soil matrix has shown to significantly affect the deposition pattern of calcium carbonate. When compared to silica sand, carbonaceous sand has shown to promote the widespread and abundant precipitation of calcium carbonate by promoting the deposition of bacteria as well as by providing surfaces that promote the growth and nucleation of calcium carbonate crystals. However, these were broadly distributed over the particles' surfaces indicating that higher precipitation efficiency could come at the cost of reduced efficacy of the treatment; especially when the treatment is designed to produce a mild cementation. Failure surfaces in carbonaceous sand could not be clearly identified indicating that the newly formed calcium carbonate is intimately bound to the soil particles. Therefore, failure models of carbonaceous matrixes should be extended to include particle-particle failure surfaces at the pore scale; in particular when considering heavily cemented soils.

Provided that the particle size of the matrix allows for effective treatment, its impact is seen to be limited to the bioaugmentation injection. In fact, fine sand has shown to retain larger amounts of biomass during this phase when compared to medium sand. The consequences would be more evident in oligotrophic treatments where the initial bioaugmentation is required to deliver sufficient urease

enzyme for the completion of the treatment. Conversely, when employing eutrophic protocols, biomass appears to be controlled by the amount of nutrients added to the cementation solution. This is considered a key finding because improved mathematical models will have to account for changes in the retained urease activity occurring as a result of nutrient additions. Therefore, future research on this aspect of MICP should focus on providing quantitative relationships between the amount and type of nutrients added to the cementation solution, and the urease activity present in the soil.

When compared to saturated soils, the treatment of unsaturated soils resulted in the formation of substantially different bonding structures. A key feature of the bond formed in unsaturated soils is represented by the possible formation of a dual bond meniscus structure between particles. The presence, or absence, of the secondary bond has shown to be strongly related to the shape of the meniscus formed during the cementation phase. This is controlled by the occurring capillary forces which are in turn determined by the soil's saturation regime and by the ionic strength of the cementation solution. Therefore, characterising the dual bond meniscus structure has allowed to improve the interpretation and understanding of macro scale properties of MICP applications in unsaturated soils. Evidence suggest that a higher efficacy should be expected when treating unsaturated soil, which further reiterates the need to contextualise any correlation that might be established between the calcium carbonate content of a sample and its mechanical properties. The literature to date has mostly focussed on the biogrout of saturated soils, future research should be directed at providing further knowledge on the application of biogrout to unsaturated soils in order to assist the development of dedicated computational tools.

## 2) ATOMISED DELIVERY OF PROCESS REAGENTS

The results demonstrated the viability of aerosol delivery methods for *in-situ* MICP when eutrophic protocols are employed. A key advantage is represented by the ability to prevent the loss of liquid reagents by percolation. Some limitations have been, however, identified in the present technology which make medical jet nebuliser unsuitable for large scale applications. As shown in Table 7.1, a substantial improvement would be produced if the air flow and the atomisation process were independent of each other.

**Table 7.1** Limitations and potential improvement delivered by a delivery system where atomisation is independent of air flow.

<b>Issue</b>	<b>Improvement</b>
Elevated/increasing injection pressure	Independent control of the air pressure/flow would allow to adjust the injection system to the reducing porosity of the soil.
Limited flow of nebulised liquid	A nebulizer unit independent of the airflow would allow to deliver larger volumes of fluid. Complete independence cannot however be achieved as a high liquid/carrier flow ratio would lead to droplet coalescence.
Low uniformity of distribution	In a dual system, the size of the droplets could be adjusted during the process to control the distance at which droplets are deposited. Additionally, air could be injected (without aerosol) to improve uniformity by displacing previously deposited liquids.
Low overall conversion efficiency	The low conversion efficiency is mostly associated with a proportion of fine droplets being transported beyond the treatment area. This is considered a minor limitation in the context of large scale applications. However it highlights the need to select a nebulizer unit capable of producing a fine band of droplet size which can be adjusted to suit specific field conditions.

The use of atomised delivery systems, however, was unsuitable for the application of oligotrophic protocols. This was ascribed to the effect that biological stress had on *S. pasteurii* as a result of exposure to the high energy environment of the nebulisation process. The presence of nutrients in eutrophic cementation liquids would have mitigated the negative effects of nebulisation by sustaining the recovery of microbes once these became deposited in the soil.

Atomised delivery of MICP reagents in unsaturated soils is a promising technology and future research should focus on overcoming the issues identified in Table 7.1. Interestingly, the technology could also be extended to the MICP treatment of saturated soil. In fact, the dewatering of a soil brought about by the introduction of a gaseous carrier such as air would lead to the establishment of a temporary partially saturated regime. This could potentially lead to the development of widely applicable technological solutions.

### **3) DEPOSITION OF DOLOMITE**

The results obtained in this study showed that the deposition of primary dolomite is an unlikely occurrence in the present context of MICP for soil improvement. However, future research should investigate the potential role of additives in assisting the precipitation of low temperature dolomite from solutions containing calcium and magnesium ions.

The addition of magnesium ions to the cementation solution has proven to promote the formation of stable calcite over a less stable vaterite cement. However this was not investigated further in this study. Future research should investigate the role of small magnesium additions as an MICP additive.

#### **4) LIMITATIONS OF THIS STUDY**

One of the main limitations in this study is represented by the use of relatively uniformly graded soil samples. Therefore, the results and conclusions presented are mostly valid within the context of this limitation. However, some of the conclusions could be cautiously extended to graded soils where the fine component is mostly represented by fine to medium sand.

Another relevant limitation is represented by the scale of the study. Bench-top experiments were deemed sufficient for the investigation of pore scale phenomena. However, the use of medical jet nebulisers in small test columns highlighted the unsuitability of such a nebuliser unit in the context of field applications. It is therefore assumed that, while informative, the validity of considerations regarding uniformity of the treatment and overall conversion efficiency is limited to small scale experiments when atomised delivery is considered.

## REFERENCES

---

- Abu-Ashour, J., D. M. Joyi, et al. (1994). "Transport of microorganisms through soil." Water, Air, and Soil Pollution **75**(1-2): 141-158.
- Adamson, A. W. and A. P. Gast (1997). Physical chemistry of surfaces. New York, Wiley.
- Al Qabany, A. and K. Soga (2013). "Effect of chemical treatment used in MICP on engineering properties of cemented soils." Géotechnique **63**(4): 331-339.
- Al Qabany, A., K. Soga, et al. (2012). "Factors Affecting Efficiency of Microbially Induced Calcite Precipitation." Journal of Geotechnical and Geoenvironmental Engineering **138**(8): 992-1001.
- Amyx, J. W., D. M. Bass, et al. (1960). Petroleum Reservoir Engineering, Physical Properties. New York, R.L. McGraw-Hill.
- Bachmeier, K. L., A. E. Williams, et al. (2002). "Urease activity in microbologically-induced calcite precipitation." Journal of Biotechnology **93**(2): 171-181.
- Balleur, S. D. and O. Girinski (2008). Amélioration de la résistance d'un matériaux poreux ou perméable, ou de la calcification bactérienne. I. N. d. I. P. Industrielle. **FR 2 911 887 - A1**.
- Banfield, J. F. and K. H. Nealson (1997). Geomicrobiology : interactions between microbes and minerals. Washington, D.C., Mineralogical Society of America.
- Bang, S. S., J. J. Lippert, et al. (2010). "Microbial calcite, a bio-based smart nanomaterial in concrete remediation." International Journal of Smart and Nano Materials **1**(1): 28-39.

- Banks, E. D., N. M. Taylor, et al. (2010). "Bacterial calcium carbonate precipitation in cave environments: A function of calcium homeostasis." Geomicrobiology Journal **27**(5): 444-454.
- Barkouki, T. H., B. C. Martinez, et al. (2011). "Forward and Inverse Bio-Geochemical Modeling of Microbially Induced Calcite Precipitation in Half-Meter Column Experiments." Transport in Porous Media.
- Bayvel, L. and Z. Orzechowski (1993). Liquid Atomization. Washington DC, Taylor and Francis.
- Benini, S., W. R. Rypniewski, et al. (1999). "A new proposal for urease mechanism based on the crystal structures of the native and inhibited enzyme from *Bacillus pasteurii*: Why urea hydrolysis costs two nickels." Structure **7**(2): 205-216.
- Berner, R. A. (1975). "The role of magnesium in the crystal growth of calcite and aragonite from sea water." Geochimica et Cosmochimica Acta **39**(4): 489-504.
- Bhattacharjee, S., C. H. Ko, et al. (1998). "DLVO interaction between rough surfaces." Langmuir **14**(12): 3365-3375.
- Boelsma, F., E. C. L. Marnette, et al. (2000). In situ air sparging - A technical guide Dutch Research Programme In-Situ Bioremediation. **vers. 1.1**.
- Bosak, T. and D. K. Newman (2003). "Microbial nucleation of calcium carbonate in the Precambrian." Geology **31**(7): 577-580.
- Bradford, S. A., J. Simunek, et al. (2003). "Modeling colloid attachment, straining, and exclusion in saturated porous media." Environmental Science and Technology **37**(10): 2242-2250.
- Bradford, S. A., J. Simunek, et al. (2006). "Significance of straining in colloid deposition: Evidence and implications." Water Resources Research **42**(12).
- Bradford, S. A., S. Torkzaban, et al. (2007). "Coupling of physical and chemical mechanisms of colloid straining in saturated porous media." Water Research **41**(13): 3012-3024.

- Braissant, O., E. P. Verrecchia, et al. (2002). "Is the contribution of bacteria to terrestrial carbon budget greatly underestimated?" Naturwissenschaften **89**(8): 366-370.
- Bressler, E. (1977). "Trickle-drip irrigation principles and application to soil-water management." Advances in Agronomy **29**: 343-393.
- Burbank, M. B., T. J. Weaver, et al. (2011). "Precipitation of calcite by indigenous microorganisms to strengthen liquefiable soils." Geomicrobiology Journal **28**(4): 301-312.
- Burbank, M. B., T. J. Weaver, et al. (2012). "Urease Activity of Ureolytic Bacteria Isolated from Six Soils in which Calcite was Precipitated by Indigenous Bacteria." Geomicrobiology Journal **29**(4): 389-395.
- Cacchio, P., C. Ercole, et al. (2003). "Calcium carbonate precipitation by bacterial strains isolated from a limestone cave and from a loamy soil." Geomicrobiology Journal **20**(2): 85-98.
- Castanier, S., G. Le Métayer-Levrel, et al. (1999). "Ca-carbonates precipitation and limestone genesis -- the microbiogeologist point of view." Sedimentary Geology **126**(1-4): 9-23.
- Cheng, L. and R. Cord-Ruwisch (2012). "In situ soil cementation with ureolytic bacteria by surface percolation." Ecological Engineering **42**(0): 64-72.
- Cheng, X. and J. Shen (2008). Microorganism cause concrete or concrete, producing method and application thereof. **CN101270369 (A)**.
- Chieffi, G. (1994). Biologia. Roma, Antonio Delfino Editore.
- Chu, J. (2012). Session 7 - BiogROUT and other grouting methods - General Report. ISSMGE - TC 211 International Symposium on Ground Improvement IS-GI Brussels.
- Chu, J., S. Varaksin, et al. (2009). Construction Processes. 17th International Conference on Soil Mechanics and Geotechnical Engineering, Alexandria, Egypt.
- Cölfen, H. and S. Mann (2003). "Higher-Order Organization by Mesoscale Self-Assembly and Transformation of Hybrid Nanostructures." Angewandte Chemie International(42): 2350-2365.



- Craig, R. F. (2004). Craig's soil mechanics. London ; New York, Spon Press.
- Crawford, R. L. and D. L. Crawford (2005). Bioremediation : principles and applications. Cambridge ; New York, Cambridge University Press.
- Cuthbert, M. O., M. S. Riley, et al. (2012). "Controls on the rate of ureolysis and the morphology of carbonate precipitated by *S. Pasteurii* biofilms and limits due to bacterial encapsulation." Ecological Engineering **41**(0): 32-40.
- DavidBall Ltd. (2011). "Product information sheet."
- De Vos, P., G. M. Garrity, et al., Eds. (2009). Bergey's Manual of Systematic Bacteriology Volume 3: The Firmicutes.
- Deelman, J. C. (1999). "Low-temperature nucleation of magnesite and dolomite." Neues Jahrbuch fur Mineralogie, Monatshefte **7**: 289-302.
- DeJong, J. T., M. B. Fritzges, et al. (2006). "Microbially induced cementation to control sand response to undrained shear." Journal of Geotechnical and Geoenvironmental Engineering **132**(11): 1381-1392.
- DeJong, J. T., B. M. Mortensen, et al. (2010). "Bio-mediated soil improvement." Ecological Engineering **36**(2): 197-210.
- DeJong, J. T., K. Soga, et al. (2011). "Soil engineering in vivo: Harnessing natural biogeochemical systems for sustainable, multi-functional engineering solutions." Journal of the Royal Society Interface **8**(54): 1-15.
- Dejong, J. T., K. Soga, et al. (2013). "Biogeochemical processes and geotechnical applications: progress, opportunities and challenges." Géotechnique **63**(4): 287-301.
- Di Cuia, R., A. Riva, et al. (2011). "Dolomite characteristics and diagenetic model of the Calcarei Grigi Group (Asiago Plateau, Southern Alps - Italy): An example of multiphase dolomitization." Sedimentology **58**(6): 1347-1369.
- Dupraz, C., R. P. Reid, et al. (2009). "Processes of carbonate precipitation in modern microbial mats." Earth-Science Reviews **96**(3): 141-162.

- Dupraz, C. and P. T. Visscher (2005). "Microbial lithification in marine stromatolites and hypersaline mats." Trends in Microbiology **13**(9): 429-438.
- Dyer, M., N. Glew, et al. (2012). "The delivery of bulk liquids as aerosols in granular soils for engineering purposes." Geotechnique Letters **2**: 181-185.
- Dyer, M., E. Marnette, et al. (2006). "Full-scale stimulation of reductive dechlorination using the Liner® technique." Engineering Geology **85**(1-2): 39-45.
- Ehrlich, H. L. (1998). "Geomicrobiology: its significance for geology." Earth-Science Reviews **45**(1-2): 45-60.
- Ehrlich, H. L. (1999). "Microbes as geologic agents: Their role in mineral formation." Geomicrobiology Journal **16**(2): 135-153.
- Ehrlich, H. L. and D. K. Newman (2009). Geomicrobiology. Boca Raton, CRC Press.
- Ellis, D. E. and P. W. Hadley (2009). "Sustainable remediation white paper—Integrating sustainable principles, practices, and metrics into remediation projects." Remediation Journal **19**(3): 5-114.
- Fang, Y. and B. E. Logan (1999). "Bacterial transport in gas-sparged porous medium." Journal of Environmental Engineering **125**(7): 668-673.
- Ferris, F. G., W. S. Fyfe, et al. (1987). "Bacteria as nucleation sites for authigenic minerals in a metal-contaminated lake sediment." Chemical Geology **63**(3-4): 225-232.
- Ferris, F. G., V. Phoenix, et al. (2004). "Kinetics of calcite precipitation induced by ureolytic bacteria at 10 to 20°C in artificial groundwater." Geochimica et Cosmochimica Acta **68**(8): 1701-1722.
- Filet, A. E., J. Gadret, et al. (2011). "Biocalcis, un nouveau procédé de consolidation de sols par voie biologique." Travaux **877**(Décembre Janvier 2011): 62-65.
- Folk, R. L. and L. S. Land (1975). "Mg/Ca Ratio and Salinity; Two Controls over Crystallization of Dolomite." AAPG Bulletin **59**(1): 60-68.

- Foppen, J. W. A. and J. F. Schijven (2005). "Transport of *E. coli* in columns of geochemically heterogeneous sediment." Water Research **39**(13): 3082-3088.
- Fujita, Y., F. G. Ferris, et al. (2000). "Calcium carbonate precipitation by ureolytic subsurface bacteria." Geomicrobiology Journal **17**(4): 305-318.
- Gal, J. Y., J. C. Bollinger, et al. (1996). "Calcium carbonate solubility: A reappraisal of scale formation and inhibition." Talanta **43**(9): 1497-1509.
- Gannon, J. T., V. B. Manilal, et al. (1991). "Relationship between cell surface properties and transport of bacteria through soil." Applied and Environmental Microbiology **57**(1): 190-193.
- Genes, P.-G. d., F. Brochard-Wyart, et al. (2004). Capillarity and wetting phenomena : drops, bubbles, pearls, waves. New York, Springer.
- Ghaly, A. E., Y. A., et al. (2013). "Effects of biostimulation and bioaugmentation on the degradation of pyrene in soils." J. Bioremed. Biodeg.(S5).
- Glew, N. (2009). Delivery of Atomised Carbon Substrates for In Situ Bioremediation of Chlorinated Solvents using Medical Jet Nebulisers. Glasgow, UK, University of Strathclyde. **PhD Thesis**.
- Gollapudi, U. K., C. L. Knutson, et al. (1995). "A new method for controlling leaching through permeable channels." Chemosphere **30**(4): 695-705.
- Gray, N. F. (2004). Biology of wastewater treatment. London, Imperial College Press.
- Grunwald, P. (1984). "Experimental section: Imparting some biochemical fundamentals in the course of basic education of chemistry students with the system urease/urea as an example." Biochemical Education **12**(4): 170-173.
- Hamdan, N., E. Kavazanjian, et al. (2011). Carbonate mineral precipitation for soil improvement through microbial denitrification, Dallas, TX.

- Han, Y. S., G. Hadiko, et al. (2005). "Effect of flow rate and CO<sub>2</sub> content on the phase and morphology of CaCO<sub>3</sub> prepared by bubbling method." Journal of Crystal Growth **276**(3-4): 541-548.
- Han, Y. S., G. Hadiko, et al. (2006). "Crystallization and transformation of vaterite at controlled pH." Journal of Crystal Growth **289**(1): 269-274.
- Han, Y. S., G. Hadiko, et al. (2006). "Influence of initial CaCl<sub>2</sub> concentration on the phase and morphology of CaCO<sub>3</sub> prepared by carbonation." Journal of Materials Science **41**(14): 4663-4667.
- Harkes, M. P., L. A. van Paassen, et al. (2010). "Fixation and distribution of bacterial activity in sand to induce carbonate precipitation for ground reinforcement." Ecological Engineering **36**(2): 112-117.
- Harkes, M. P., L. A. van Paassen, et al. (2008). Co-relation of unconfined compressive strength and carbonate content in the BioGrout process. 1st International Conference on BioGeoCivil Engineering. The Netherlands.
- Heibloem, M., K. Prins, et al. (1990). Methodes d'irrigation, Manuel de formation n. 5 Division de la mise en valeur des terres et des eaux, FAO.
- Ivanov, V. (2011). Environmental microbiology for engineers. Boca Raton, FL, CRC Press.
- Jahns, T. (1996). "Ammonium/urea-dependent generation of a proton electrochemical potential and synthesis of ATP in *Bacillus pasteurii*." Journal of Bacteriology **178**(2): 403-409.
- James, S. R., S. J. Dobson, et al. (1990). "Halomonas meridiana, a New Species of Extremely Halotolerant Bacteria Isolated from Antarctic Saline Lakes." Systematic and Applied Microbiology **13**(3): 270-278.
- Johnson, W. P., X. Li, et al. (2007). "Colloid retention in porous media: Mechanistic confirmation of wedging and retention in zones of flow stagnation." Environmental Science and Technology **41**(4): 1279-1287.
- Jonkers, H. M. and M. C. M. van Loosdrecht (2010). "BioGeoCivil Engineering." Ecological Engineering **36**(2): 97-98.

- Karol, R. H. (2003). Chemical grouting and soil stabilization. New York, M. Dekker.
- Keller, A. A. and M. Auset (2007). "A review of visualization techniques of biocolloid transport processes at the pore scale under saturated and unsaturated conditions." Advances in Water Resources **30**(6-7): 1392-1407.
- Knoll, A. H. and K. Swett (1990). "Carbonate deposition during the late Proterozoic era: an example from Spitsbergen." American Journal of Science **290 A**: 104-132.
- Konhauser, K. (2007). Introduction to geomicrobiology. Malden, MA, Blackwell Pub.
- Krajewska, B. (2009). "Ureases I. Functional, catalytic and kinetic properties: A review." Journal of Molecular Catalysis B: Enzymatic **59**(1-3): 9-21.
- Kralj, D., L. Brečević, et al. (1997). "Vaterite growth and dissolution in aqueous solution III. Kinetics of transformation." Journal of Crystal Growth **177**(3-4): 248-257.
- Kralj, D., L. Brečević, et al. (1990). "Vaterite growth and dissolution in aqueous solution I. Kinetics of crystal growth." Journal of Crystal Growth **104**(4): 793-800.
- Kralj, D., L. Brečević, et al. (1994). "Vaterite growth and dissolution in aqueous solution II. Kinetics of dissolution." Journal of Crystal Growth **143**(3-4): 269-276.
- Kucharski, E., G. Price, et al. (1997). Engineering Properties of CIPS cemented Calcareous Sand. Engineering Geology: Proceedings of the 30th International Geological Congress.
- Kucharski, E. S., R. Cord-Ruwisch, et al. (2006). Microbial Biocementation. W. I. P. Organization. **WO 2006/066326 A1**.
- Kucharski, E. S., R. Cord-Ruwisch, et al. (2008). Microbial Biocementation. **US 2008/024572 A1**.
- Land, L. S. (1998). "Failure to precipitate dolomite at 25 °C from dilute solution despite 1000-fold oversaturation after 32 years." Aquatic Geochemistry **4**(3-4): 361-368.

- Lefebvre, A. H. (1989). Atomization and sprays. New York, Hemisphere Pub. Corp.
- Li, L., C. X. Qian, et al. (2013). "Enzyme kinetic characterization of microbe-produced urease for microbe-driven calcite mineralization." Reaction Kinetics, Mechanisms and Catalysis **108**(1): 51-57.
- Li, X., C. L. Lin, et al. (2006). "Role of grain-to-grain contacts on profiles of retained colloids in porous media in the presence of an energy barrier to deposition." Environmental Science and Technology **40**(12): 3769-3774.
- Liebermann, O. (1967). "Synthesis of dolomite." Nature **213**(5073): 241-245.
- Lioliou, M. G., C. A. Paraskeva, et al. (2007). "Heterogeneous nucleation and growth of calcium carbonate on calcite and quartz." Journal of Colloid And Interface Science **308**(2): 421-428.
- Long, X., Y. Ma, et al. (2011). "In vitro synthesis of high Mg calcite under ambient conditions and its implication for biomineralization process." Crystal Growth & Design(11 (7)): 2866–2873.
- López-García, P., J. Kazmierczak, et al. (2005). "Bacterial diversity and carbonate precipitation in the giant microbialites from the highly alkaline Lake Van, Turkey." Extremophiles **9**(4): 263-274.
- Loste, E., R. M. Wilson, et al. (2003). "The role of magnesium in stabilising amorphous calcium carbonate and controlling calcite morphologies." Journal of Crystal Growth **254**(1-2): 206-218.
- Lourenço, S. D. N., D. Gallipoli, et al. (2012). "Formation and evolution of water menisci in unsaturated granular media." Géotechnique **62**(3): 193-199.
- Lumsden, D. N. (1979). "Discrepancy between thin-section and X-ray estimates of dolomite in limestone." Journal of Sedimentary Research **49**(2): 429-435.
- Martinez, B. C. and J. T. DeJong (2009). "Bio-Mediated soil improvement: Load transfer mechanisms at the micro- and macro- scales." Advances in Ground Improvement: Research to Practice in the United States and China: 242-251.

- Mastandrea, A., E. Perri, et al. (2006). "Microbial primary dolomite from a Norian carbonate platform: Northern Calabria, southern Italy." Sedimentology **53**(3): 465-480.
- McCallion, O. N. M., K. M. G. Taylor, et al. (1996). "Jet nebulisers for pulmonary drug delivery." International Journal of Pharmaceutics **130**(1): 1-11.
- McConnaughey, T. A. and J. F. Whelan (1997). "Calcification generates protons for nutrient and bicarbonate uptake." Earth-Science Reviews **42**(1-2): 95-117.
- Meldrum, F. C. and H. Cölfen (2008). "Controlling mineral morphologies and structures in biological and synthetic systems." Chemical Reviews **108**(11): 4332-4432.
- Mitchell, J. K. and J. C. Santamarina (2005). "Biological considerations in geotechnical engineering." Journal of Geotechnical and Geoenvironmental Engineering **131**(10): 1222-1233.
- Mobley, H. L. T., M. D. Island, et al. (1995). "Molecular biology of microbial ureases." Microbiological Reviews **59**(3): 451-480.
- Montoya, B. M., J. T. DeJong, et al. (2013). "Dynamic response of liquefiable sand improved by microbial-induced calcite precipitation." Géotechnique **63**(4): 302-312.
- Moore, D. M. and R. C. Reynolds (1997). X-ray diffraction and the identification and analysis of clay minerals. Oxford ; New York, Oxford University Press.
- Mullin, J. W. (2001). Crystallisation, Reed Educational and Professional Publishing.
- National Research Council (2006). Geological and geotechnical engineering in the new millennium: opportunities for research and technological innovation. Washington, DC, Committee on Geological and Geotechnical Engineering in the New Millennium: Opportunities for Research and Technological Innovation. National Research Council (U.S.): xiv, 206 p.
- NCIMB (2008). Revival of cultures. QF-77.
- NCIMB (2010). "NCIMB Culture Media v2.0."

- O'Callaghan, C. and P. W. Barry (1997). "The science of nebulised drug delivery." Thorax **52**(SUPPL. 2): S31-S44.
- Rawlings, D. E. (2002). "Heavy metal mining using microbes." Annual Review of Microbiology **56**: 65-91.
- Redman, J. A., S. L. Walker, et al. (2004). "Bacterial Adhesion and Transport in Porous Media: Role of the Secondary Energy Minimum." Environmental Science and Technology **38**(6): 1777-1785.
- Riding, R. (2000). "Microbial carbonates: The geological record of calcified bacterial-algal mats and biofilms." Sedimentology **47**(SUPPL. 1): 179-214.
- Riha, B. D., L. C. Murdoch, et al. (2010). Aerosol injection into vadose zone. Google Patents. U. S. P. Office. **US20100307754**.
- Sánchez-Román, M., J. A. McKenzie, et al. (2009). "Presence of sulfate does not inhibit low-temperature dolomite precipitation." Earth and Planetary Science Letters **285**(1-2): 131-139.
- Sánchez-Román, M., C. S. Romanek, et al. (2011). "Aerobic biomineralization of Mg-rich carbonates: Implications for natural environments." Chemical Geology **281**(3-4): 143-150.
- Sánchez-Román, M., C. Vasconcelos, et al. (2008). "Aerobic microbial dolomite at the nanometer scale: Implications for the geologic record." Geology **36**(11): 879-882.
- Scholl, M. A., A. L. Mills, et al. (1990). "The influence of mineralogy and solution chemistry on the attachment of bacteria to representative aquifer materials." Journal of Contaminant Hydrology **6**(4): 321-336.
- Schulz, H. (1998). "Mechanisms and factors affecting intrapulmonary particle deposition: Implications for efficient inhalation therapies." Pharmaceutical Science and Technology Today **1**(8): 336-344.
- Shellenberger, K. and B. E. Logan (2002). "Effect of molecular scale roughness of glass beads on colloidal and bacterial deposition." Environmental Science and Technology **36**(2): 184-189.



- Short, M. B., J. C. Baygents, et al. (2005). "Stalactite growth as a free-boundary problem: A geometric law and its platonic ideal." Physical Review Letters **94**(1).
- Srivithayapakorn, S. and A. Keller (2003). "Transport of colloids in saturated porous media: A pore-scale observation of the size exclusion effect and colloid acceleration." Water Resources Research **39**(4): SBH111-SBH1111.
- Stocks-Fischer, S., J. K. Galinat, et al. (1999). "Microbiological precipitation of CaCO<sub>3</sub>." Soil Biology and Biochemistry **31**(11): 1563-1571.
- Suer, P., N. Hallberg, et al. (2009). "Biogrouting compared to jet grouting: Environmental (LCA) and economical assessment." Journal of Environmental Science and Health - Part A Toxic/Hazardous Substances and Environmental Engineering **44**(4): 346-353.
- Suthersan, S. S. (1997). Remediation engineering : design concepts. Boca Raton, Fl., CRC-Lewis Publishers.
- Tagliaferri, F., J. Waller, et al. (2011). "Observing strain localisation processes in bio-cemented sand using x-ray imaging." Granular Matter **13**(3): 247-250.
- Taylor, G. and M. Gumbleton (2004). "Aerosols for macromolecule delivery: Design challenges and solutions." American Journal of Drug Delivery **2**(3): 143-155.
- Threlfall, T. (2003). "Structural and Thermodynamic Explanations of Ostwald's Rule." Organic Process Research and Development **7**(6): 1017-1027.
- Torkzaban, S., S. S. Tazehkand, et al. (2008). "Transport and fate of bacteria in porous media: Coupled effects of chemical conditions and pore space geometry." Water Resources Research **44**(4).
- van der Ruyt, M. and W. van der Zon (2009). "Biological in situ reinforcement of sand in near-shore areas." Proceedings of the Institution of Civil Engineers: Geotechnical Engineering **162**(1): 81-83.
- van der Star, W. R. L., Taher, E., Harkes, M. P., Blauw, M., van Loosdrecht, M. C. M. and van Paassen, L. A. (2010). "Use of waste streams and microbes for in situ transformation of sand into sandstone."

International Symposium on Ground Improvement Technologies and Case Histories, 2009 Singapore. Geotechnical Society of Singapore, 177-182.

van Lith, Y., R. Warthmann, et al. (2003). "Sulphate-reducing bacteria induce low-temperature Ca-dolomite and high Mg-calcite formation." Geobiology **1**(1): 71-79.

van Paassen, L. A. (2009). BioGrout, ground improvement by Microbially Induced Carbonate Precipitation. Department of Biotechnology, Delft University of Technology. Delft, The Netherlands. **Doctoral dissertation**.

van Paassen, L. A. (2011). Bio-mediated ground improvement: From laboratory experiment to pilot applications. Geo-Frontiers 2011: Advances in Geotechnical Engineering. Dallas, TX: 4099-4108.

van Paassen, L. A., C. M. Daza, et al. (2010). "Potential soil reinforcement by biological denitrification." Ecological Engineering **36**(2): 168-175.

van Paassen, L. A., R. Ghose, et al. (2010). "Quantifying biomediated ground improvement by ureolysis: Large-scale biogROUT experiment." Journal of Geotechnical and Geoenvironmental Engineering **136**(12): 1721-1728.

van Veen, J. A., L. S. van Overbeek, et al. (1997). "Fate and activity of microorganisms introduced into soil." Microbiology and Molecular Biology Reviews **61**(2): 121-135.

van Wijngaarden, W. K., F. J. Vermolen, et al. (2013). "A mathematical model for BiogROUT: Bacterial placement and soil reinforcement." Computational Geosciences **17**(3): 463-478.

Vasconcelos, C. and J. A. McKenzie (1997). "Microbial mediation of modern dolomite precipitation and diagenesis under anoxic conditions (Lagoa Vermelha, Rio De Janeiro, Brazil)." Journal of Sedimentary Research **67**(3): 378-390.

Walsh, R. (2012). Alternative Perspectives of Enzyme Kinetic Modeling Medicinal Chemistry and Drug Design. D. Ekinici. Rijeka, Croatia, InTech.

- Wang, W. H., B. Köhler, et al. (2008). "Molecular and physiological aspects of urea transport in higher plants." Plant Science **175**(4): 467-477.
- Whiffin, V. S. (2004). Microbial CaCO<sub>3</sub> precipitation for the production of biocement. School of Biological Science & Biotechnology, Murdoch University. Perth, Western Australia. **Doctoral dissertation**: p. 154.
- Whiffin, V. S., L. A. van Paassen, et al. (2007). "Microbial carbonate precipitation as a soil improvement technique." Geomicrobiology Journal **24**(5): 417-423.
- Wiedemeier, T. H. (1999). Natural attenuation of fuels and chlorinated solvents in the subsurface. New York, John Wiley.
- Wright, D. T. and A. Oren (2005). "Nonphotosynthetic bacteria and the formation of carbonates and evaporites through time." Geomicrobiology Journal **22**(1-2): 27-53.
- Zeebe, R. E. and D. Wolf-Gladrow (2001). CO<sub>2</sub> in Seawater - Equilibrium, Kinetics, Isotopes, Elsevier.
- Zevi, Y., A. Dathe, et al. (2005). "Distribution of colloid particles onto interfaces in partially saturated sand." Environmental Science and Technology **39**(18): 7055-7064.
- Zhao, J. (2008). Rock Mechanics Course Material - Ch. 4: Properties of Rock Materials., École Polytechnique Fédérale de Lausanne, Switzerland.
- Zhou, G. T., Q. Z. Yao, et al. (2010). "Controlled crystallization of unstable vaterite with distinct morphologies and their polymorphic transition to stable calcite." European Journal of Mineralogy **22**(2): 259-269.

## ACKNOWLEDGMENTS

---

The work presented here would not have been possible without the financial support of the Irish Research Council for which I am grateful. Numerous individuals have contributed to this work through the years. It is with great pleasure and gratitude that I acknowledge their contribution.

I start by thanking Mark Dyer, my supervisor, who brought me in his team and gave me the courage to move back to Academia after several years in industry. Ronnie Russell, who became my co-supervisor and hosted me for many a day in his microbiology laboratory. Connie Crowley-Cribbin, who always took the time to answer my microbiology questions. Martin Carney and Eoin Dunne, who assisted and guided me in the geotechnical lab. Robbie Goodhue, who shared with me his knowledge of XRD analysis. Derek Simpson and all the staff at the Centre for Microscopy and Analysis, who introduced me to scanning electron microscopy. David Mc Aulay, who helped me with the construction of the test columns. Tom Grey and Ruth Jackson, colleagues and, above all, friends, who helped me with my English and were always available to discuss ideas.

A PhD though, is also a personal journey and a difficult one that is. I wish to thank those who accompanied me on it.

Silvia, my beloved wife. Her thoughtful words and relentless support have gotten me through the difficult times and made the good ones wonderful. I would not have made it without her. My parents and my brother whose support and affection were with me at all times. Federico and Andy, who were always there for a chat and a laugh when I needed one. Thank you all.

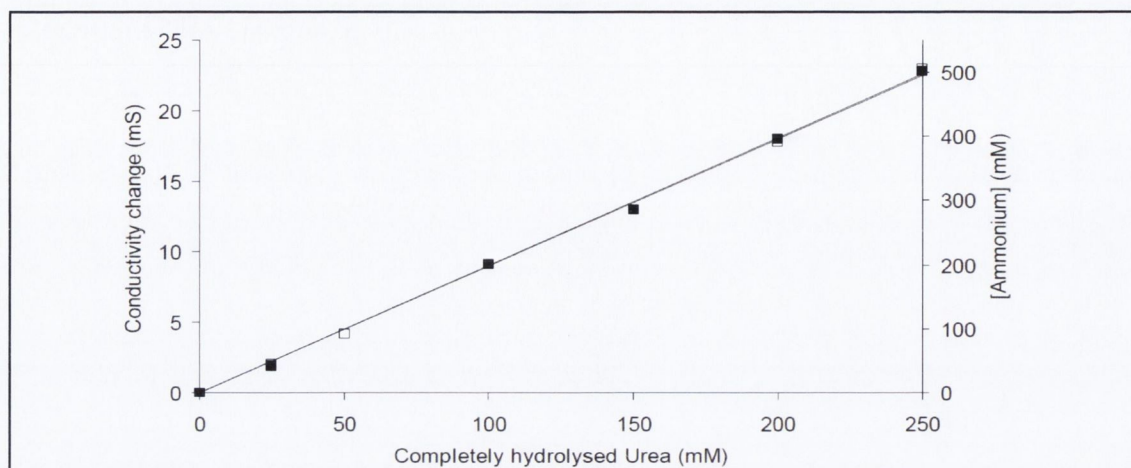


# APPENDIX ONE

---

MATERIALS AND METHODS

## Urease Activity from Electrical Conductivity Measures



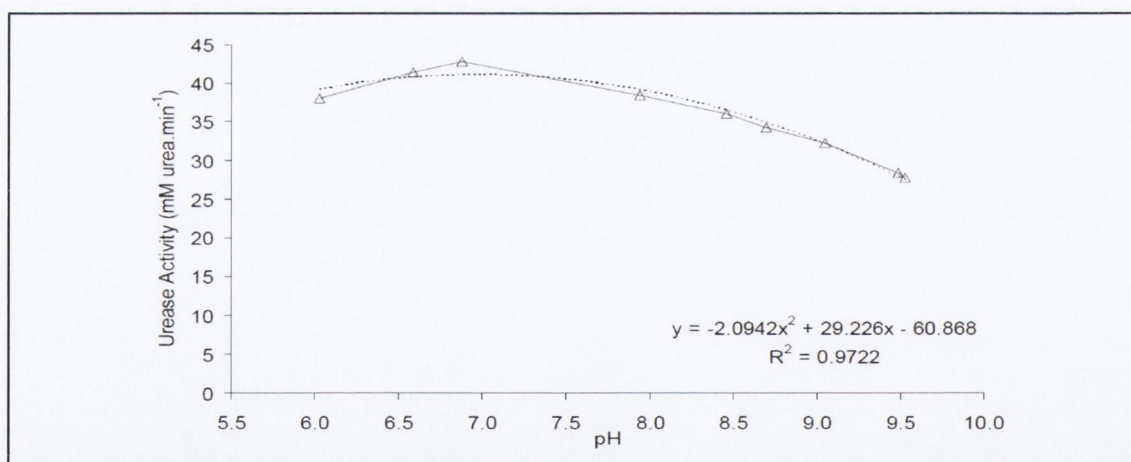
**Annex 1** Standard curve of electrical conductivity change and ammonium concentration after complete hydrolysis of urea (Whiffin 2004).

### Derived correlations:

$$\Delta_{Urea} (mM) = 11.11 \Delta_{EC} (mS) \quad (R^2 = 0.9988)$$

$$\Delta_{Urea} (mM) = 0.5 \Delta_{NH_4} (mM) \quad (R^2 = 0.9991)$$

## Urease Activity pH Correction Curve

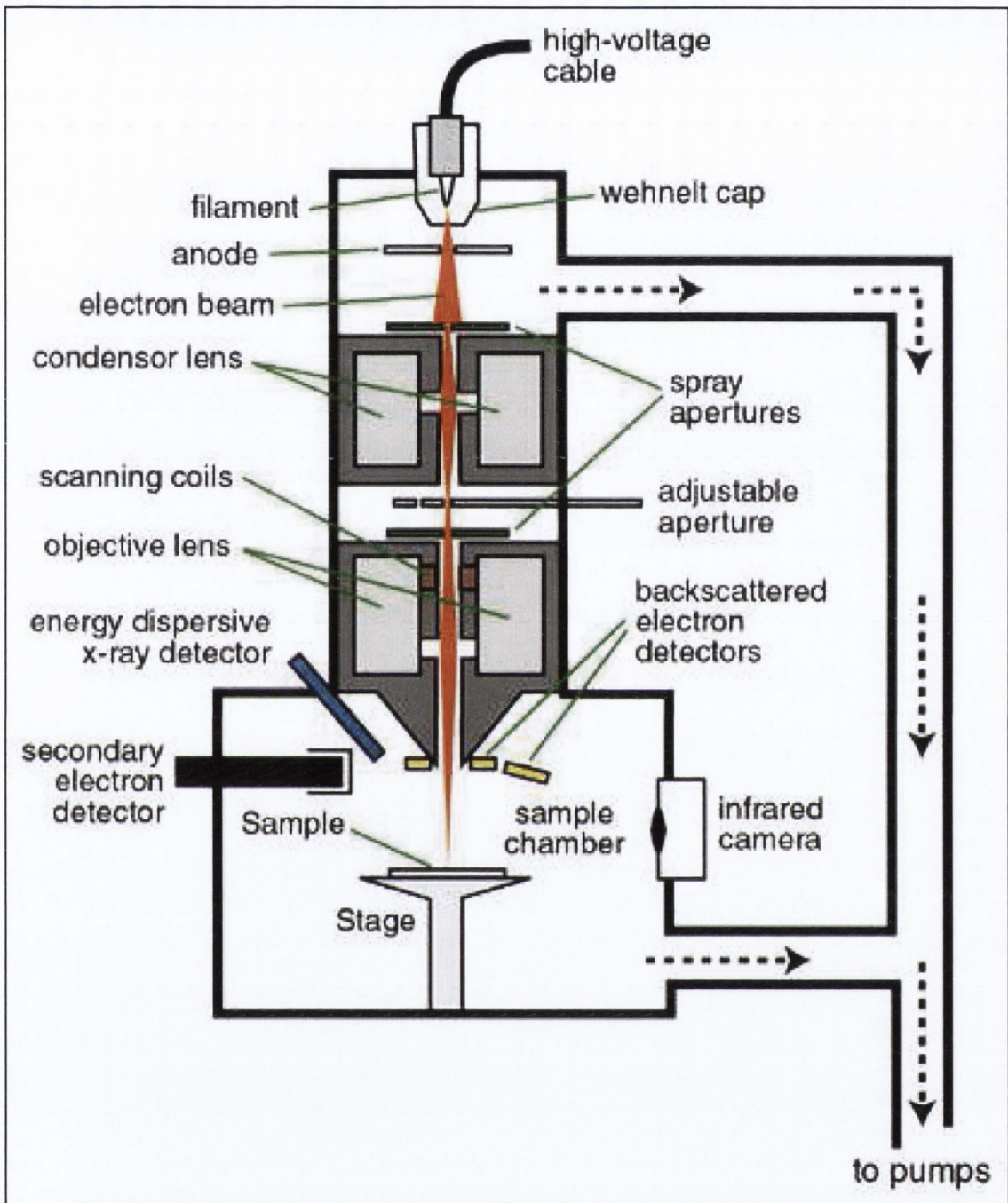


**Annex 2** Effect of pH on urease (standard) activity and fitted polynomial curve (Whiffin 2004).

### Correction factor:

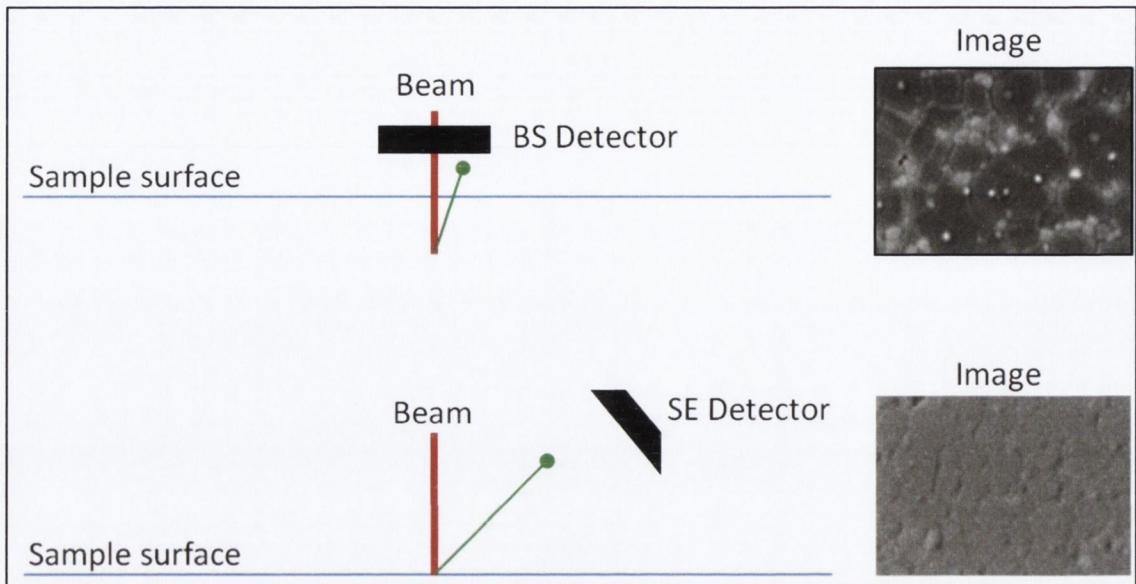
$$Activity_{pH7} = \left( \frac{Std. Activity_{pH7}}{Std. Activity_{pHx}} \right) \times Activity_{pHx}$$

## Scanning Electron Microscopy

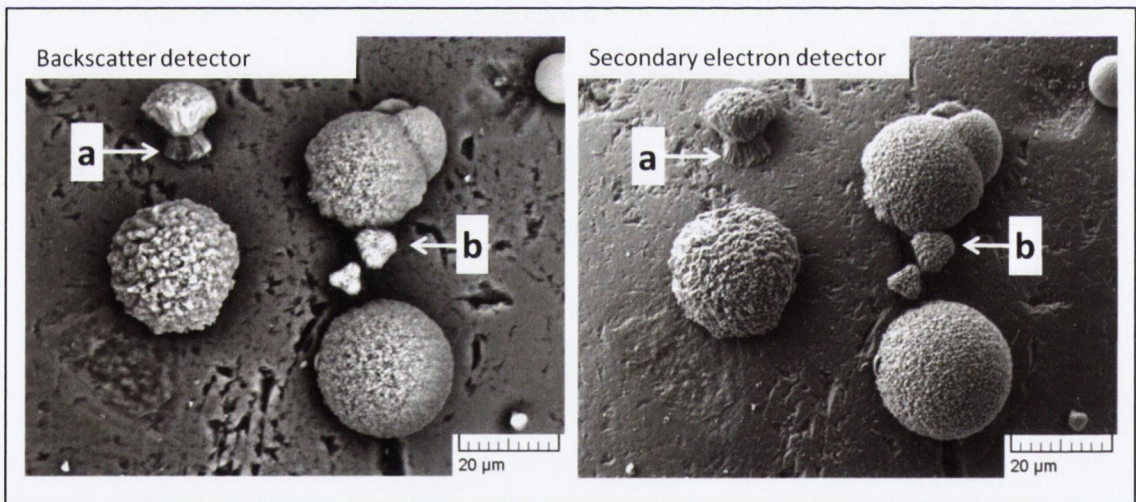


**Annex 3** Schematic representation of an SEM with EDX capability (<http://www4.nau.edu>).



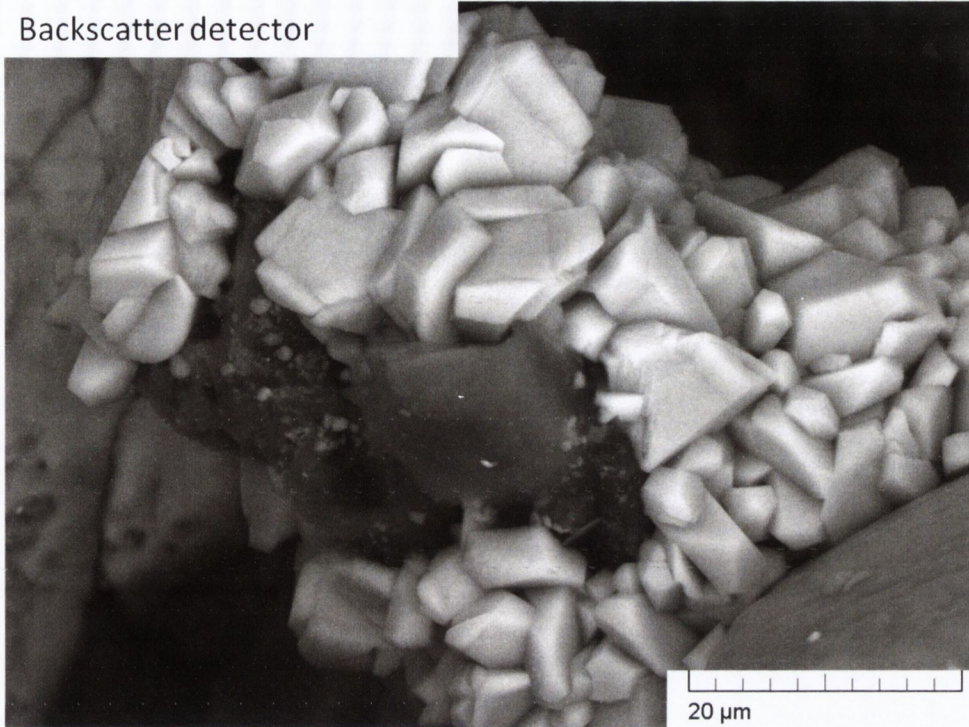


**Annex 4** Difference between backscatter detection (BSD) and secondary electron detection (SED). BSD greyscale are determined by the density (composition) of the material. SED greyscale represents topography: samples appear illuminated from the side because of the position of the detector.

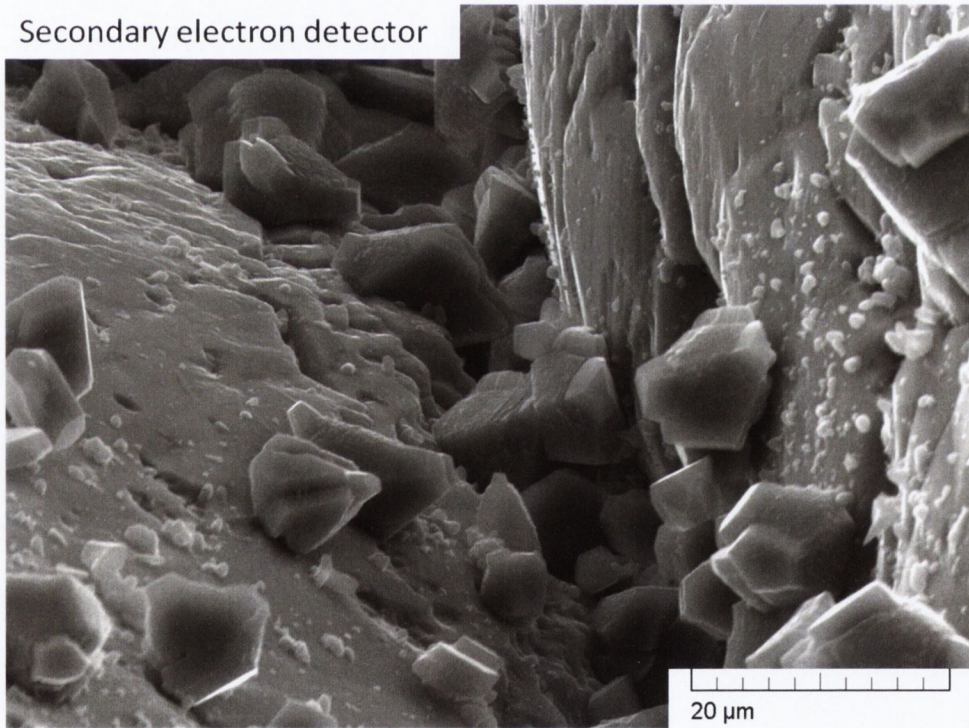


**Annex 5** The two images show the same portion of a silica sand particle covered by a number of small calcium carbonate deposits. The image on the left was acquired through the BSD and allows to discriminate between materials on the basis of density (carbonate is a lighter shade of grey). However, SED provides a better view of surface roughness, topography and structure (lighting from top left corner is clearly identifiable). **a** and **b** indicate locations where the difference is particularly evident.

Backscatter detector

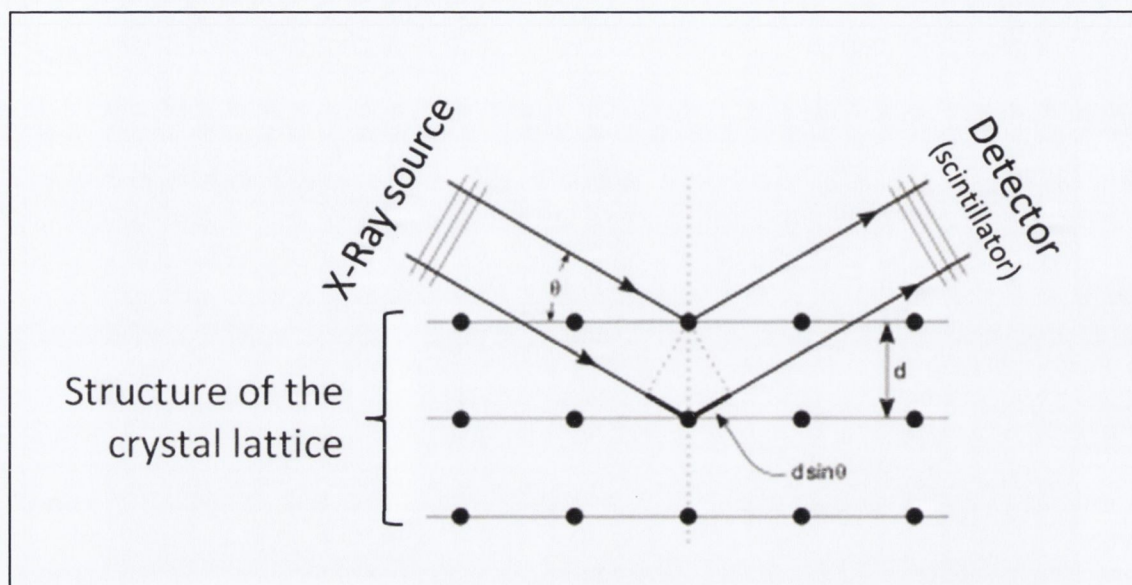


Secondary electron detector

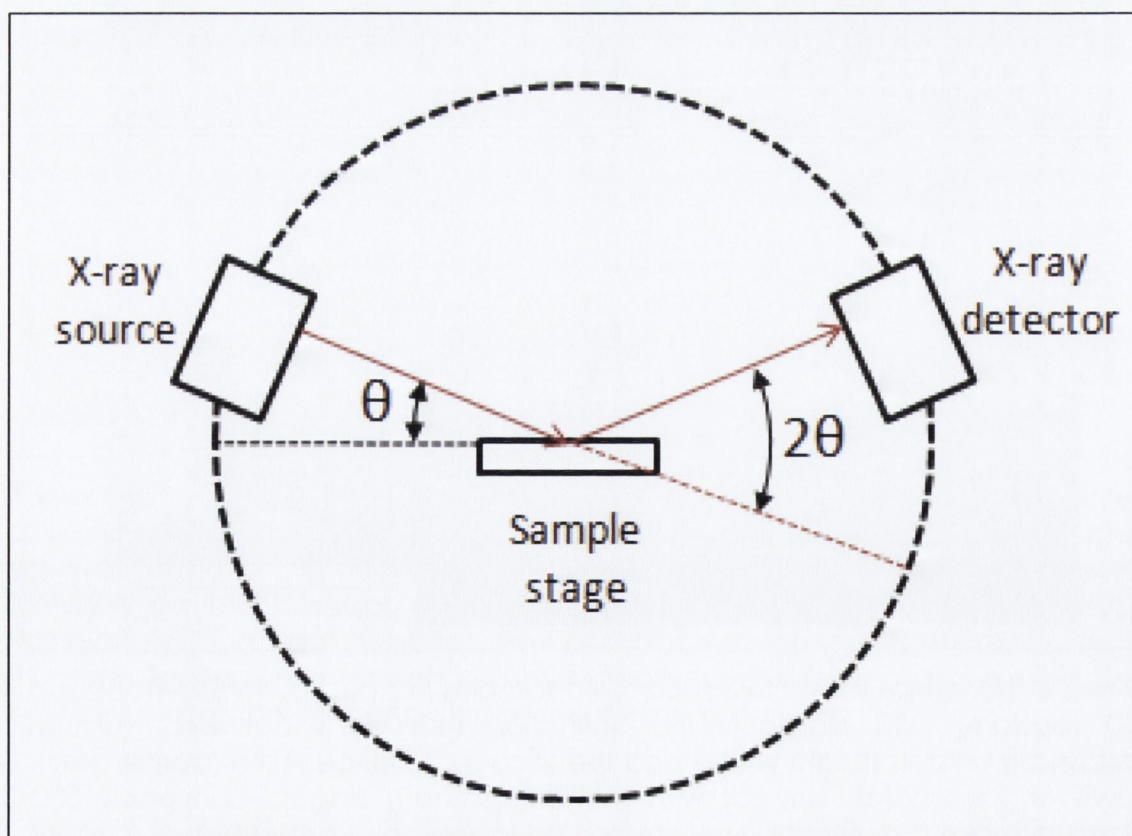


**Annex 6** The image shows two silica sand samples imaged using BSD (top) and SED (bottom). BSD highlights the distinction that exists between calcium carbonate crystals (bright white) and the silica material beneath (darker grey). However the crystals appear with rounded smooth edges. Conversely SED allows to make a distinction solely based on topography and structure. Calcite crystals formed between the two sand particles clearly identified and display sharp, distinct edges.

## X-Ray Diffraction Peak Analysis



**Annex 7** Schematic representation of an x-ray beam scattered by the atoms in a crystalline structure. When Bragg's law is satisfied the waves interfere constructively generating a peak (in-phase refraction).



**Annex 8** Schematic representation of a set-up for X-Ray diffraction analysis. Source and detector are moved along the circumference in steps ( $2\theta$  is incremented). Image from <http://chemwiki.ucdavis.edu>.

**Bragg's Law (constructive interference):**

$$\sin \theta = \frac{n\lambda}{2d}$$

where:

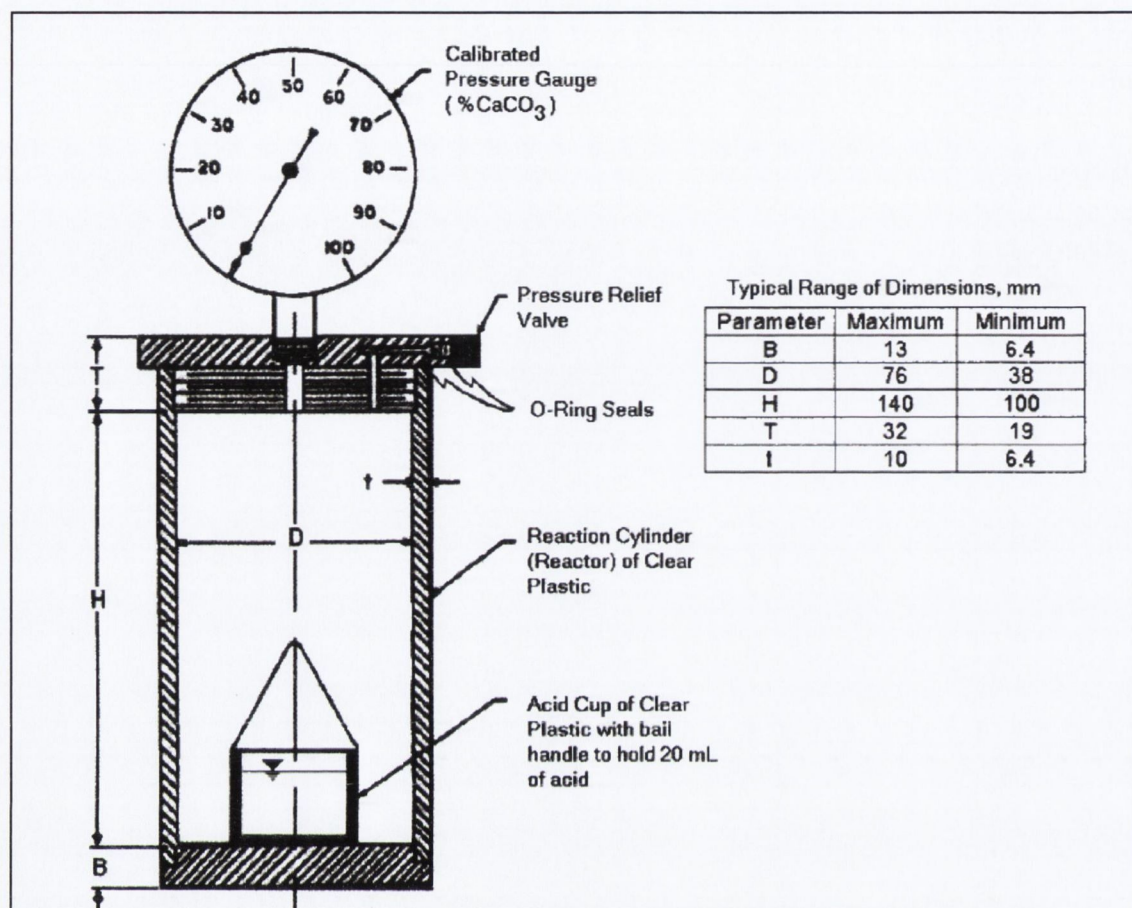
$\theta$  = incident angle

n = integer

$\lambda$  = wave length (1.54Å for Cu ka)

d = distance between planes in the crystal lattice

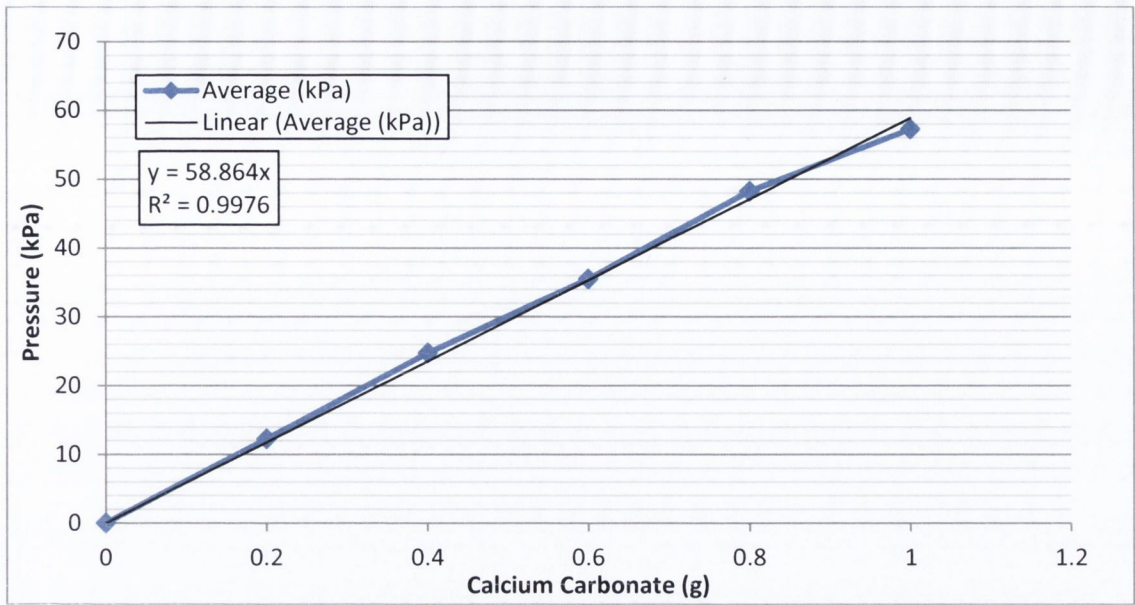
## Barometric Determination of Calcium Carbonate Equivalent



**Annex 9** Schematic representation of an apparatus for the barometric determination of calcium carbonate (ASTM D4373-02).

**Annex 10** Summary of calcite equivalent values for different carbonates (ASTM D4373-02).

Carbonate Specie	Cation	Calcite Equivalent
Magnesite	Mg	117.0%
Dolomite	Mg, Ca	108.6%
Calcite	Ca	100.0%
Aragonite	Ca	100.0%
Rhodocrosite	Mn	87.1%
Siderite	Fe	86.4%
Smithsonite	Zn	79.8%
Whiterite	Ba	50.7%
Cerrusite	Pb	37.5%

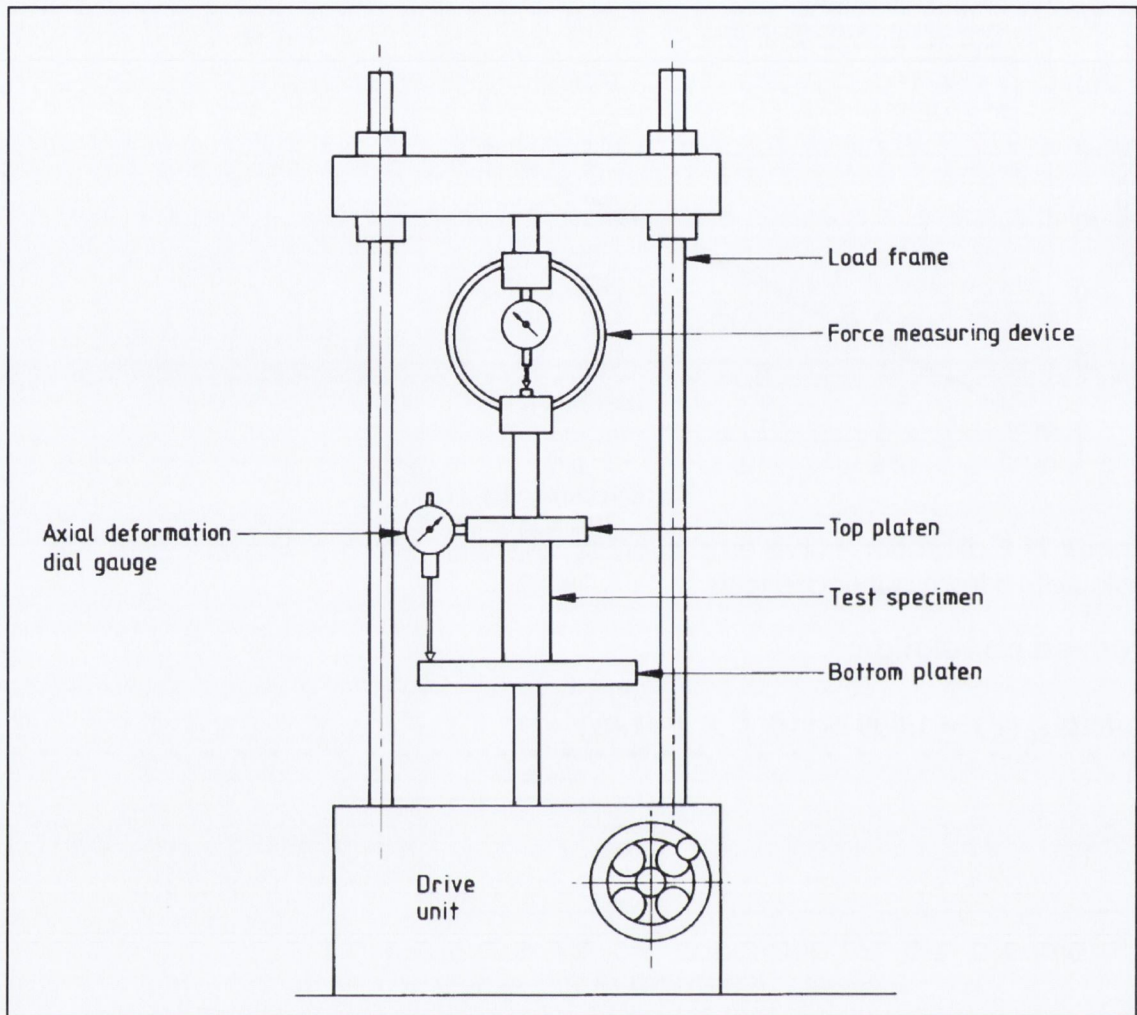


**Annex 11** Calibration curve employed in this study. Average values were calculated from duplicate tests.

**Derived correlation:**

$$Calcite_{EQ}(g) = 1.699 \times 10^{-3} \times P (kPa) \quad (R^2 = 0.9976)$$

## Unconfined Compressive Strength Test



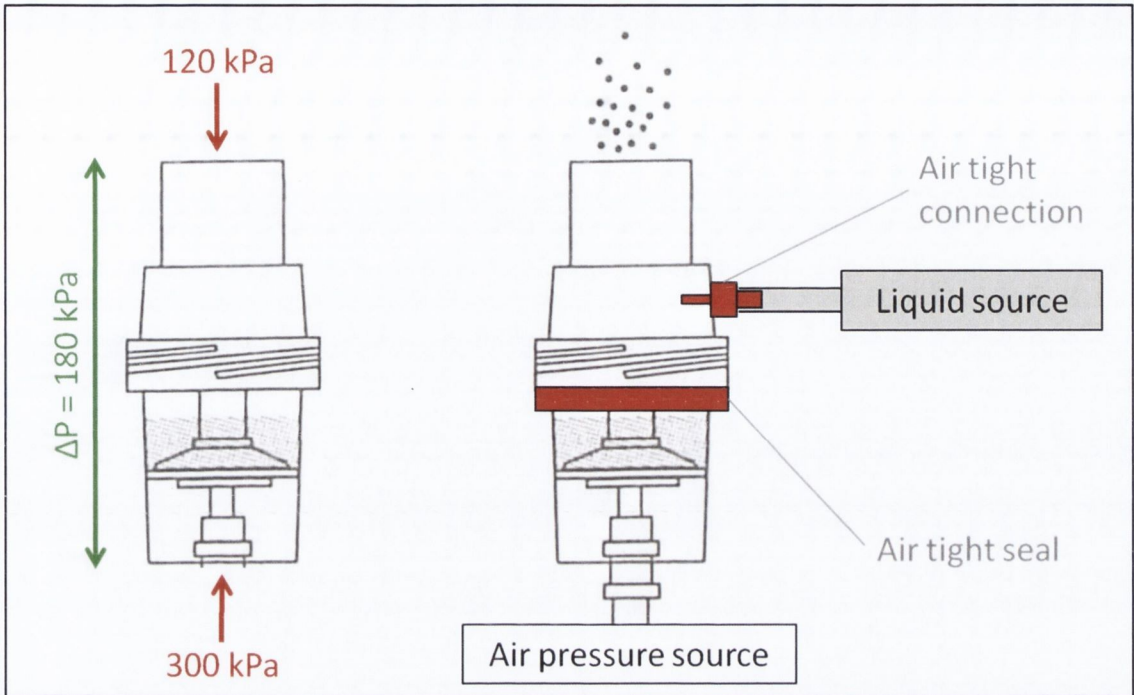
**Annex 12** Schematic representation of a load frame for unconfined compression strength test (BS 1377-7:1990).

**Annex 13** Details of the proving rings (force measuring device) employed in this study. Rings were selected on the basis of visual observation of the sample.

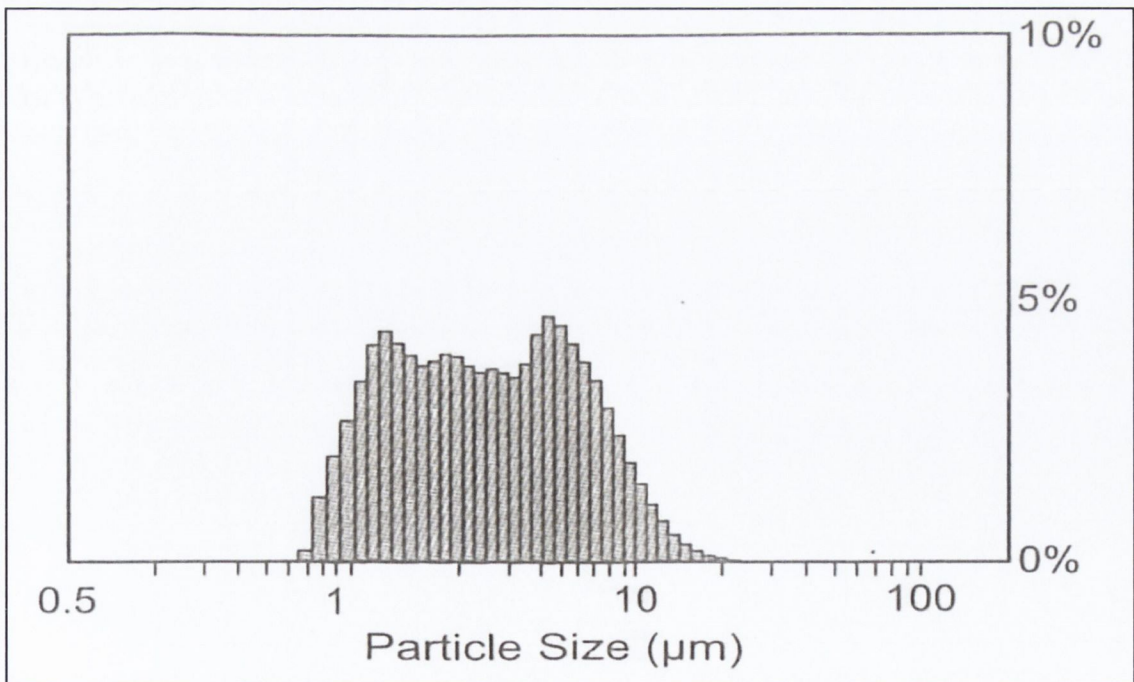
Visual	Ring N <sup>o</sup>	Range*	Constant (k)*
Soft	10588	0 – 0.05 kN	$1.93 \times 10^{-4}$ kN/div
		0.05 – 0.1 kN	$1.91 \times 10^{-4}$ kN/div
Hard	10858	0 – 0.2 kN	$7.7 \times 10^{-4}$ kN/div
		0.2 – 0.6 kN	$7.6 \times 10^{-4}$ kN/div

\* Calibration values provided by the supplier.

## Medical Jet Nebulisers



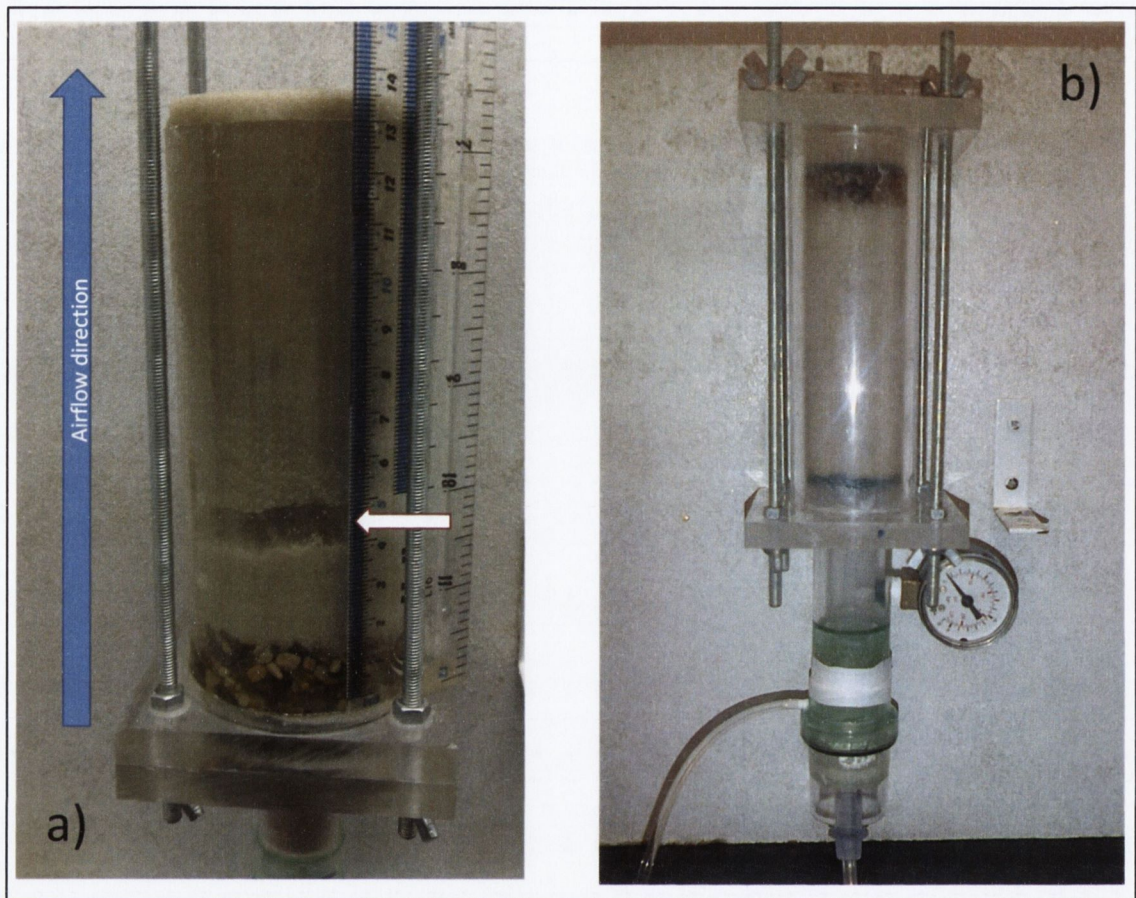
**Annex 14** Schematic representation of the modifications (red) carried out on Cirrus<sup>®</sup> nebuliser to adapt it to the working conditions encountered in this study. The seal was obtained using a suitably sized rubber o-ring whereas the connection was a PVC 3/32" to 1/16" reducer (The West Group Ltd.)



**Annex 15** Particle size distribution of aerosol generated by a Cirrus<sup>®</sup> nebuliser operating at  $8 \text{ L min}^{-1}$  (180 kPa). Data provided by the supplier (Intersurgical Ltd. 2009).



## Test column set-up



**Annex 16 (a)** Preliminary column design showing a sample where pressure fracture occurred (white arrow). The design was abandoned. **(b)** Revised column design where a confinement system was introduced at the top of the column. The gravel pack was placed at the top of the sand sample to improve the distribution of the confining forces.

## **References**

ASTM D4373-02 Standard test method for rapid determination of carbonate content of soils, American Society for Testing and Materials

BS 1377-7:1990 Methods of test for Soils for civil engineering purposes.  
Part 7: Shear strength tests (total stress).

Intersurgical Ltd. (2009). Cirrus information leaflet.

Whiffin, V. S. (2004). Microbial CaCO<sub>3</sub> precipitation for the production of biocement. School of Biological Science & Biotechnology, Murdoch University. Perth, Western Australia. **Doctoral dissertation:** p. 154.

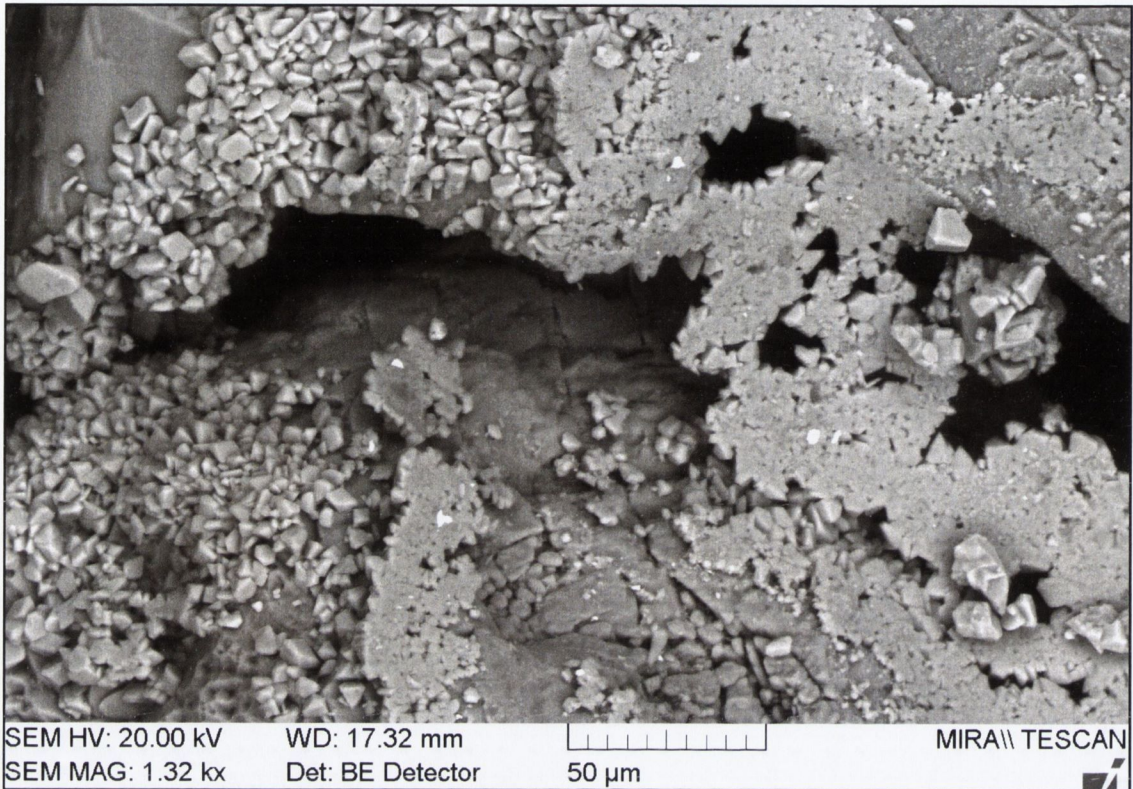


# APPENDIX TWO

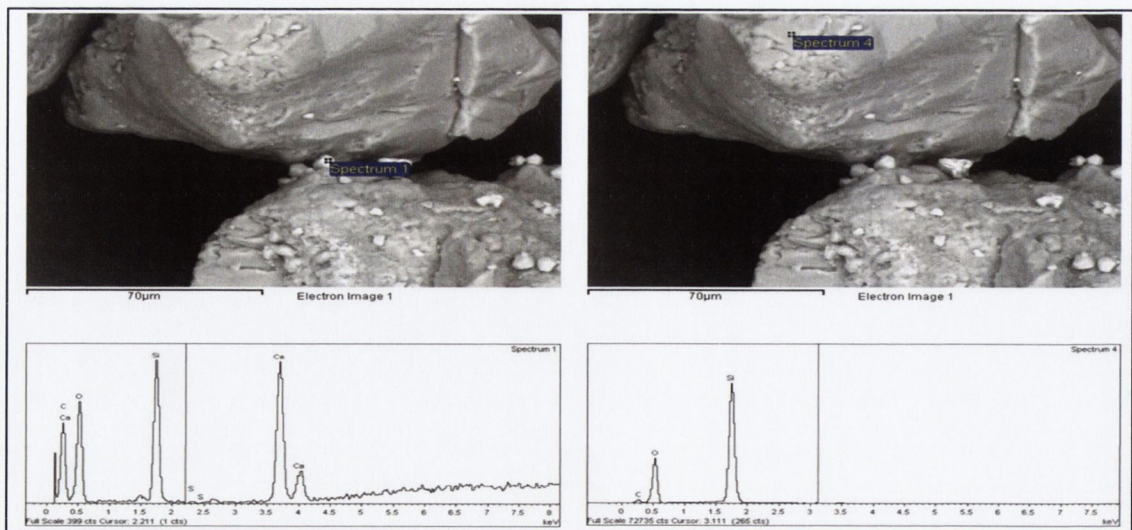
---

EXPERIMENTAL RESULTS AND DISCUSSION

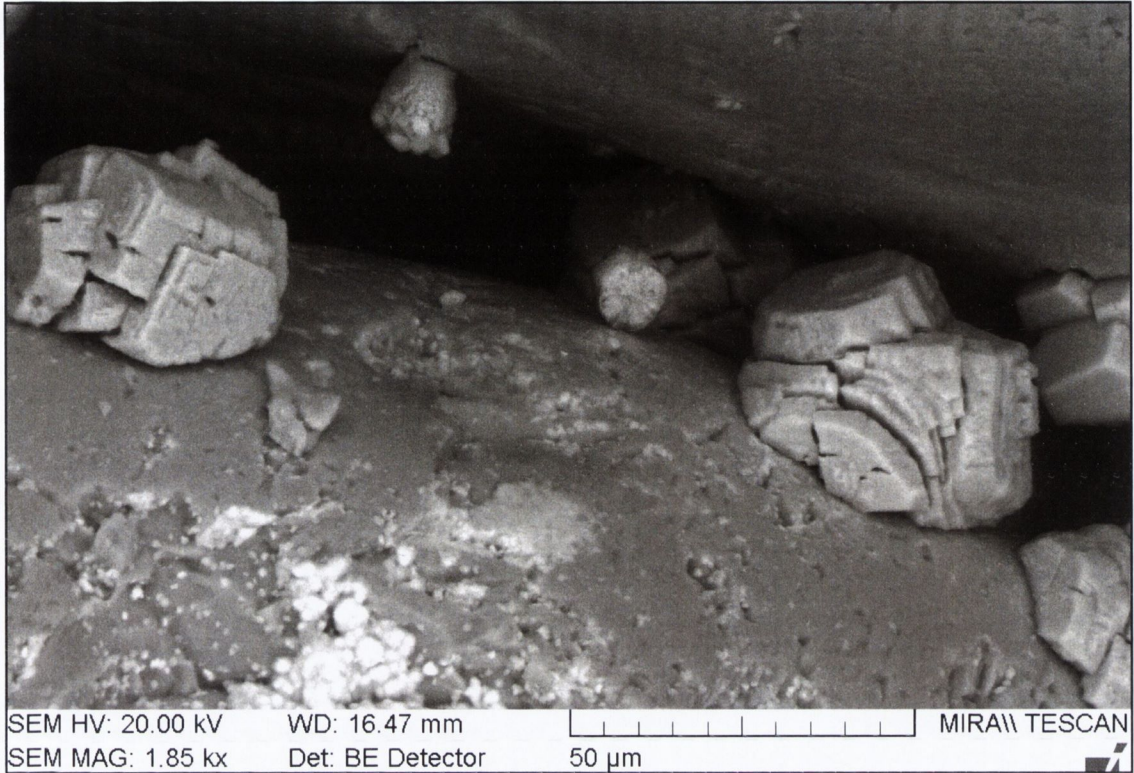
## Experiment N. 1: Carbonate distribution



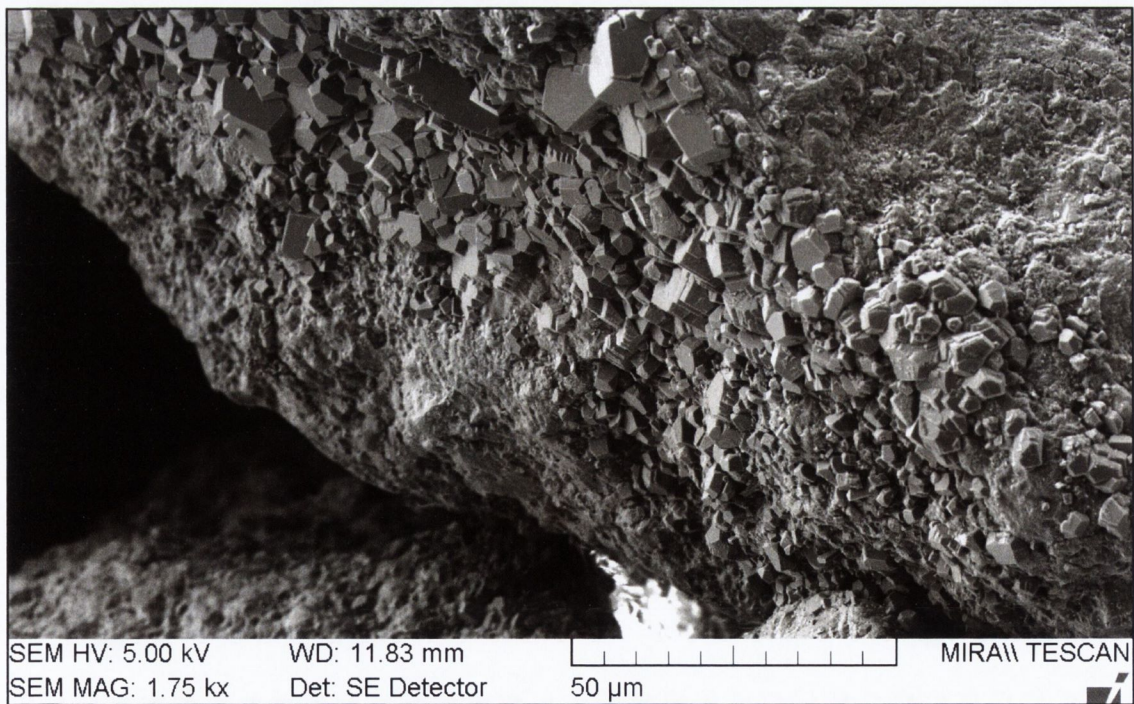
**Annex 1** SEM image of silica sand samples prepared as part of preliminary work. The preliminary experiment replicated work from the literature (van Paassen 2009). Calcite crystals are seen to coalesce in to polycrystalline structures. The imprint of a detached particle is visible in the left half of the image.



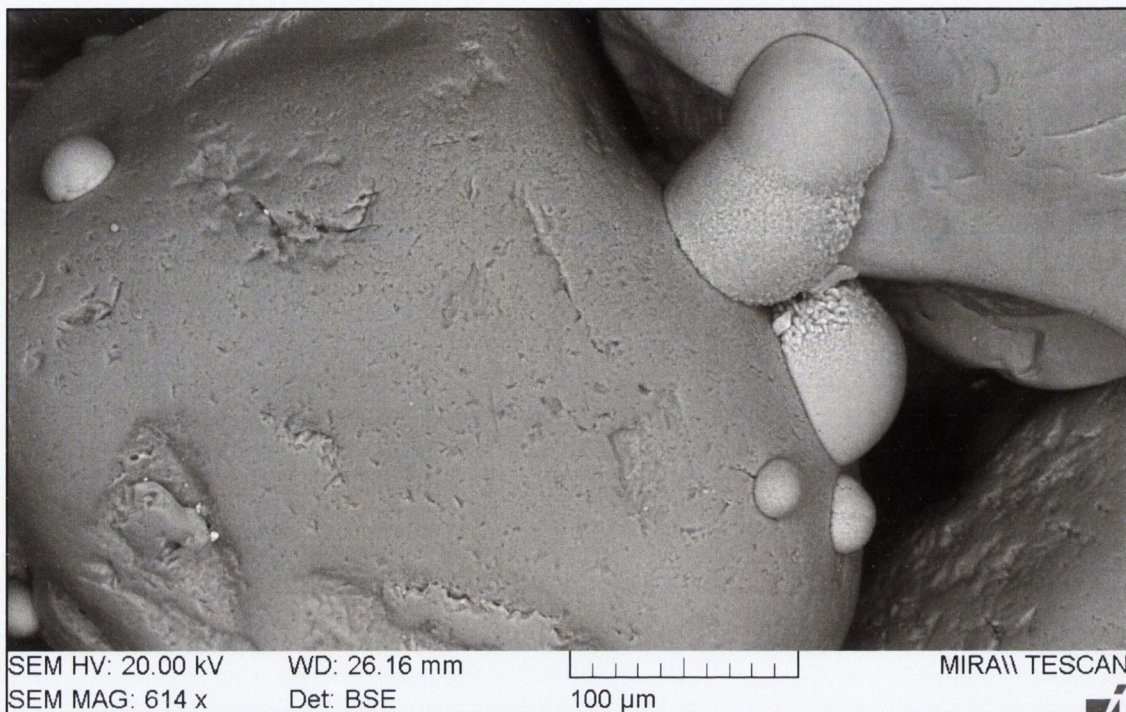
**Annex 2** Element analysis of sample OB3. The EDX functionality allows confirming the nature of the solid being observed: **(left)** calcium carbonate bond, **(right)** silica sand particle.



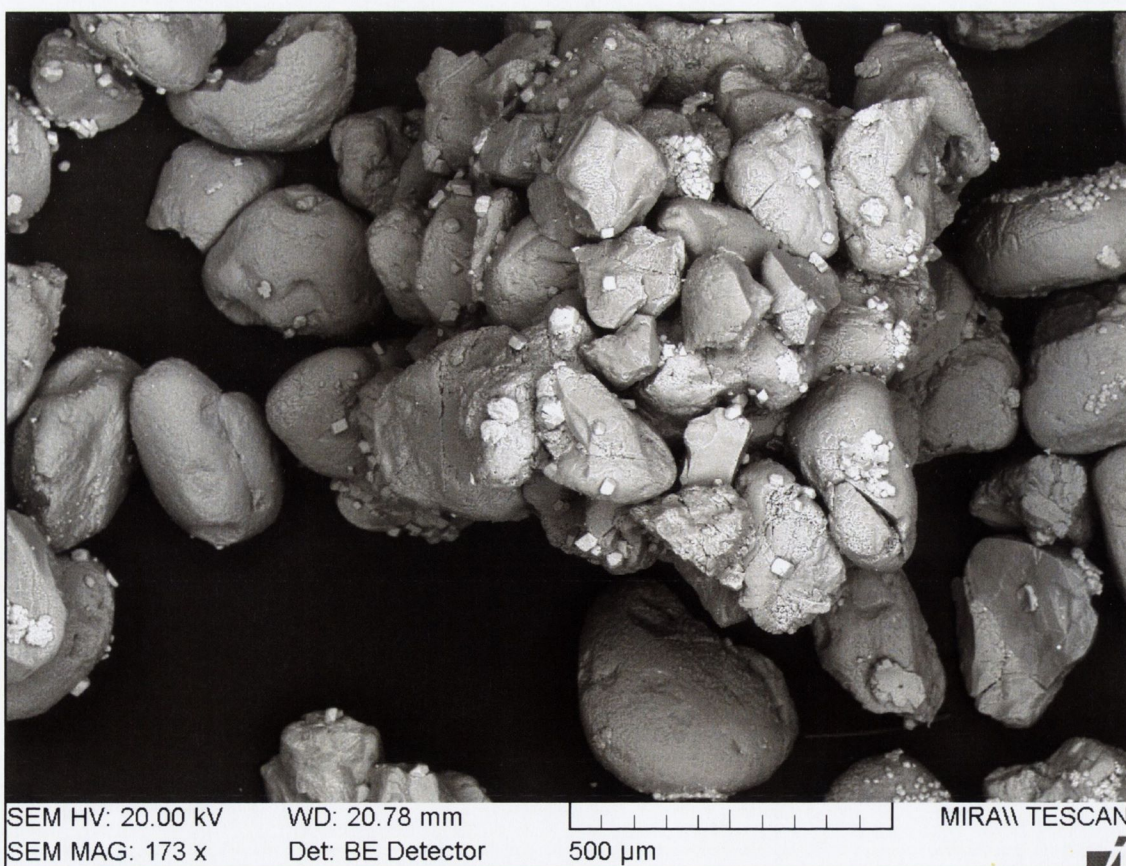
**Annex 3** SEM image of sample OA1 showing crystalline calcite forming in between particles of silica sand.



**Annex 4** Sample OD1 showing wide spread precipitation of calcite over the exposed surfaces of a carbonate sand particle.

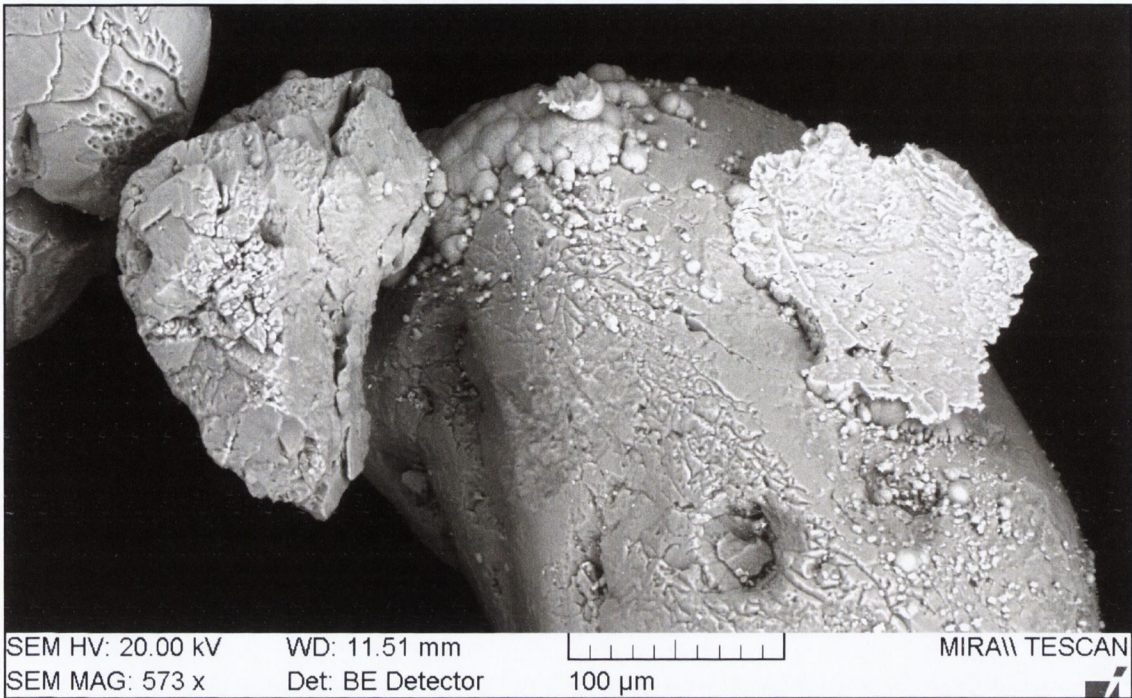


**Annex 5** Sample EA2 showing the carbonate bond formed between silica sand particle employing eutrophic treatments.

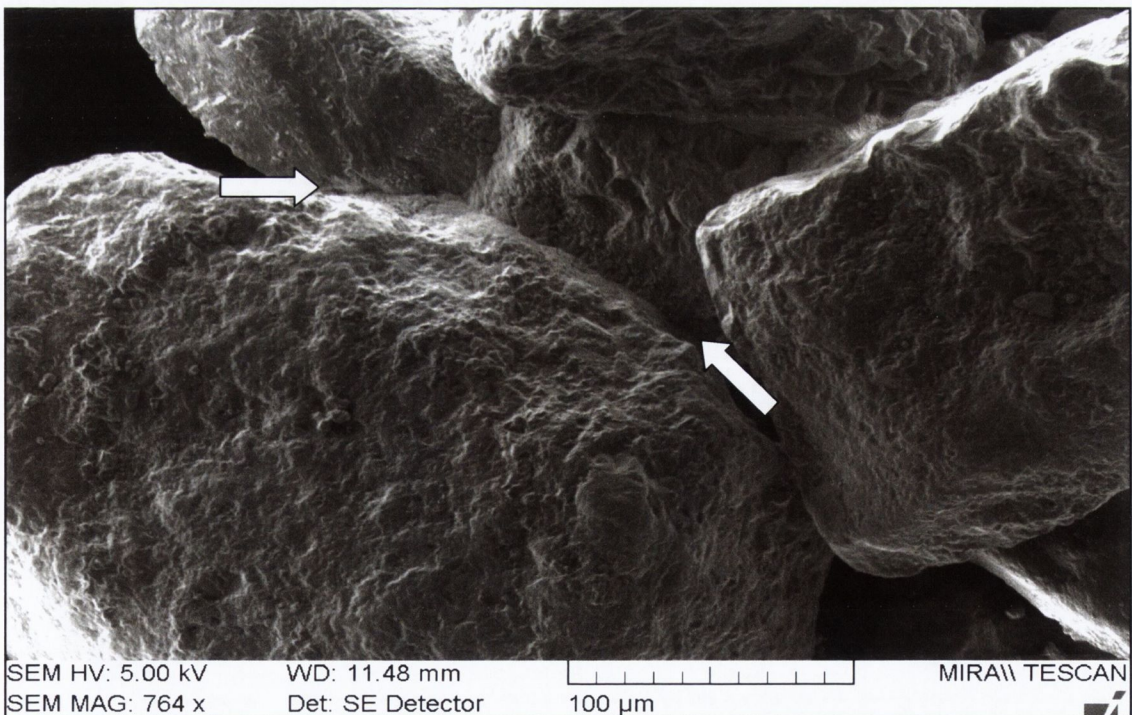


**Annex 6** Sample OB4 showing a large group of silica sand particles held together by calcite bonds.

## Experiment N. 2: Carbonate bond

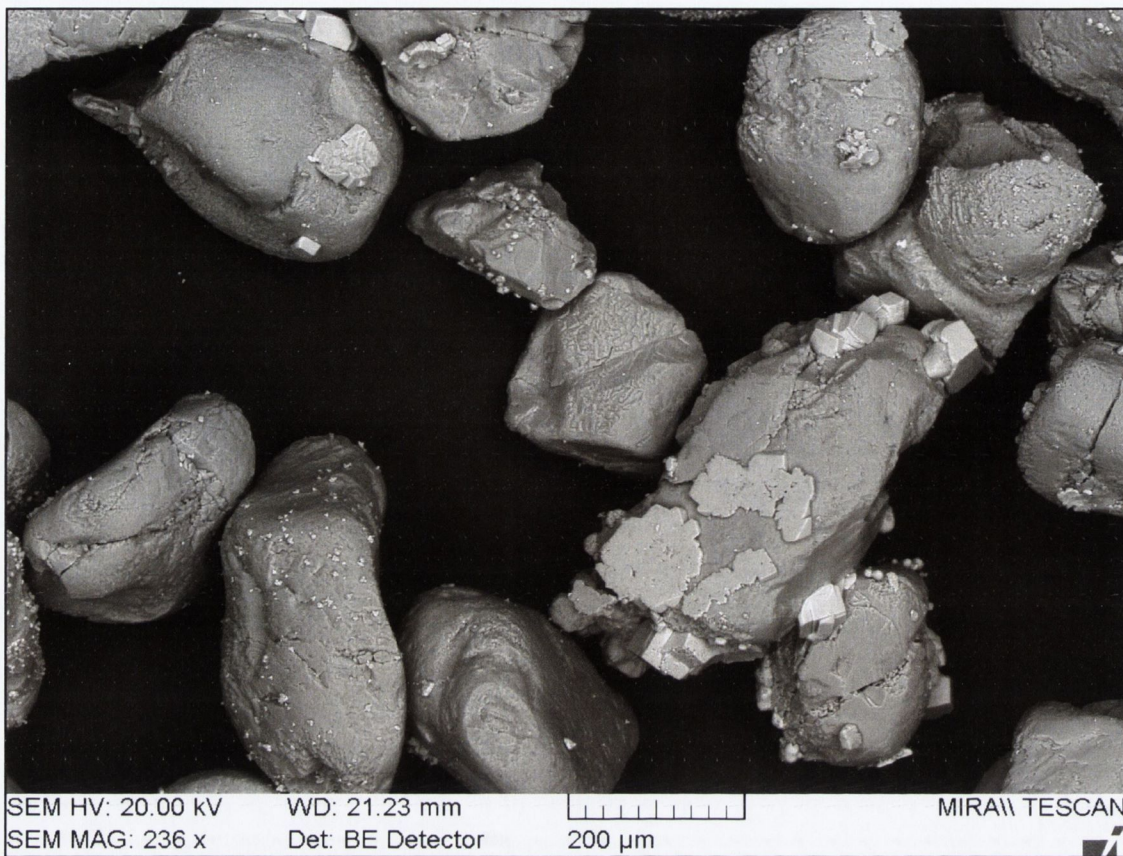


**Annex 7** Sample EE1 showing a bond particle failure surface where the imprint of the detached particle is clearly visible. An intact bond is also visible where calcium carbonate domes are “colonising” the surface of the silica particle as a result of eutrophic treatment.

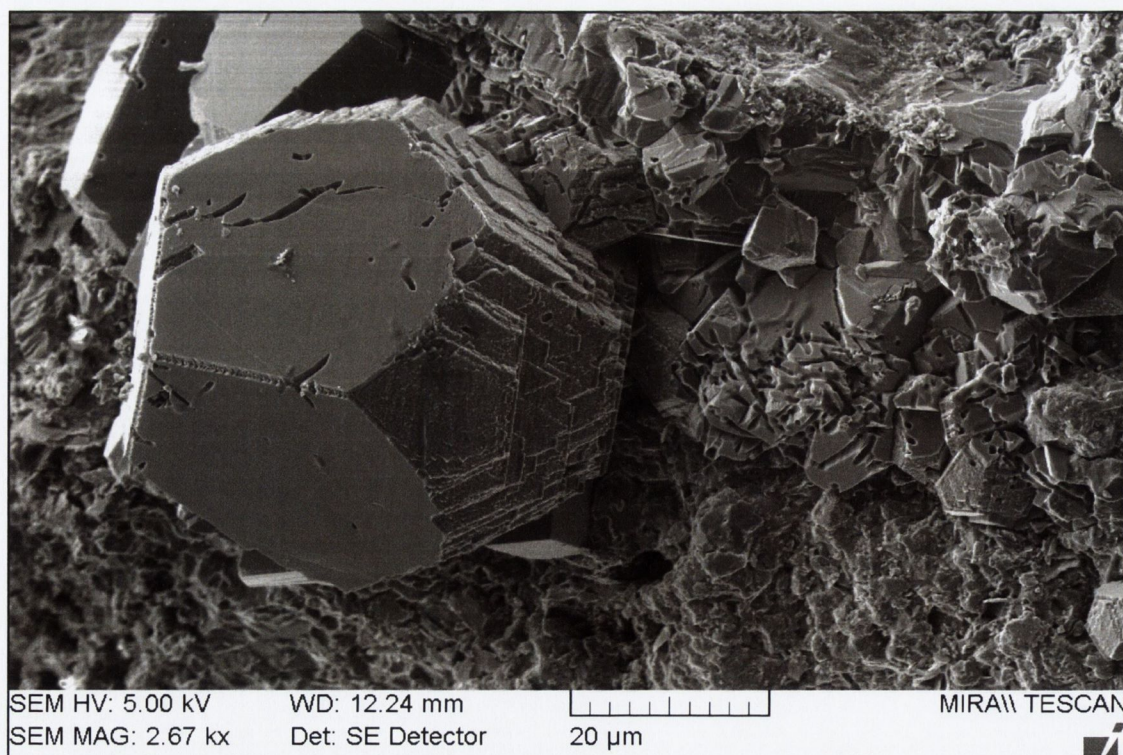


**Annex 8** Sample EE2 showing an eutrophic bond formed in carbonaceous sand. Calcium carbonate is mostly precipitated as micro calcite as a result of the carbonaceous nature of the sand particle. The arrows show the “suture”.

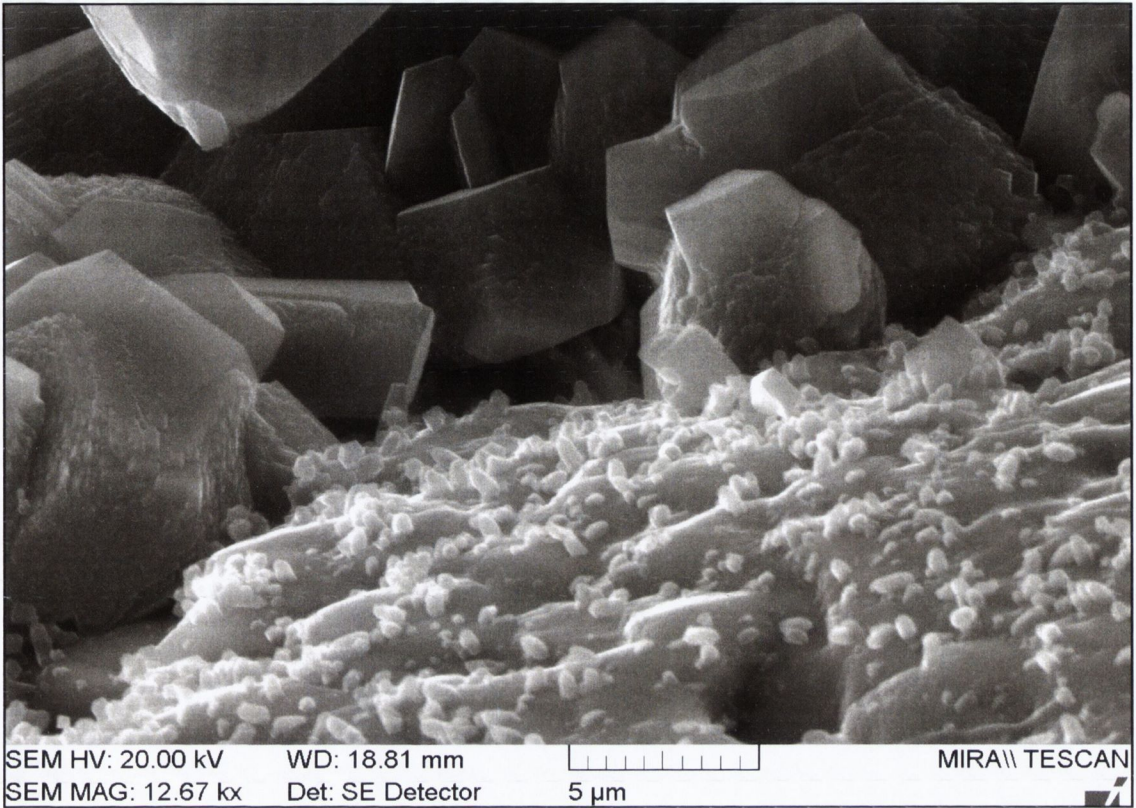




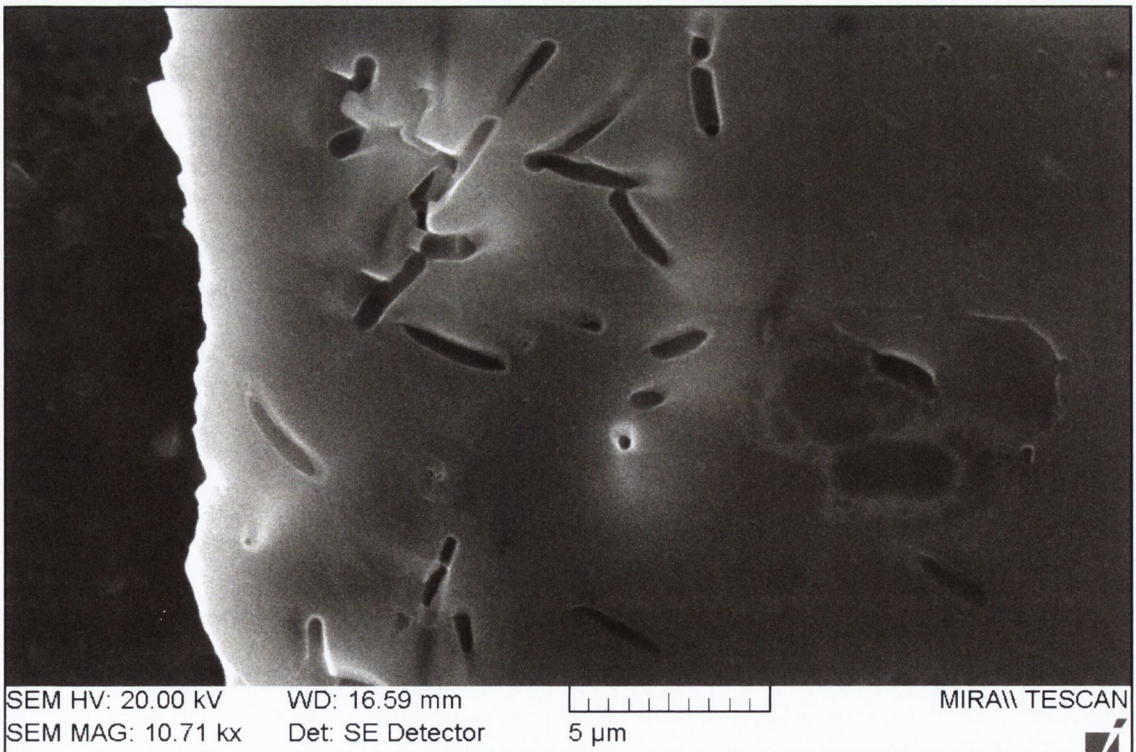
**Annex 9** Sample OE1 showing large monolithic bonds formed between silica particles during oligotrophic treatment.



**Annex 10** Sample OE2 showing the detail of a calcite crystal on a carbonaceous sand particle.

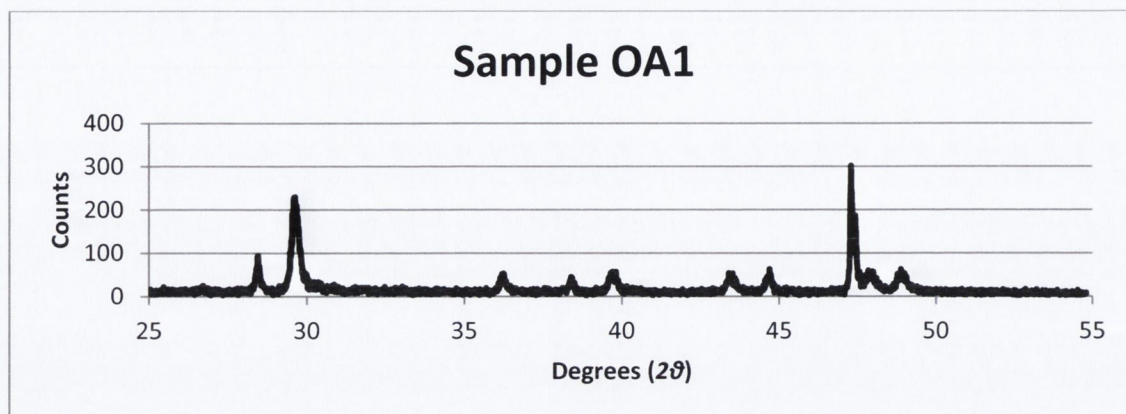


**Annex 11** Detail of calcite crystals growing on the surface of silica sand. The sample was obtained during preliminary work employing oligotrophic injection methods.

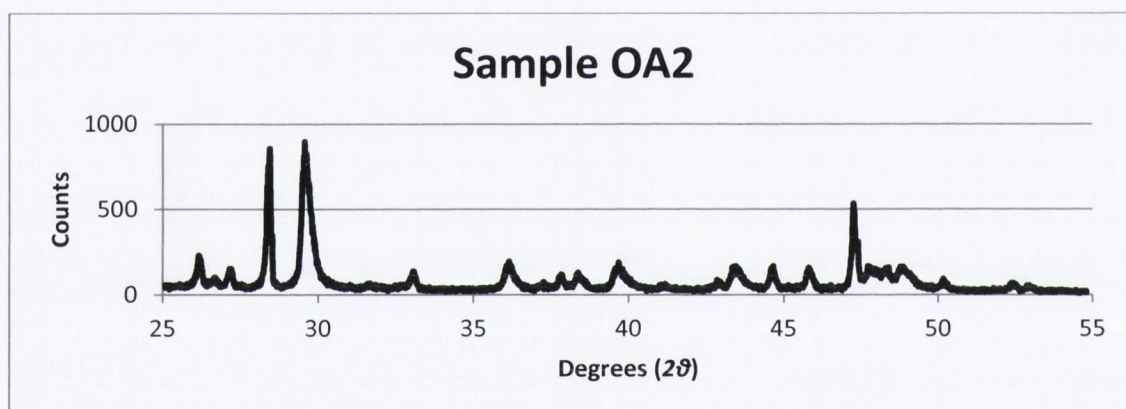


**Annex 12** Sample OE1 showing the detail of bacterial imprints left in newly formed calcium carbonate.

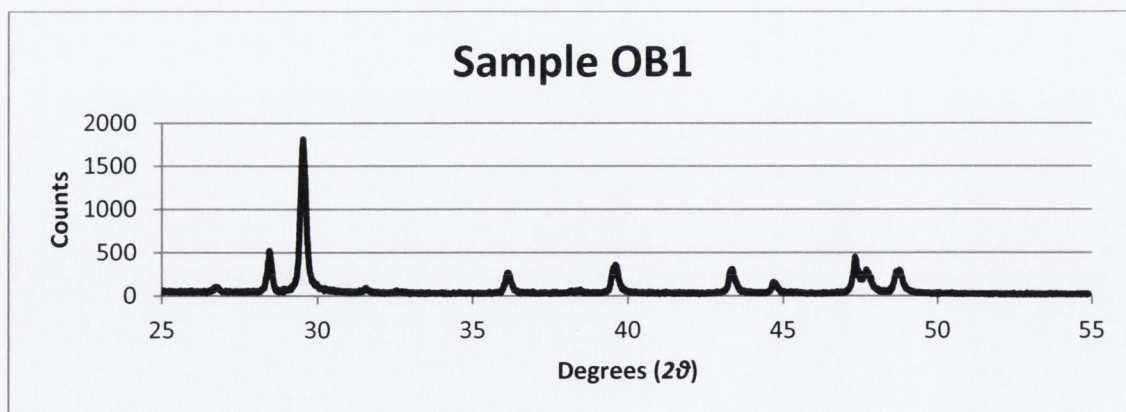
### Experiment N. 3: Magnesium in MICP applications



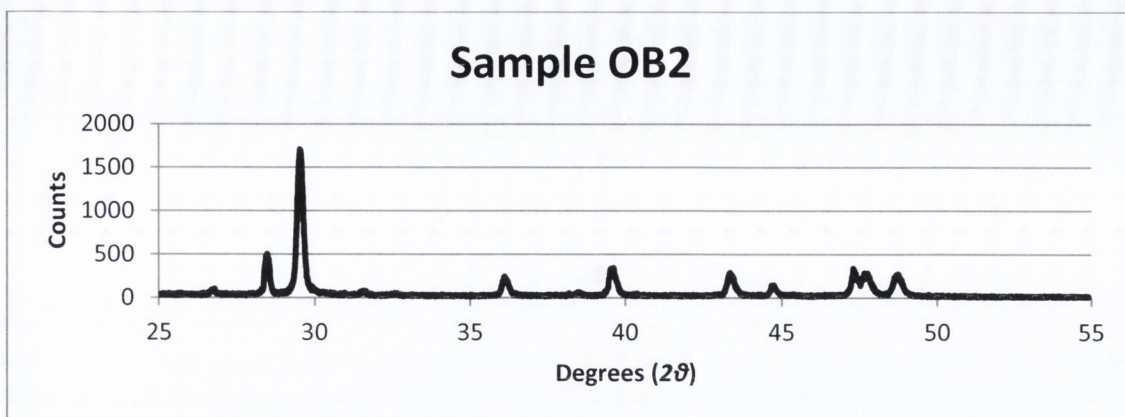
**Annex 13** Powder XRD, diffraction pattern of sample OA1



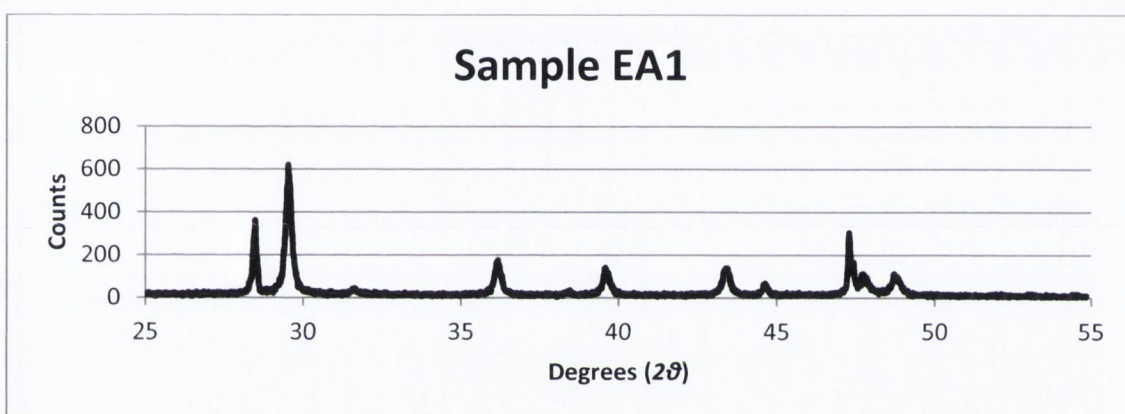
**Annex 14** Powder XRD, diffraction pattern of sample OA2



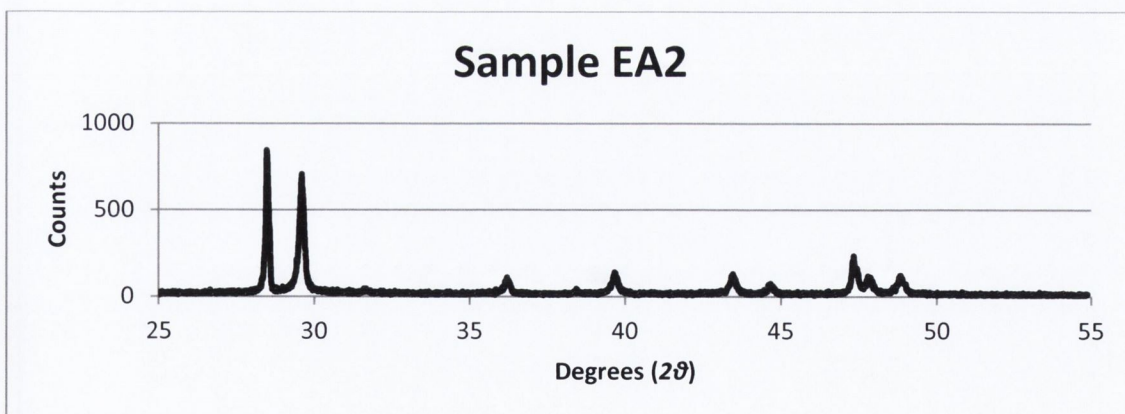
**Annex 15** Powder XRD, diffraction pattern of sample OB1



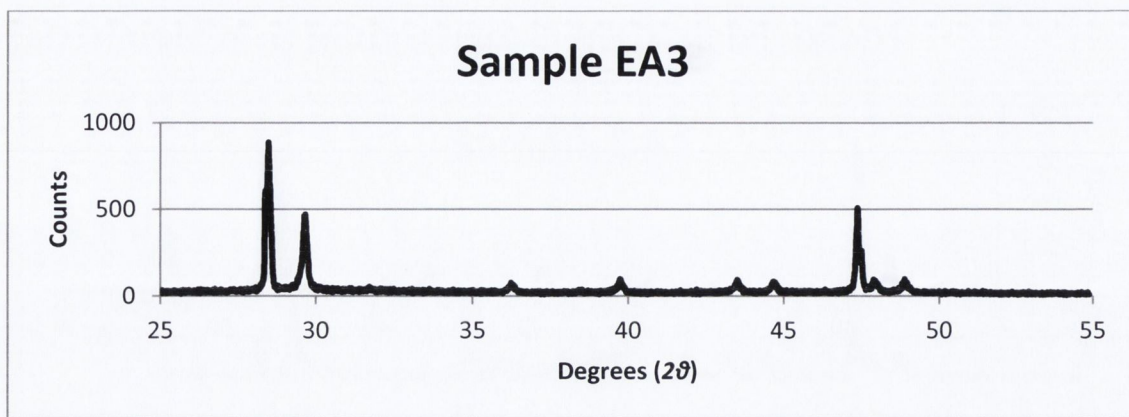
**Annex 16** Powder XRD, diffraction pattern of sample OB2



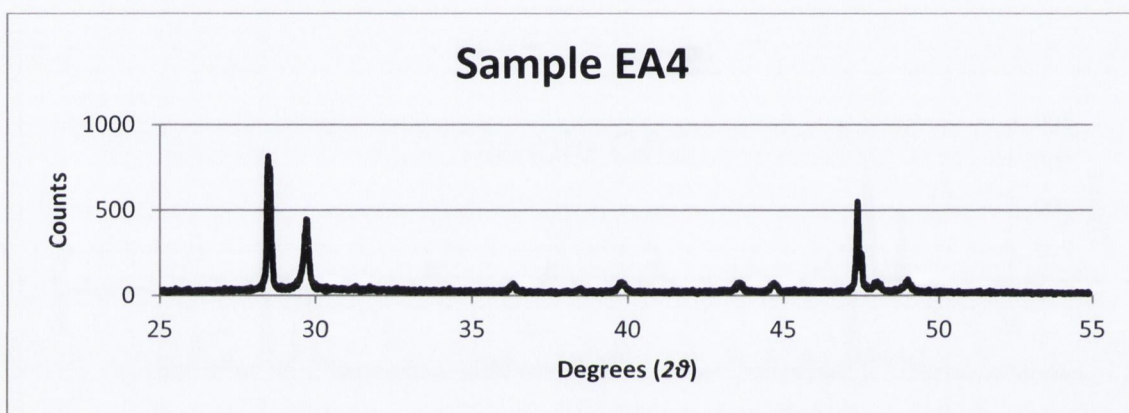
**Annex 17** Powder XRD, diffraction pattern of sample EA1



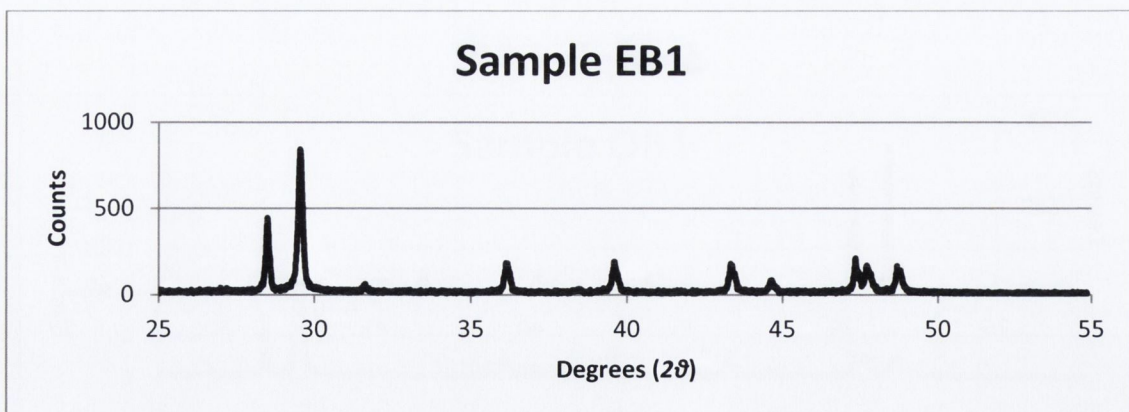
**Annex 18** Powder XRD, diffraction pattern of sample EA2



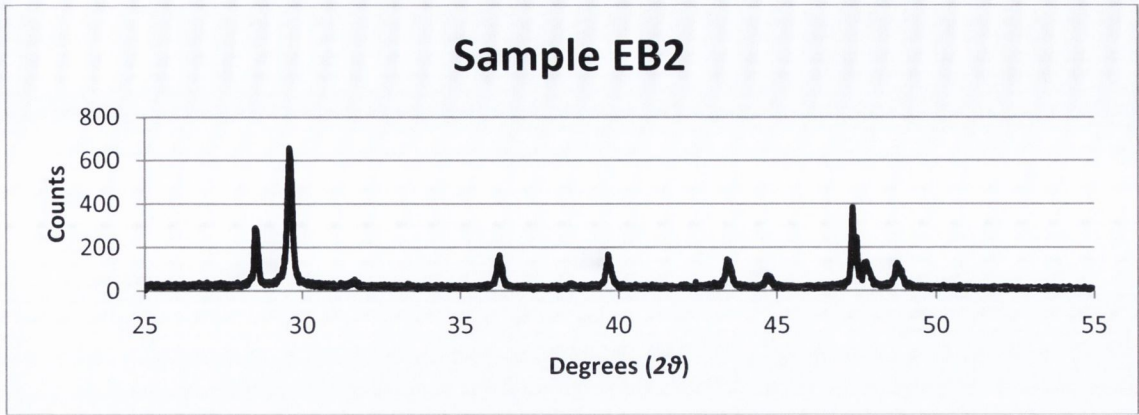
**Annex 19** Powder XRD, diffraction pattern of sample EA3



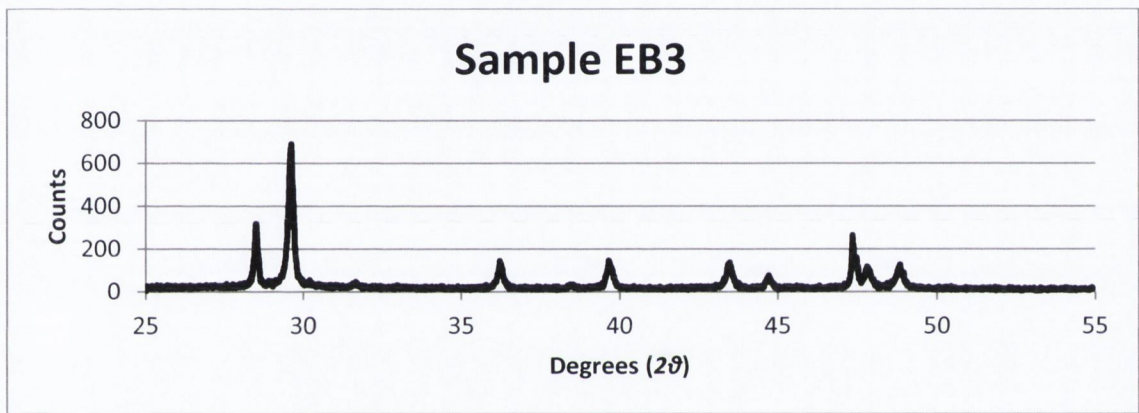
**Annex 20** Powder XRD, diffraction pattern of sample EA4



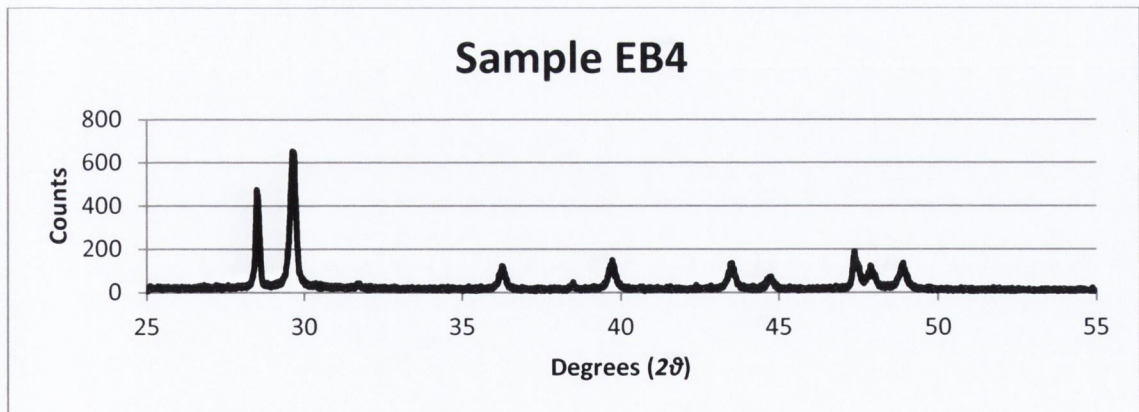
**Annex 21** Powder XRD, diffraction pattern of sample EB1



**Annex 22** Powder XRD, diffraction pattern of sample EB2



**Annex 23** Powder XRD, diffraction pattern of sample EB3

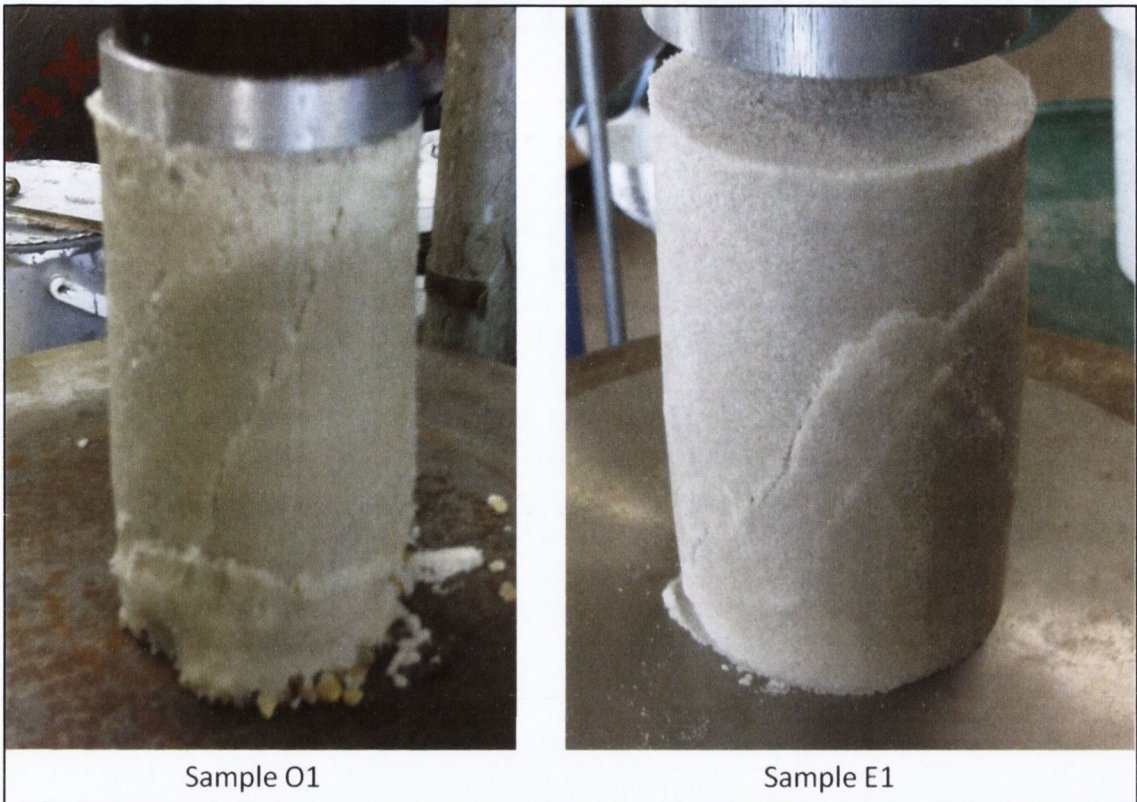


**Annex 24** Powder XRD, diffraction pattern of sample EB4

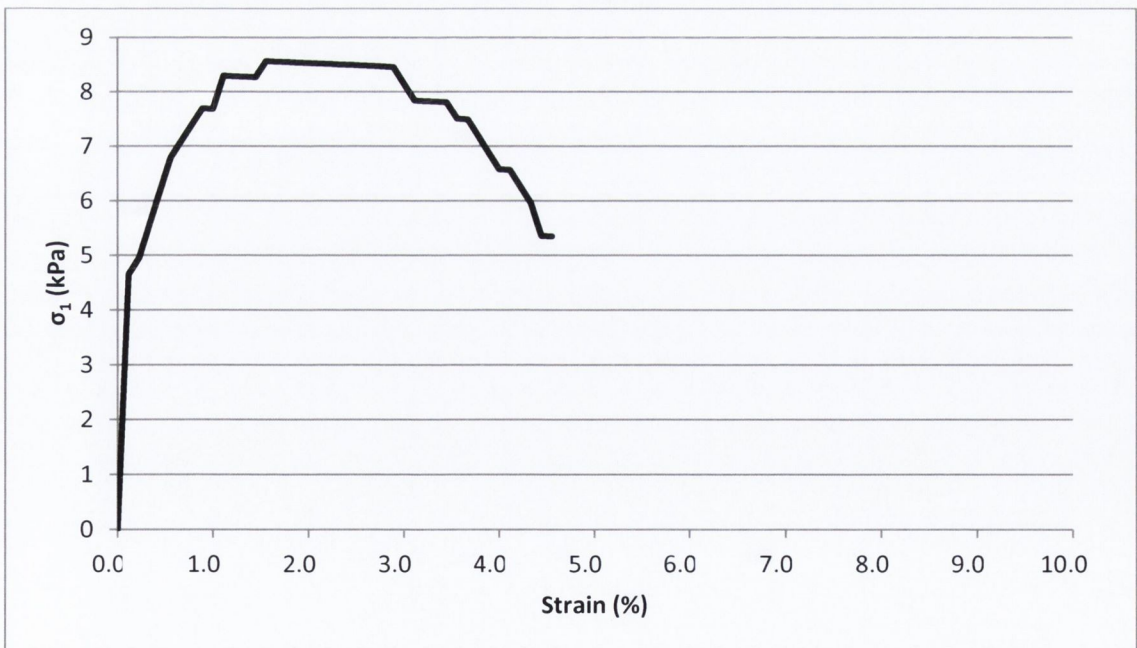


**Annex 25** Reactor vessels employed in Experiment N. 1

## Experiment N. 4: Feasibility of aerosol delivery

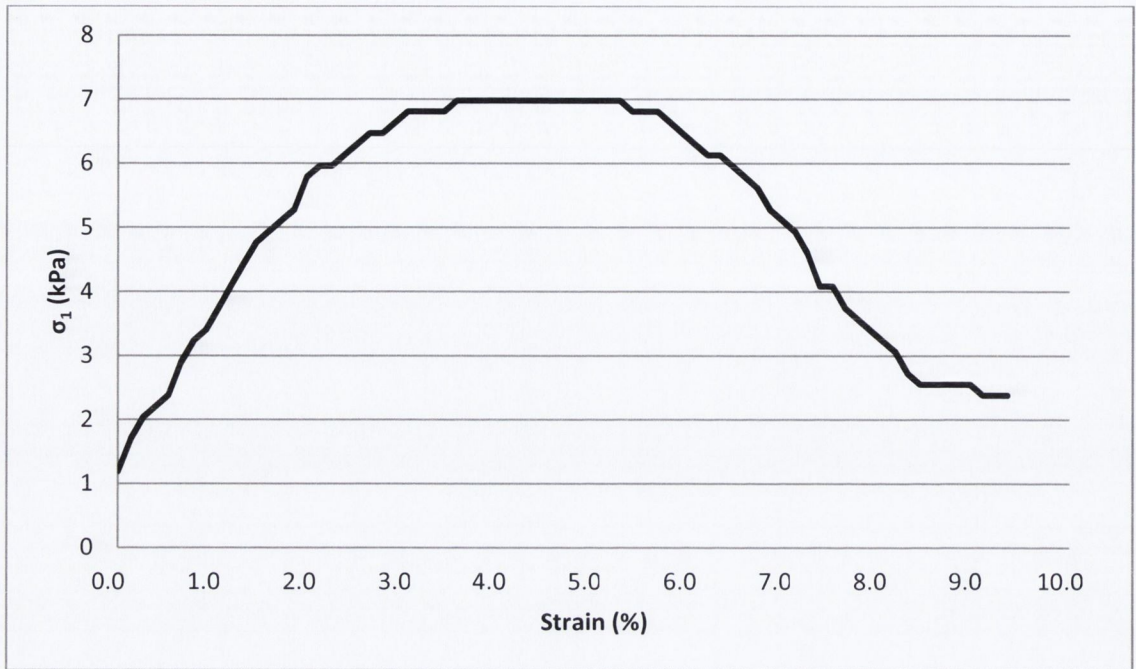


Annex 26 UCS test samples after failure.



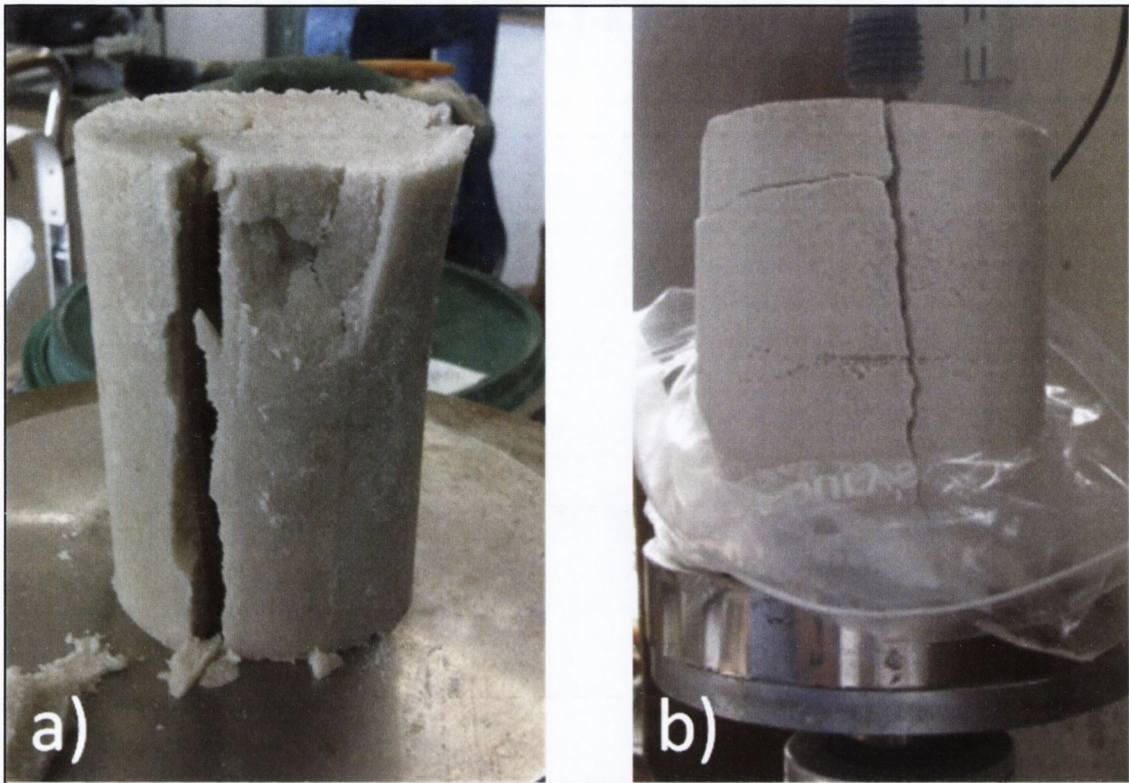
Annex 27 Sample O1 UCS (wet) stress-strain curve.



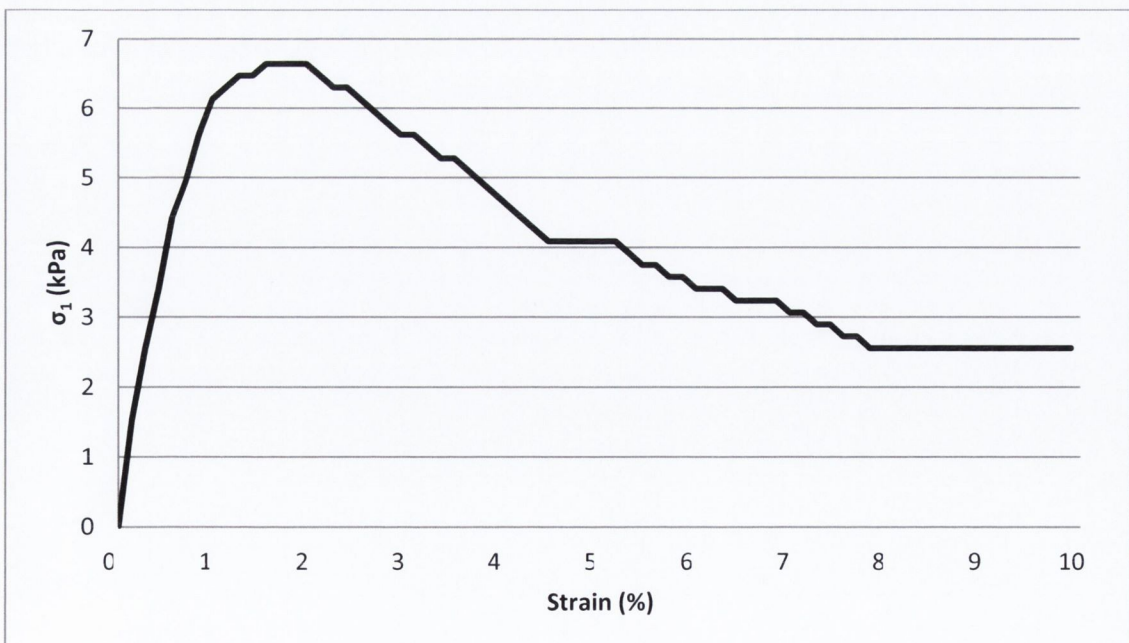


**Annex 28** Sample E1, UCS (wet) stress-strain curve.

## Experiment N. 4: Feasibility of aerosol delivery



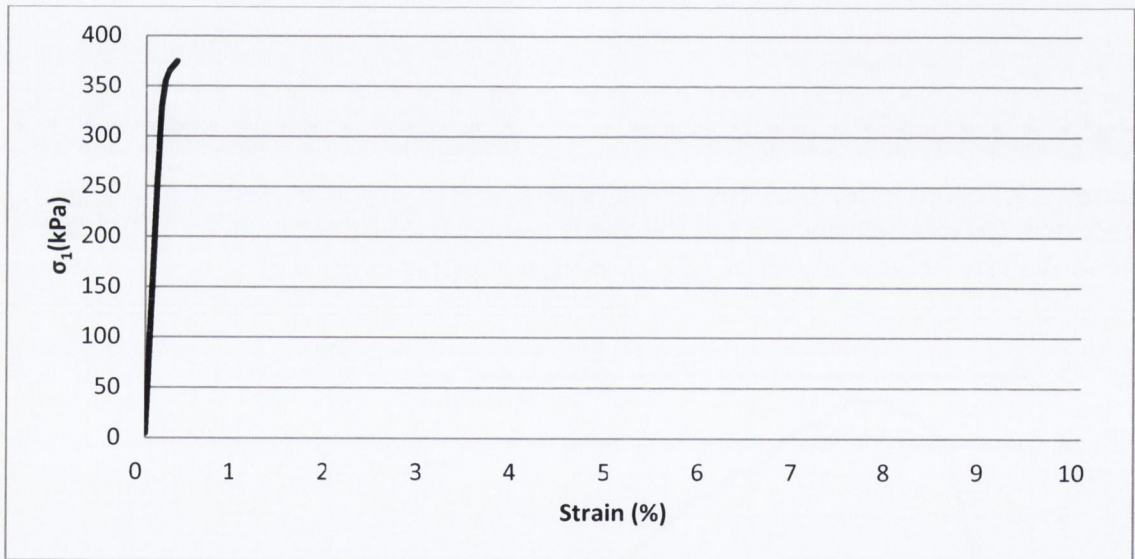
**Annex 29** Failure after UCS test of sample treated with conventional injection methods. **(a)** preliminary work in this study using oligotrophic protocols. **(b)** work presented by Al Qabany et al. (2013) using eutrophic protocols.



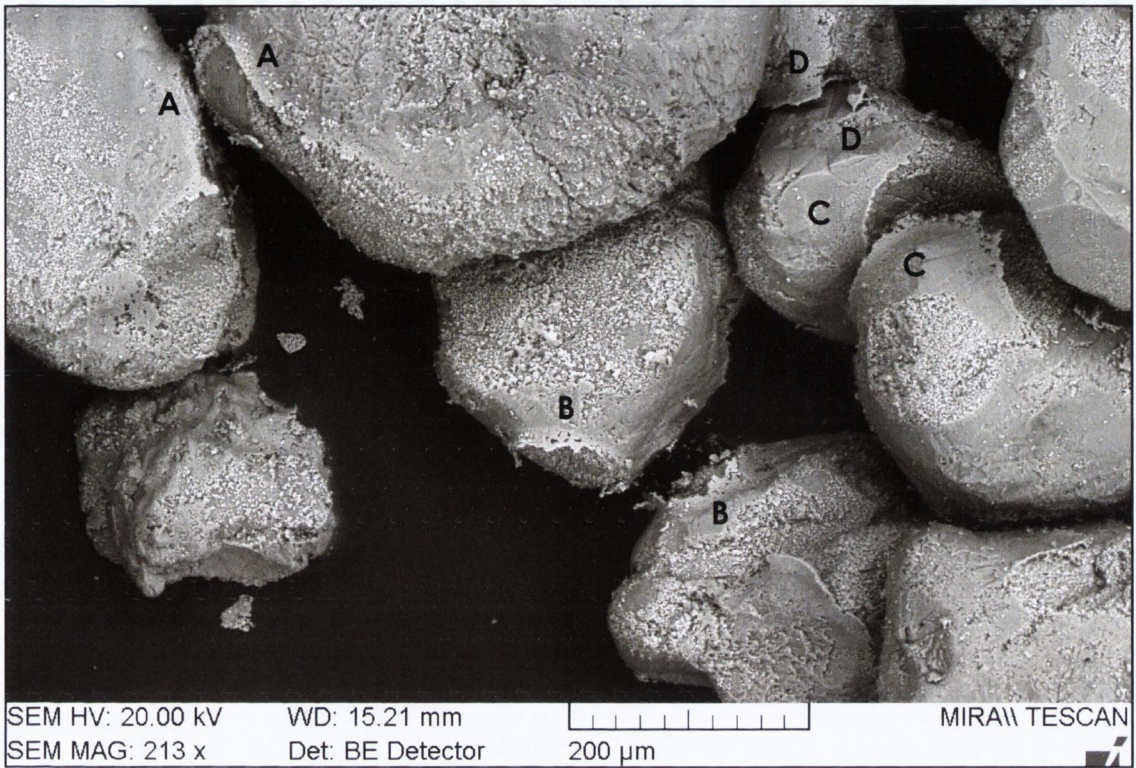
**Annex 30** Sample E150 UCS (wet) stress-strain curve.



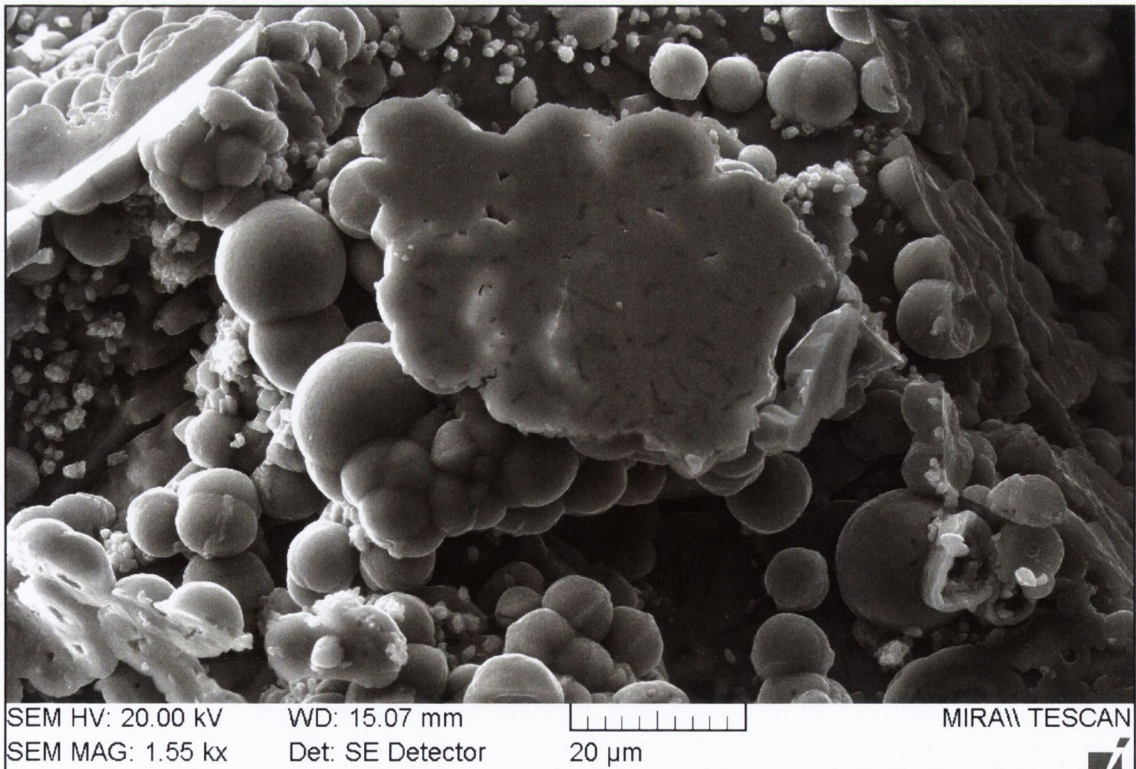
**Annex 31** Sample E500 UCS (wet) stress-strain curve. Data beyond the point of failure could not be recorded due to the complete collapse of the sample.



**Annex 32** Sample E1000 UCS (wet) stress-strain curve. Data beyond the point of failure could not be recorded due to the complete collapse of the sample.



**Annex 33** Sample E150 showing a cluster of particles where numerous primary and secondary bonds can be seen to fail. Letters indicate matching parts of a bond.



**Annex 34** Sample E1000 showing calcium carbonate deposited between the AWI and the surface of a particle. Bacteria imprints are visible in the foreground deposit. Widespread formation of spherulites is evident.

## **References**

Al Qabany, A. and K. Soga (2013). "Effect of chemical treatment used in MICP on engineering properties of cemented soils." Géotechnique **63**(4): 331–339.

van Paassen, L. A. (2009). BioGrout, ground improvement by Microbially Induced Carbonate Precipitation. Department of Biotechnology, Delft University of Technology. Delft, The Netherlands. **Doctoral dissertation.**

